Ebola virus nucleocapsid-like particles demonstrate consistent assembly, but a wide range of helical condensation

by

Melissa J. Rabb

A Thesis submitted to the Faculty of Graduate Studies of

The University of Manitoba

In partial fulfillment of the requirements of the degree of

Doctor of Philosophy

Department of Medical Microbiology and Infectious Diseases

University of Manitoba

Winnipeg, Canada

Abstract

Filoviruses were named after their thread-like appearance in the transmission electron microscope. As filamentous viruses, the protein shell that protects their single-stranded, negative-sense RNA genomes must be flexible, but strong. As a result, Ebola and Marburg viruses construct complex helical nucleocapsid structures. Five of the eight viral proteins encoded by these viruses are components of the helical nucleocapsid; however, only the nucleoprotein (NP), VP24, and VP35 are required to assemble nucleocapsid-like particles in transfected cells. The protein-protein interactions and stoichiometry of these 3 proteins, as well as a fourth nucleocapsid protein VP30 and the viral matrix protein VP40 within Ebola and Marburg virus nucleocapsids are not well understood.

Structural analyses of the Ebola virus nucleocapsid have been previously limited by the presence of the viral envelope, matrix, and glycoproteins. The overall goal of this thesis was to generate envelope-free nucleocapsids that could be analyzed by transmission electron microscopy to produce higher resolution nucleocapsid reconstructions. To do this we investigated a) the release of nucleocapsids from native Ebola virus and b) the generation and isolation of nucleocapsid-like particles from transfected cells. Treatment with a low concentration of detergent was not sufficient to release nucleocapsids from Ebola virus particles; however, the late stage of infection enabled the detection of novel nucleocapsid-like particles that we have termed "proto-nucleocapsids". These proto-nucleocapsids were ~30.5 nm in diameter and image analysis revealed a hollow structure with small lobes, attributed to individual NP molecules. In addition, no large external protuberances on this structure were observed. As such, we hypothesize that the proto-nucleocapsids are the inner NP-RNA layer of the Ebola virus nucleocapsid, which has previously been shown to be ~25 nm in diameter.

Heterologous expression of Ebola virus NP, VP24, VP30, VP35, and VP40 followed by density gradient ultracentrifugation of cell lysates enabled the isolation of novel nucleocapsid-like particles. While these structures had been previously observed within cell sections, we were the first to isolate and characterize them. These nucleocapsid-like

particles had a similar diameter to the Ebola virus nucleocapsid, but had a helical pitch slightly larger than the native nucleocapsid. Characterization of the nucleocapsid-like particles under various conditions demonstrated that the overall integrity of the helical structure was maintained, although a wide range of helical condensation was observed.

Ebola virus infection can cause severe hemorrhagic fever, with a case-fatality rate ranging from 50-90%. The current Ebola virus epidemic in Western Africa is suspected to have infected close to 25 000 people and has resulted in the death of at least 10 000. Although vaccines are currently undergoing clinical trials, there is still no treatment for individuals infected with Ebola. The rational design of anti-viral drugs that can target essential aspects of the Ebola virus lifecycle, such as the assembly of its nucleocapsid, requires greater understanding of this virus.

Dedication

To my grandfather Dr. George Harvey, who instilled a love of science and geology in me at a very young age. I'm so happy to be following in your footsteps.

And to my cousin Devika, who passed away just before completing her own PhD. This one is for you as well.

Acknowledgements

There are many people who have helped me get here and I will try to thank them all, but please forgive me if I forget anyone!

To my advisors Dr. Tim Booth and Dr. Dan Beniac, a very deep-felt thank you for always being available for questions, problem-solving, or a quick chat. It's been a pleasure to work with you both and to advance my skills so much in terms of molecular biology and the TEM. I love being able to tell people that I get to see not only viruses, but also exactly how my research is going. So thank you!

Thanks also to my committee members Dr. Kevin Coombs and Dr. Brian Mark, who were very helpful in their suggestions and always willing to answer questions.

I was very lucky to have received funding from the Natural Sciences and Engineering Research Council of Canada. Thank you for your support.

To Lindsey, Shannon, and Christine thanks for the many laughs and help along the way! No one understands the quirks (and pains) of using the TEM like you!

Thanks also to the Mass Spectrometry department at the NML. They performed the in-gel digestions for me and trained me in the protocol. Thanks to Andrea Taylor for the statistics help and a special thanks to Lynn Burton at CFIA who taught me all there is to know about sectioning! Lastly, thanks for the Special Pathogens group, and Shane Jones in particular for performing my Ebola virus experiment for me.

To the faculty and support staff of the Medical Microbiology department, thanks for running the smooth ship that is the Medical Microbiology department! The department is such a strong community and I've really benefited from that.

To the distinguished Ladies and Gentlemen of the Theodore Roberts Association for the Disenfranchised Graduate Students. I'm not sure I've ever had as many good, kind friends with the bonus of fully understanding what a graduate degree is like. Thank you so much for the laughs, cries, ridiculousness, and heart-warming friendship!

To my parents who have always been so supportive, thank you. They let me move across the country to pursue my bachelor degree and never said a peep about the cost of flights. I'm so glad that we are closer now and able to see each other more often (and for cheaper!). Thank you for pushing me and instilling in me a sense of curiosity, wonder, and drive. I wouldn't be who I am without you.

And to my Husband, who has kept me laughing even when I want to pull my hair out because my thesis formatting has gone wonky again: thank you. Thank god you are a computer genius, Google only knows so much. Thank you for listening to my project woes and for giving advice from a different angle that is almost always useful. Thank you for your love and support, xo.

Table of Contents

List of Tables

List of Figures

List of Movies

Abbreviations

Å	Angstrom
BHK cells	Baby hamster kidney fibroblasts
BSL4	Biosafety level 4
Cryo-EM	Cryo-electron microscopy
Cryo-ET	Cryo-electron tomography
DC-SIGN	Dendritic cell-specific ICAM3 grabbing non-integrins
DDSA	Dodecenylsuccinic anhydride
DMP-30	2,4,6-Tris(dimethylaminomethyl)phenol
DMSO	Dimethylsulfoxide
DRC	Democratic Republic of Congo
dsRNA	Double stranded RNA
DSS	Disuccinimidyl suberate
EBOV	Ebola virus

EGS	Ethylene glycolbis(disuccinimidyl succinate)
FDA	Food and Drug Administration
GAGs	Glycosaminoglycans
GP; sGP; ssGP	Glycoprotein; soluble; small soluble
HBV	Hepatitis B virus
HEK 293T	Human embryonic kidney cells
HIV	Human immunodeficiency virus
HRP	Horseradish peroxidase
IEM	Immuno-electron microscopy
IFN	Interferon
IID	Interferon inhibitory domain
IRF	Interferon regulatory factor
KCl	Potassium chloride
L protein	RNA dependent RNA polymerase of filoviruses
L-domain	Late budding domain
L-SIGN	Liver and lymph node endothelial cell- specific ICAM3 grabbing non-integrins
mAbs	Monoclonal antibodies
MALDI-TOF	Matrix-assisted laser desorption ionization-time of flight
MARV	Marburg virus
MCP-1	Monocyte chemoattractant protein-1
MgCl2	Magnesium chloride
MIP-1α	Macrophage inflammatory protein-1alpha
µl	microliter
MWCO	Molecular weight cut-off
NaAc	Sodium acetate
NaCl	Sodium chloride
NHP	Nonhuman primate
nm	nanometer
NML	National Microbiology Laboratory, Winnipeg, Canada

NNS	Nonsegmented negative-stranded
NO	Nitric oxide
NP	Nucleoprotein
NPC1	Niemann-Pick C1 protein
Nt	Nucleotide
ORF	Open reading frame
PBS	Phosphate buffered saline
PCR	Polymerase chain reaction
PE	Promoter element
PFA	Paraformaldahyde
Pfu	Plaque-forming units
PIC	Protease inhibitor cocktail
PTA	Phosphotungstic acid
PVDF	Polyvinylidene difluoride
RNP	Ribonucleoprotein
SDS-PAGE	Sodium dodecyl sulfate polyacrylamide gel electrophoresis
siRNA	Short, interfering RNA
SIRT	Simultaneous iterative reconstruction technique
STAT-1	Signal transducer and activator of transcription 1
TEM	Transmission electron microscopy
TG	Tween20-glycine
TIM-1	T-cell Ig and mucin domain 1
TNF-α	Tumor Necrosis Factor-alpha
TRAIL	TNF-related apoptosis-inducing ligand
trVLP	Transcription and replication competent virus-like particles
UTR	Untranslated region
VeroE6	African green monkey kideny cells
VLP	Virus-like particle
WHO	World Health Organization

Chapter 1. Introduction

The protein shell or capsid of a virus particle surrounds the viral genome to protect the nucleic acid during transmission and infection (Caspar and Klug, 1962). Environmental conditions, including desiccation, sunlight, and changes to pH must be endured for the successful transmission and replication of a virus (Caspar and Klug, 1962). Once inside the host cell, the nucleocapsid often continues to protect the viral genome from anti-viral attacks led by host cell proteins. Newly replicated genomes are quickly surrounded by capsid proteins for protection, but also as a means of distinguishing genomes that are ready to be further assembled and released as complete virus particles (Flint et al. 2004).

There are two types of virus, non-enveloped and enveloped. Non-enveloped viruses have an outer protein coat (the capsid), which can be multi-layered. Enveloped viruses are surrounded by a lipid bilayer (usually including virally-encoded trans-membrane proteins) that is derived from the host cell (Flint et al. 2004). Picornaviruses, such as poliovirus, do not have a viral envelope and rely on their icosahedral capsids for protection. The four capsid proteins of poliovirus self-assemble to form a T=1 (pseudo-T=3) symmetrical structure, that is relatively robust in the environment (Flint et al. 2004; Tuthill et al., 2010). Herpesviruses are much larger, enveloped viruses that also encode capsid proteins that self-assemble into an icosahedral structure (Flint et al. 2004). Herpes simplex virus type 1 assembly is a more complex system than poliovirus, with seven different viral proteins (some encoded by multiple genes) involved in the assembly. The hexons and pentons of the icosahedral nucleocapsid consist of quasi-equivalent VP5 interactions, which are linked together by VP19C and VP23 (Flint et al. 2004). Three additional proteins (VP24, VP21, and VP22a) assist in capsid formation, with VP22a acting as a scaffold for VP5 assembly (Flint

et al. 2004). Other viruses, such as poxviruses, retroviruses, and coronaviruses have more complex capsids. Coronaviruses and retroviruses encode nucleocapsid proteins that coat their RNA genomes, but also encode capsid and matrix proteins (retroviruses) or membrane proteins (coronaviruses) that provide additional structure to the virus particle (Flint et al. 2004). Poxviruses encode core proteins that self-assemble into the core wall that surrounds the genomic DNA (Flint et al. 2004). The last major type of capsid has a helical symmetry. The viruses of the *Mononegavirales*, including rhabdoviruses, paramxyoviruses, and filoviruses express proteins that assemble into helical nucleocapsids around their negative sense, single-stranded RNA genome (Flint et al. 2004; Reviewed in Booth et al. 2013). In addition, orthomyxoviruses and some plant viruses, such as tobacco mosaic virus form helical nucleocapsids (Flint et al. 2004; Booth et al. 2013). Filoviruses and rhabdoviruses package their helical nucleocapsids within linear and bullet-shaped particles, respectively. Unlike rhabdoviruses, filoviruses have several types of particle morphology (Beniac et al. 2012; Flint et al. 2009). Paramyxoviruses package multiple copies of their helical nucleocapsid within pleomorphic particles (Loney et al. 2009). Ebola virus particles have also been shown to package multiple genome copies, yet the overall particle shape remains linear (Beniac et al. 2012).

For each of these viruses, the capsid is made up of the same repetitive arrangement of proteins. The capsid of tobacco mosaic virus consists of just one protein; whereas many viruses, including filoviruses, poliovirus, and herpesviruses require the assembly of multiple distinct protein subunits (Beniac et al. 2012; Flint et al. 2010). Regardless of the number of different proteins, self-assembly can only occur if each newly synthesized protein subunit contains the proper interaction sites that enable protein-protein bonds

(Caspar and Klug, 1962). Proteins folded or synthesized incorrectly will lack these interaction sites and will not self-assemble, preventing their incorporation into the capsid (Caspar and Klug, 1962). As Caspar and Klug (1962) describe, self-assembly tends to generate a structure that has "the maximum number of most stable bonds". Thus, in this theory, the assembled structure is favoured since it has the lowest energy state. This does not necessarily mean that each protein subunit must be assembled into the exact same environment. The process is driven by each protein subunit tending to form the most stable bonds possible within that environment. In the case of many viruses, this is accomplished through quasi-equivalent interactions, rather than completely identical bonds (Caspar and Klug, 1962).

In this thesis, I investigated the assembly of the Ebola virus nucleocapsid. I expressed the Ebola virus nucleocapsid proteins in 293T cells and successfully isolated Ebola virus nucleocapsid-like particles. I discovered that these particles were dynamic, with a wide range of helical condensation observed, but were also highly stable. Only the most severe (low pH, 0 mM NaCl) lysis conditions were capable of damaging the assembled nucleocapsid-like particles. Overall, my research has demonstrated that the Ebola virus nucleocapsid is capable of self-assembly and suggests that a final helical condensation step might occur during envelopment and/or budding of virus particles.

1.1 The Ebola virus

Of all the known viruses, the *Filoviridae* family has one of the most unique and recognizable morphologies (Booth et al. 2013). Ebola and Marburg virus species have been imaged as linear, branched, spherical, check mark, or comma-shaped particles using the transmission electron microscope (TEM); however, the internal quaternary structure of these viruses is still not well understood.

Filoviruses were first identified in 1967, when lab workers in Marburg, Frankfurt, and later Belgrade were exposed to an unknown pathogen after handling African Green Monkeys and their tissues, imported from Uganda (Slenczka and Klenk, 2007). A total of 32 individuals became sick with a haemorrhagic illness that could not be diagnosed. It took an international group of scientists approximately three months to identify the unknown pathogen and electron microscopy played a critical role in that discovery. It was the TEM observation of filamentous virus particles in formalin-fixed guinea pig blood that gave us the first look at this new virus family (Slenczka and Klenk 2007). Today, TEM continues to provide novel information on virus structure, life cycle, and emerging pathogens.

Filoviruses are enveloped, filamentous viruses belonging to the order *Mononegavirales* (Elliott et al. 1985; Feldmann et al. 1993; Feldmann et al. 2003; Mehedi et al. 2011; Sanchez et al. 1993; Sanchez et al. 1996; Volchkov et al. 1999). Within the *Filoviridae* family there are 3 genera: the recently discovered *Cuevavirus* from bats in Spain and the original members *Marburgvirus* and *Ebolavirus* (Kuhn et al. 2014; Negredo et al. 2011). Currently, there are 5 species of *Ebolavirus* identified that are associated with varying degrees of pathogenesis: *Zaire*, *Sudan*, *Reston*, *Taï Forest*, and *Bundibugyo*

(Anonymous 1978a; Anonymous 1978b; Cox et al. 1983; Le Guenno et al. 1995; Miranda et al. 1999; Richman et al. 1983; Rollin et al. 1999; Wamala et al. 2010). With the exception of *Zaire ebolavirus*, all of the other species contain one virus that is named after that species (e.g. the *Sudan ebolavirus* group contains Sudan virus). The nomenclature has changed for the *Zaire* species such that the virus in that group is now called Ebola virus (Kuhn et al. 2014). While it is likely that all of these viruses circulate as different strains and variants, only Ebola and Sudan viruses have multiple different isolates recorded at the moment (Kuhn et al. 2014). The most recent Ebola virus isolates are the Makona variant that caused the 2014-2015 West Africa outbreak, as well as the Lomela variant which caused a much smaller, unrelated outbreak in the Democratic Republic of Congo (DRC) in mid to late 2014 (Baize et al. 2014; Kuhn et al. 2014; Maganga et al. 2014). The Ebola virus genes used in this thesis will be from the 1976 Mayinga strain (Volchkov et al. 1999; Volchkov et al. 2000).

The non-segmented negative sense RNA genome of Ebola virus is 18,959 bp long and encodes 8 known proteins: nucleoprotein (NP), VP35, VP30, glycoprotein (GP), soluble GP (sGP), small soluble GP (ssGP), VP24, and the RNA-dependent RNA polymerase (L protein; RdRp) (Figure 1) (Elliott et al. 1985; Feldmann et al. 1993; Feldmann et al. 2003; Mehedi et al. 2011; Sanchez et al. 1993; Sanchez et al. 1996; Volchkov et al. 1999). NP, VP35, VP30, VP24, and L protein are all components of the helical Ebola virus nucleocapsid; however, only NP, VP35, VP30, and L protein are required for replication and transcription of the Ebola virus genome (Figure 1) (Huang et al. 2002; Muhlberger et al. 1999; Noda et al. 2006; Volchkov et al. 2001). The Ebola virus displays high gene efficiency, with each viral protein having multiple functions throughout the virus life cycle.

Figure 1. Organization of the Ebola virus genome. Expression of NP, VP35, and VP24 are required for the formation of nucleocapsid-like structures in transfected cells (yellow outline). Expression of VP30 and L are not required for nucleocapsid assembly, but are present within the nucleocapsid (orange outline) (Huang et al. 2002; Muhlberger 2007).

1.2 The West Africa outbreak

Prior to the 2014/15 Ebola virus outbreak in West Africa, the disease burden for filovirus infections was relatively low in comparison to malaria and other tropical diseases (Rougeron et al. 2015). From the identification of Marburg in 1967 up until 2014, only 2,989 clinical cases of filovirus infection had been identified. However, with an average case-fatality rate of 70% among these cases and a fatality range of 25-90% when looking at specific outbreaks, filovirus infections were still a public health concern in central Africa (Feldmann et al. 2003; Rougeron et al. 2015). The unexpected Ebola virus outbreak in Guinea, Liberia, and Sierra Leone beginning in early 2014 highlighted the transmissibility and pathogenicity of this virus, as well as the cultural and socioeconomic factors involved in filovirus infections (Baize et al. 2014; MacNeil and Rollin 2012; Rougeron et al. 2015). With a current total of 28,639 cases, 15,217 that are confirmed, 2,619 that are probable, and 10,767 that are suspected, this outbreak has an average case-fatality rate of 40%; however, experts believe it could be much higher (WHO 2016). A slow global response to the outbreak, paired with the overwhelmed treatment facilities that lacked the resources to isolate all suspected infections were some of the major contributing factors to the high case numbers (WHO 2016). The West Africa outbreak also highlighted the importance of effective knowledge translation (MacNeil and Rollin 2012). Performing funeral rites, which

involved washing of the body was a major risk factor for acquiring filovirus infection (WHO 2016). While researchers and doctors understood that these actions were a significant source of new infections, getting the general population to understand this was difficult. Fear of hospitals and Westerners also played a large part in this knowledge translation barrier. As a result, knowledge uptake of infection control practices within the populations of Guinea, Liberia, and Sierra Leone was slow and in some respects, the length of the outbreak reflects this (Rougeron et al. 2015; WHO 2016).

It is probable that the number of cases recorded for filovirus outbreaks is higher than estimated due to the suspected cases that were not included in the final case counts (Meltzer et al. 2014; WHO 2016). In addition, the overwhelming number of patients likely prevented reporting of all infections due to sheer volume (Meltzer et al. 2014). The isolated nature of many of the rural communities could also obscure the number of filovirus cases and deaths (MacNeil and Rollin 2012). The prevalence of Ebola virus antibodies in the Central African population ranges from 5-15%, indicating that the disease burden may be higher than the number of confirmed cases suggests (Becquart et al. 2010; Busico et al. 1999; Gonzalez et al. 2000; MacNeil and Rollin 2012). On the other hand, asymptomatic cases of Ebola virus have been documented and rural populations in Gabon display strong humoral and cellular immune responses to Ebola virus (Becquart et al. 2010; Leroy et al. 2000; Leroy et al. 2001). Thus, the relatively high antibody prevalence does not necessarily correlate with a higher number of unrecognized filovirus cases. However, the possibility of undetected cases should be taken into account when estimating disease burden (MacNeil and Rollin 2012).

1.3 Filovirus transmission

Filoviruses are a significant public health concern due to their high pathogenicity, infectivity, and transmissibility (Judson et al. 2015). Nonhuman primates (NHP) were susceptible to aerosolized Ebola virus at doses of 10 plaque-forming units (pfu) or less, suggesting a very low lethal dose 50 (LD_{50}) *via* that route of transmission (Reed et al. 2011). Experimentally, NHP have been infected with Ebola virus after intramuscular, submucosal, intraperitoneal, oral, conjunctival, or respiratory inoculation (Jaax et al. 1996; Johnson et al. 1995; Judson et al. 2015; Reed et al. 2011). In actuality, epidemiological data suggests that the most common route of filovirus transmission is through direct contact with infected individuals (Judson et al. 2015). Direct contact with infectious mucous membranes is a major risk factor for filovirus infection, as is contact between broken skin and infectious blood or other bodily fluids including saliva, breast milk, urine, and semen (Bausch et al. 2007; Judson et al. 2015).

1.3.1 Zoonotic reservoirs

The index case for the West Africa outbreak is thought to have been a 2-year-old boy in Guinea who died in early December 2013 (Baize et al. 2014). Anecdotally, it was noted that the child had played in a hollow tree close to his home village that housed a colony of insectivorous free-tail bat (*Mops condylurus*) (Mari Saez et al. 2014). Experimentally, *M. condylurus* bats survived inoculation with Ebola virus and displayed high viremia, but very little research on virus shedding or transmission from this bat species has been performed (Swanepoel et al. 1996). Prior to the West Africa outbreak, the majority of research focused on the susceptibility of fruit bat species to filovirus infection, as well as field studies of fruit bats in filovirus endemic areas. Ebola virus RNA has been detected in three wild-caught

fruit bat species and Ebola virus-specific antibodies have been detected in six different fruit bat species, suggesting a wide range of susceptible reservoirs (Leroy et al. 2005; Olival et al. 2013). Viable Ebola virus was also recovered from the feces of experimentally infected fruit bats (*Epomophorus wahlbergi*) for up to three weeks after infection (Swanepoel et al. 1996).

While the evidence is suggestive of bats being the major reservoir of Ebola virus, it is conclusive for Marburg virus. Marburg virus has been directly isolated from Egyptian fruit bats (*Rousettus aegyptiacus*) caught in southwestern Uganda (Amman et al. 2012; Towner et al. 2009). Infection of this species under biosafety level 4 containment (BSL4) conditions demonstrated no negative signs of infection in two different studies, supporting the identification of this species as a natural reservoir for Marburg virus (Amman et al. 2015; Paweska et al. 2012). Egyptian fruit bats shed virus both orally and rectally, with higher viral loads detected from oral swabs (Amman et al. 2015). Horizontal transmission between bats may be due to biting with infected saliva, a route that is common for rabies virus, another member of the *Mononegavirales* (Amman et al. 2015). Transmission to other animal species could occur after contact with, or ingestion of, half-chewed fruits (test-bites) that are dropped by feeding bats (Amman et al. 2015).

In addition to the 2014 West Africa outbreak, in which contact with infectious guano, urine, or a bat bite possibly lead to the infection of the index case, other filovirus outbreaks can be associated with human-bat interactions. The 1976 Ebola virus outbreak in Sudan started in a cotton factory with roosting bats and the 2007 outbreak in the DRC was associated with an annual migration and hunting of fruit bats (Anonymous 1978a;

Leroy et al. 2009). Two outbreaks of Marburg virus have been linked to gold mining in caves that contain bat populations, the first in Uganda in 2007-2008 and the second in the DRC in 1998-2000 (Amman et al. 2012; Bausch et al. 2003; Olival and Hayman 2014). Two cases of filovirus infection, one of which was fatal, have also been linked to cave exploring in the Python Cave in Uganda. In both cases, the tourists returned to their home countries and subsequently developed symptoms and were diagnosed with Marburg virus infection (Centers for Disease Control and Prevention (CDC) 2009; Timen et al. 2009). The Python cave harbours a large colony of *R. aegyptiacus* bats (Amman et al. 2012).

1.4 Filovirus pathogenicity

The incubation period for human filovirus infection is 2 to 21 days; however, most individuals develop symptoms within 4-9 days. Initial symptoms are nonspecific and include fever, headache, nausea, fatigue, and muscle pain (Rougeron et al. 2015). Rapid deterioration of patients accompanies a high fever and multi-organ involvement including the central nervous system, the gastrointestinal tract, and respiratory system. Symptoms are wide ranging and can include: stomach pain, vomiting, diarrhea, anorexia, throat and chest pain, cough, shortness of breath, confusion, delirium, prostration, and seizures (Rougeron et al. 2015). Only about 1 in 3 patients develop haemorrhagic manifestations, which can result in skin rashes, nosebleeds, dark stool due to gastrointestinal bleeding, and vomiting of blood. Multi-organ failure occurs in fatal disease, resulting in shock, tachypnea, convulsions, coma, and severe metabolic disruption (Rougeron et al. 2015). Non-fatal disease is characterized by an extended fever of 5-9 days that improves in tandem with the detection of host antibody and T cell responses and subsequent viral clearance (Rougeron et al. 2015).

Although the routes of infection might be variable, once filoviruses enter the body they very specifically target dendritic cells, macrophages, and monocytes (Geisbert et al. 2003b; Mahanty et al. 2003; Ryabchikova et al. 1999; Stroher et al. 2001). Early infection of these cell types effectively disables the immune response and disseminates the virus to other tissues including liver, spleen, and secondary lymphoid organs (Geisbert et al. 2003b; Rougeron et al. 2015). Infection of hepatocytes, endothelial cells, fibroblasts, and epithelial cells then occurs (Baskerville et al. 1985; Ryabchikova et al. 1999). Filovirus infection is characterized by immune dysregulation, virus- and cell-induced cell death, and vascular leakage. Together, these phenomena lead to the severe symptoms observed during filovirus infection (Rougeron et al. 2015). Whereas non-lethal infections are typified by prompt and restrained innate immune responses and subsequent adaptive immunity, lethal infections produce destructive cytokine storms and almost no humoral or cell-mediated responses (Baize et al. 1999; Baize et al. 2002; Leroy et al. 2001; Wauquier et al. 2010).

In a lethal infection, uncontrolled and over-activity of the innate immune response is seen as a major confounding factor (Rougeron et al. 2015). A positive feedback loop is produced in which infected monocytes and macrophages release pro-inflammatory and chemoattractant cytokines such as macrophage inflammatory protein-1α (MIP-1α) and monocyte chemoattractant protein (MCP-1), resulting in the migration and subsequent infection of more phagocytic immune cells (Gupta et al. 2001a; Hensley et al. 2002; Stroher et al. 2001; Wauquier et al. 2010). Additionally, Tumor Necrosis Factor-α (TNF-α), interleukin (IL)-1β, IL-6, IL-8, IL-10, IL-1 receptor antagonist, soluble TNF receptor, and nitric oxide (NO), among others, are over produced (Baize et al. 1999; Baize et al. 2002; Hensley et al. 2002; Leroy et al. 2001; Stroher et al. 2001; Wauquier et al. 2010). Of note,

not found in this list of cytokines are the type 1 interferons (IFNα/β). As a crucial pathway for the cellular antiviral response, filoviruses specifically inhibit IFNα/β expression in a variety of ways. VP35 prevents IFNα/β synthesis by inhibiting kinases responsible for interferon regulatory factor (IRF)-3 activation and by increasing the degradation of IRF-7 (Basler et al. 2000; Basler et al. 2003; Chang et al. 2009; Prins et al. 2009). This viral protein also interferes with IFNα/β production by sequestering dsRNA in order to prevent activation of the retinoic acid-inducible gene 1 (RIG-I) pathway (Cardenas et al. 2006). Direct interactions between VP24 and both a) karyopherin-α1, an importin responsible for the nuclear accumulation of signal transducer and activator of transcription 1 (STAT-1), and b) STAT-1 itself, results in the inhibition of IFN-induced gene expression (Reid et al. 2006; Reid et al. 2007; Zhang et al. 2012). Mutations in Ebola virus VP24 or VP35 that abrogated the ability to evade the type I IFN response produced less virulent strains in mouse models (Ebihara et al. 2006; Hartman et al. 2008; Prins et al. 2010b). Thus, the lack of a cellular antiviral state, due to reduced IFN expression and signalling, enables the escalation of filovirus infection and pathogenicity.

The cytokine storm produced by the ongoing migration and infection of monocytes and macrophages can trigger vascular dysregulation (Hensley et al. 2002; Rougeron et al. 2015). Vasoactive compounds released by these cells, such as TNF-α, act on endothelial cells leading to increased vascular permeability and altered endothelial cell function (Hensley et al. 2002; Schnittler and Feldmann 1998; Stroher et al. 2001). Full-length GP has also been shown to be cytotoxic to endothelial cells (Yang et al. 2000). Endothelial cells stimulated by MCP-1, IL-8, and soluble GP begin to express adhesion molecules that will be used by neutrophils and monocytes to infiltrate the site of infection. The invasion of

immune cells through the vascular wall can lead to further tissue damage (Geisbert et al. 2003b; Gerszten et al. 1999; Rougeron et al. 2015; Wahl-Jensen et al. 2005). In addition to this vascular leakage, high levels of tissue factor expressed on infected macrophages can trigger activation of the clotting cascade (Geisbert et al. 2003a). Multi-organ damage from widespread blood clots, combined with the lack of clotting factors needed to prevent dangerous bleeding at other sites (disseminated intravascular coagulation) is the final stage of filovirus haemorrhagic fever (Baize et al. 1999; Hensley et al. 2002; Schnittler and Feldmann 1998; Wauquier et al. 2010).

The last key difference in filovirus infection outcomes is the presence of an adaptive immune response. Individuals who succumbed to fatal infections had only low levels of filovirus-specific IgM and IgG antibodies, whereas an early humoral response in patients was found to be indicative of a positive outcome (Baize et al. 1999; Gupta et al. 2001b; Khan et al. 1999; Ksiazek et al. 1999). Similarly, a strong T cell response was noted in asymptomatic patients (Leroy et al. 2000). Severe filovirus infections are characterized by dramatic T lymphocyte and natural killer cell apoptosis, due in part to the expression of TNF-related apoptosis-inducing ligand (TRAIL) and other soluble apoptotic factors, which effectively destroys the T cell response before it has even begun (Baize et al. 1999; Hensley et al. 2002; Reed et al. 2004; Wauquier et al. 2010). The cell-mediated and humoral immune responses are further suppressed by the inactivation of infected dendritic cells, which do not mature or produce cytokines during Ebola virus infection (Bosio et al. 2003; Geisbert et al. 2003b; Mahanty et al. 2003). Thus, the severe pathogenicity of filovirus infections derives from both immune- and pathogen-mediated cellular damage (Rougeron et al. 2015).

1.5 The Ebola virus life cycle

1.5.1 Entry and attachment

The Ebola virus GP is a type I transmembrane glycoprotein that undergoes several posttranslational edits (Sanchez et al. 1996; Sanchez et al. 1998; Volchkov et al. 1998). The addition and maturation of N-glycans *via* the Golgi complex is followed by the proteolytic cleavage of GP at a multibasic amino acid motif (Sanchez et al. 1998; Volchkov et al. 1998). The two proteins generated by this cleavage vary in size substantially, with GP_1 approximately 140 kDa and GP_2 only 26 kDa. Although cleaved, the two proteins remain attached by a disulfide bond, forming a heterodimer $GP_{1,2}$ (Sanchez et al. 1998; Volchkov et al. 1998). $GP_{1,2}$ is expressed as a homotrimer on the surface of infected cells and is acquired by virus budding (Sanchez et al. 1998). While covalently attached, the two domains play different roles in filovirus infection. GP_1 contains the receptor-binding domain and is responsible for cellular attachment (Dube et al. 2009; Kuhn et al. 2006; Manicassamy et al. 2005). The much smaller GP_2 subunit contains the hydrophobic fusion peptide required for release of the nucleocapsid into the cytosol (Ito et al. 1999; Weissenhorn et al. 1998a; Weissenhorn et al. 1998b). A number of different cellular attachment factors have been identified for Ebola virus depending on the cell type investigated. The principal target cells of filoviruses (monocytes, macrophages, dendritic cells, hepatocytes, and endothelial cells) express various C-type lectins that are thought to be important cellular entry factors as they enhance infection in cell culture (Alvarez et al. 2002; Geisbert and Hensley 2004; Takada et al. 2004). These include the asialoglycoprotein receptor on liver cells, the dendritic cell-specific ICAM3 grabbing non-integrins (DC-SIGN) on immature dendritic cells, and a homologue to DC-SIGN found on liver and lymph node endothelial cells (L-

SIGN) (Alvarez et al. 2002; Becker et al. 1995; Takada et al. 2004). T-cell Ig and mucin domain 1 (TIM-1) has also been shown to directly interact with the Ebola virus GP receptor-binding domain and strongly enhance infection (Kondratowicz et al. 2011). Interestingly, TIM-1 has also been shown to mediate a GP-independent method of entry. TIM-1 can interact with phosphotidylserine on the envelope of Ebola virus-like particles (VLPs) and trigger internalization. VLPs lacking the Ebola virus GP were still macropinocytosed by cells expressing TIM-1 (Moller-Tank et al. 2013). The Tyro3 family member Axl is also a phosphotidylserine binding protein that has been demonstrated to enhance infection of Ebola VLPs *via* a phosphotidylserine interaction (Brindley et al. 2011; Jemielity et al. 2013). The number of filovirus attachment and entry factors identified mirrors the wide variety of cells susceptible to filovirus infection, both early and late in disease. It is highly likely that with continued research, more attachment and entry factors will be found.

Interaction of filovirus GP with the attachment factors listed above results in the internalization of the virus by macropinocytosis and, to a lesser degree, by clathrin-mediated endocytosis (Aleksandrowicz et al. 2011; Nanbo et al. 2010; Saeed et al. 2010). The macropinosome merges with an early endosome and the virus is trafficked through the endosomal pathway (Saeed et al. 2010). Maturation and acidification of the virus-carrying early endosome to a late endosome or lysosome results in the proteolytic cleavage of the O-linked glycosylation-rich mucin-like domain of GP_1 by cathepsins B and L (Chandran et al. 2005; Schornberg et al. 2006). The exposed receptor-binding domain of GP_1 then interacts with the Niemann-Pick C1 protein, resulting in a conformational change that releases the GP_2 fusion peptide. GP_2 interacts with the endosomal/lysosomal membrane and leads to

membrane fusion and virus uncoating (Carette et al. 2011; Cote et al. 2011; Miller et al. 2012; Wang et al. 2016). Unlike the attachment factors listed above, NPC1 is universally expressed and is an absolute requirement for filovirus infection (Carette et al. 2011; Cote et al. 2011).

1.5.2 Replication

The ~19 kb Ebola virus genome contains various *cis*-acting signals for replication, transcription, and packaging. At the extreme ends of the genome are the 3' and 5' untranslated regions (UTRs) that flank the viral open reading frames (ORFs) (Weik et al. 2005). The 3' UTR is 470 nucleotides (nt) in length and consists of the Leader sequence (1-55 nt), the NP transcription start site (56-67 nt), a transcription-relevant RNA secondary structure (56-78 nt), the beginning of the NP gene (56 nt), and the replication promoter. The NP ORF begins at nucleotide 470 (Weik et al. 2002; Weik et al. 2005). In contrast, the 5' UTR is almost double the length at 742 nt, but contains only the antigenomic promoter required for viral genome replication and the overlapping Trailer region (18283-18959 nt) (Hoenen et al. 2010). While the 3' and 5' UTR sequences are required for experimental packaging of filovirus-specific minigenomes, the specific encapsidation signals within these sequences are still unknown (Johnson et al. 2006).

Filovirus genome replication requirements are conserved among all species. Three viral proteins, NP, VP35, and the L protein are necessary and sufficient for genome replication (Becker et al. 1998; Muhlberger et al. 1998; Muhlberger et al. 1999). The functional replicase complex consists of the RdRp (L protein) and its cofactor VP35 (Becker et al. 1998; Muhlberger et al. 1999; Trunschke et al. 2013). This replicase complex is likely

bound to the NP-encapsidated filovirus genome through a VP35-NP interaction (Becker et al. 1998; Muhlberger et al. 1999). Although the mechanism is not fully understood, similar studies on other members of the *Mononegavirales* suggest that homo-oligomers of VP35 (or the phosphoproteins of other nonsegmented, negative-stranded [NNS] RNA viruses) recruit the L protein to the genome and interact with adjacent NP molecules. The sequential binding and release of individual Marburg virus VP35 monomers (from the homo-oligomer complex) results in the progression of the polymerase down the NP-coated genome (Curran 1998; Moller et al. 2005). In addition, homo-oligomerization of VP35 is thought to trigger a conformational change that enables the differentiation of structural (nucleocapsid) and functional (polymerase co-factor) activities of VP35, as homo-oligomerization is not required for VP35 association with NP-derived inclusion bodies (Moller et al. 2005). Further research is required to confirm this mechanism *in vivo* for both Marburg and Ebola viruses. The ability of the Ebola virus L protein to form homo-oligomers has also been described, and while homo-oligomerization of the NNS RNA virus Sendai virus' RdRp is necessary for viral activity, the relevance of this finding for filovirus replication and transcription is not yet known (Trunschke et al. 2013).

1.5.3 Transcription

In addition to its replicase function, the VP35-L protein complex also functions as the transcriptase. Starting at the 3' end of the filovirus genome, the polymerase complex can either replicate a full complementary genome or transcribe viral mRNAs. Seven monocistronic mRNA species are produced from filovirus genomes; however, the GP mRNA of Ebola virus undergoes transcriptional editing that results in the expression of 3 different GP variants (Mehedi et al. 2011; Sanchez et al. 1998). Each viral mRNA is capped and

polyadenylated, generating translation-ready transcripts (Muhlberger et al. 1996). Filoviruses have highly conserved transcription start and stop sequences that can overlap between genes due to a conserved sequence of 3'UAAUU that is found in both the start and stop signals. Genes that do not overlap have short intergenic regions that range in length and sequence (Muhlberger et al. 1996; Muhlberger 2007; Sanchez et al. 1993). Each transcription start site is thought to form an RNA secondary structure; however, only the NP transcription start site has been fully characterized (Muhlberger et al. 1996; Sanchez et al. 1993; Weik et al. 2002).

The NP transcription start site is found within the 3' UTR and forms a stable stem-loop structure (Weik et al. 2002; Weik et al. 2005). The RNA secondary structure is thought to impede the transcription process unless a third viral protein, VP30, is present (Weik et al. 2002). VP30 is a transcription activator that is required for Ebola virus minigenome transcription and the rescue of Ebola virus *in vitro* (Halfmann et al. 2008; Muhlberger et al. 1999; Weik et al. 2002). Whereas previous work with Marburg virus minigenomes found no role for VP30 in transcription, more recent research demonstrated that VP30 was also required for rescue of Marburg virus (Enterlein et al. 2006; Muhlberger et al. 1999). Thus, it seems likely that VP30 plays a similar role in both species of *Filoviridae*; however, the mechanism behind Marburg virus VP30-dependent transcription has not been confirmed (Enterlein et al. 2006).

Ebola virus transcription can be initiated without VP30 by removing the transcription start site stem-loop structure, enabling the polymerase complex to begin transcription barrier-free (Weik et al. 2002). Minigenomes lacking this RNA structure and

expressed in the absence of VP30 produced reporter activity similar to the control, suggesting that the presence of VP30 was unnecessary for the assembly of the transcription complex between VP35 and the L protein (Weik et al. 2002). In addition, removal of VP30 did not negatively influence the length of mRNAs produced from the mutated minigenome, demonstrating that VP30 is not required for mRNA elongation (Weik et al. 2002). In contrast, the absence of VP30 abolished transcription of wild-type Ebola virus minigenomes and inhibited the transcription of downstream genes both in the minigenome and full-length Ebola virus rescue system (Martinez et al. 2008; Weik et al. 2002). Together, this data suggests that VP30 is a critical component of the Ebola virus transcription complex. As a transcription activator and reinitiation factor, VP30 prevents the premature termination of transcription due to the presence of RNA secondary structures. It is likely that all of the Ebola virus genes contain an RNA secondary structure at their transcription start sites, making VP30 a necessity for the Ebola virus life cycle (Martinez et al. 2008; Muhlberger et al. 1996; Weik et al. 2002). This is clearly demonstrated by the deletion of the Ebola virus VP30 gene, which produces a lethal mutation (Halfmann et al. 2008; Martinez et al. 2008). The mechanism behind VP30-dependent initiation/reinitiation function is unknown, but it has been suggested that VP30 resolves, hides, or prevents the RNA secondary structure from forming in the first place (Weik et al. 2002).

In addition to being a transcriptional activator, VP30 is thought to play a key role in the switch from replication to transcription and *vice versa*. Specifically, it is the phosphorylation status of VP30 that appears to regulate an interaction with VP35 in the polymerase complex (Biedenkopf et al. 2013; Martinez et al. 2011; Modrof et al. 2002).

Non-phosphorylated VP30 is functionally active and binds to the VP35-L protein complex, enabling transcription to occur (Biedenkopf et al. 2013). Phosphorylation of VP30 by unknown cellular kinases inhibits the VP30-VP35 interaction causing VP30 to dissociate from the transcriptase complex. In the absence of VP30, the polymerase complex switches to its replicase function, producing genomic and antigenomic RNA. Phosphorylation of VP30 was demonstrated to increase viral replication (Biedenkopf et al. 2013; Martinez et al. 2011). Upon dephosphorylation by cellular phosphatases, VP30 can be recruited back to the polymerase complex resulting in transcription initiation (Biedenkopf et al. 2013; Martinez et al. 2011; Modrof et al. 2002). It is of interest to note that phosphorylated VP30 interacts strongly with NP and has been detected in infectious virions (Martinez et al. 2011). Thus, dephosphorylation upon viral entry must occur for efficient primary transcription (Biedenkopf et al. 2013; Martinez et al. 2011).

The matrix protein VP40 is also implicated in transcription regulation. An RNA-binding ring structure consisting of eight VP40 molecules was originally noted in Ebola virus infected cells and has since been further characterized (Bornholdt et al. 2013; Gomis-Ruth et al. 2003). This octameric, pore-like structure does not associate with the plasma membrane and is not required for VLP release (Bornholdt et al. 2013; Gomis-Ruth et al. 2003). Expression of WT VP40 or a mutant ring-forming VP40 reduced minigenome transcription by 70% or 80%, respectively (Bornholdt et al. 2013; Hoenen et al. 2010). However, mutation of the VP40 RNA-binding interface in these strictly ring-forming mutants interfered with the negative regulation of transcription (Bornholdt et al. 2013). Furthermore, knockout of the RNA-binding interface alone was sufficient to generate a lethal mutation to full-length Ebola virus infection (Hoenen et al. 2005). The surprising

discovery of VP40 co-localizing with the RNP proteins in perinuclear inclusions early in Ebola virus infection has led to the hypothesis that VP40 may be an important regulator of early viral transcription, while its role switches to packaging of release of virions late in infection (Bornholdt et al. 2013; Nanbo et al. 2013).

1.5.4 Packaging and release

The role of Ebola virus VP24 is controversial in virus replication and transcription. Initial studies using overexpression of VP24 in minigenome assays found that VP24 negatively inhibited both genome replication and transcription (Hoenen et al. 2006; Hoenen et al. 2010a; Watanabe et al. 2007). However, a recent study found that when VP24 was expressed in a regulated fashion using a tetracistronic minigenome, the effect of this viral protein on genome replication and transcription was minimal (Watt et al. 2014). Surprisingly, VP24 did influence the infectivity of minigenomes in a length-dependent fashion. Short, monocistronic genomes did not require VP24 to be provided *in trans* to producer cells in order to generate infectious transcription and replication competent VLPs (trVLPs). In these monocistronic experiments, VP24 was also not required for reporter activity in target cells that expressed NP, VP35, VP30, and L proteins *in trans* (the proteins involved in the viral ribonucleoprotein complex; RNP) (Watt et al. 2014). In contrast, long, tetracistronic minigenomes that encoded a reporter gene, and Ebola virus VP40, VP24, and GP genes had dramatically reduced infectivity of trVLPs when VP24 expression was knocked out in producer cells and not provided *in trans* in target cells (Watt et al. 2014). This data suggested a novel role for VP24 in RNA packaging, in which VP24 is responsible for the condensation of the NP-RNA complex. Condensation was not required for effective packaging of the short monocistronic genomes, but appears to be crucial for the longer

tetracistronic minigenomes and the ~19 kb Ebola virus RNA genome (Hoenen et al. 2006; Watt et al. 2014). Watt et al. (2014) also suggested that VP24 may play a role in recruiting and/or securing the L protein to the 3' end of the Ebola virus genome during packaging; however this has not been experimentally confirmed (Watt et al. 2014). Reporter activity in naïve (untransfected) target cells was reduced by 90% when infected by monocistronic minigenomes generated in the absence of VP24 (Hoenen et al. 2006). Addition of VP24 to the producer cell transfection panel generated infectious VLPs that were able to undergo primary transcription in naïve target cells (Hoenen et al. 2006). Thus, the role of VP24 in RNA condensation may be required both for packaging, by compressing the length of the Ebola virus genome and for primary transcription/replication, by locking the L protein at the 3' end to ensuring correct genome processing upon naïve cell infection (Hoenen et al. 2006; Watt et al. 2014).

1.6 The Ebola virus nucleocapsid

The filovirus nucleocapsid is the most complex of all the *Mononegavirales (*Booth et al. 2013). Whereas rhabdovirus and paramyxovirus nucleocapsids are constructed with the use of three viral proteins, the filovirus nucleocapsid has five associated proteins: NP, VP24, VP30, VP35, and the L protein (Booth et al. 2013). Altogether, these proteins form a left-handed helical nucleocapsid that protects and scaffolds the nonsegmented, single-stranded, negative-sense RNA genome (Beniac et al. 2012). The analysis of cryo-EM and cryo-ET data from chemically-inactivated Ebola virus suggests a multi-layered nucleocapsid model in which NP subunits form the inner ~25 nm helical layer and VP24-VP35 form the outer ~41 nm layer (Figure 2) (Beniac et al. 2012). The reconstruction of the Ebola virus nucleocapsid indicates an inner layer of large subunits that are the approximate size of a NP monomer (Beniac et al. 2012). The diameter of this inner layer has been measured in reconstructions as 22.3 nm, with an inner diameter of approximately 16 nm (Figure 2) (Beniac et al. 2012). Using a circular fixed radius based on the diameter of the inner layer, as well as the 18.9 kb size of the RNA genome, Beniac et al. (2012) have calculated that the nucleotide-to-NP ratio for the Ebola virus nucleocapsid is 13:1. Biochemical studies on the nucleocapsid of Marburg virus have predicted a nucleotide-to-NP ratio of 12 to 15, which is consistent with the above calculation (Mavrakis et al. 2002). Analysis of the Ebola virus nucleocapsid indicates approximately 10.81 NP subunits per turn, with a pitch of 6.96 nm (Beniac et al. 2012). Interestingly, it is only the inner NP layer that interacts vertically with adjacent NP subunits; the outer nucleocapsid layer appears to contain only horizontal protein-protein interactions (Figure 2) (Beniac et al. 2012; Booth et al. 2013).

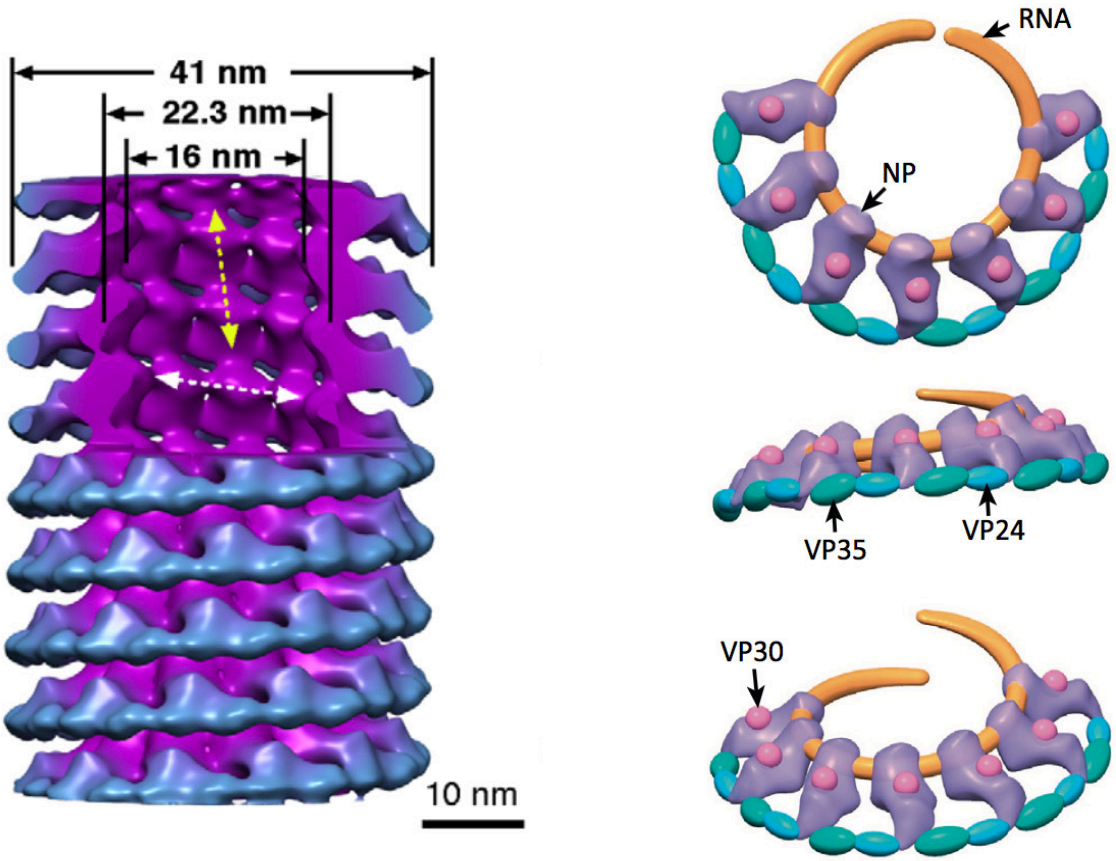

Figure 2. Structure of the Ebola virus nucleocapsid. (Left) 3D reconstruction of a nucleocapsid from chemically-inactivated Ebola virus from Beniac et al. (2012). Resolution is 19Å. **(Right)** A schematic model indicating where the nucleocapsid-associated proteins are located within the Ebola virus nucleocapsid, adapted from Booth et al. (2013). Both figures used with permission.

The formation of Ebola virus nucleocapsid-like particles in transfected cells requires the expression of NP, VP24, and VP35 exclusively (Huang et al. 2002; Noda et al. 2006). The diameter of these structures measured in cell sections is approximately 50 nm, consistent with the diameter of Ebola virus nucleocapsids (Huang et al. 2002; Noda et al. 2006). Expression of these three nucleocapsid proteins results in inclusion bodies that appear very similar to those observed in virus infected cells, suggesting that these three proteins are the major contributors to the structure of the Ebola virus nucleocapsid (Huang et al. 2002; Noda et al. 2006). Since the location of NP has been defined within the inner layer of the nucleocapsid, the remaining proteins VP24 and VP35 are thought to form the outer layer (Beniac et al. 2012). Two different globular densities are visible in the 3D reconstruction of the outer layer and together they form a bridge-like structure (Figure 2). The two lobes are the correct densities for VP24 and VP35 subunits and when combined they generate a complex that is approximately 60 kDa. This would be the appropriate size for a heterodimer of VP24 (~24 kDa) and VP35 (~35 kDa) (Beniac et al. 2012). Stoichiometrically, the reconstructed Ebola virus nucleocapsid exhibits one putative VP24-VP35 heterodimer per NP molecule, which is in agreement with biochemical analysis of protein content from native Ebola virus (Beniac et al. 2012; Elliott et al. 1985). The VP24-VP35 complex interacts with adjacent heterodimers and the inner NP subunit horizontally, but not vertically (Figure 2). As a result, the nucleocapsid is able to bend like a spring: as the inner NP layer condenses, the outer VP24-VP35 heterodimers can expand away from each other. The flexibility of the nucleocapsid prevents RNA damage and is clearly an effective method, since so many filovirus particles exhibit bends and curves (Figure 3) (Beniac et al. 2012; Booth et al. 2013).

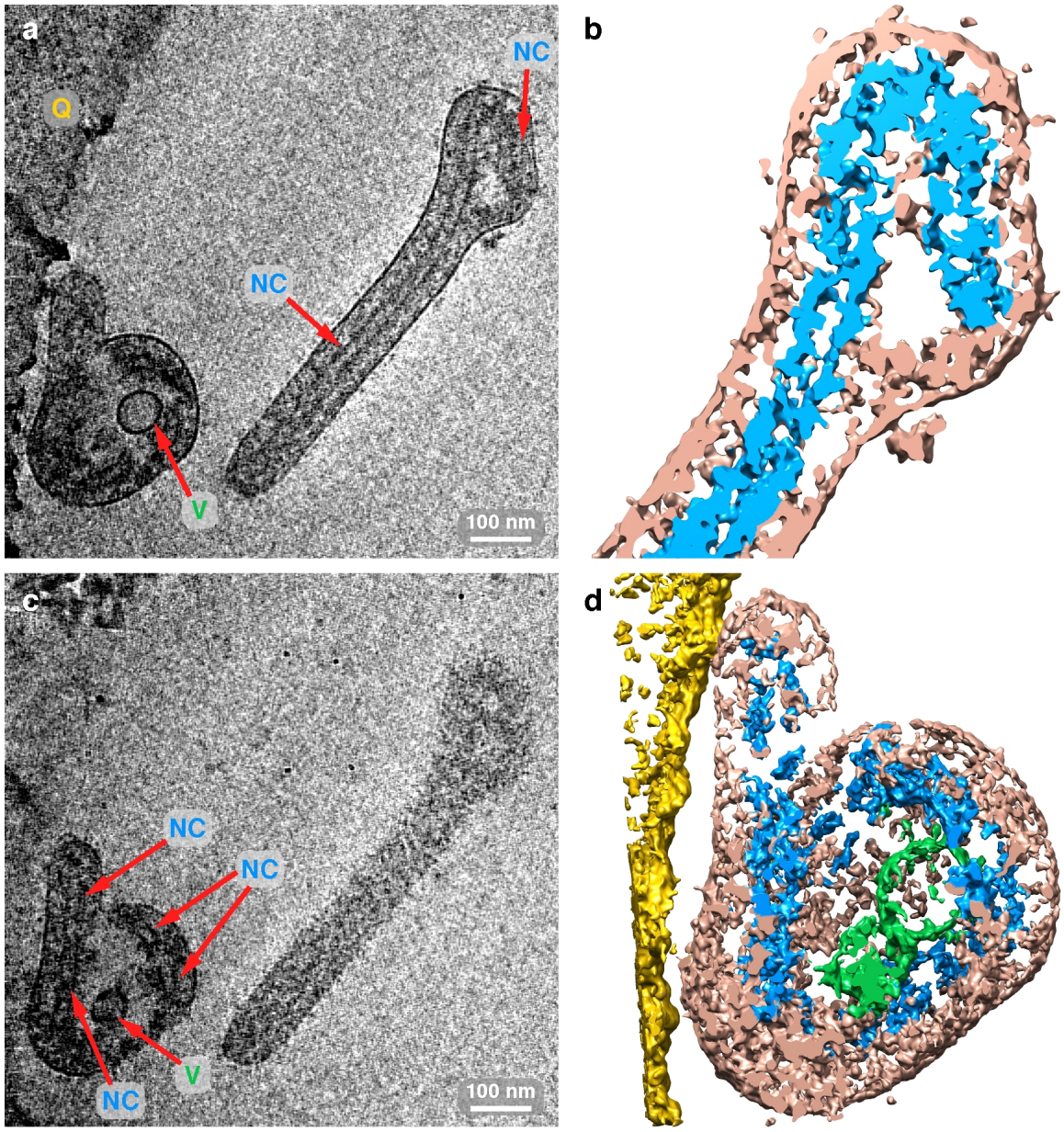

Figure 3. Examples of curved nucleocapsids within Ebola virus particles. (A,C) Tomograms of cryo-preserved Ebola virus particles. **(B,D)** Solid-surface density maps of nucleocapsids (blue), viral envelope (beige), vesicles (green), and grid line (yellow). NC: nucleocapsid; V: vesicles; Q: Quantifoil grid.

The role of the last two nucleocapsid proteins in nucleocapsid structure is less well defined. The L protein is thought to be a low-copy number protein, with biochemical analysis suggesting that around 50 proteins are incorporated within the nucleocapsid (Beniac et al. 2012; Elliott et al. 1985). For comparison, the copy numbers of NP, VP24, VP30, and VP35 estimated by the Beniac et al. (2012) nucleocapsid reconstruction are all equivalent to 1454 per virion, further supporting the 1:1 ratio of NP to heterodimer model discussed above (Beniac et al. 2012; Booth et al. 2013). Where the L protein is located within the virion has not yet been elucidated, likely due to its low copy number (Beniac et al. 2012; Booth et al. 2013). Neither the L protein or VP30 are required to generate nucleocapsid-like particles in transfected cells, suggesting that neither plays a key role in nucleocapsid assembly (Huang et al. 2002). Huang et al. (2002) noted no difference in nucleocapsid particles when VP30 was present or absent. Beniac et al. (2012) hypothesize that VP30 may be binding to an upper groove within the NP subunit, adjacent to the VP24-VP35 heterodimer. On solid-surface density maps this region contains a globular bump that is ~30 kDa in mass; however, this location remains unconfirmed (Figure 2) (Booth et al. 2013).

The matrix protein VP40 also plays a role in stabilizing the nucleocapsid structure, although it is not a nucleocapsid protein. The VP40 hexameric lattice formed on the cytoplasmic side of the plasma membrane is able to interact with the nucleocapsid proteins NP and VP35 (Bornholdt et al. 2013; Johnson et al. 2006b; Licata et al. 2004; Noda et al. 2007a). The periodicities of the hexameric lattice and the nucleocapsid are closely matched. While the VP40 protofilaments have a periodicity of 5 and 7 nm, the Ebola virus nucleocapsid has a pitch of ~7 nm (Beniac et al. 2012; Bornholdt et al. 2013). As a result,

the nucleocapsid and VP40 matrix likely form quasi-equivalent interactions that are easily shifted to stabilize a nucleocapsid that is constantly in flux (Booth et al. 2013). Furthermore, a 7 nm space can be found between the nucleocapsid and the matrix/viral envelope, giving the nucleocapsid "wiggle room" for additional curvature (Beniac et al. 2012; Booth et al. 2013).

A second, much lower resolution (~40 Å) model for the Ebola virus nucleocapsid has been generated by Bharat et al. (2012) (Figure 4). The pitch (~7 nm) and number of subunits per turn (~ 11) were approximately similar to those determined by Beniac et al. (2012), but the shape and proposed structural organization of each nucleocapsid model were quite different (Figure 2, Figure 4) (Beniac et al. 2012; Bharat et al. 2012). Whereas Beniac et al. (2012) described a "bridge-like" VP24-VP35 outer structure; Bharat et al. (2012) suggested "boomerang protrusions" of these two proteins. In the latter, only VP35 was in direct contact with NP, with VP24 projecting out from VP35. In addition, they hypothesized that there were 2 NP subunits per VP35-VP24 protrusion (Bharat et al. 2012). As a result, the Bharat et al. (2012) nucleocapsid model also contained a greater number of NP subunits (~24) within the inner nucleocapsid layer which decreased the predicted nucleotide-to-NP ratio to ~6. A nucleoptide to NP ratio of 12-15 has been measured biochemically in Marbug virus NP (Mavrakis et al, 2002), which is consistent with the structure as determined by Beniac et al (2012). In addition, the Bharat et al. (2012) model predicts a non-stoichiometric ratio of the nucleocapsid proteins, whereas the Beniac et al model implies 1:1:1 ratios of NP:VP24:VP35. Both Elliot et al. (1985) and Beniac et al. (2012) measured approximately 1:1 ratios of nucleocapsid proteins by gel densitometry of purified virus particles; whereas, the model of Bharat et al. (2012) implies

two NP per VP24/VP35 subunit. It is difficult to envision an efficient assembly process that requires alternating protein-protein interactions, as suggested by their model (Bharat et al. 2012).

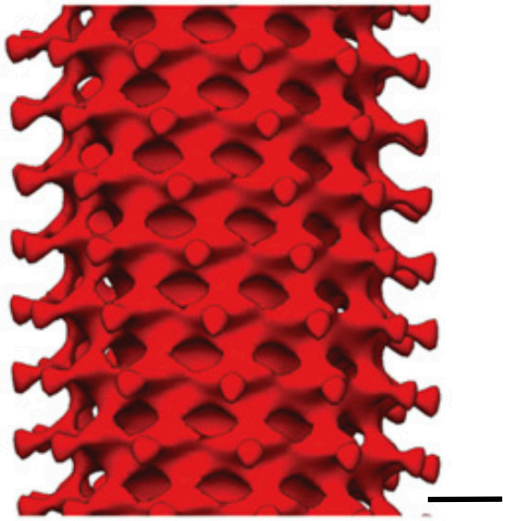

Figure 4. A second model of the Ebola virus nucleocapsid. Figure adapted from Bharat et al. (2012), used with permission. Resolution is 41Å. Scale bar is 10 nm.

1.7 The Ebola virus nucleocapsid proteins

1.7.1 Nucleoprotein (NP)

The Ebola virus encodes the largest NP of all the *Mononegavirales*. At 739 amino acids in length, approximately half of the Ebola virus NP is hydrophobic (1-450 amino acids) while the C-terminal domain is hydrophilic (Sanchez et al. 1989; Watanabe et al. 2006). The N-terminal amino acid sequences of Ebola and Marburg virus species are highly conserved. Structurally, the Ebola virus NP N-terminal domain also shares common features with other *Mononegavirales*, such as an RNA-binding domain and a NP

oligomerization domain (Barr et al. 1991; Kirchdoerfer et al. 2015; Sanchez et al. 1989; Sanchez et al. 1992). Recent studies have demonstrated that there are two smaller domains within the first 380 amino acids of the Ebola virus NP (NP_{core}). Together, these domains form a folded bi-lobed structure that is homologous to the NP of other NNS viruses (Dong et al. 2015; Kirchdoerfer et al. 2015; Leung et al. 2015). The two globular domains of the NP_{core} frame a positively charged groove (Dong et al. 2015; Kirchdoerfer et al. 2015; Leung et al. 2015). Alanine substitutions of the three lysines or one arginine (K160, K171, R174, and K248) that make up this basic groove drastically reduced the amount of bound single-stranded RNA, suggesting that this region is the RNA-binding domain (Dong et al. 2015; Kirchdoerfer et al. 2015; Leung et al. 2015). Both NP_{core} lobes consist of mainly α-helices, with the N-terminal domain also forming two β-strands (Dong et al. 2015; Kirchdoerfer et al. 2015; Leung et al. 2015). The amino acids on the extreme ends of the NP_{core} region are predicted to be the oligomerization arms, as deletion of these regions generated only NP monomers (Kirchdoerfer et al. 2015). This result is consistent with earlier research which demonstrated that $NP_{\Delta 451\text{-}739}$ mutants were capable of oligomerizing to form the inner 20 nm nucleocapsid particles, but could not form the 50 nm full nucleocapsid or support replication or transcription (Watanabe et al. 2006). Full-length N- terminal deletions resulted in no visible nucleocapsid particles (Watanabe et al. 2006). Thus, the N-terminal region of the Ebola virus NP is key to successful RNA interactions and NP oligomerization, both of which are required for productive viral infection (Dong et al. 2015; Kirchdoerfer et al. 2015; Leung et al. 2015; Watanabe et al. 2006).

In contrast to the conserved sequence and structure of the Ebola virus NP N-terminal domain, the highly acidic, hydrophilic C-terminal domain is unique. Structural

analysis found no homology between the C-terminal domain and any known protein; however, sequence similarities between filovirus species can be found when the last 100 amino acids are compared (Dziubanska et al. 2014). Analysis of a C-terminal $NP_{641-739}$ crystal structure indicates that it is a globular domain made up of a central α-helix that scaffolds the remaining mix of antiparallel α-helices and β-strands (Dziubanska et al. 2014). NP deletion mutants that lacked the last 138 amino acids were able to form 50 nm nucleocapsid-like particles and support replication and transcription of minigenomes; however, they were not incorporated into VLPs (Watanabe et al. 2006). Further functional studies identified the last 50 amino acids of the NP sequence as being the key requirements for NP-VP40 interactions and successful nucleocapsid encapsidation (Licata et al. 2004). Intriguingly, while there is a lack of sequence and structural homology amongst the C-terminal NP domains of the *Mononegavirales*, the functional capabilities are often conserved (Noda et al. 2007a). Virion incorporation of Sendai virus and human parainfluenza virus type 1 are also dependent on an interaction between their respective matrix proteins and NP C-terminal domains (Coronel et al. 1999; Coronel et al. 2001; Stricker et al. 1994). Further research is needed to determine the specific VP40 interaction sites within the C-terminal region of NP, as well as the binding conformations of these proteins. In addition, the relevance of this interaction in regards to the nucleocapsid structure is unclear. Transfection of NP with VP40 results in NP incorporation and greater VLP production; however, addition of VP24 and VP35 to this transfection panel does not negatively influence VLP production or nucleocapsid incorporation (Johnson et al. 2006b; Licata et al. 2004). Thus, additional factors must also play a role in nucleocapsid budding, such as VP40 interactions with the other nucleocapsid proteins and/or flexible, low-density

NP loops that span the nucleocapsid and are currently undetected by crystal structure or cryo-EM analysis (Beniac et al. 2012; Booth et al. 2013).

VP35 interaction sites have been identified in both the N- and C-terminal domains of NP. Expression of the $NP_{\Delta 451\text{-}739}$ mutant with VP35 did not result in co-purification of these two proteins, suggesting that the binding site of VP35 is in the C-terminal domain (Noda et al. 2011). This result is in agreement with the lack of 50 nm nucleocapsid-like particles visible when $NP_{\Delta 451\text{-}739}$, VP24, and VP35 are expressed (Watanabe et al. 2006). Recent functional and structural studies have identified a second VP35 binding site in the NP_{core} (Kirchdoerfer et al. 2015; Leung et al. 2015). A peptide from the N-terminal domain of VP35 has been crystallized bound to the C-terminal domain of NP_{core} (Kirchdoerfer et al. 2015). The 80 amino acid peptide does not block the RNA-binding domain or prevent NP conformational changes. Instead, VP35 is predicted to bind to the same approximate location as the N-terminal oligomerization arm, preventing NP-NP interactions (Kirchdoerfer et al. 2015). The authors suggest that this mechanism allows VP35 to chaperone monomeric NP to the nascent RNP molecule during genome replication; however, the mechanism behind NP-VP35 disassociation and whether this triggers a conformational change in NP that promotes RNA binding is unclear (Kirchdoerfer et al. 2015). Furthermore, how the multiple functions of VP35 (interferon antagonist, polymerase co-factor, chaperone, and nucleocapsid component) are balanced during viral replication is unknown.

Initial studies on the Ebola virus NP demonstrated a slower migration through sodium dodecyl sulfate polyacrylamide gel electrophoresis (SDS-PAGE) than was expected

based on molecular weight calculations (Elliott et al. 1985; Huang et al. 2002). NP is predicted to be ~ 85 kDa in size, but size estimation from SDS-PAGE suggests a molecular weight closer to 115 kDa (Elliott et al. 1985; Huang et al. 2002; Sanchez et al. 1989). Research into this size discrepancy initially pointed to O-glycosylated and sialyation of NP (Huang et al. 2002; Watanabe et al. 2006). Further biochemical studies including glycomic analysis by matrix-assisted laser desorption ionization-time of flight (MALDI-TOF) could not identify any glycosylated residues (Shi et al. 2008). Instead, it was concluded that the highly acidic C-terminal domain was most likely responsible for the slower SDS-PAGE migration of NP, a phenomenon noted for other viral and cellular proteins (Shi et al. 2008). Mass spectrometry was also used to identify four phosphorylation sites within the C-terminal domain of NP: Thr_{563}, Ser_{581}, Ser_{587}, and Ser_{647} (Peyrol et al. 2012). Analysis of these residues demonstrated dynamic phosphorylation states except for Ser_{587}, which was constitutively phosphorylated under experimental conditions (Peyrol et al. 2012).

1.7.2 VP35

VP35 is the second gene encoded by the filovirus genome (Sanchez et al. 1993). It is 340 amino acids in length, with an N-terminal coiled-coil domain and a C-terminal double-stranded (ds)RNA-binding domain (Cardenas et al. 2006; Hartman et al. 2004; Moller et al. 2005; Reid et al. 2005; Sanchez et al. 1993). Amino acids 82-118 form a coiled-coil motif that is required for homo-oligomerization of VP35, with trimers and larger complexes detected after gel filtration and SDS-PAGE (Reid et al. 2005). Disruption of this coiled-coil motif reduced the ability of VP35 to inhibit activation of a reporter gene under control of an interferon stimulated gene promoter, suggesting that oligomerization facilitates VP35's function as an IFN antagonist (Reid et al. 2005). Furthermore, mutation of the coiled coil

domain of Marburg virus VP35 led to a reduction in viral replication and transcription due to the inability of VP35 to homo-oligomerize and interact with the RdRp (Moller et al. 2005). VP35 deletion mutants lacking the C-terminal domain could still be immunoprecipitated with the L protein (Prins et al. 2010a).

The C-terminal domain of VP35 contains a unique interferon inhibitory domain (IID) that is comprised of two different basic amino acid regions. The IID is currently the only region of VP35 that has been elucidated by x-ray crystallography (Leung et al. 2009; Leung et al. 2010a; Leung et al. 2010b). The IID consists of two subdomains: (i) four α-helices generated by residues 221-283, which contain the first basic patch (FBP) and (ii) a mixed, four-stranded β-sheet with a short helical domain generated by residues 294-340, which contain the central basic patch (CBP) (Leung et al. 2009). The FBP contains four basic residues that are conserved among filovirus species: K222, R225, K248, and K251. Individual substitution of these residues for alanine or glutamic acid resulted in complete inhibition of Ebola virus minigenome reporter activity, with the exception of K222. In contrast, substitution to a different basic amino acid, for example from lysine to arginine, did not inhibit reporter gene expression (Prins et al. 2010a). The FBP was also shown to be critical for VP35-NP interactions, as alanine or glutamic acid substitutions of R225 and K248 prevented co-immunoprecipitation (co-IP) of these two proteins. This result was observed to a lesser degree with K251A/E (Prins et al. 2010a). As all of these mutants could still interact with the L protein, it has been suggested that VP35 bridges the NP and L protein together within the polymerase complex, resulting in successful RNA replication and transcription (Prins et al. 2010a).

The CBP consists of six conserved residues: R305, K309, R312, K319, R322, K339 (Prins et al. 2010a). Substitution of any of these residues for alanine resulted in the inability of VP35 to bind to dsRNA (Cardenas et al. 2006). Recombinant Ebola viruses expressing VP35 CBP mutations had reduced growth *in vitro*, while infected VeroE6 cells displayed greater immune responses (Hartman et al. 2006). Furthermore, guinea pigs inoculated with Ebola virus expressing VP35 with a double point mutation K319A/R322A showed rapid clearance of the virus with no sign of pathogenesis (Prins et al. 2010b). Conversely, mutations in the FBP did not affect dsRNA binding or IFN antagonism (Leung et al. 2009). Thus, the dsRNA binding capabilities of VP35 appear to be directly related to immune suppression and virus pathogenesis, likely by preventing viral dsRNA detection by the cell (Cardenas et al. 2006; Hartman et al. 2006; Hartman et al. 2008; Leung et al. 2009; Leung et al. 2010b). In addition, it appears that both the N- and C-terminal domains of VP35 are required for efficient IFN suppression. Expression of VP35 N- or C-terminal truncation mutants was either ineffective or weakly effective at inhibiting IFN responses, respectively. Full IFN inhibitory activity could only be demonstrated with expression of the wild-type protein or a VP35 fusion protein consisting of the C-terminal domain fused to a bacteriophage T4 trimerization motif (Reid et al. 2005). Thus, while VP35 oligomerization itself is not sufficient to suppress cellular IFN responses, it appears to be a necessary component for this function of VP35 (Reid et al. 2005).

The Ebola virus VP35 protein is now recognized to share some homologous functions to the phosphoproteins of the other *Mononegavirales*. It is a required cofactor for the viral polymerase and has recently been shown to act as a chaperone for monomeric NP, similar to VSV and Nipah virus P proteins (Elliott et al. 1985; Kirchdoerfer et al. 2015;

Muhlberger et al. 1999). However, studies into post-translational modifications of VP35 are lacking. Initial biochemical analysis of VP35 did not detect any phosphorylation of this protein, which is unusual for a phosphoprotein homolog (Elliott et al. 1985). It has been suggested that VP35 and VP30 share the role of filovirus phosphoprotein, as VP30 phosphorylation appears to regulate the switch between replication and transcription (Biedenkopf et al. 2013; Biedenkopf et al. 2016; Martinez et al. 2008; Martinez et al. 2011; Modrof et al. 2002). In addition, protein-protein interaction sites between VP35 and VP24, VP30, and to some respects NP in relation to the nucleocapsid structure are still undetermined. It is currently unknown which domains of either protein are involved in this interaction. VP35 and nonphosphorylated VP30 interact *via* co-IP (Biedenkopf et al. 2013). Immunofluorescence assays (IFA) illustrated that this interaction was able to recruit VP35 into NP-induced inclusion bodies; however, whether this interaction was important for nucleocapsid assembly or strictly for transcription activation was unclear (Biedenkopf et al. 2013). While VP35-NP interactions have been mapped to the C-terminal domain of VP35 and the N- and C- terminal domains of NP, these studies investigated minigenome expression rather than the possible structural ramifications after binding site mutations (Kirchdoerfer et al. 2015; Prins et al. 2010a; Watanabe et al. 2006). Kirchdoerfer et al. (2015) reported a stronger NP-VP35 interaction when VP35 residues 80-340 were expressed, suggesting that oligomerization might also play a role in this interaction. Lastly, VP35 can be detected in VLPs when expressed alone with VP40 and this interaction was sufficient to package and encapsidated Ebola virus minigenomes, suggesting a direct interaction between VP35 and VP40 (Johnson et al. 2006b). The binding sites have not

been mapped for either protein. Thus, greater analysis of VP35 and its binding partners would be beneficial in understanding the structure of the Ebola virus nucleocapsid.

1.7.3 VP24

VP24 is a filovirus unique protein, with no known homologs (Watt et al. 2014). The protein is 239 amino acids in length and forms a single domain, pyramidal-like structure upon crystallization (Zhang et al. 2012). The three-sided structure consists mainly of α-helices, with a three-stranded and five-stranded β-sheet on adjacent sides (Zhang et al. 2012). The protein also contains two pockets at the base of those two sides, one hydrophobic (L57, L75, L79, L198, L221) and the other hydrophilic (S178, E180, I189, T191, E200; rim: P77, T193, K206, M209). Both regions contain highly conserved amino acids within the *Ebola virus* genus (Zhang et al. 2012). Additional conserved amino acids, residues 96-98 and 106-121, on an outside face of the pyramidal fold have been identified as binding sites for STAT-1 (Zhang et al. 2012). Residues on a different face, 42 and 142-146, have been shown experimentally to be important for VP24 and karyopherin α-1 interactions (Mateo et al. 2010). Both karyopherin α-1 and STAT-1 are involved in the same pathway of antiviral IFN response (Mateo et al. 2010; Reid et al. 2006). Dimerized and phosphorylated STAT-1 is imported into the nucleus by karyopherin α-1, triggering an antiviral state within the cell *via* the transcriptional regulation of genes (Mateo et al. 2010; Reid et al. 2006). Thus, VP24 redundantly inhibits IFN signalling, suggesting that this is an important pathway for anti-Ebola virus immune responses (Mateo et al. 2010; Reid et al. 2006; Reid et al. 2007). Indeed, serial passaging experiments demonstrate that this is the case, as wild type Ebola virus becomes pathogenic to mice and guinea pigs only after point mutations arise in NP and VP24 (Ebihara et al. 2006; Mateo et al. 2011). A direct

correlation between pathogenicity and evasion of the IFN response was noted in the mice model (Ebihara et al. 2006).

Functional studies for VP24 in relation to the nucleocapsid structure are lacking. Deletion of either the N- or C-terminal domain, even just the first or last five amino acids, completely abrogated VP24's role in nucleocapsid formation. No 50 nm particles were visible in cells expressing any version of a truncated VP24 with NP and VP35 (Noda et al. 2007b). Interestingly, these VP24 mutants could only be tagged with the FLAG peptide on their N terminus. Tagging of the C-terminal also consistently abolished the assembly of the 50 nm nucleocapsid-like particles (Noda et al. 2007b). Whether this observation is due to conformational changes, steric hindrance, or the inhibition of direct protein-protein interactions is unknown (Noda et al. 2007b). VP24 and NP were shown to very weakly interact by co-IP, whereas similar studies could not demonstrate a direct interaction between VP24 and VP35 (Huang et al. 2002; Noda et al. 2006). However, IFA and TEM studies suggest co-localization of these two proteins, which was demonstrated by overlapping signals and changes to internal cellular structures, respectively (Bamberg et al. 2005; Noda et al. 2006). Whether there is a direct interaction between VP24 and VP30 is also unknown; however, short interfering RNA (siRNA) knockdown of VP24 resulted in diminished incorporation of VP30 into virions (Hoenen et al. 2006). The finding that VP24 had lipophilic properties prompted earlier studies to consider it a minor matrix protein, rather than a component of the viral nucleocapsid (Han et al. 2003). Co-localization of VP24 and VP40 has been observed at the plasma membrane and VP24 has been documented within VLPs; however, there is currently no evidence of a direct interaction between VP24

and VP40 (Bamberg et al. 2005; Han et al. 2003). Thus, many details are still lacking when it comes to the role of VP24 in the nucleocapsid.

1.7.4 VP30

VP30 is an essential transcription factor encoded by Ebola viruses (Modrof et al. 2002; Muhlberger et al. 1999). The 288 amino acid protein is necessary for activation and reinitiation of the transcription function as the polymerase complex travels the Ebola virus genome (Martinez et al. 2008; Modrof et al. 2002; Sanchez et al. 1993; Weik et al. 2002). The N-terminus of VP30 consists of residues 1-141 and contains a zinc-binding domain, a putative RNA binding domain, and an oligomerization domain (Hartlieb et al. 2003; John et al. 2007; Modrof et al. 2003). The amino acids 68-95 form a Cys_3-His motif which binds specifically to zinc ions (Modrof et al. 2003). Substitution of these VP30 residues resulted in a loss of transcription activation function; however, these mutations did not affect the association of VP30 with NP inclusion bodies (Modrof et al. 2003). Hydrophobic residues upstream of this region have been implicated in RNA binding. VP30 mutants lacking residues 26-40 were unable to bind to single-stranded RNA, whereas wild type VP30 demonstrated a relatively strong interaction. Intriguingly, VP30 only bound to single-stranded RNA or stem-loop RNA structures that contained long 5' or 3' extensions and not with dsRNA (John et al. 2007).

Directly downstream of the Cys_3-His motif is the homo-oligomerization domain of VP30. Residues 94-112 form a α-helical structure with four leucines at residues 100 to 103 (Hartlieb et al. 2003). An alanine substitution of any of these residues produced oligomerization deficient mutants (Hartlieb et al. 2003). Importantly, these mutants were

unable to support VP30-induced transcription of minigenomes, but could still co-localize with NP inclusion bodies (Hartlieb et al. 2003). Furthermore, oligomerization deficient mutants inhibited Ebola virus growth in cell culture (Hartlieb et al. 2003). As such, homo-oligomerization appears to be key for VP30's function as Ebola virus transcription factor. VP30 dimers and hexamers have been identified experimentally and from Ebola virus virions (Hartlieb et al. 2007).

Most research on VP30 has focused on the importance of two serine clusters in the N-terminal domain, which are phosphorylatable. Serine residues at positions 29-31 and 42, 44, and 46 are dynamically phosphorylated and dephosphorylated, resulting in a switch from viral RNA replication to transcription. The phosphorylation state of VP30 appears to be independent of its ability to homo-oligomerize, as dimers of both alanine and aspartate mutants could still be detected (Biedenkopf et al. 2013). The phosphorylation sites do overlap the putative RNA binding domain and there has been speculation that phosphorylation might inhibit RNA binding (and therefore the transcription activation activity of VP30) due to electrostatic repulsion; however, experimentally this has not yet been shown (Biedenkopf et al. 2013).

Phosphorylation of the serine residues of VP30 also appears to play a role in protein-protein interactions. Wild type VP30 and VP30 containing alanine substitutions could be co-IP with VP35; whereas, the aspartate VP30 mutant demonstrated only a weak interaction, suggesting that nonphosphorylated VP30 interacts more readily with VP35 (Biedenkopf et al. 2013). In contrast, NP was pulled down by phosphorylated VP30 or the aspartate mutant (Biedenkopf et al. 2013). This interaction was mapped to the C-terminal

domain of VP30, specifically residue E197. Structurally, only the C-terminal domain of VP30 has been crystallized. Residues 142-272 form a globular structure consisting of seven α-helices (Hartlieb et al. 2007). The E197A mutant did not co-localize or co-IP with NP, but the addition of VP35 enabled the recruitment of $VP30_{E197A}$ to NP inclusion bodies. The $VP30_{E197A}$ mutant was transcriptionally active in producer cells of trVLPs, however, transfer of these trVLPs to naïve target cells did not result in reporter activity and $VP30_{E197A}$ was barely detectable within the trVLPs (Biedenkopf et al. 2013). Thus, a model has been proposed that suggests that nonphosphorylated VP30 interacts with VP35 and L to form the transcriptase complex with possibly direct VP30-RNA interactions. Phosphorylation of VP30 results in the dissociation of VP30 from VP35 and/or RNA. As the polymerase complex can no longer overcome the RNA secondary structures for transcription, the VP35-L complex switches to its replicase function. Phosphorylated VP30 may then interact with NP, resulting in its incorporation into nascent virion particles (Biedenkopf et al. 2013; Biedenkopf et al. 2016; John et al. 2007; Martinez et al. 2008; Martinez et al. 2011; Modrof et al. 2002; Weik et al. 2002). However, there still remain a number of questions about the role of VP30 in transcription and nucleocapsid assembly.

Furthermore, there is conflicting evidence as to whether VP30 does require phosphorylation for its interactions with NP. Nonphosphorylated VP30 mutants were detected in trVLPs; however, whether this was due to VP30-VP35, or VP30-NP, or both interactions was unclear (Biedenkopf et al. 2016; Martinez et al. 2011). These non-phosphorylated mutants were also able to co-localize with NP inclusion bodies even though they lacked phosphorylation (Martinez et al. 2011). In addition, VP30 N- (residues 1-141) and C- (residues 142-272) terminal truncated mutants both co-localized with NP inclusion

bodies; however, only the wild type and C-terminal VP30 mutant could be co-IP with NP and were found in VLPs (Hartlieb et al. 2007). While the phosphorylation status of the N-terminal domain is not known for this experiment, it is clear that the C-terminal domain of VP30 also plays an important role in NP interactions (Hartlieb et al. 2007). It is possible that two different interactions are occurring, one involving phosphorylation and transcriptional regulation and the other nucleocapsid assembly (Hartlieb et al. 2007). While hexameric VP30 has been detected in native virus, structural studies have not elucidated any of these structures, suggesting that the organization is random or that this organization is rare within the nucleocapsid (Hartlieb et al. 2007). In fact, as mentioned earlier, the location of VP30 within the nucleocapsid is still unknown (Beniac et al. 2012; Booth et al. 2013). The binding sites of VP30 and VP35 are also unknown and direct interactions between VP30 and VP24 or VP40 have yet to be demonstrated.

1.7.5 VP40

VP40 is the matrix protein of Ebola virus and as such is responsible for virion budding and release from infected cells (Jasenosky et al. 2001). VP40 is 326 amino acids in length and contains an N-terminal homo-oligomerization domain and a C-terminal membrane-association domain (Dessen et al. 2000; Jasenosky et al. 2001; Ruigrok et al. 2000; Sanchez et al. 1993). The N- and C-terminal domains of VP40 are connected by a flexible linker, which enables the protein to rearrange into different conformations (Bornholdt et al. 2013; Dessen et al. 2000). While the N-terminal domain is characterized by two three-stranded β-sheets that bend towards each other and are surrounded by four small α-helices, the C- terminal domain is less organized with only two β-sheets and two α-helices that are linked by a disordered loop (Bornholdt et al. 2013; Dessen et al. 2000).

VP40 is capable of forming multiple oligomerization states including an octameric ring structure, a butterfly-shaped dimer, and a hexameric filament that forms the matrix of the virus particle (Bornholdt et al. 2013; Gomis-Ruth et al. 2003). It has been suggested that each of these oligomers plays a different role within the virus life cycle and involves different homo-oligomer interactions (Bornholdt et al. 2013). The octameric ring structure consists of four VP40 dimers interacting in an antiparallel manner. The octameric ring can be produced by expression of just the VP40 N-terminal domain, demonstrating that direct interactions within this structure occur *via* the N-terminal domains of VP40 dimers (Gomis-Ruth et al. 2003). The butterfly-shaped dimer formed by VP40 is instrumental in shuttling VP40 to the plasma membrane (Bornholdt et al. 2013). Upon interaction with the plasma membrane VP40 rearranges into a linear structure consisting of six VP40 molecules (Bornholdt et al. 2013). The multiple hexameric filaments form a multilayered lattice that coats the plasma membrane and interacts with the nucleocapsid proteins, resulting in the incorporation of the nucleocapsid and budding of the virion (Bornholdt et al. 2013). Thus, VP40 is a dynamic protein that reorganizes through multiple conformations depending on its function in the virus life cycle (Bornholdt et al. 2013).

The N-terminal domain of VP40 consists of residues 1-194. Expression of this domain alone is capable of producing multi-order oligomers (Gomis-Ruth et al. 2003; Hoenen et al. 2010b). The dimeric interface between two VP40 monomers consists of residues 52-65 and 108-117 (Bornholdt et al. 2013). Point mutations within this region inhibited VP40 migration to the plasma membrane and VLP release from transfected cells (Bornholdt et al. 2013). Additional studies on dimerization-deficient mutants also demonstrated a loss of membrane association and budding, as well as an inability of the

VP40 mutant to regulate minigenome transcription (Hoenen et al. 2010a; Hoenen et al. 2010b). Thus, initial dimerization of VP40 is not only required for transcription regulation, but also for trafficking, matrix assembly, and budding at the plasma membrane (Bornholdt et al. 2013; Hoenen et al. 2010a; Hoenen et al. 2010b).

Formation of the hexameric lattice involves interdimeric interactions between the C- terminal domains of VP40, specifically residues L203, I237, M241, M305, and I307 (Bornholdt et al. 2013). Substitution of M241 for an arginine resulted in VP40 proteins that were able to dimerize, but could not form the filamentous hexamers. These C-terminal oligomerization-interface mutants could not support VLP release, but were trafficked to the plasma membrane (Bornholdt et al. 2013). These results imply that the multi-layered lattice formed by filamentous hexamers of VP40 is required for virion budding (Bornholdt et al. 2013). In addition, VP40 contains conserved basic regions within its C-terminal domain that directly interact with the negatively charged plasma membrane. Deletion of the six lysine residues that form this patch or substitution to neutral or negatively charged amino acids resulted in a loss of VP40-induced budding activity (Bornholdt et al. 2013; Jasenosky et al. 2001). Thus, electrostatic forces dictate the interaction between VP40 and the plasma membrane. Furthermore, this interaction triggers a conformational reorganization of VP40 that enables the formation of the hexameric matrix lattice (Adu-Gyamfi et al. 2013; Bornholdt et al. 2013; Jasenosky et al. 2001).

VP40 also contains two overlapping late budding domains (L-domains) within its N terminus. L-domains are key for cell-virus separation late in the infection cycle, but the mechanism behind this event is unclear (Harty et al. 2000; Jasenosky et al. 2001; Licata et

al. 2003). VP40 encodes a first L-domain starting at residue 7 (PTAP) and a second L-domain overlaps this motif by re-using the proline residue at position 10 to form a PPEY motif (Harty et al. 2000; Jasenosky et al. 2001; Licata et al. 2003; Martin-Serrano et al. 2001). Deletion of both motifs resulted in dramatically reduced VLP production; however, removal of just one motif did not negatively affect VLP release (Licata et al. 2003).

The interaction of VP40 with the nucleocapsid proteins is relatively well studied in comparison to some of the other viral proteins. Co-expression of NP and VP40 resulted in enhanced VLP release compared to VP40 alone, whereas co-expression of VP24 and VP40 did not (Licata et al. 2004). Similarly NP and VP40, but not VP24 and VP40, have been shown to co-localize *via* IFA and co-IP (Hoenen et al. 2010b; Licata et al. 2004; Nanbo et al. 2013; Noda et al. 2007a). While no direct interaction between VP24 and VP40 has been shown, the addition of NP to VP24/VP40 transfections led to greater VLP production than was observed with NP and VP40 alone. As such, it is possible that VP24 may be bridging the NP-VP40 interaction, facilitating budding (Licata et al. 2004). Dimerization-deficient VP40 mutants were able to co-IP NP and were also found to co-localize with NP in transfected cells, suggesting that oligomerization is not required for VP40-NP interactions (Hoenen et al. 2010b). In addition, the RNA-binding capability of VP40 is not required for VP40-NP interactions, as RNA binding-deficient mutants could still incorporate NP into VLPs (Hoenen et al. 2005). While the VP40 binding sites have been mapped to the C-terminus of NP, the reverse has not been performed (Licata et al. 2004).

The co-expression of VP35 and VP40 does not result in enhanced VLP release; however, protease protection assays do show that VP35 is packaged in VP40 VLPs

(Johnson et al. 2006a; Johnson et al. 2006b). Mammalian two-hybrid assays demonstrated a direct interaction between VP35 and VP40, which is further supported by co-localization of these two proteins (Johnson et al. 2006b). Co-localization of VP40 and VP35 can also be observed when NP is present (Nanbo et al. 2013). The VP40-VP35 interaction does not require RNA, but this interaction is sufficient to incorporate Ebola virus minigenome RNA into VLPs in the absence of NP (Johnson et al. 2006b). The binding sites of VP35 and VP40 are currently not elucidated.

1.8 Transmission electron microscopy

1.8.1 Negative stain

TEM sample preparation begins with a liquid specimen applied to the surface of a small circular metal grid, 3.05mm in diameter. Depending on the sample and TEM technique being used, the grid may be pre-treated with a support film of plastic (polyvinyl formal; Formvar) and/or carbon (Curry et al. 2006). Negative stain is the major TEM technique used within this thesis. For this technique, a heavy metal salt solution (stain) is applied to a grid previously loaded with the sample of interest. As the stain air-dries it encases and conforms to all structures within the sample, increasing their electron density and thus, their contrast within the TEM (Curry et al. 2006; Gentile and Gelderblom 2014). This is particularly useful because biological samples are usually comprised of light atoms that are difficult to visualize in the TEM without stain (Boekema et al. 2009; Gentile and Gelderblom 2014). Negative staining is most often performed on grids that are both Formvar and carbon-coated. The Formvar provides the surface for the sample to adhere to,

while the carbon adds thermal and mechanical stability, as well as additional contrast. In addition, these carbon-coated grids are made more hydrophilic by glow discharge (generation and subsequent deposition of negatively charged ions in a vacuum) (Curry et al. 2006; Gentile and Gelderblom 2014).

There are a number of different metal salts currently used for negative staining that can influence our ability to differentiate pathogens. Uranyl acetate is beneficial for stabilizing viral envelopes, but has a very low pH that can affect biological structures (Gentile and Gelderblom 2014). The ultrastructure of poxviruses is more apparent after staining with uranyl acetate compared to other stains (Curry et al. 2006). Phosphotungstic acid (PTA) can be used at a more relevant physiological pH, but tends to provide less contrast than uranyl acetate (Gentile and Gelderblom 2014). Furthermore, PTA can disrupt some viral and cellular membranes (Nakata et al. 1987). Rotaviruses stained in PTA with a pH higher than 4.5 appeared broken and reduced in number compared to the same sample stained with uranyl acetate or PTA at a pH of 4.5 (Nakata et al. 1987). Lead citrate directly interacts with both uranyl acetate and the fixative/stain osmium tetroxide (Pandithage 2013). This double stain produces high contrast images and as a result, is the most popular choice for thin-section microscopy. Whereas uranyl acetate binds to a) sialic acid carboxyl groups of proteins and lipids and b) DNA and RNA phosphate backbones, lead citrate is less specific and will bind to lipid and cytoskeletal cellular components, as well as any osmium or uranyl ions (Pandithage 2013). Methylamine tungstate is considered a more gentle stain (in comparison with PTA) and provides good contrast for membranes and macromolecules (Kolodziej et al. 1997; Stoops et al. 1991). Negative stain is the method of choice for rapid TEM diagnostics; however, it does have disadvantages when used for structural analysis. As

the stain air-dries onto the sample, the structures contained within that sample may become flattened or distorted (Baker et al. 1999). As a result, the structures visualized may not be exact representations of native protein conformations. Nonuniform staining and radiation damage can also affect structural analysis, although more recent low dose techniques have reduced the latter issue. The ability of some stains to disrupt important structures within a specimen can also prevent accurate structural analysis. Most significantly, the densities highlighted by negative stain are attributed to the heavy metal salt coating the sample and not the protein densities themselves (Baker et al. 1999; Boekema et al. 2009; Kolodziej et al. 1997). This can lead researchers to "make a mountain out of a mole hill" where lesser protein densities may become exaggerated due to negative stain (Baker et al. 1999). Negative staining is a useful technique for rapid visualization of samples and with the proper appreciation of its shortcomings can still be a valuable method for structural analysis (Massower et al. 2001).

1.8.2 Cryo-electron microscopy

To better preserve a protein's native structure, cryo-electron microscopy (cryo-EM) was developed (Adrian et al. 1984). This technique flash freezes a sample at liquid ethane temperatures (~170°C), enabling the native structures within to be preserved by a thin layer of vitrified water (Adrian et al. 1984; Baker et al. 1999). The sample is kept at liquid nitrogen temperature (~196°C) during storage and while within the TEM. No support film is needed as the sample is encased within the vitrified water. Unlike negative stain, contrast of cryo-preserved structures is produced by the density difference between the water and protein molecules and is emphasized by defocusing the image. No external metal salt is applied (Baker et al. 1999). Samples prepared for cryo-EM can be analysed by single

particle imaging or tomography (cryo-ET). Both analysis methods can result in high-resolution images and 3D reconstructions of your structure of interest; however, they differ in the process of image collection and analysis. Single particle imaging and cryo-ET are based on the projection theorem, which states that the Fourier transform of a 2D projection image will contain the same information as one plane (through the centre of the reciprocal space) of the Fourier transform of a 3D projection image. As a result, 2D Fourier transforms of the same structure from different orientations can "fill in" the reciprocal space of the 3D Fourier transform. The inverse Fourier transform can then be calculated generating a 3D reconstruction of the structure of interest (De Rosier and Klug 1968; Frank 2002). An important caveat for this process being that a majority of possible structural orientations must be present in the data set to prevent artifacts, such as elongation of the final 3D reconstruction (De Rosier and Klug 1968; Frank 2002).

1.8.3 Single particle image analysis

Single particle imaging analysis is the averaging of individual, randomly orientated particle projections in order to resolve the structure of interest (Baker et al. 1999; Boekema et al. 2009; De Rosier and Klug 1968; Frank 2002). Thousands to tens of thousands of particle projections are collected from image fields containing many structures, all in different orientations. These individual projections must first be aligned in terms of rotational and translational differences, followed by alignment based on their planar orientation using multivariate statistical analysis. Finally these images are computationally grouped into specific classes based on similarities. After classification, the processed images are averaged together, generating a novel projection image that is both higher contrast and higher resolution than the individual projections (Boekema et al. 2009;

van Heel et al. 2000). The resolution and contrast of an averaged image is dependent on the number of projections summed in its class. The more data present (processed images), the higher quality the averaged image will be. These averages can then be used for Fourier transform calculations and 3D reconstructions (Boekema et al. 2009; van Heel et al. 2000).

The greatest strength and weakness of single particle image analysis is the image averaging. Microscope, image processing, and sample limitations can all negatively affect the final image sum, and thus the resolution of the final reconstruction. Variations in magnification and defocus, as well as CCD camera distortion or aberrations can affect image quality (Frank 2002). Furthermore, there are several limitations related to the electron beam that affect image quality as well, usually resulting in a blurring of the image, some of which can be corrected for (Frank 2002; van Heel et al. 2000). Improper alignment of individual projections can lead to loss of image resolution, as can an insufficient number of particles and/or missing particle orientations (Boekema et al. 2009; Frank 2002). Most importantly, single particle imaging analysis requires homogeneous 3D structures. This can be a major drawback for structural analysis as many proteins or macromolecular complexes are dynamic, and while distinct conformational changes can be accounted for using projection classification, structures that are constantly in flux are not suitable for single particle image analysis (Cope et al. 2010; Frank 2002).

1.8.4 Tomography

Cryo-ET suffers some of the same microscope and processing limitations as single particle imaging; however, cryo-ET is not limited to homogeneous 3D structures (Cope et al. 2010; De Rosier and Klug 1968). Whereas single particle imaging utilizes numerous

particles frozen in various orientations, cryo-ET utilizes only one particle with the various orientations created by tilting the sample within the microscope. At each angle change, a new image projection is recorded until the vitreous water is too thick to image through (Cope et al. 2011). Each projection is first aligned to each other based on cross-correlational calculations, and then further aligned using the fiducial markers (colloidal gold; 10-15 nm in diameter) that were added during sample prep. The second alignment corrects for subtle changes in image magnification, defocus, rotation, and translation and is an iterative process that repeats until the alignment no longer improves (Cope et al. 2011). The aligned images can then be processed into a tomogram, which can be displayed as a movie that travels through the sample in the Z-axis, with rotation occurring along the Y-axis (Chapter 9.4: Movie S1, Movie S2). Similar to single particle image analysis, these aligned projections can then be back-projected into Fourier space to generate a 3D model of the structure (Cope et al. 2011). A tilt series usually contains an oversampling of low frequency Fourier components, as a result, the back-projection is weighted against this to balance out the missing high frequency data (Cope et al. 2011). In addition, the ice thickness of the sample can limit the range of angles used in the tilt series. Once the ice becomes too thick, usually between ± 56° to 70°, what little signal-to-noise ratio that was apparent is lost in further images. As a result, when the images are back-projected not all of the 3D reciprocal space is filled because some orientations are absent. The "missing wedge" of data in the Z-axis (parallel to the electron beam) can lead to lower resolution and artifacts such as elongation (Cope et al. 2011). These artifacts are comparable to what occurs if an insufficient variation of angles is processed during single particle image analysis. In the latter technique, the collection and analysis of more images in the missing

orientations can decrease these artifacts (Boekema et al. 2009; van Heel et al. 2000). In cryo-ET, a dual-axis tilt series can be used to reduce the "missing wedge" (Guesdon et al. 2013; Mastronarde 1997; Penczek et al. 1995). Dual-axis tomography entails rotating a specimen 90° in-plane after completing the first tilt series and imaging a second tilt series of that same area (Mastronarde 1997; Penczek et al. 1995). The two tilt series can then be processed separately and added into the same reciprocal space. Data missing in the Z-axis from the first tilt series can be recovered from the second series, effectively reducing the "missing wedge" and providing greater resolution (Guesdon et al. 2013; Mastronarde 1997; Penczek et al. 1995). Z-axis slices of the tomogram and computed 3D reconstructions can provide knowledge on the subunits and conformation of the structure of interest (Cope et al. 2011). If the particle displays symmetrical components or multiple identical structures occur within one tomogram, subtomogram (or subvolume) averaging can be performed. These identical components are selected, aligned, and averaged to generate summed projections that have a higher resolution (Cope et al. 2011). Cryo-ET is a valuable technique because it does not require symmetry in your structure of interest. The ability to select symmetrical units for subtomogram averaging is advantageous, but not the goal of this technique (Cope et al. 2011). Negative stain, single particle- and tomographic image analysis will all be used within this thesis to better elucidate the internal quaternary structure of the Ebola virus.

1.9 Study Rationale, Hypothesis, and Objectives

1.9.1 Study Rationale

The arrangement and stoichiometry of NP, VP24, VP30, and VP35 within the Ebola virus nucleocapsid remains unconfirmed due to moderate-resolution reconstructions and missing or incomplete protein-protein interaction data. Initial studies demonstrated that Ebola virus infected cell sections and cells expressing NP, VP24, and VP35 both displayed very similar inclusion bodies that contained 50 nm cylindrical particles (Huang et al. 2002; Noda et al. 2006). As no high magnification TEM or image analysis was performed in these studies to confirm this similarity, I sought to determine whether tomographic analysis of transfected cell sections could identify structural differences. Significantly, there was also an absence of data in the literature concerning the isolation and characterization of filovirus nucleocapsids. Many groups have studied the Ebola virus nucleocapsid structure as part of the virus particle; however, the study of artificial Ebola virus nucleocapsid-like particles has not been reported. In this thesis, my goal was to generate, isolate, and characterize Ebola virus nucleocapsid-like particles from transfected cells.

As a dynamic macromolecular complex, the structure and function of the filovirus nucleocapsid is interconnected. The nucleocapsid acts as a scaffold and protector of the RNA genome, but must also be capable of disassembly and reassembly for replication and transcription. A greater understanding of the structure of the Ebola virus nucleocapsid may lead to the better appreciation of its functions in genome packaging, budding, replication, and transcription.

1.9.2 Hypotheses

1) Ebola virus nucleocapsids released from their viral envelopes will remain stable, symmetrical particles.
2) Co-expression of the Ebola virus nucleocapsid proteins NP, VP24, VP35, and/or VP30 and VP40 will result in the self-assembly of near-native nucleocapsid-like particles which display helical symmetry.

1.9.3 Objectives

1) To generate nucleocapsid-like particles in 293T cells by co-transfection of expression plasmids for a) cell section experiments and b) for purification
2) To isolate, purify, and assess the stability of the nucleocapsid-like particles using ultracentrifugation and negative stain techniques
3) To investigate the structure of purified nucleocapsid-like particles using TEM and image analysis
4) To isolate envelope-free nucleocapsids from detergent (NP-40) disrupted Ebola virus and perform TEM and image analysis on these structures

Chapter 2. Materials and Methods

2.1 Cells and viruses

HEK 293T human embryonic kidney cells and Vero E6 African Green Monkey kidney cells were maintained in Dulbecco's modified Eagle's medium (DMEM; Life Technologies, Carlsbad, U.S.A) with 10% fetal bovine serum (FBS; Life Technologies) and 1% penicillin/streptomycin/L-glutamine (PSL; Life Technologies) at 37°C with 5% CO_2.

Shane Jones and the Special Pathogens Group at the National Microbiology Laboratory (NML) in Winnipeg, Manitoba propagated, detergent-treated, and fixed the Zaire Ebola virus Kikwit strain for this thesis in their biosafety level 4 (BSL4) laboratory. Briefly, Ebola virus was grown in VeroE6 cells until 3+ cytopathic effects were observed, approximately 14 days post-infection. The medium was removed from infected flasks and both the media and flasks were placed at -80°C. Medium and cells were thawed and separately clarified by centrifugation at 1,500 rpm for 10 min at 4°C; after which the separate supernatants were loaded onto 20% sucrose cushions (Thermo Fisher Scientific, Inc., Waltham, U.S.A) in TNE buffer (Chapter 9.1) and centrifuged at 28,000 x g for 2 hours at 4°C, using an SW32 rotor (Beckman Coulter Inc., Brea, U.S.A) (Cutts et al. 2016; Melito et al. 2008). Pelleted virus was washed in sterile PBS and centrifuged at 28,000 x g for 30 min at 4°C. Pellets were resuspended in sterile PBS, or sterile PBS containing 0.15% Nonidet P-40 for 10 min at room temperature (NP-40; Sigma-Aldrich, St. Louis, U.S.A) followed by incubation in 4% paraformaldehyde (Sigma-Aldrich) for 24 hours at 4°C (Cutts et al. 2016). Excess fixative was removed by dialysis in PBS using Slide-A-Lyzer G2 cassettes with a 10,000 molecular weight cut-off (MWCO) (Thermo Fisher Scientific) (Melito et al. 2008).

Plasmids

Plasmids encoding Ebola virus structural proteins NP, VP35 and VP24 were originally received from Dr. Gary Nabel (NIH/VRC) in the plasmid pVR2000; however, due to expression difficulties, new plasmids were designed (Huang et al. 2002). cDNA encoding Ebola virus NP, VP24, VP35, VP30, VP40, and GP (GenBank Accession # EU224440.2) were individually synthesized to include restriction enzyme sites by GenScript U.S.A, Inc., Piscataway, New Jersey, U.S.A. Genscript then subcloned each gene into the expression plasmid pCAGGs, generously provided by Darwyn Kobasa (NML) (Table 1) (Kobasa et al. 1997; Niwa et al. 1991). Gene direction and integrity was confirmed by Genscript Inc, and gene expression was subsequently confirmed by SDS-PAGE and mass spectrometry at the NML (Chapter 9.2).

Table 1. Restriction enzymes used for gene insertion.

Gene	Restriction enzymes
NP	EcoRI, XhoI
VP24	ClaI, XhoI
VP30	EcoRI, XhoI
VP35	SacI, SmaI
VP40	EcoRI, XhoI
GP	EcoRI, XhoI

Plasmids were initially propagated in One Shot TOP10 Chemically Competent *E. coli* (Life Technologies), using 50 ng of plasmid per 25 µl of *E. coli*. Plasmid and *E. coli* were incubated for 30 min on ice, followed by heat shock at 42°C for 30 sec. After a 2 minute incubation on ice, heat shocked *E. coli* were incubated for an hour at 37°C with shaking and

then plated onto 200 µg/ml carbenicillin Lennox Broth agar plates, made inhouse at the NML. Plates were incubated for 24 hours at 37°C, after which single colonies were selected and streaked onto new carbenicillin plates to confirm growth.

Further plasmid propagation was performed using the Endofree Maxi Plasmid Purification kit (Qiagen Inc., Hilden, Germany). A single colony from a streaked confirmation plate was inoculated into 100 ml of Lennox-Miller broth with 100 µg/ml of Ampicillin. Colonies were grown overnight at 37°C, shaking at ~200 rpm. Following the Endofree kit protocol, bacteria were pelleted at 6,000 x g for 15 min at 4°C, followed by resuspension, lysis, and filtration steps. Plasmids were redissolved in 100 µl of UltraPure water (Life Technologies) and stored at 4°C or -20°C. Final plasmid concentrations were determined using a Nanodrop Spectrophotometer ND-1000 and Nanodrop Software (Thermo Fisher Scientific). Plasmids were diluted to 200-400 µg/µl for storage.

2.2 Transfection

Twenty-four hours prior to transfection, HEK 293T or BHK cells were seeded at ~5 x 10^5 cells/ml into a Corning®CellBIND® 75cm^2 flask (Corning Inc., Corning, U.S.A). Transfections were performed using the Effectene Transfection Reagent (Qiagen) and volumes were scaled up for use in 75cm^2 flasks (Table 2). Plasmids were mixed with the appropriate amount of Buffer EC and Effector and incubated at room temperature for 2-5 min (Table 2). After which, the Effectene reagent was added and the transfection solution was incubated for 5-10 min. During this time, cells were washed with 10 ml DMEM with 10% FBS and 1% PSL and media was replaced with 10 ml of supplemented DMEM. After incubation, 4 ml of supplemented DMEM was carefully added to the transfection solution

and the final mixture was gently added to the flask. Transfected cells were incubated at 37°C with 5% CO_2 in supplemented DMEM. Cells and supernatant were harvested 48 - 72 hours after transfection.

Table 2. Volumes of Effectene reagents used for transfection of T75 flasks.

Qiagen Effectene Transfection Reagent	Volume or Concentration	Example of NP/VP24/VP35 transfection
DNA	3.5 - 7 µg per plasmid	NP 3.5 µg VP24 3.5 µg VP35 3.5 µg
Effector	Total DNA (µg) x 8	10.5 x 8 = 84 µl
Buffer EC	= 500 µl – Total DNA (µl) – Effector (µl)	= 500 – volume of NP/VP24/VP35 plasmids – 84 µl
Effectene	Total DNA (µg) x 10 or 25	10.5 x 10 = 105
Media to transfection solution	4 ml	4 ml
Media to cells	10 ml	10 ml

2.3 Staggered transfection

Multiple combinations of Ebola virus plasmids were used to investigate the Ebola virus nucleocapsid structure including staggered transfection of plasmids (Table 3). Cells were plated 24 hours prior to transfection in T75 flasks, as above. The initial transfection followed the protocol described in the previous section. For the second round of transfections, cell monolayers were not washed nor media removed. After being mixed with 4 ml media, the second transfection solution was added at either 2 or 6 hours post-initial transfection. The staggered combinations are listed in Table 3. Transfected cells

were incubated at 37°C with 5% CO_2 in supplemented DMEM. Cells and supernatant were harvested 48 hours after initial transfection. These experiments were performed in duplicate.

Table 3. Study design for staggered transfections.

Initial Transfection	Incubation time (hours)	Secondary Transfection
NP/VP35	2	VP24
NP/VP40	2	VP24/VP35
NP	6	VP24/VP35
NP/VP35	6	VP24
NP/VP40	6	VP24/VP35

2.4 Cell lysis methods

Multiple methods of cell lysis were performed (Table 4). HEK 293T cells transfected with the Ebola virus expression plasmids were lysed

A-B) with hypotonic lysis buffer with or without 1% NP-40,

C) in isotonic salt concentration (150 mM NaCl) with 1% NP-40,

D) by 3 freeze-thaw cycles in 150 mM NaCl at -80°C,

E) by 3 freeze-thaw cycles in 50 mM NaCl at -80°C,

F) by a tissue homogenizer,

G-H) in isotonic salt buffer in the absence of EDTA

For all methods, cells were harvested by gentle pipetting in culture medium. The cell/medium suspension was clarified by centrifugation for 5 min at 1,500 rpm at 4°C. Cell pellets were resuspended in 1-2 ml of PBS and spun a second time for 5 min at 1,500 rpm at 4°C. Cell pellets were resuspended in the appropriate buffer. For methods A-C and G-H,

transfected cells were lysed for 30 min on ice, followed by centrifugation for 5 min at 1,500 rpm at 4°C (Elliott et al. 1985; Iseni et al. 1998; Noda et al. 2010; Noda et al. 2011). For methods D-F, transfected cells were resuspended in either 150 mM or 50 mM NaCl PBS containing protease inhibitor cocktail (PIC; Roche; Diagnostics, Basel, Switzerland). Cell pellets were frozen three times at -80°C or homogenized for 60 sec using an Omni tissue homogenizer (Omni International, Kennesaw, U.S.A) then clarified for 5 min at 1,500 rpm and stored at 4°C. All transfections were performed in triplicate.

2.5 Iodixanol gradients

Clarified cell lysates were loaded onto continuous 15-30% iodixanol (Optiprep; Sigma-Aldrich) density gradients (Nielsen et al. 2006). Iodixanol gradients were chosen for two main reasons. First, as an inert solution, it would not interact with the protein structures, and second, any remaining iodixanol after purification would disrupt the negative stain less than other gradient materials such as sucrose (Nielsen et al. 2006). In addition, when sucrose was used as a gradient material during preliminary experiments, the separation of proteins was not as clean as with iodixanol. As such, iodixanol was chosen as the gradient material. To ensure equal NaCl concentration throughout the gradient, iodixanol dilutions were prepared in NaCl-supplemented PBS to equalize the NaCl concentration to 50 mM or 150 mM, depending on the experiment. Continuous gradients were prepared 24-48 hours in advance in Ultra-Clear centrifuge tubes (Beckman Coulter) and stored at 4°C. Gradients consisted of 4 ml of 15% iodixanol gently layered on top of 8 ml of 30% iodixanol. After addition of ~ 1 ml lysate, gradients were ultracentrifuged at 230,501 x g for 2 hours at 4°C using an SW40 Ti rotor (Figure 5) (Beckman Coulter).

Table 4. Reagent concentrations for the buffers used within this thesis.

	Hypotonic lysis buffer		Physiological lysis buffer	Freeze-thaw (3X)		Homogen-ization	Divalent salt and/or sucrose lysis buffer	
Reagent	**A**	**B**	**C**	**D**	**E**	**F**	**G**	**H**
Tris-HCl pH 7.5 (mM)	10	10	10	0	0	0	10	10
NaCl (mM)	50	50	150	150	50	150	150	150
EDTA (mM)	1	1	1	0	0	0	0	0
NP-40	0	1%	1%	0	0	0	1%	0.1%
PIC	yes	yes	yes	yes	yes	yes	yes	yes
$MgCl_2$ (mM)	0	0	0	0	0	0	1.5	1.5
KCl (mM)	0	0	0	0	0	0	10	10

Reagent sources: Tris-HCl pH 7.5 (Thermo Fisher Scientific); EDTA, $MgCl_2$, and KCl (Life Technologies); PIC without EDTA (Roche Diagnostics); NP-40 and sucrose (Sigma-Aldrich)

2.6 Fractionation

Fractions were collected in 1 ml aliquots, starting at the top of the gradient, using an Auto Densi-Flow Density Gradient Fractionator (Labconco, Kansas City, U.S.A). Tubing was rinsed with sterile PBS between gradients. Fractions were stored at 4°C. Density of fractions was determined by weighing 1 ml fractions of control gradients.

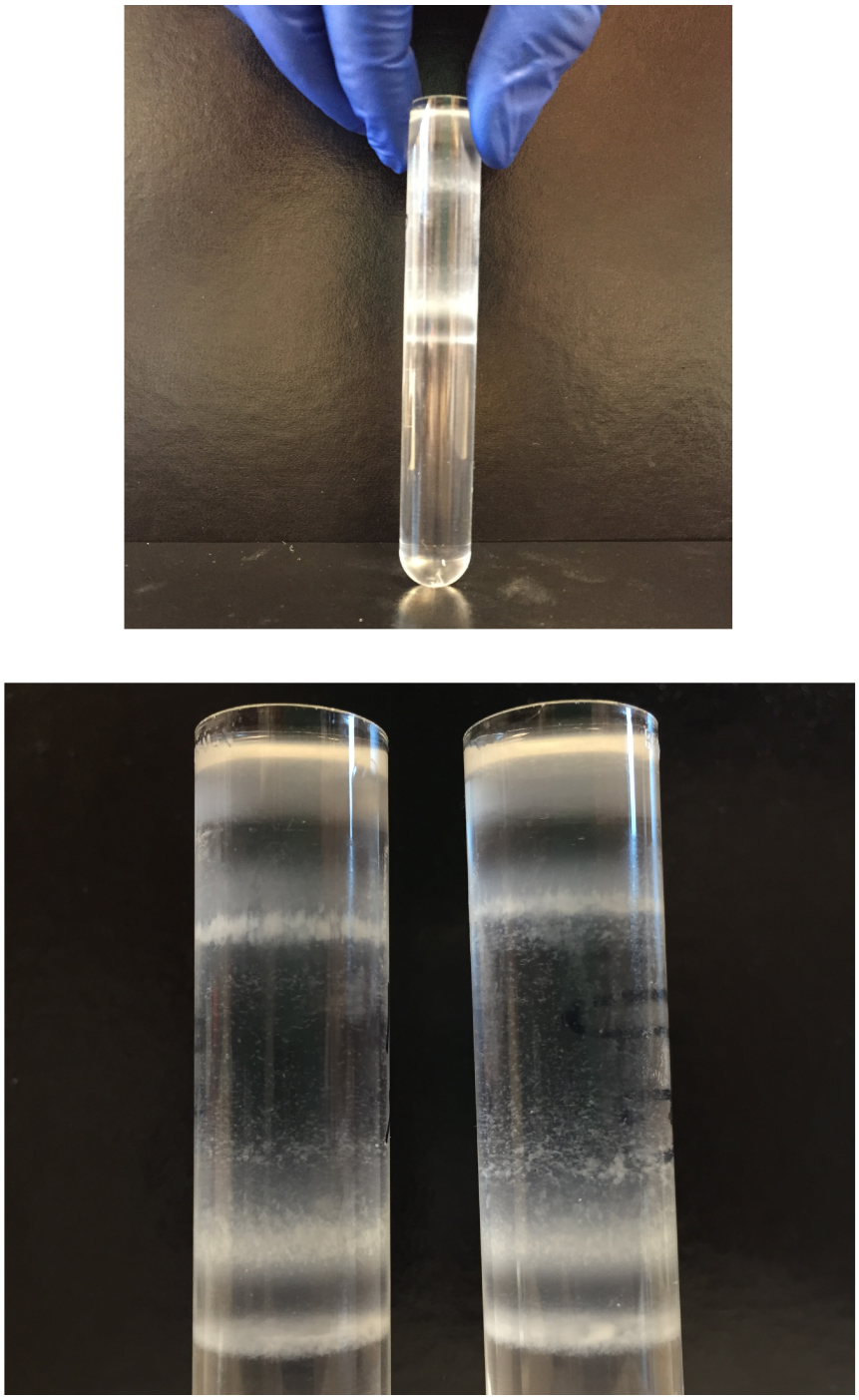

Figure 5. Representative images of 15-30% iodixanol gradients after ultracentrifugation. Cells were homogenized in 150 mM NaCl PBS and lysate was layered on top of gradient.

2.7 pH experiments

293T cells were transfected as described above with either NP alone, or NP/VP24/VP35 with or without VP30. Cells were harvested 72 hours post-transfection and lysed in isotonic lysis buffer. Two different experiments were done to determine the effect of low pH on Ebola virus nucleocapsid-like particles. In the first, cell lysate was layered onto 15-30% iodixanol gradients containing 150 mM NaCl and ultracentrifuged. The fractions were collected and fractions 5-7 were dialysed in either neutral (PBS) or low pH (5 mM NaAc, pH 5) buffers using 10K MWCO Slide-a-Lyzers (Table 5). Dialysis products were collected and stored at 4°C. In the second experiment, cells were transfected and harvested as above; however, the gradients were generated to match the dialysis buffer. For example, the low pH gradient would consist of 15% and 30% iodixanol in 5 mM NaAc, pH 5. The fractions from this gradient would then be dialyzed in 5 mM NaAc, pH 5 (Table 5). As above, dialysis products were collected and stored at 4°C. Each experiment was performed in triplicate.

Table 5. Study design for pH experiments.

	Experiment 1 (NP only)		**Experiment 2 (NP only, NP/VP24/VP35±VP30)**	
Buffers	**Gradient**	**Dialysis**	**Gradient**	**Dialysis**
PBS pH 7	✓	✓		
150 mM NaCl, 5 mM Tris-HCl pH 7.5			✓	✓
5 mM Tris-HCl pH 7.5		✓	✓	✓
5 mM NaAc pH 5		✓	✓	✓

Reagent sources: Tris-HCl pH 7.5 (Thermo Fisher Scientific); NaCl and PBS (Life Technologies); NaAc (NML).

2.8 Fixation methods

Two methods of fixation of nucleocapsid-like particles were investigated. Cross-linking of live cells was performed using three different chemicals: paraformaldehyde (PFA), disuccinimidyl suberate (DSS), and ethylene glycolbis(disuccinimidyl suberate) (EGS) (Creative Molecules Inc., Victoria, Canada). Five percent dimethylsulfoxide (DMSO) was used as a negative control (Sigma-Aldrich). Cells were washed and harvested by gentle pipetting 48 hours post-transfection and clarified by an 800 x g spin for 15 min in a JS7.5 rotor (Beckman Coulter). Approximately 1.4 x 10^7 cells were used per crosslinker. A 2% PFA solution was generated in PBS by heating 1 g of PFA in 50 ml of PBS until it had dissolved. A new PFA stock was generated for each experiment. Cells were treated with room temperature PFA for 10 or 20 min, with continuous end over end rotation. DSS and EGS were generated as 50 mM stocks in DMSO. The 50 mM stocks were then diluted to 1 or 2 mM concentrations in 3% DMSO PBS. Clarified cells were mixed with DSS or EGS for 32 or 42 min. The crosslinker concentrations and incubation times are summarized in Table 6. PFA, DSS, and EGS were inactivated with 125 mM glycine in PBS (Sigma-Aldrich) for 15 min, followed by centrifugation (as above) to re-pellet the cells. The supernatant was discarded, and the inactivation steps were performed twice more. Cells were lysed in isotonic lysis buffer and stored at 4°C. Experiments were performed in duplicate.

Table 6. Study design for the cross-linker experiment.

Cross-linker	Concentration	Incubation time (min)
PFA	2%	10
PFA	2%	20
DSS	1 mM	32
DSS	2 mM	32
DSS	1 mM	42
DSS	2 mM	42
EGS	1 mM	32
EGS	2 mM	32
EGS	1 mM	42
EGS	2 mM	42

PFA: paraformaldehyde; DSS: disuccinimidyl suberate; EGS: ethylene glycolbis(disuccinimidyl suberate)

A second method of fixation was based on the Grafix method by Kastner et al. (2008). In this method, a fixative is added to the density gradient, rather than the cells. A final gluteraldehyde concentration of 0.15% was added to either the 15% iodixanol solution or to both the 15% and 30% iodixanol solutions in order to generate Grafix density gradients (Electron Microscopy Sciences, Hadfield, Pennsylvania, U.S.A) (Kastner et al., 2008). Transfected cells lysed by hypotonic lysis buffer were loaded onto Grafix gradients and centrifuged as described in Section 2.6 (Kastner et al. 2008).

2.9 VLP collection

Forty-eight hours post-transfection, cell culture media was removed from the flasks, clarified for 5 min at 1,500 rpm and loaded onto a 20% sucrose cushion in TNE buffer and centrifuged at 15,100 rpm for 2 hours at 4°C, using an SW32 rotor (Beckman Coulter). Pellets were carefully washed and resuspended in sterile PBS and stored at 4°C (Melito et al. 2008).

2.10 SDS-PAGE

Fraction samples were mixed equally with Laemmli sample buffer (Bio-Rad Laboratories, Inc., Hercules, U.S.A) containing 5% betamercaptoethanol (Bio-Rad Laboratories), boiled for 5 min at 97°C and loaded onto a 12% Bis-Tris gel (Life Technologies). Gels were stained with Coomassie blue (SimplyBlue SafeStain; Life Technologies) for one hour and imaged using a Gel Doc™ EZ Imager (Bio-Rad Laboratories). The Novex Pre-Stained protein standard was used (Life Technologies).

2.11 Purification of nucleocapsid-like particles

Based on protein gel results, fractions with relatively high levels of Ebola virus nucleocapsid proteins and lower levels of cellular proteins were chosen for further investigation (usually fractions 5-7). Selected fractions were either dialyzed in PBS using Slide-A-Lyzer G2 cassettes with a 10,000 MWCO or layered onto PBS in Ultra-Clear centrifuge tubes and ultracentrifuged at 129,657 x g for 45 min at 4°C using an SW40 Ti rotor (Melito et al. 2008). Pellets were resuspended in PBS and stored at 4°C. Dialysis buffers were changed at 2 hour intervals, twice. A final incubation overnight at 4°C was performed, and dialysis products were collected with a syringe as per manufacturers instructrions. Dialysis products were stored at 4°C.

2.12 Immunoblotting

Samples were mixed in a 1:1 ratio with Laemmli sample buffer containing 5% beta-mercaptoethanol, boiled for 5 min and loaded onto a 12% Bis-Tris gel for SDS-PAGE. Proteins were transferred to nitrocellulose or polyvinylidene difluoride (PVDF) membranes using the iBlot Gel Transfer System, setting 3 (Life Technologies). Two immunoblotting methods were used during this study. Proteins were visualized using horseradish peroxidase (HRP) chemiluminescence or infrared imaging using the Licor system. As such, membranes were blocked for 1 hour at room temperature with either 5% bovine serum albumin (BSA; Santa Cruz Biotechnology) or Odyssey Blocking Buffer (Licor Biosciences, Lincoln, USA) in TBS with 0.1% Tween20, respectively (TBST; Bio-Rad Laboratories). Membranes were then rinsed twice for 5 min in TBST, after which the primary antibody was added in blocking buffer. Following primary antibody incubation overnight, membranes were washed 3 times for 5 min with TBST. The secondary antibody was incubated for 1 hour at room temperature in TBST. Finally, the membrane was washed 3-6 times for 5 min in TBST and/or TBS and the membranes were imaged *via* chemiluminescence using the VersaDoc 5000 MP and Quantity One software (Bio-Rad Laboratories) or the Odyssey Classic imager and Image Studio Lite software (Licor Biosciences).

Shane Jones and the Special Pathogens Unit at the NML kindly donated an inhouse anti-Zaire Ebola virus polyclonal antibody from rhesus macaques which was used at 1:1600 dilution, overnight at 4°C. A goat anti-human IgG secondary antibody conjugated to HRP was used to detect the anti-Zaire Ebola virus antibody at a dilution 1:5000 (Santa Cruz Biotechnology). Primary antibodies against NP (Cat #0301-012: IBT Bioservices, Rockville,

USA; Cat #ZEB-NP-01: Eenzyme LLC, Gaithersburg, USA), VP35 (IBT Bioservices, Cat #0301-040), and VP40 (IBT Bioservices, Cat # 0301-010) were used at a 1:1000 dilution for NP and VP35 or a 1:2000 dilution for VP40. For the Licor system, secondary antibodies goat anti-mouse IRDye 680LT (Mandel Scientific, Guelph, Canada; LIC-926-68020) and goat anti-rabbit IRDye 800CW (Mandel Scientific; LIC-926-32211) were used at a dilution of 1:25,000.

2.13 Mass spectrometry

After SDS-PAGE, bands suspected to be NP, VP24, VP35, VP30, or VP40 were cut from the gel and aliquoted separately. In-gel digestion was performed to reduce and alkylate the protein using dithiothreitol and iodoacetamide (Sigma-Aldrich). Protein was digested using trypsin (Promega Corporation, Madison, USA) and peptides were run on the Orbitrap XL (ThermoFisher Scientific). Results were analyzed using Scaffold software (Proteome Software Inc., Oregon, USA) and proteins were identified using the full SwissProt database or with the SwissProt virus database only (Chapter 9.2).

2.14 Support grid preparation

2.14.1 Cleaning

Four hundred mesh square copper or nickel grids were washed for 2 min in acetic acid, followed by consecutive 2 minute washes in acetone, 70% ethanol, and lastly 100% ethanol. Grids were dried on filter paper in a covered petri dish.

2.14.2 Formvar plastic preparation and grid coating

One percent formvar in chloroform (Electron Microscopy Sciences) was poured into an ethanol cleaned coplin jar and covered with parafilm between uses. Ethanol cleaned

glass slides were dipped into the formvar chloroform solution and rapidly removed. The glass slide was held in hand while the formvar chloroform quickly dried. The quality of plastic was assessed by light microscope and slides were discarded if plastic was too holey. To remove the plastic from the slide, each side was etched with a razor blade and the glass slide was slowly lowered into ddH_20 at an angle, allowing the plastic to float on the surface of the water. Cleaned grids were then placed on the plastic. To remove the plastic and grids, a piece of cardstock paper was lowered into the water bath. The cardstock paper was carefully lifted up out of the water from underneath the formvar plastic and grids, collecting them. Grids, plastic, and paper were air dried overnight in a covered petri dish.

2.14.3 Carbon-coating grids

To layer a carbon film on top of formvar-coated grids, the cardstock containing grids were placed in an Agar 208 Turbo Carbon Coater (Agar Scientific Ltd., Stansted, U.K.). Carbon rods were polished to remove residual charcoal and one side was sharpened to a point. Once a suitable vacuum was reached, the carbon rods were degassed for 30 sec with the protector shield in place to cover the grids. The protector shield was then removed and carbon was evaporated onto grids for 4 sec. Grids were carefully pealed from the cardstock to maintain the plastic and carbon films and placed in grid holders.

2.14.4 Glow-discharge treatment of grids

To reduce the hydrophobicity of the carbon-coated grids, grids were temporarily charged using the Agar 208 Turbo Carbon Coater. Grids were placed in the machine and a vacuum of ~ 2 x 10^{-1} mbar was produced. Grids were irradiated for 30 sec at a current of 15 mA. Glow-discharged grids were used within the hour.

2.15 Negative staining

Along with pelleted or dialysed fraction samples, lysates and gradient volumes were also investigated for nucleocapsid-like particles. To stain, 3 µl of sample was adsorbed onto a glow-discharge treated, carbon coated formvar film on 400 mesh copper grid for 1 minute. For gradient samples, 2 µl of the gradient fraction and 2 µl of the corresponding PBS were adsorbed for 1 minute. The grids were then washed 3-6 times with 3 µl UltraPure water and stained for 30 sec with 3 µl of 2% methylamine tungstate (Nano-W; Nanoprobes Inc., New York, U.S.A) (Melito et al. 237-43).

A FEI Tecnai 20 transmission electron microscope (FEI Company, Hillsboro, USA) operating at 200 kV was used to image these specimens at various magnifications. An AMT Advantage XR-12 CCD camera (AMT; Danvers, U.S.A) was used to acquire the images (Melito et al. 2008).

2.16 Measurement of pitch and diameter

Pitch and diameter measurements of nucleocapsid-like particles were made using Image J, an open-source software platform (www.imagej.net) (Abramoff et al. 2004). For each lysis method and transfection combination, measurements were taken to determine the median and mean with standard deviation (Table 7, Table 8). To do so, the scale of each micrograph was calculated using the length of the scale bar in pixels and inputted under analyze/set scale in Image J. Once calibrated, the straight line or segmented tool was used for measurements, and "m" on the keyboard was hit to record a new measurement. For pitch lengths, measurements were made from centre to centre of adjacent spines of the particle. For diameter lengths, measurements were made from end to end of one spine. The

zoom tool of Image J was used to enlarge the particles. If particles had blurred/fuzzy ends of spines, these pixels were included in the diameter measurements. Microsoft Excel was used to calculate medians and means with standard deviation, as well as summary bar graphs.

Table 7. Number of diameter measurements for each protein combination and lysis method.

	LB50	**LB150**	**FT50**	**FT150**	**Media**		
NP/VP24/VP35	550	453	492	553	111	**Cryo**	181
NP/VP24/VP35/VP30	599	694	649	704	551	**Ebola**	119
NP/VP24/VP35/VP40	961	843	505	899	534	**P-NP**	625
NP/VP24/VP35/VP30/VP40	636	504	684	507	511		

LB50: hypotonic lysis buffer; LB150: isotonic lysis buffer; FT50: hypotonic freeze/thaw; FT150: isotonic freeze/thaw; Media: cell culture media; Cryo: NP/VP24/VP35 particles in vitrified water; Ebola: measurements from cryo-preserved Ebola virus tomogram; P-NP: Proto-nucleocapsids.

Table 8. Number of pitch measurements for each protein combination and lysis method.

	LB50	**LB150**	**FT50**	**FT150**	**Media**		
NP/VP24/VP35	910	510	748	634	194	**Cryo**	286
NP/VP24/VP35/VP30	798	559	576	881	583	**Ebola**	219
NP/VP24/VP35/VP40	912	986	712	621	733	**P-NP**	641
NP/VP24/VP35/VP30/VP40	540	592	586	670	690		

LB50: hypotonic lysis buffer; LB150: isotonic lysis buffer; FT50: hypotonic freeze/thaw; FT150: isotonic freeze/thaw; Media: cell culture media; Cryo: NP/VP24/VP35 particles in vitrified water; Ebola: measurements from cryo-preserved Ebola virus tomogram; P-NP: Proto-nucleocapsids.

2.17 Statistical analysis

The individual data sets were observed by frequency histogram to visualize data characteristics. It was noted that the majority of pitch frequency histograms were skewed to the left, while the diameter measurements were normally distributed. As such, diameter measurements were compared using the two-tailed student T test and the pitch measurements were compared using the nonparametric Mann-Whitney U test. For student t tests, an F test was first performed to determine equal or unequal variance. The total number of statistical analyses performed for each category (pitch, diameter) was 80. The Bonferroni correction was calculated for each category in order to reduce the number of false positives (0.05/80 = 0.000625 = p). This p value was used to determine significance of each individual student t test and Mann-Whitney test. Even with this stringent p value, many of the calculated p values were highly significant. Student t tests and Mann-Whitney tests were performed in Excel, using the data analysis add-in.

Linear regression was also performed in Excel. Lysis method was dummy-coded such that hypotonic lysis buffer was the comparator. Likewise, protein combination was dummy-coded such that NP/VP24/VP35 was the comparator. A p value of 0.05 was maintained for these analyses.

2.17.1 Densitometry

To estimate the stoichiometry of the nucleocapsid proteins from SDS-PAGE for the isotonic freeze/thaw, gels were imaged with a desktop scanner. Scanned images were imported into the SPIDER software and lanes were subfiled and each subfile was saved as an individual image. These images were then averaged and converted to a one-dimensional array of numbers that could be imported into Excel for final analysis and generating density plots. The density plot was corrected for background noise and the area under the curves were measured to calculate the signal value. The signal value is equal to molecular mass multiplied by protein copy number, thus if the molecular weight of the protein is known, the estimated stoichiometry of each protein can be calculated.

2.18 Immuno-electron microscopy (IEM)

Although results were not shown in this thesis, IEM was performed. Seventy-two hours post-transfection, NP/VP24/VP35 transfected cells were lysed with hypotonic lysis buffer with 1% NP-40 and ultracentrifuged through a 50 mM NaCl iodixanol gradient. Fraction 5 and 6 were collected and pelleted through 50 mM NaCl PBS and the pellet collected, as described previously. To perform IEM, the grid-on-drop method was performed in which all reagents were pipetted onto a piece of parafilm in order of use, usually 20-40 µl of each. To prevent oxidation, nickel rather than copper grids were used. The glow-discharge treated, carbon coated formvar film, 400 mesh nickel grid was placed on a drop of sample (NP/VP24/VP35 pellet) for 1 minute, after which it was placed onto 6 consecutive drops of PBS for 1 minute to wash it. Next, the grid was placed onto a drop of blocking buffer which consisted of PBS, 0.2% Tween20, 0.2% glycine (PBS-TG), and 2% BSA for 10 min at room temperature. Half of a large petri dish was placed over top to

reduce evaporation. The grid was then washed in 6 consecutive drops of PBS-TG for 1 minute per drop. The primary antibodies used in this experiment were rabbit anti-Zaire Ebola virus NP polyclonal (1:100) or rabbit anti-Zaire Ebola virus VP35 polyclonal antibodies (1:100) (IBT Bioservices, Gaithersburg, U.S.A). Primary antibodies were diluted in PBS-TG-BSA and the grid was incubated on drop for 1 hour, covered. As a negative control, grids were treated with PBS-TG-BSA rather than the primary antibody. After 6 more consecutive washes with PBS-TG, the grid was placed on a drop containing a 1:40 ratio of Protein A-coated 10 nm gold particles in PBS-TG for 30 min (Aurion Immuno Gold Reagents & Accessories, Wageningen, The Netherlands). Three consecutive 1 minute washes in PBS-TG, followed by 3 consecutive 1 minute washes in UltraPure water completed the washing stage. The grid was then lifted off the water using forceps and the excess water wicked away with a filter paper. The grid was stained for 30 sec with 3 µl of methylamine tungstate.

2.19 Embedding and sectioning

Forty-eight hours post-transfection, HEK 293T cells were harvested by gentle pipetting in PBS and pelleted by low speed centrifugation. Cell pellets were fixed with 2% PFA/2.5% glutaraldehyde for 1 hour at room temperature. Following fixation, cells were pelleted and the excess fixative was removed. Cell pellets were mixed with liquid 3% Ultra-pure Low Melting Point agarose in ddH_20 (Life Technologies). Once solidified, cell/agarose pellets were cut into 1 mm pieces and added to tissue processing 'baskets'. The entire tissue-processing program can be found in Chapter 9.3 and solutions can be found in Chapter 9.1. In brief, cells were stained with 1% osmium tetraoxide for 1 hour (Electron Microscopy Sciences), followed by a step-wise dehydration using increasing concentrations

of ethanol and propylene oxide. Cells were embedded in Epon 812 and accelerator DMP-30 (Electron Microscopy Sciences). Once embedded, tissue was placed in the bottom of beam capsules and resin with accelerator was added over top. Beam capsules were placed in a 68°C oven for 24-36 hours. Once hardened, the plastic resin was removed from the beam capsules.

Thin sectioning of cells was performed using an ultramicrotome, the Ultracut UCT (Leica, Solms, Germany). The resin block was first roughly trimmed using a razor blade to get closer to the embedded tissue. The block was then finely trimmed to generate a tip similar in size to a large sharpie. The tip of the block was then further smoothed and levelled with a glass knife made the same week (Leica). The block was then moved to the ultramicrotome holder, rather than the rough-trim holder. A glass knife with a plastic "boat" attached to it by wax was then placed in the ultramicrotome and the boat was filled with water to the top of the knife. As thin sections were cut on the glass knife, they floated on top of the water. Chloroform was used to smooth out the sections before they were applied to a grid. Acetone-washed, uncoated 300 mesh copper grids were carefully dipped into the "boat" water and brought underneath of the sections. The grids were then brought up underneath the section, picking it up. Grids were wicked and placed on filter paper to dry for 24 hours.

Thin sections were stained with a combination of 2% uranyl acetate and 0.05% lead citrate. Uranyl acetate was generated in warm water with mixing. Lead citrate was generated by dissolving lead citrate powder into boiled MilliQ water, with the addition of ~1 pellet of NaOH to raise the pH to ~12 (Sigma-Aldrich; Canemco Inc., Lakefield, Canada).

To stain, grids were placed on filtered uranyl acetate droplets for 10 min in the dark. Grids were then transferred to water droplets. Each grid was washed twice in 3 beakers of water and then transferred to a fresh droplet of water. Grids were then placed on droplets of filtered lead citrate in a petri dish that also contained NaOH pellets to reduce CO_2. Grids were incubated for 5 min and then washed as above and wicked dry. Lastly, sections were carbon-coated for radiation stability.

2.20 Indirect carbon evaporation and coating

Carbon was prevented from directly landing on grids by indirect carbon evaporation. Two ethanol cleaned glass slides hold up a third slide within the Agar 208 evaporator. Underneath the top horizontal slide was placed a thin slice of mica, ~ 75 mm by 25 mm. Carbon rods were cleaned of past char and the evaporator was run for 15 min to allow a strong vacuum to build. The carbon rods were then de-gassed for 30 sec, followed by carbon evaporation for 5-10 sec at setting 4. As a result of the upper glass slide, evaporated carbon did not directly hit the mica sheet, but instead was reflected off the slanted glass slides, allowing the mica to become indirectly covered with carbon.

To remove the thin film of carbon from the mica sheet, a large bowl was cleaned with ethanol and filled with UltraPure water. The mica was scored with a razor into small square sections and carefully lowered at an angle into the water, allowing the carbon to float off and remain on the surface of the water. Quantifoil grids, with the quantifoil side up were individually lowered under the surface of the water using forceps and brought underneath the thin layer of carbon (Quantifoil MicroTools GmbH, Jena, Germany). As the grids were brought to the surface of the water they picked up the thin carbon film. Grids were left on

forceps for 1 hour to allow for proper drying of the carbon onto the quantifoil grid. This process was then repeated for the other side of the grid. Glow-discharge was found to break the carbon/quantifoil and was therefore omitted.

2.21 Vitrobot

For cryo-EM, 3 µl of sample was loaded onto holey quantifoil grids and then plunge cooled in liquid ethane at liquid nitrogen temperature using a Vitrobot Mark IV (FEI). Grids were stored in liquid nitrogen. The Gatan CT3500TR single tilt rotation low-temperature specimen holder was cooled to- and maintained at liquid nitrogen temperature during imaging of these samples. Grids were discarded after cryo-EM use due to radiation and thawing.

2.22 Single particle imaging

Indirect carbon-coated square quantifoil grids were prepared prior to staining. Dialysed intracellular nucleocapsids from Zaire Ebola virus Kitwit strain, diluted 1:5 with PBS, were applied to these grids for 1 minute, washed 3 times with Ultrapure water and stained for 30 sec with 2% methylamine tungstate. After drying for 1 hour, the grid was loaded into a FEI Tecnai 20 G2 transmission electron microscope operated at 200 kV. Images were recorded using the Falcon CMOS direct electron detector (FEI). Images were taken at 50,000X magnification at -1.5 µ defocus, with a dose of 10 electrons/$Å^2$. As a result, the pixel size at the CCD detector was 1.998 Å/pixel. Data collection was performed using the Xplore 3D software, low-dose unit and TEM Imaging and Analysis (TIA) software (FEI) (Beniac et al. 2012).

2.22.1 Single particle imaging analysis

Image analysis of the proto-nucleocapsids was performed on 5620 images. Particle selection was performed using the EMAN program. The EMAN2 software was used to calculate the contrast transfer function correction using the "e2ctf.py" function (Frank et al. 1996; Ludtke et al. 1999). Resolution was estimated by Fourier shell correlation using the FSC 0.5 criteria. The SPIDER/WEB software was used to reconstruct the proto-nucleocapsid structure. As a baseline for the proto-nucleocapsid reconstruction, a previous Ebola virus nucleocapsid model was loaded into the software (Beniac et al. 2012). Using this previous data, the iterative helical real space reconstruction method (IHRSR) was applied to the 5620 proto-nucleocapsid images (Egelman 2000; Egelman 2007). The UCSF Chimera software package (Computer Graphics Laboratory, University of California, San Francisco, USA) was used to model and visualize the calculated reconstructions (Pettersen et al. 2004). 2D and 3D images present in this thesis were generated using UCSF Chimera by Dr. Daniel Beniac (NML).

2.23 Tomography

2.23.1 Data collection

BSA-coated 10 or 15 nm gold particles were applied to grids containing stained and carbon-coated cell sections at a 1:5 ratio (gold:water) (Aurion). Three µl of the gold mixture was applied to the cell sections for 30 sec. The grids were then washed in 3 water droplets and the grid was wicked dry. Specimens were placed in a Gatan CT3500TR single tilt rotation low-temperature specimen holder and imaged by a FEI Tecnai 20 G2 transmission electron microscope operated at 200 kV. Micrographs were recorded using an Eagle 4K CCD camera (FEI). Dual axis tomograms were generated by performing one

complete tomogram and then rotating the sample 90° within the microscope and completing a second tomogram. Sections were imaged at 25,000X magnification at -1 μ defocus, with angle steps of 1°. Data were collected within tilt ranges of ±56°, with a total cumulative dose/tomographic data set of 100 electrons/Å^2. Data collection was performed using the low-dose and TIA software. In addition, the Xplore3D data acquisition software (FEI) was used for automated eucentricity and focusing (Beniac et al. 2012).

2.23.2 Image processing

Tomography data from cell sections was analyzed using the Inspect3D Xpress software package (FEI). A two-step alignment process was performed for each data set. First, cross-correlation of adjacent images was completed in multiple cycles until the cross-correlational shift between images was less than 1 pixel in either the X or Y plane. Second, the entire tomographic data set (image stack) was aligned using the 10 or 15 nm colloidal gold added to the sample before imaging. At least 10 gold particles were selected as fiducial markers, which were then identified and tracked in each individual image by the Inspect3D software. Using the known tilt angles for each image and the location of the fiducial gold markers, the software could then globally align the image stack. The aligned stack could be output as a movie file or as a data file for the generation of 3D reconstructions. To do so, 10 iterations of the simultaneous iterative reconstruction technique (SIRT) were performed (Beniac et al. 2012). Initial alignments were performed by Melissa Rabb. Final analysis was performed by Dr. Daniel Benaic (NML).

2.23.3 Sub-tomogram analysis

Sub-tomogram image analysis of the cell section tomography was performed using the Automated Recognition of Geometries, Objects, and Segmentations (ARGOS) version 2.0.2 software package (FEI). Sub-tomograms at 60, 80, and 120 pixels were extracted from the cell section data using the Chimera software (Pettersen et al. 2004). These sub-tomograms contained a circular (vertical cross-section) segment of the nucleocapsid-like particles or NP tubes. The ARGOS software was then employed to search the original tomogram for similar structures using a six dimensional search matrix (3 positional variants and 3 rotational variants). Identified sub-tomograms were then aligned to the original template sub-tomogram and averaged with a filter to minimize the missing wedge effect. This process was then repeated using the average structure as the initial sub-tomogram template. The whole procedure was repeated several more times to enhance analysis. The UCSF Chimera software was used by Dr. Daniel Beniac to model and visualize the 3D reconstruction of the NP/VP24/VP35 nucleocapsid-like particles within a cell section.

Chapter 3. Analysis of novel Ebola virus proto-nucleocapsids and thin sections of cells transfected with Ebola virus NP, VP24, VP30, VP35, and VP40

3.1 Rationale

Cryo-EM has enabled the preservation of near native Ebola virus in vitrified water. Single particle and tomographic image analysis of frozen-hydrated Ebola virus has solved the nucleocapsid structure to 19 Å (Beniac et al. 2012). At this resolution protein densities are visible; however, more specific details of the protein arrangements and stoichiometry within the nucleocapsid remain elusive (Beniac et al. 2012). Structural analysis of the Ebola virus nucleocapsid within native virions is hindered by the presence of the viral envelope, which consists of the lipid bilayer, the VP40 hexameric lattice, and randomly distributed glycoproteins (Beniac et al. 2012; Booth et al. 2013; Bornholdt et al. 2013). These additional viral components are not helically ordered and since they add density and thickness to the specimen they reduce the contrast and detail of the nucleocapsids. Thus, the imaging and analysis of envelope-free nucleocapsids might be expected to result in a higher resolution structure than reconstructions from whole virus particles. Tomographic analysis of the Ebola virus enables the separation of nucleocapsid from the lipid bilayer by choosing (subvolumes) from the middle of the tomogram. However, the quality of data is still reduced by the viral envelope, as the images are of whole virus particles (Beniac et al. 2012; Cope et al. 2010). The principle aim of this thesis was to isolate and characterize envelope-free Ebola virus nucleocapsids derived from either whole virus or heterologous expression of nucleocapsid proteins. As a first step, I sought to release nucleocapsids from enveloped Ebola virus particles.

In addition, conventional electron microscopy of ultrathin sections of cells expressing the Ebola virus NP, VP24, and VP35 proteins suggested that the ~50 nm diameter

cylindrical particles produced by transfection were indistinguishable from those observed in Ebola virus-infected cells at selected magnifications (Huang et al. 2002; Noda et al. 2006). Before I attempted to isolate envelope-free nucleocapsid-like particles, I first needed to confirm that nucleocapsid protein expression and protein-protein interactions were occurring as expected within transfected cells. Furthermore, I was curious as to whether higher magnification images or tomographic image processing could provide more information on the assembly and structure of Ebola virus nucleocapsid-like particles.

3.2 Hypothesis

Treatment of Ebola virus particles with a non-ionic detergent (NP-40) will result in the disruption of viral envelopes and release of native viral nucleocapsids that are free of lipid bilayers, VP40 matrix interactions, and glycoprotein trimers.

3.3 Objectives

1. Assess the effects of detergent treatment on Ebola virus particles and nucleocapsids
2. Analyze proto-nucleocapsids by single-particle imaging analysis and generate a 3D reconstruction of this structure
3. Generate expression vectors for Ebola virus NP, VP24, VP30, VP35, VP40
4. Confirm protein expression by SDS-PAGE, western blot, and/or mass-spectrometry
5. Fix and embed transfected cells in resin for ultramicrotomy
6. Section resin-embedded cells and stain for electron microscopy
7. Perform tomography on select cell sections

3.4 Results

3.4.1 Imaging of envelope-free proto-nucleocapsids

To generate envelope-free nucleocapsids, Shane Jones from the Special Pathogens Group at the NML kindly propagated Ebola virus (Zaire, Kitwit strain) for us in the BSL 4 laboratory. The virus particles were harvested 14 days post-infection, treated with 0.15% NP-40 or PBS as a control, and fixed with 4% PFA. This protocol was based on a similar study by Bharat et al. (2012), in which Ebola VLPs were treated with 0.15% NP-40 to release NP-RNA structures. I dialyzed the fixed samples to remove the PFA and subsequently observed them using negative stain TEM. While the concentration of NP-40 (0.15%) was greater than the critical micelle concentration of NP-40 (0.02%), incubation of virus particles at this NP-40 concentration was not sufficient to release nucleocapsids from their viral envelopes (Figure 6).

Surprisingly, TEM of the control Ebola virus sample revealed the presence of nucleocapsid-like particles after negative stain (Figure 7). Initial measurements of these nucleocapsid-like particles using ImageJ software assigned an average diameter of 29.67±2.93 nm and average pitch of 5.56±1.36 nm. Subsequent image analysis (discussed in Section 3.4.2) calculated a more accurate outside diameter of 30.5 nm diameter and inside diameter of 20 nm, which is narrower than the 41 nm diameter of the full Ebola virus nucleocapsid. In addition, image analysis calculated a pitch of 6.96 nm with 10.81 repeats per helical turn, which is identical to the pitch of the full nucleocapsid. These condensed helical particles were relatively straight and ordered with regions of loosely coiled protein/RNA at one or both ends of the helical rod and sometimes connecting

multiple particles together (Figure 8). End on views of these particles suggested that they were hollow cylinders (Figure 9).

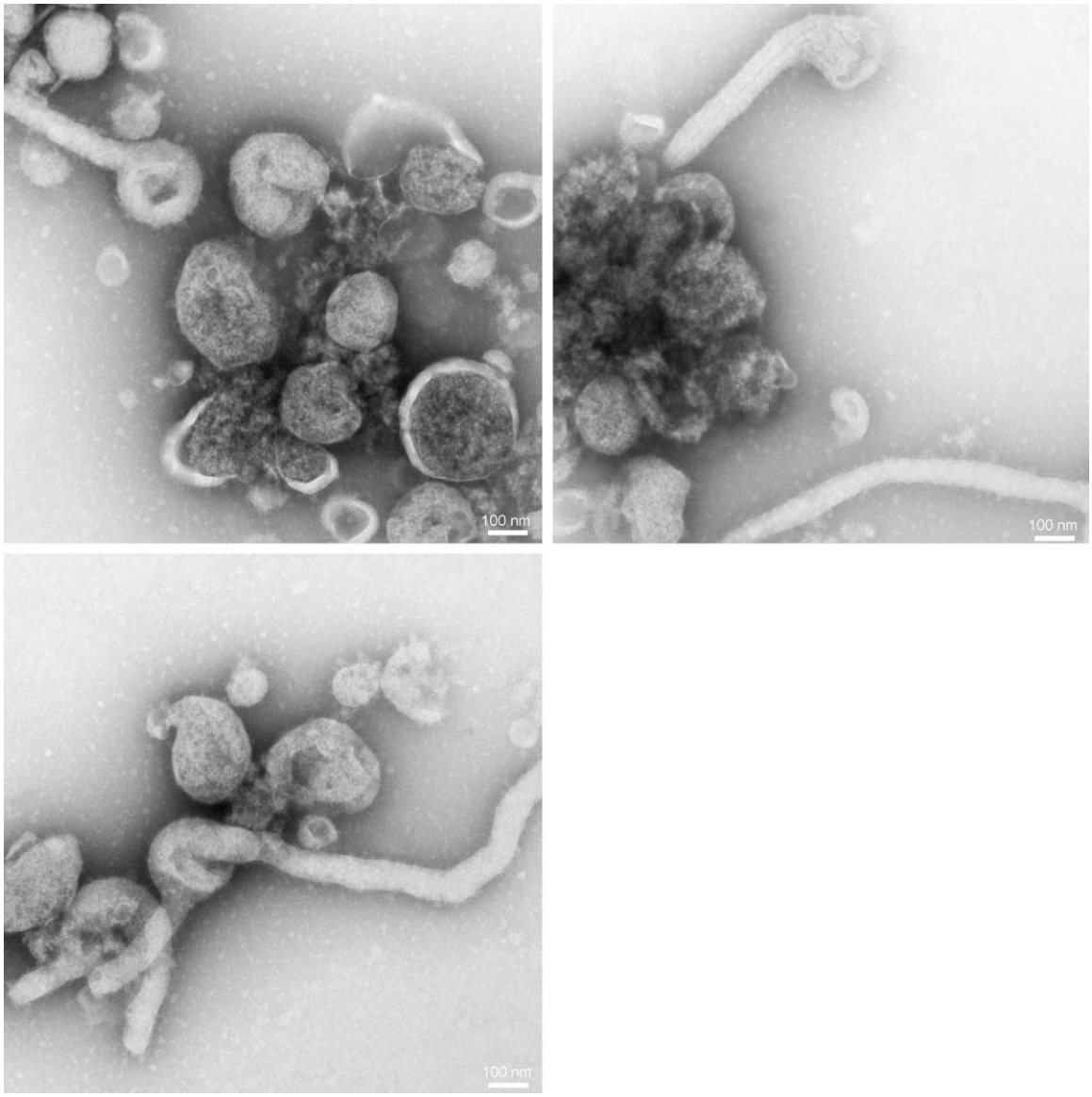

Figure 6. Treatment of Ebola virus particles with 0.15% NP-40. Ebola virus was propagated in VeroE6 cells for 14 days. Purified virus was treated for 10 min with 0.15% NP-40 in 50 mM NaCl lysis buffer and fixed overnight with 4% PFA. Samples were dialyzed and stained with methylamine tungstate.

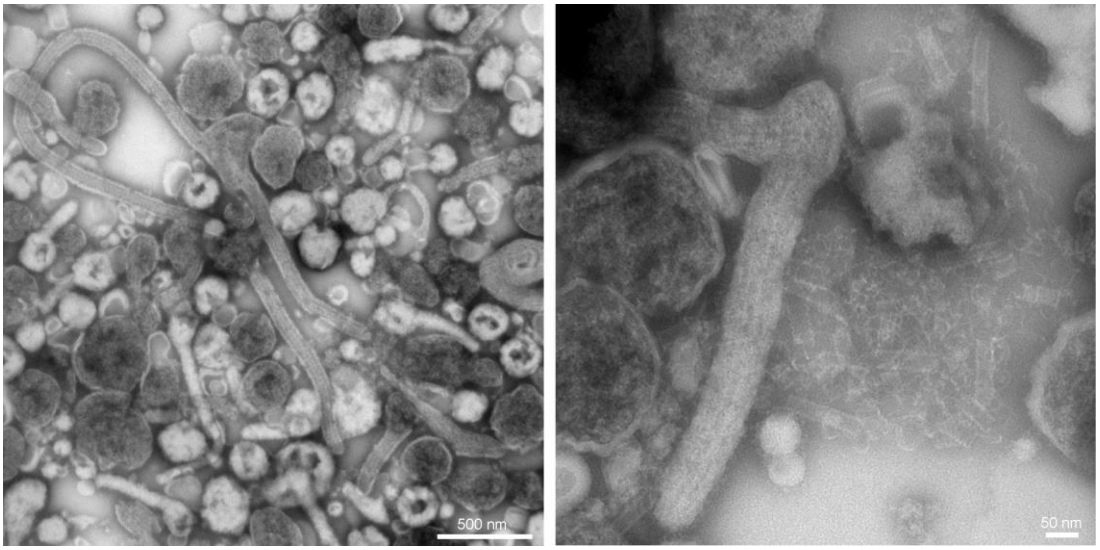

Figure 7. Nucleocapsid-like particles observed in control Ebola virus sample. Fourteen days post-infection, viral particles were collected and fixed with 4% PFA. Samples were dialyzed and stained with methylamine tungstate.

As these samples were previously fixed, immunogold labeling to confirm protein identification was not attempted. However, particles similar in size and appearance have been generated in the past by expression of a NP C-terminal truncated mutant (NP_{1-451}) (Bharat et al. 2012; Watanabe et al. 2006). In addition, the inner NP helix of the Ebola virus nucleocapsid has been calculated as ~20 nm in diameter (Beniac et al. 2012). As such, the 30.5 nm particles observed in my control Ebola virus sample are consistent with a single-layered NP helix and we have named these "proto-nucleocapsids" (Booth et al. 2013)(manuscript in process) (Figure 9). Based on the high number of intact viral particles observed and relatively long propagation, these proto-nucleocapsids were likely released from infected cells late in infection and/or during the freeze-thaw process (Booth et al. 2013).

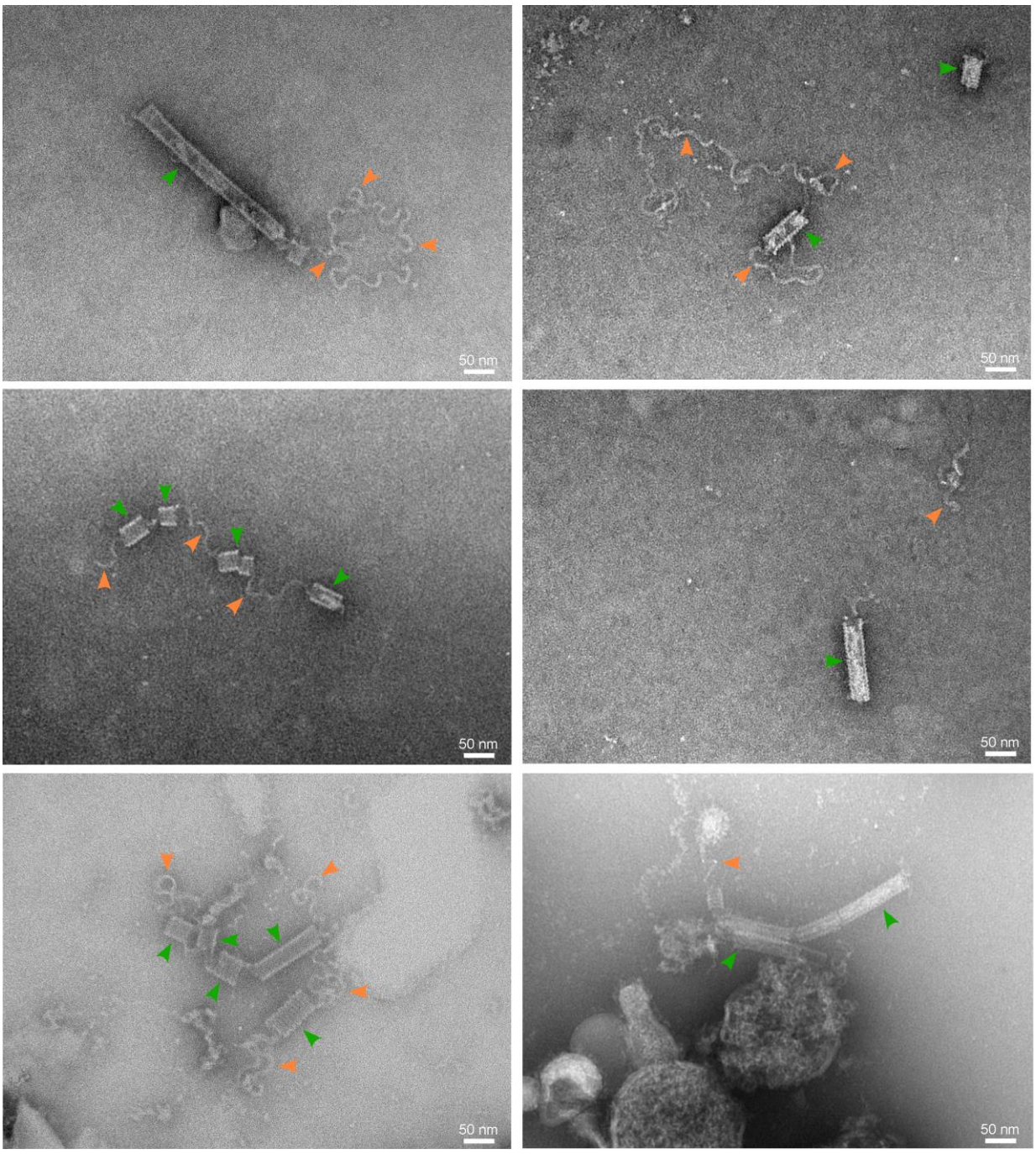

Figure 8. Higher magnification electron micrographs of novel proto-nucleocapsids. Ebola virus was propagated for 14 days, purified by ultracentrifugation and fixed with 4% PFA. Samples were dialyzed, applied to thin-carbon Quantifoil grids, and stained with methylamine tungstate. Orange arrowheads indicate loose protein-RNA threads and green arrowheads indicate longitudinal cross-sections of proto-nucleocapsids.

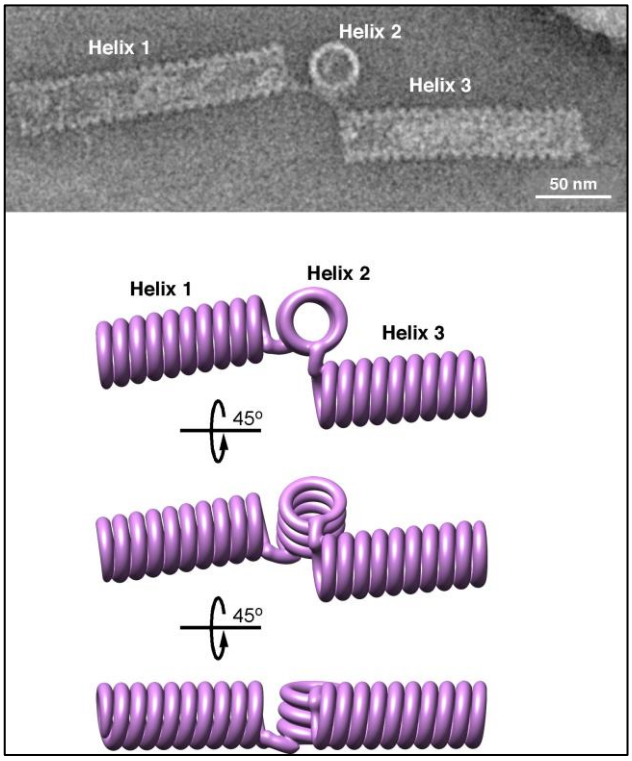

Figure 9. 3D schematic model of helical proto-nucleocapsids. The proto-nucleocapsid was stained with methylamine tungstate on thin-carbon Quantifoil grid and modeled using USCF Chimera.

3.4.2 Single particle image analysis of proto-nucleocapsids

While single-layered nucleocapsids, which we call proto-nucleocapsids have been reported previously, we were the first to describe this structure as a single-layered NP helix, rather than the full nucleocapsid (Booth et al. 2013; Noda et al. 2006). To further study these particles, control Ebola virus samples were applied to previously prepared thin-carbon coated Quantifoil grids and stained with methylamine tungstate (Figure 8). Indirect carbon evaporation provides the same thermostability and mechanical strength as direct carbon-coating, but lacks the thickness irregularities that are common with direct carbon-coating. To determine the structure of the proto-nucleocapsids, 5620 images were evaluated by linear reference-free single particle 2D analysis to identify common structural motifs and sort images into classes based on these commonalities. 2D class averages of the proto-nucleocapsid demonstrated a left-handed, condensed helical particle with short spokes or ribs (Figure 10). Each "spoke" was globular with no exterior densities, suggesting the absence of a bridge or arm-like structure which further supports the hypothesis that this particle is comprised of NP only. In addition, a cross-section of the proto-nucleocapsid illustrates the 20 nm internal diameter and strongly helical nature of these particles. A 3D reconstruction of the proto-nucleocapsid based on the 2D class averages and previous Ebola virus nucleocapsid tomographic data established an 18.5 Å model in which each spoke on the rod represents an individual NP molecule (Figure 10).

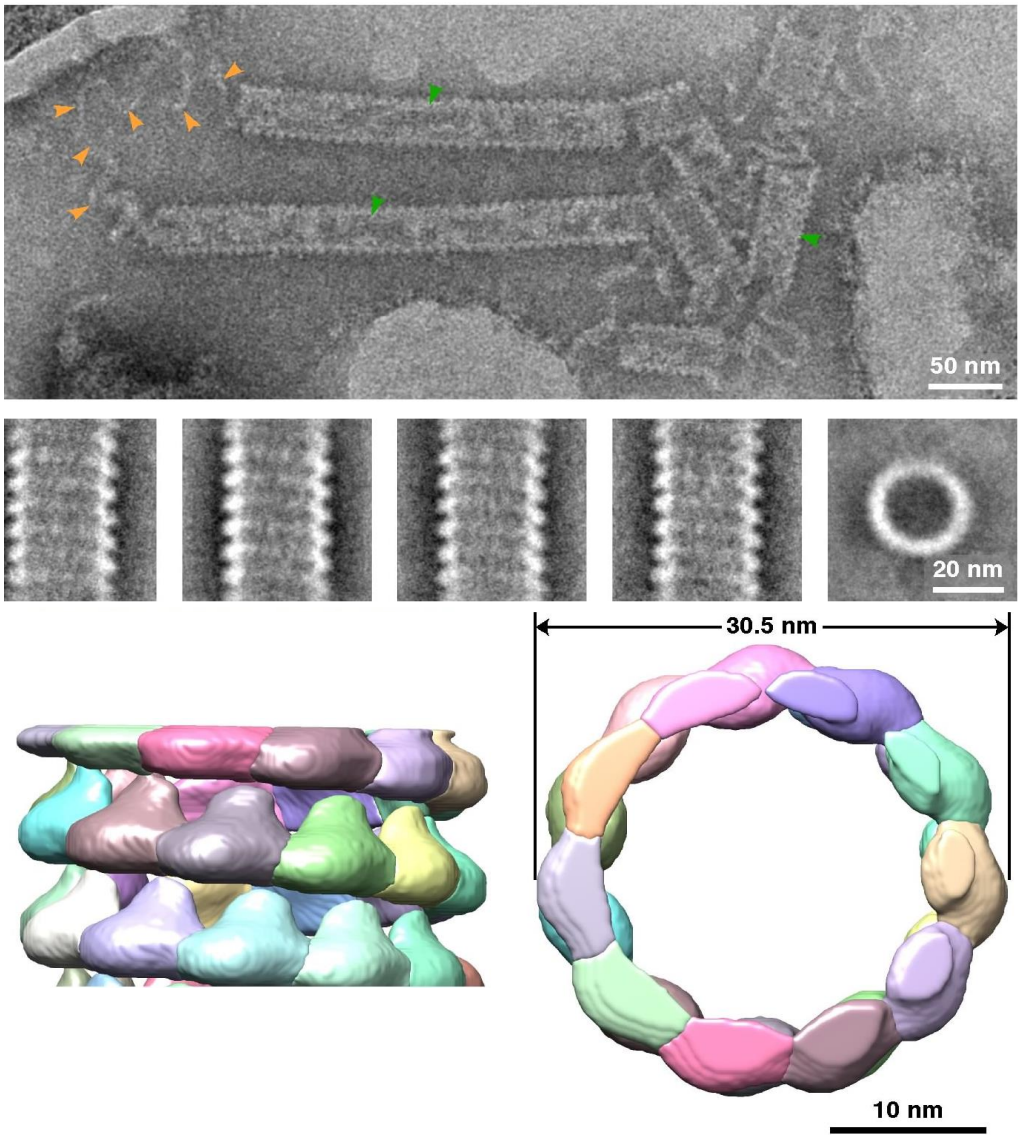

Figure 10. Image processing of proto-nucleocapsids. Top panel: Negative stained proto-nucleocapsids imaged on thin-carbon Quantifoil grids. Orange arrowheads indicate loose protein-RNA threads and green arrowheads indicate longitudinal cross-sections of proto-nucleocapsids. **Middle panel:** Linear 2D averages of proto-nucleocapsids, showing longitudinal and end-on cross-section averages. **Bottom panels:** 18.5Å reconstructions of the proto-nucleocapsid showing longitudinal (left) and end-on (right) views with individual NP subunits represented as different colours.

3.4.3 Transfection of 293T cells

Ebola virus cDNA was synthesized and subcloned into the pCAGGS vector by Genscript Inc. after the addition of appropriate restriction enzyme sites (as described in Chapter 2.2). Expression of NP, VP24, VP30, and VP35 was visible by SDS-PAGE after gradient ultracentrifugation and Coomassie blue stain (Figure 11). Expression of NP, VP35, and VP40 was further confirmed by Western blot and mass spectrometry (Figure 12; Chapter 9.2). Expression of VP40 was difficult to differentiate in cell lysate samples by SDS-PAGE; however, SDS-PAGE of purified VLPs strongly demonstrated the presence of VP40 (Figure 11). Expression of VP24 and VP30 was further confirmed by mass spectrometry (Chapter 9.2)

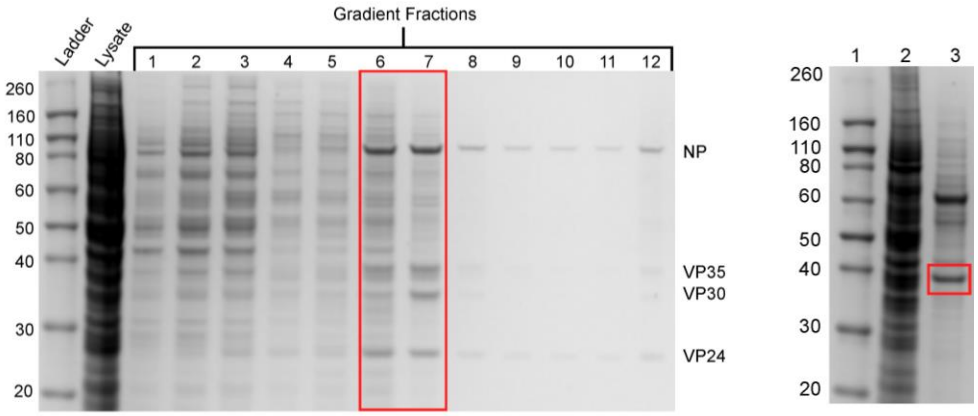

Figure 11. Detection of Ebola virus nucleocapsid-associated proteins after differential ultracentrifugation or VLP collection. Left panel: 293T cells were lysed by hypotonic freeze/thaw and layered onto a 15-30% iodixanol gradient. Fractions were collected top-down, with Fraction 1 representing the first fraction collected. SDS-PAGE results were detected by Coomassie blue stain. Red box indicates fractions chosen for further purification. **Right panel:** 48 hours post VP40 transfection, cell culture supernatant was collected and layered onto a 20% sucrose gradient. Pellets were resuspended after ultracentrifugation and SDS-PAGE was performed. Red box indicates VP40 band. Lane 1: ladder; Lane 2: VP40-transfected cell lysate; Lane 3: purified VP40 VLP.

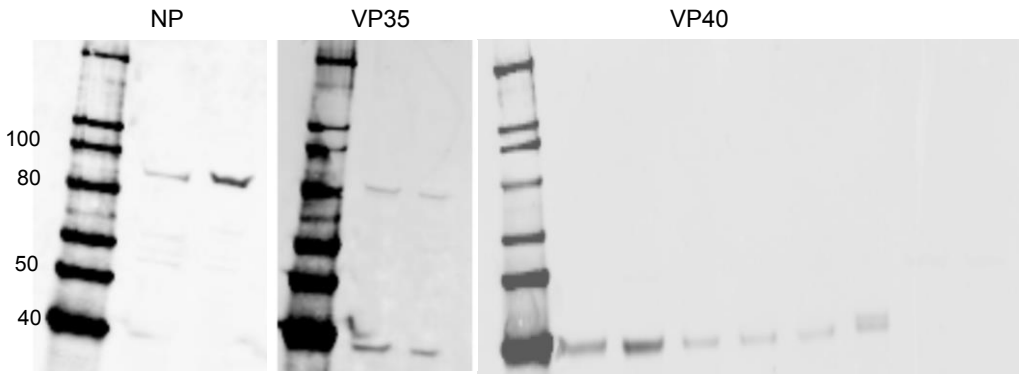

Figure 12. Western blot detection of NP, VP35, and VP40. Forty-eight hours post transfection of NP (first panel), VP35 (second panel), or VP40 (third panel), 293T cells were lysed in isotonic lysis buffer and layered onto 15-30% iodixanol gradients. **NP and VP35 blots**: Lane 1: MagicMark ladder; Lane 2: lysate; Lane 3: fraction 6. **VP40 blot**: Lane 1: MagicMark ladder; Lane 2: lysate; Lanes 3-7: fractions 1-6.

3.4.4 Thin sections

Various Ebola virus nucleocapsid protein combinations were expressed to evaluate their effect on the assembly of intracellular nucleocapsid-like particles. Forty-eight hours post-transfection cells were fixed, stained with osmium tetroxide, dehydrated and resin embedded. Sections were further stained with lead citrate and uranyl acetate prior to TEM.

3.4.4.1 NP expression

As expected, expression of NP alone resulted in the generation of ring-like particles within the cytoplasm of transfected cells (Figure 13) (Watanabe et al. 2006). These particles formed inclusion bodies that were noticeable even at low magnifications because of the illusion of striations within them (Figure 13). These NP tubes were approximately 25 nm in diameter.

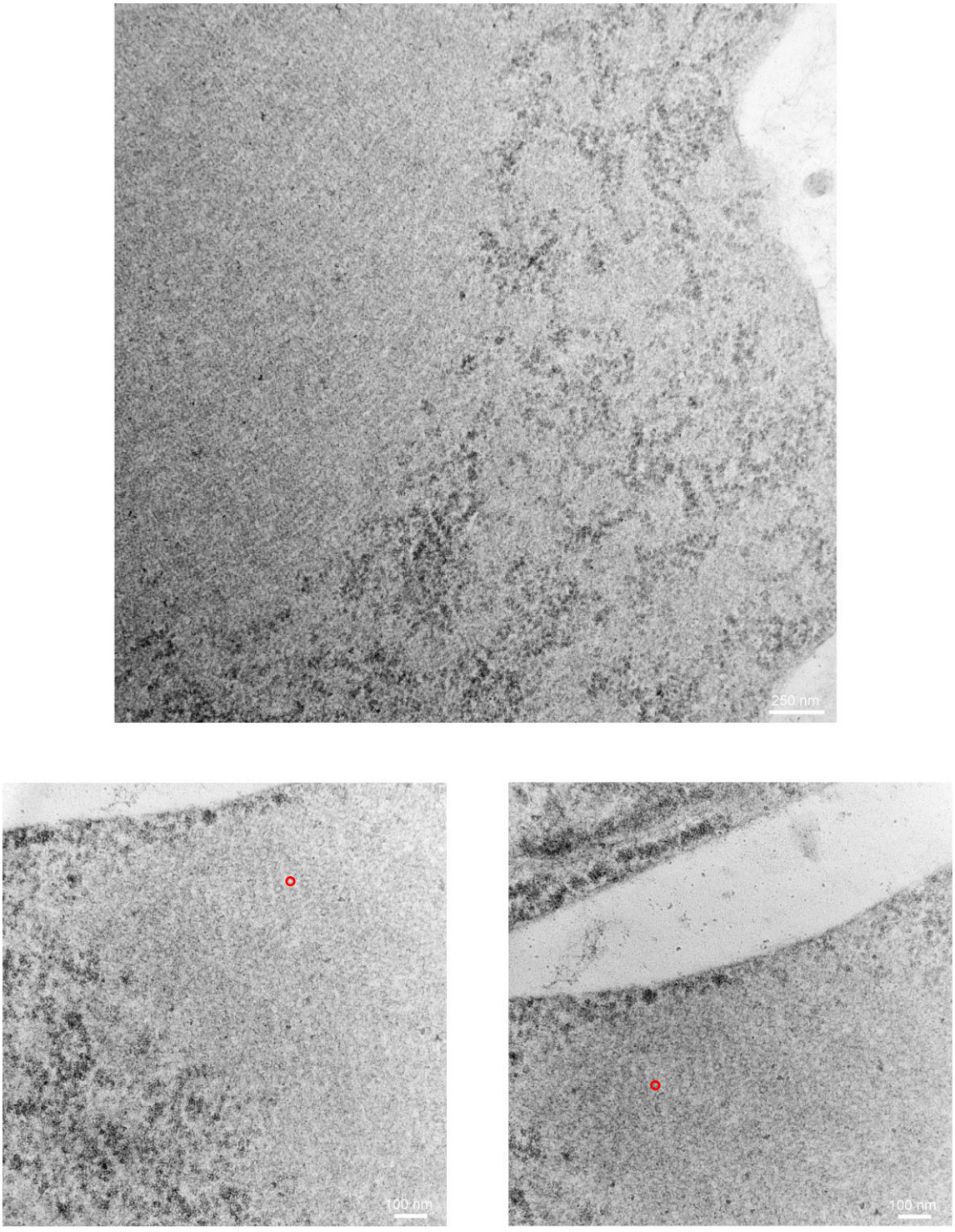

Figure 13. Expression of NP results in ~25 nm helical particles. Cells were harvested 48 hours after transfection and subjected to staining, dehydration, and embedding. Sections were stained with lead citrate and uranyl acetate. Examples of NP ring particles are outlined in red.

3.4.4.2 NP/VP24/VP35 expression

Co-expression of NP, VP24, and VP35 resulted in large, electron-dense inclusion bodies within transfected cells (Figure 14). Nucleocapsid-like particles had an average diameter of ~50 nm, which is consistent with previous research (Huang et al. 2002; Noda et al. 2006). In contrast to expression of NP alone, thin-sections of cells transfected with all three proteins resulted in both longitudinal and transverse profiles of the nucleocapsid tubes. While greater detail was observed in high magnification images, resolution was still too low to observe the characteristic "herring-bone" pattern observed in cryo-EM images of the Ebola virus nucleocapsid (Figure 14).

3.4.4.3 NP/VP24/VP35/VP30 expression

The addition of VP30 to the transfection panel did not visibly affect nucleocapsid-like particles or the transfected cells. Large inclusion bodies were observed within the cytoplasm, with cellular material pushed to the outside edge (Figure 15). High magnification images of the nucleocapsid-like particles did not indicate any alterations to their assembly when VP30 was present (Figure 15).

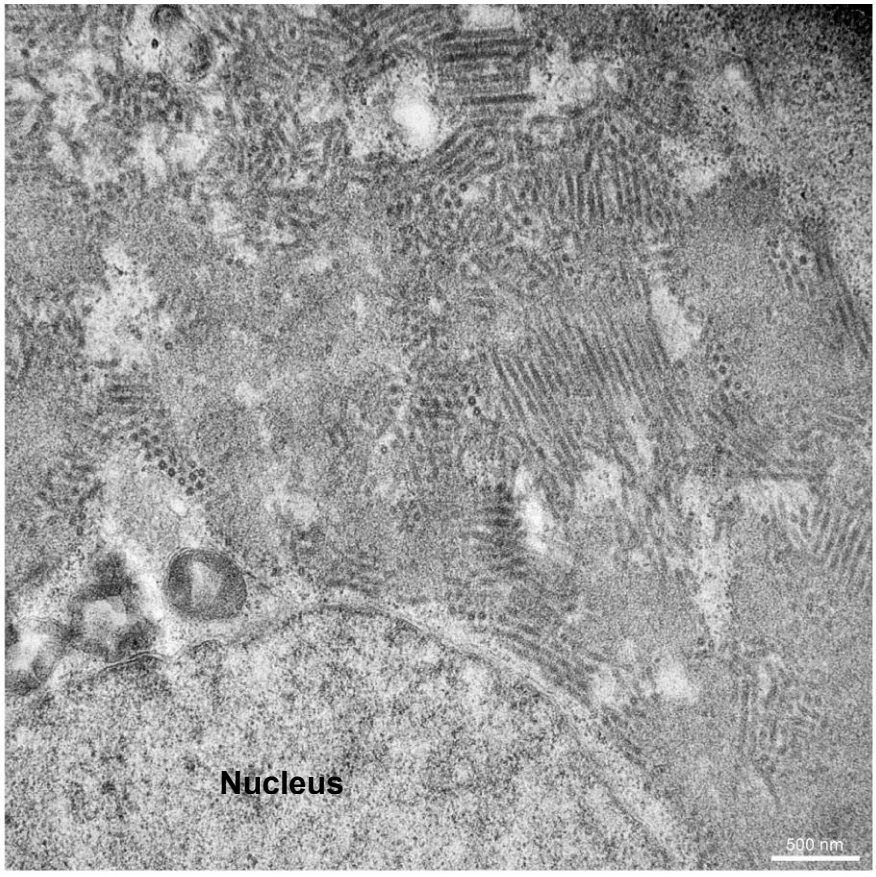

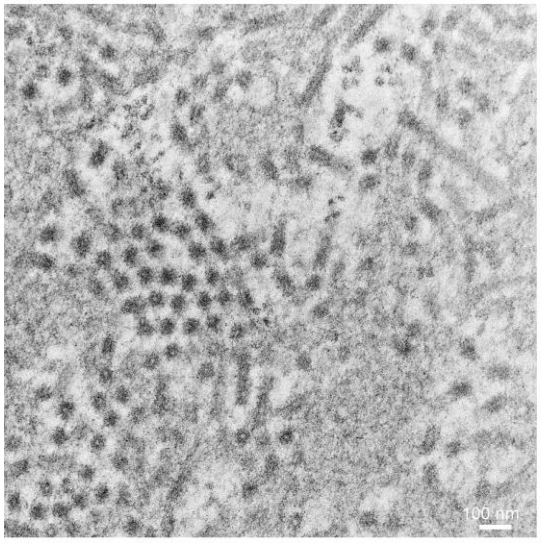

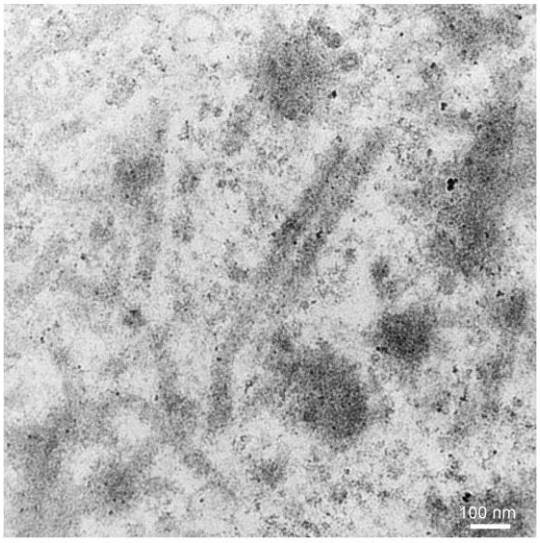

Figure 14. Co-expression of NP, VP24, and VP35 generates nucleocapsid-like particles visible by cell section. Sections were stained with lead citrate and uranyl acetate.

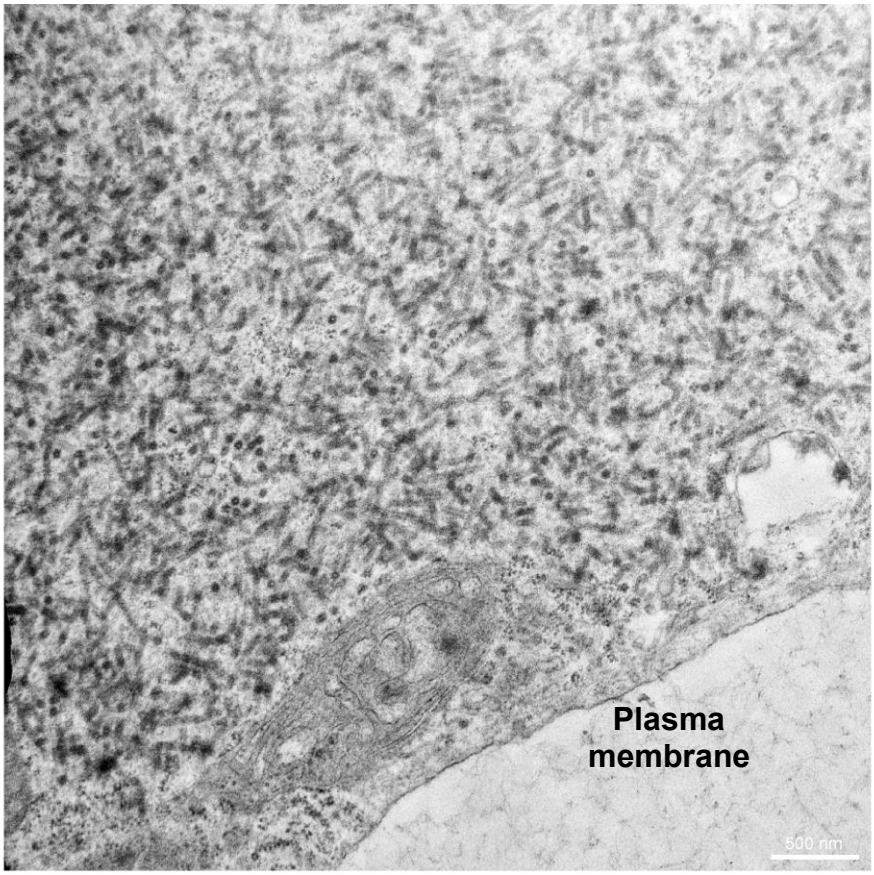

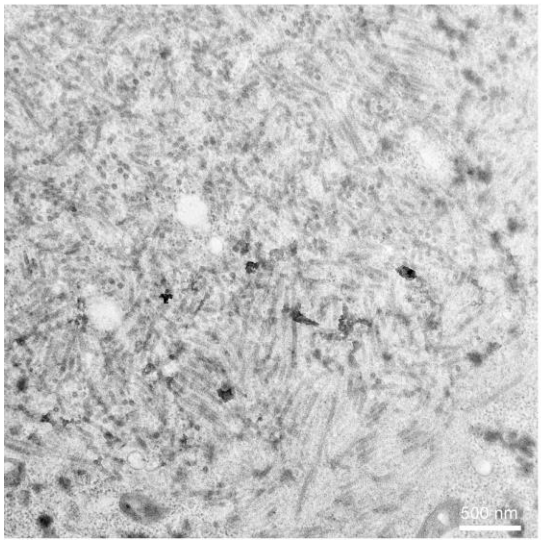

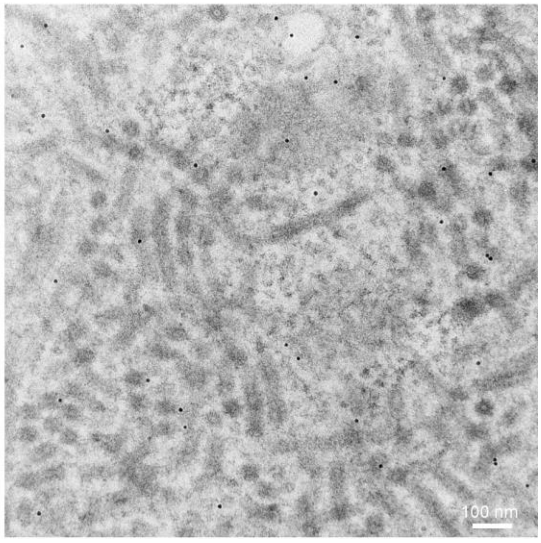

Figure 15. Transfection of NP, VP24, VP35, and VP30 generates nucleocapsid-like particles. Sections were stained with lead citrate and uranyl acetate.

3.4.4.4 NP/VP24/VP35/VP40 expression

The addition of the matrix protein VP40 resulted in a few well-characterized changes to nucleocapsid location and cell morphology. Large inclusion bodies were still observed within the cell cytoplasm; however, nucleocapsid-like particles were also observed at the plasma membrane, budding from the plasma membrane, and detached from the cell within the resin (Figure 16). The transfected cells also displayed membrane ruffling, which is a phenomenon observed in the presence of VP40. Although the mechanism is not fully understood, it is thought that the interaction between VP40 and the plasma membrane results in the production of excess plasma membrane or the expansion of the plasma membrane such that it ripples off the cell surface (Figure 16) (Bornholdt et al. 2013; Noda et al. 2002). Similar to the other protein combinations, resolution was too low to determine any specific details of the nucleocapsid-like particles.

3.4.4.5 NP/VP24/VP35/VP30/VP40 expression

Lastly, co-expression of the five Ebola virus nucleocapsid proteins was investigated to observe their combined effects on assembly. Intracellular nucleocapsid-like particles did not appear any different from previous protein combinations at low or high magnification. As described above, the presence of VP40 led to the phenomenon of plasma membrane ruffling (Bornholdt et al. 2013; Noda et al. 2002). Nucleocapsid-like particles were also observed at the plasma membrane, in the process of budding, and in VLPs outside the cell (Figure 17).

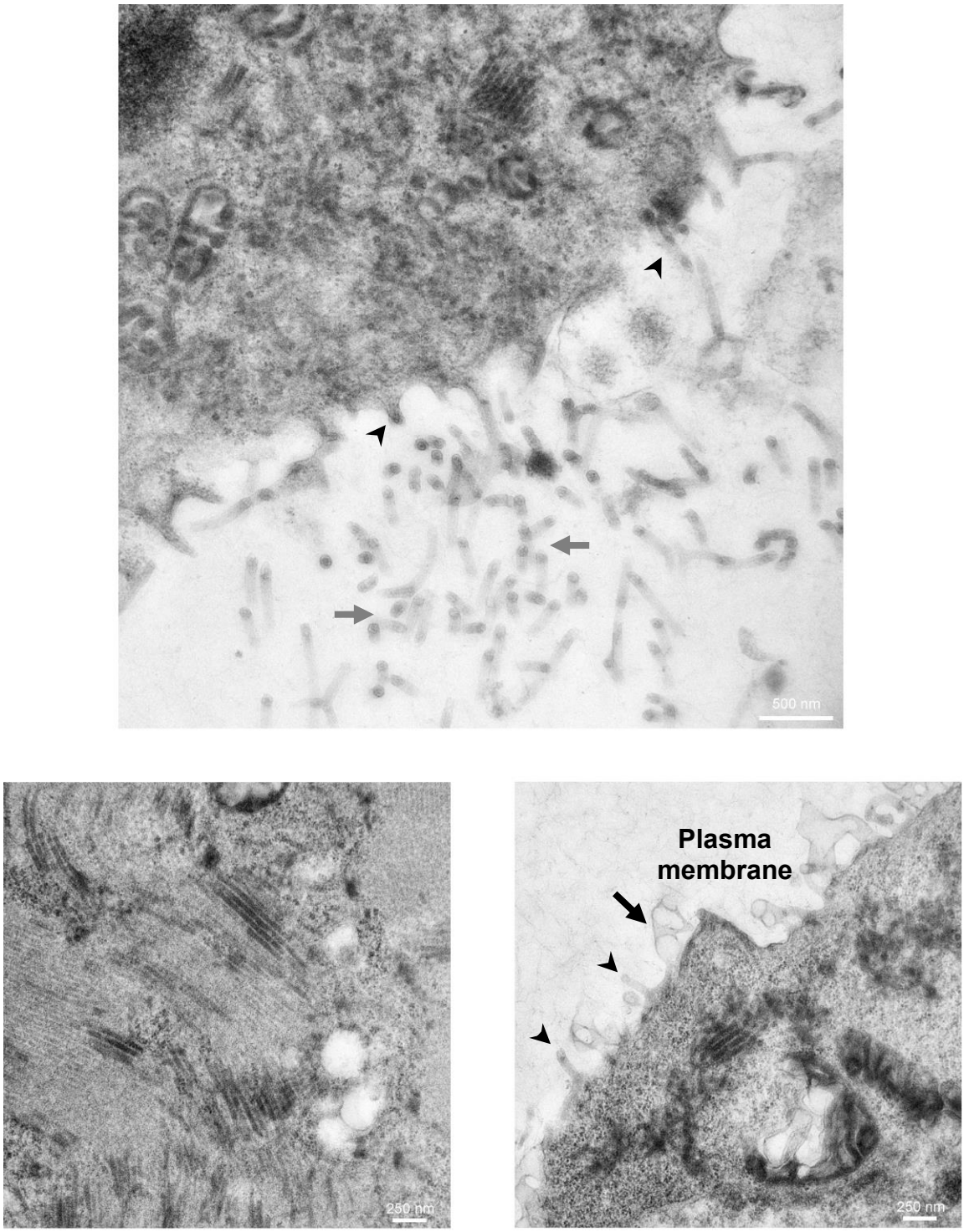

Figure 16. Expression of VP40 with NP, VP24, and VP35 results in the assembly of nucleocapsid-like particles and plasma membrane ruffling. Sections were stained with lead citrate and uranyl acetate. Black arrowheads indicate budding VLPs; black arrows indicate plasma membrane ruffles; grey arrows indicate budded VLPs.

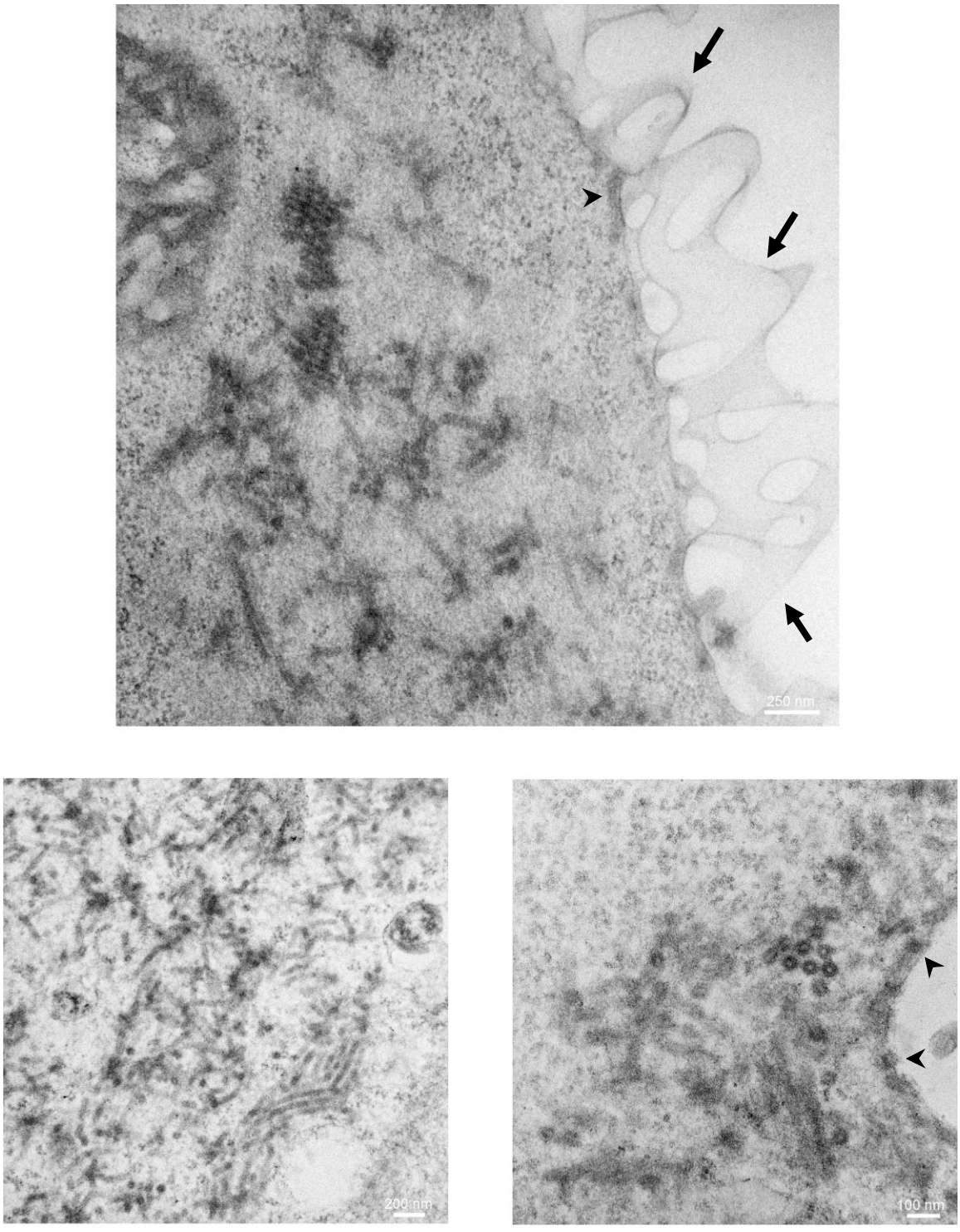

Figure 17. Expression of NP, VP24, VP35, VP30, and VP40 generates nucleocapsid-like particles within cell sections. Sections were stained with lead citrate and uranyl acetate. Black arrows indicate plasma membrane ruffles; black arrowheads indicate nucleocapsid-like particles on the cytosolic side of the plasma membrane.

3.4.5 Tomography of thin sections

To gain more information on the intracellular nucleocapsid-like particles, tomography was performed on cell sections of NP transfected alone, NP/VP24/VP35 or NP/VP24/VP35/VP30. Thicker sections (~170 nm) were chosen to increase the amount of data in the Z axis and images were taken at each degree from ±56°, with a total dose/tomogram of 100 electrons/Å^2. Tomographic image analysis of NP-transfected cell sections illustrated the ~30.5 nm tube-like particles formed by this protein when expressed alone (Figure 18). Tomograms of NP/VP24/VP35 or NP/VP24/VP35/VP30-transfected cell sections enabled the tracking of vertically and horizontally orientated tube-shaped particles through the Z axis and it was possible to observe some particles bending through the axis (Chapter 9.4: Movie S1; Movie S2). Using the tomography data, specific subsets of images were selected and averaged together. These middle Z stacks often provide the best overall representation of the tomogram. In the first column of Figure 18, adjacent images have been averaged to generate representative images of NP alone, NP/VP24/VP35, or NP/VP24/VP35/VP30 nucleocapsid-like particles. Unlike the negative stain micrographs described in Section 3.4.4, these subvolumes provide higher resolution images of the NP tubes and nucleocapsid-like particles. NP/VP24/VP35 and NP/VP24/VP35/VP30 nucleocapsid-like particles were on average 47.5 nm in diameter, which is comparable to the full Ebola virus nucleocapsid. The addition of VP30 did not result in any demonstrable changes to structure or size.

A 3D reconstruction of NP/VP24/VP35 intracellular nucleocapsid-like particles demonstrates their hollow, helical nature and their angled positions within the cell (Figure

19). Unfortunately, resolution was still not high enough to identify the "herring-bone" structure of the nucleocapsid, which is why the 3D reconstruction appears smooth.

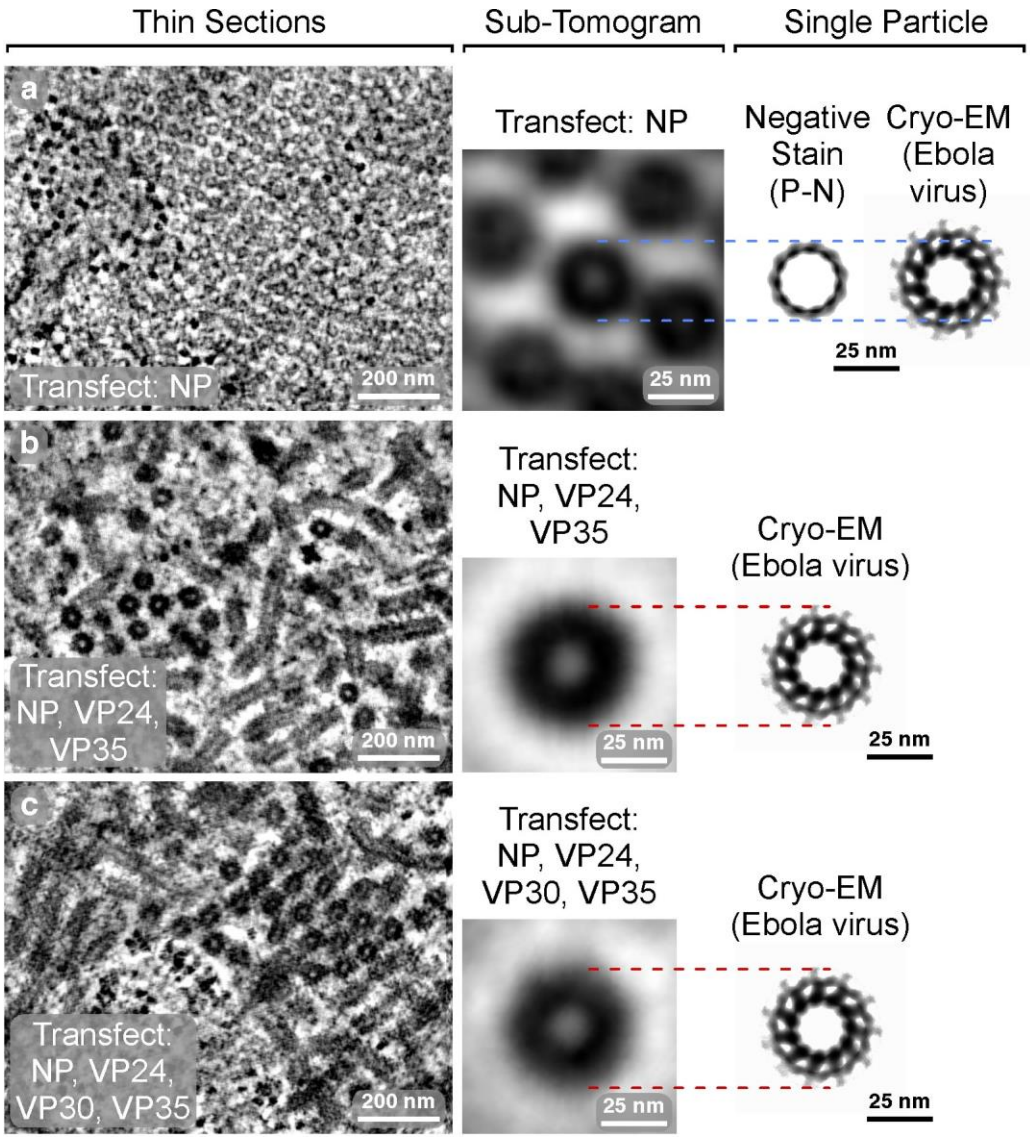

Figure 18. Image analysis of cell section tomograms. 293T cells were transfected with (A) NP; (B) NP/VP24/VP35, or (C) NP/VP24/VP35/VP30 and resin embedded 48 hours later. The first column "Thin Sections" consists of Z-slice averages from dual-axis tomograms of the transfected cell sections. The middle column contains projection images of the sub-tomogram averages from the dual-axis tomograms. The final column shows projection images calculated by single particle image analysis of either the proto-nucleocapsid or full Ebola virus nucleocapsid. (P-N): Proto-nucleocapsid.

However, analysis of sub-tomograms from each protein combination revealed that the NP tube diameter is consistent with both the diameter of the proto-nucleocapsid described in Section 3.4 and the inner layer of the full Ebola virus nucleocapsid (Figure 2; Figure 18). Transfection of NP, VP24, and VP35 with or without VP30 was sufficient to produce intracellular nucleocapsid-like particles that were equivalent in diameter to the full Ebola virus nucleocapsid (Figure 18).

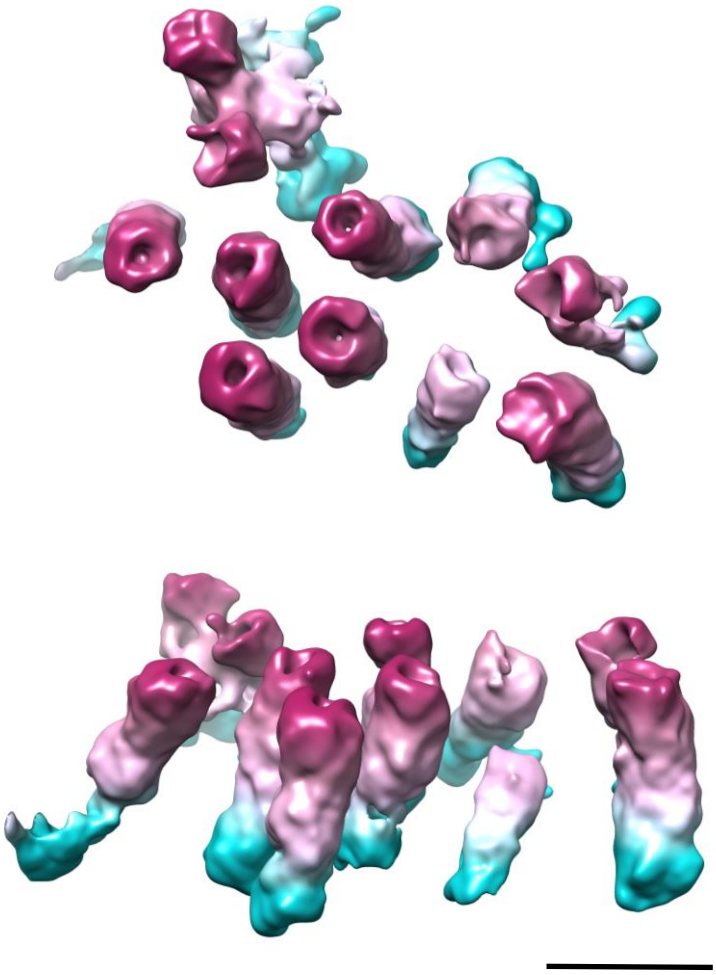

Figure 19. 3D reconstruction of nucleocapsid-like particles observed in a NP/VP24/VP35 transfected cell. Top panel: Original orientation of particles within cell section. **Bottom panel:** Orientation was rotated 90° to show section depth. Blue colour indicates the bottom of the section and the burgundy colour indicates the top of the section. Section thickness was ~170 nm. Error bar: 100 nm.

3.5 Summary

Treatment of Ebola virus particles with 0.15% NP-40 was not sufficient to release nucleocapsids from their viral envelopes. However, harvesting of the virus late in infection resulted in the surprising discovery of envelope-free proto-nucleocapsids. These particles displayed the same average pitch (6.96 nm) and number of repeats per turn (10.81) as the native Ebola virus, but were only 30.5 nm in diameter, rather than 41 nm. Single particle image analysis revealed a tightly wound helical structure with small globular spokes and no arm-like densities, attributed to single NP molecules.

Transmission electron microscopy of ultrathin sections of transfected cells confirmed that the production of ~50 nm nucleocapsid-like particles required the expression of only NP, VP24, and VP35. Expression of NP alone resulted in ring-like particles visible in cell sections. Image analysis of dual axis tomograms of transfected cell sections revealed that the NP particles were the correct diameter for the inner nucleocapsid layer and that expression of NP, VP24, and VP35 with or without VP30 was required to form the larger ~50 nm tubes. When VP40 was present, nucleocapsid-like particles were visible at the various stages budding: interaction with the plasma membrane, protruding through the plasma membrane, and budded VLPs within the section resin. The resolution of the negative stain micrographs and tomograms was not sufficient to distinguish the "herring-bone" structure of the nucleocapsid; however, our results support the theory that VP30 is located within the inner nucleocapsid, as its addition did not change the nucleocapsid-like particle diameter.

Chapter 4. Characterization of Ebola virus nucleocapsid-like particles

4.1 Rationale

Once I had confirmed that the Ebola virus nucleocapsid proteins were behaving as expected within transfected cells, I next investigated the synthesis, isolation, purification, and characterization of the nucleocapsid-like particles. Two different lysis methods and sodium chloride concentrations were examined in this Chapter. Lysis buffer containing the detergent NP-40 was chosen due to its use in previous studies. Both Bharat et al. (2012) and Noda et al. (2010) treated transfected cells with a NP-40 lysis buffer in order to isolate Ebola virus NP particles (Bharat et al. 2012; Noda et al. 2010). Cell lysis by three rounds of freeze/thaw at -80°C was the second method chosen as it is a common approach for Ebola virus propagation (Cutts et al. 2016). The Ebola virus samples discussed in Chapter 3.4 were harvested by this freeze/thaw method. Since my preliminary studies suggested that hypotonic lysis buffer lead to enhanced cell lysis/greater protein detection, I compared hypotonic (50 mM) versus isotonic (150 mM) sodium chloride concentrations for both lysis methods.

4.2 Hypotheses

1. Nucleocapsid-like particles visible in ultrathin sections of cells can be released from transfected cells and will retain a substantially similar structure to that present in intact virions.
2. I hypothesize that the method of cell lysis will not significantly affect the assembled structure of the nucleocapsid-like particles.

4.3 Objectives

1. Lyse transfected cells by hypotonic or isotonic lysis buffer, or by freeze/thaw in hypotonic or isotonic PBS
2. Purify nucleocapsid-like particles by differential ultracentrifugation
3. Isolate nucleocapsid-like particles from gradient fractions
4. Image nucleocapsid-like particles by negative stain EM
5. Measure pitch and diameter of nucleocapsid-like particles
6. Identify any significant differences between lysis methods and/or protein combinations

4.4 Results

4.4.1 Hypotonic lysis buffer

For my initial studies, a hypotonic lysis buffer (50 mM NaCl, 1% NP-40, 10 mM Tris-HCl, pH 7.5, 1mM EDTA, PIC) was used to release nucleocapsid-like particles from transfected cells.

4.4.1.1 Single transfections

Expression vectors were first transfected individually into 293T cells to confirm protein expression and evaluate protein migration through 15-30% iodixanol density gradients (Figure 20). With the exception of NP, SDS-PAGE of gradient fractions demonstrated no obvious patterns of migration and it was often difficult to differentiate the protein of interest from the cellular proteins (Figure 20). In contrast to the other nucleocapsid proteins, NP migration was distinguishable from cellular proteins, with the highest amount of protein visible in fractions 5-7 (Figure 21a). NP, VP35, and VP40 migration through the gradient was confirmed by western blot (Figure 12).

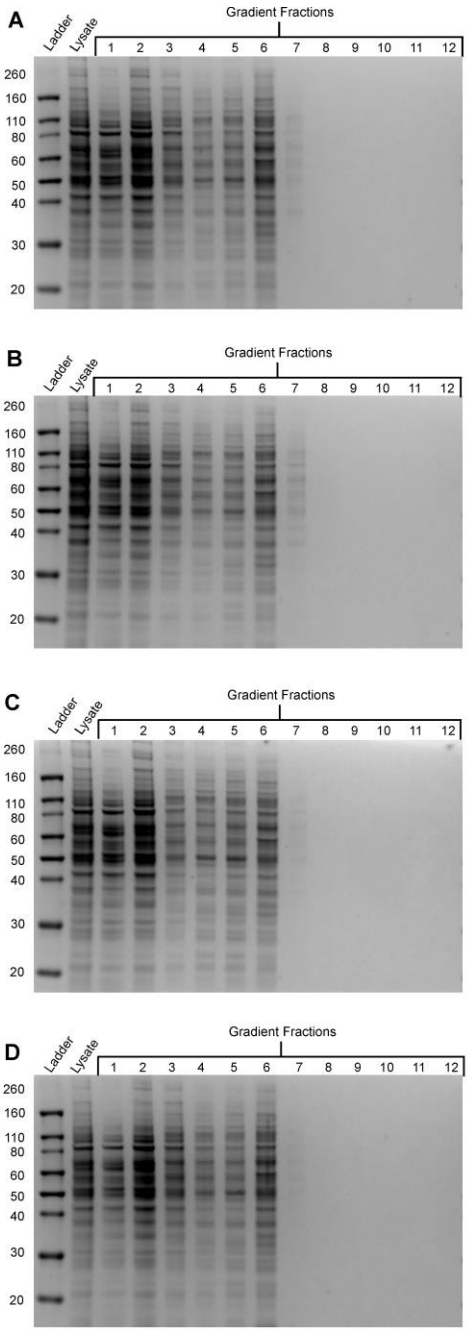

Figure 20. Ebola virus nucleocapsid protein migration after single transfection. 293T cells were transfected with (A) VP35; (B) VP24; (C) VP30 or (D) VP40. Cells were lysed with hypotonic lysis buffer and layered onto 15-30% iodixanol gradients. Fractions were collected top-down, with Fraction 1 representing the first fraction collected. Fractions were analyzed by SDS-PAGE.

4.4.1.2 Dual transfections

I next characterized the interactions between the NP and the other nucleocapsid proteins. To do this I performed co-transfections, lysed the cells in hypotonic lysis buffer and separated proteins by differential ultracentrifugation. SDS-PAGE was performed on collected gradient fractions and fractions containing high levels of nucleocapsid proteins and lower amounts of cellular proteins were chosen for further purification by ultracentrifugation. Pellets were resuspended in 50 mM NaCl PBS.

Expression of Ebola virus NP alone or in combination with one other nucleocapsid protein resulted in loose coils of NP-RNA that were purified from fractions 6 and 7 (Figure 21, Figure 22), similar to those observed by Mavrakis et al. (2002) and Noda et al. (2010). Expression of NP and VP35 resulted in the co-migration of these proteins through the density gradient (Figure 21b). Expression of NP and VP30 also lead to obvious co-migration of these proteins (Figure 21d). In contrast to VP35 and VP30, dual expression of NP and VP24 did not result in a well-defined co-migration pattern (Figure 21c). Whereas NP migration maintained a similar distribution to the previous gradients, VP24 migration through the gradient was impaired. The majority of VP24 was observed in the top two fractions with the cellular proteins. Only a trace amount of VP24 was visible in fractions 6 and 7, which contained the highest levels of NP (Figure 21c). VP40 co-migration with NP was difficult to visualize by SDS-PAGE. Detection of VP40 by Western blot demonstrated a weak co-distribution of NP and VP40 through the iodixanol gradient (Figure 21ef). No evidence of co-migration was evident when VP24 and VP35 were expressed together (Figure 21g).

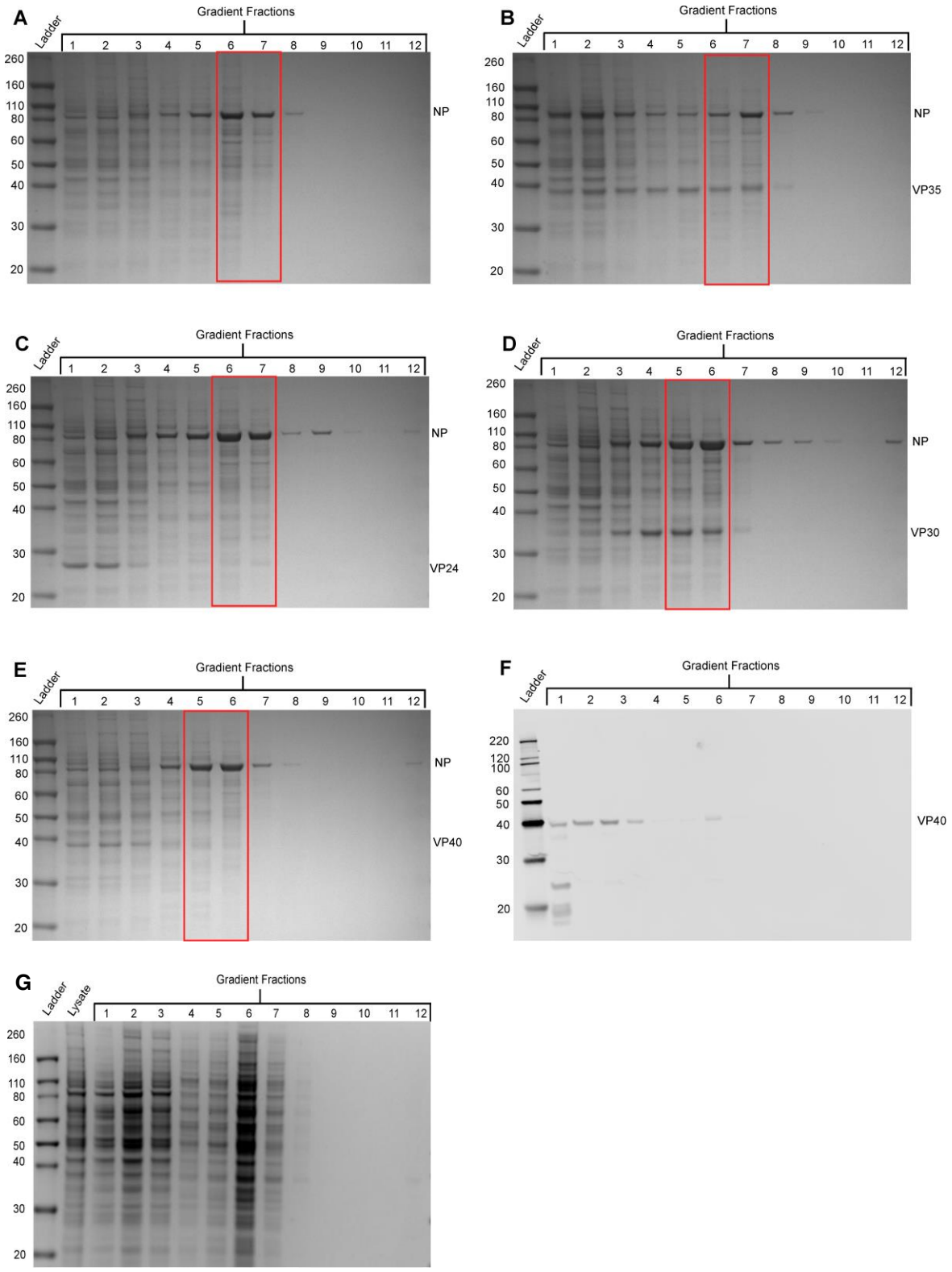

Figure 21. Migration of Ebola virus nucleocapsid proteins through iodixanol gradients after dual transfection. 293T cells were lysed in hypotonic lysis buffer. Gels were stained with Coomassie blue. (A) NP; (B) NP/VP35; (C) NP/VP24; (D) NP/VP30; (E) NP/VP40; (F) Anti-VP40 western blot of NP/VP40 gradient; (G) VP24/VP35.

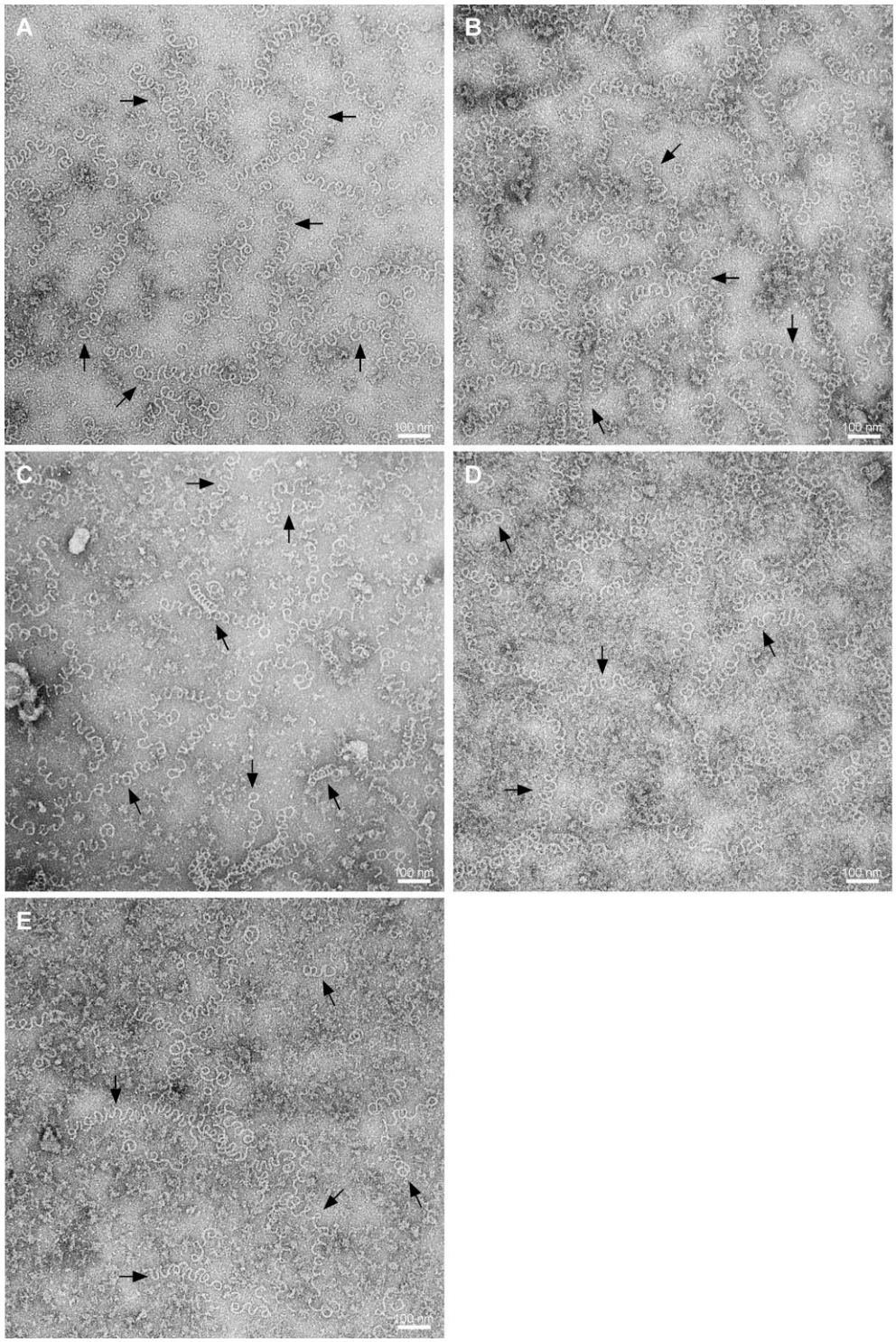

Figure 22. Negative stain results after expression of NP in combination with a second nucleocapsid protein. 293T cells were lysed in hypotonic lysis buffer and proteins were purified through a 15-30% iodixanol density gradient. Fractions 6 and 7 were pelleted and stained with methylamine tungstate. (A) NP; (B) NP/VP35; (C) NP/VP24; (D) NP/VP30; (E) NP/VP40.

4.4.1.3 Isolation and purification of NP/VP24/VP35 nucleocapsid-like particles

Previously, analysis of intracellular nucleocapsid-like particles by buoyant density gradient sedimentation resulted in the co-distribution of NP and VP35, but not VP24 (Huang et al. 2002). In the Huang et al. (2002) protocol, cell lysates were mixed with 60% iodixanol, brought to a final concentration of 30% and then ultracentrifuged to generate a continuous density gradient. In contrast, the isolation of nucleocapsid-like particles on a continuous 15-30% iodixanol density gradient resulted in the co-distribution of all three nucleocapsid proteins (Figure 23). Fractions 1-4 had an average density of 1.05-1.12 g/ml. Fractions 5-7 had an average density of 1.15-1.16 g/ml. Remaining fractions had an average density of 1.16-1.17 g/ml. Expression of NP, VP35 and VP24 resulted in the migration of VP24 through the gradient in tandem with the other two nucleocapsid-associated proteins. Furthermore, purification of fractions containing all three nucleocapsid proteins resulted in the isolation of envelope-free nucleocapsid-like particles (Figure 24).

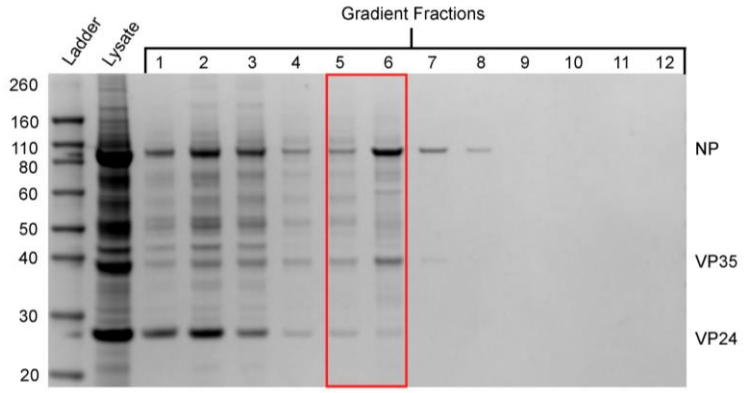

Figure 23. Gradient distribution of Ebola virus NP, VP24, and VP35 after co-expression. Cells were lysed with hypotonic lysis buffer and lysates were layered onto 15-30% iodixanol gradients. Fractions were collected top-down, with Fraction 1 representing the first fraction collected. Fractions were subjected to SDS-PAGE and gels were stained with Coomassie blue. The red box indicates fractions chosen for further purification.

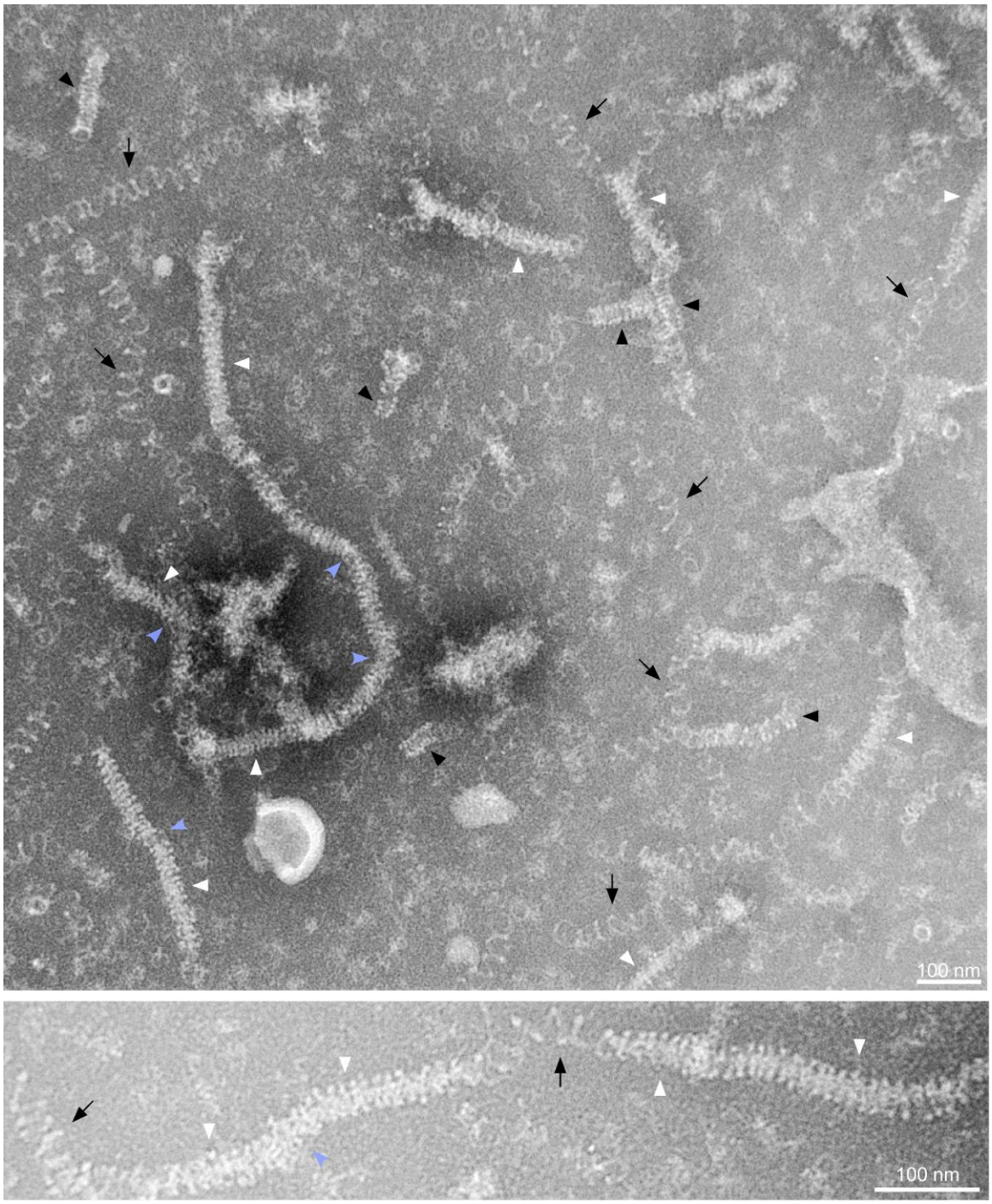

Figure 24. Nucleocapsid-like particles purified after differential ultra-centrifugation of NP/VP24/VP35-transfected cell lysates (panels above and on following page). Gradient fractions 5 and 6 were layered onto 50 mM NaCl PBS and ultracentrifuged to concentrate particles and remove iodixanol. Pellet was resuspended and stained with methylamine tungstate. Black arrows indicate loose NP-RNA coils, black arrowheads indicate tight NP-RNA coils, white arrowheads indicate nucleocapsid-like particles; and blue arrowheads indicate kinks in nucleocapsid-like particles.

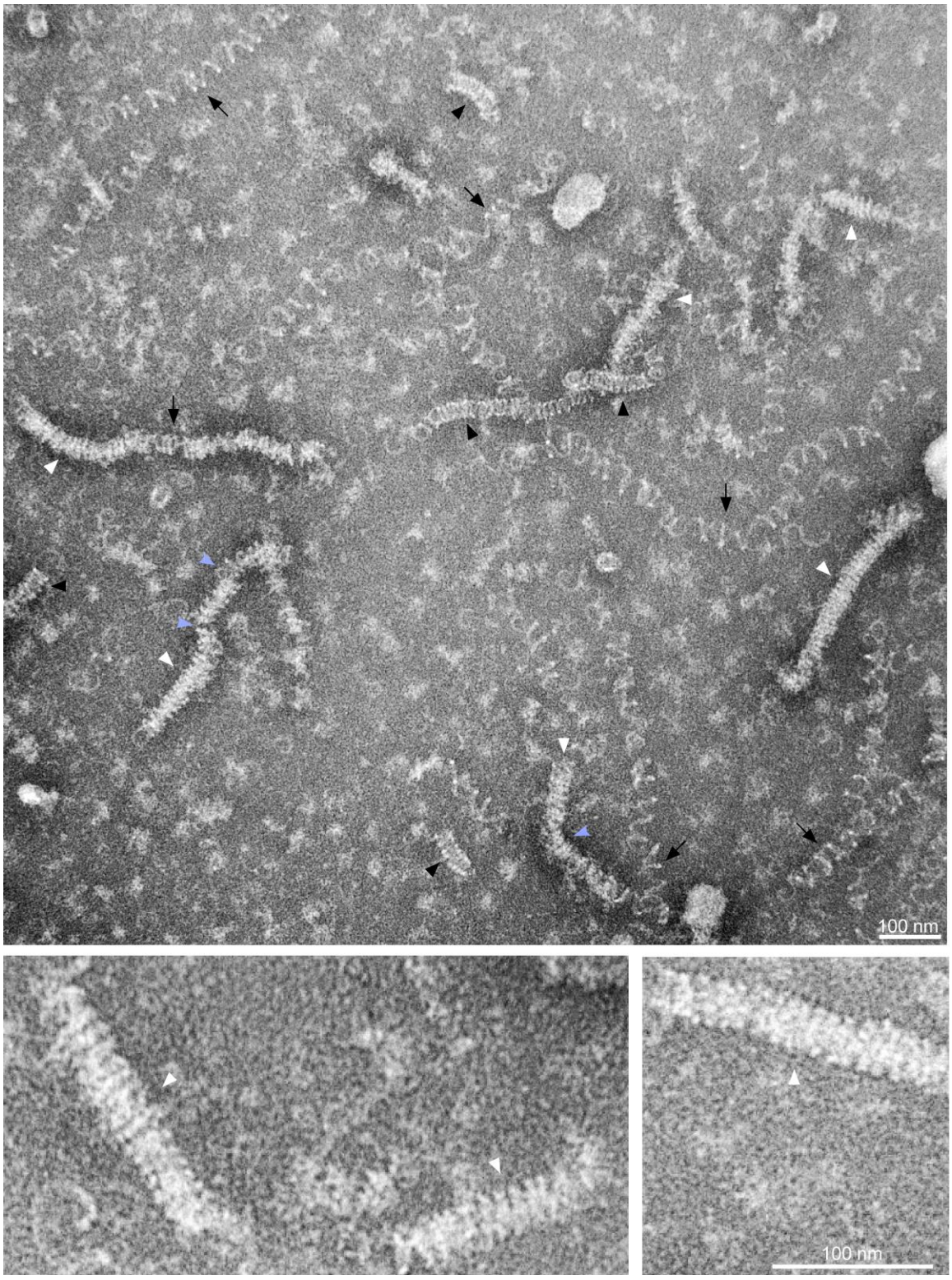

Figure 24 continued.

These helical particles had the same "herring bone"-like structure previously described in the Ebola virus nucleocapsid (Beniac et al. 2012). In addition, the filaments varied in length and were highly flexible, with multiple "kinked" areas (Figure 24). The diameter of these particles ranged from 22-47 nm, with a mean diameter of 32.8±4.18 nm, which is similar to the 41 nm diameter of the Ebola virus nucleocapsid (Figure 25). In contrast, the pitch of the isolated nucleocapsid-like particles was larger than that of the ~7 nm Ebola virus nucleocapsid calculated by Beniac et al. (2012), with a range of 2-24 nm and an average of 10.83±4.12 nm (Figure 26).

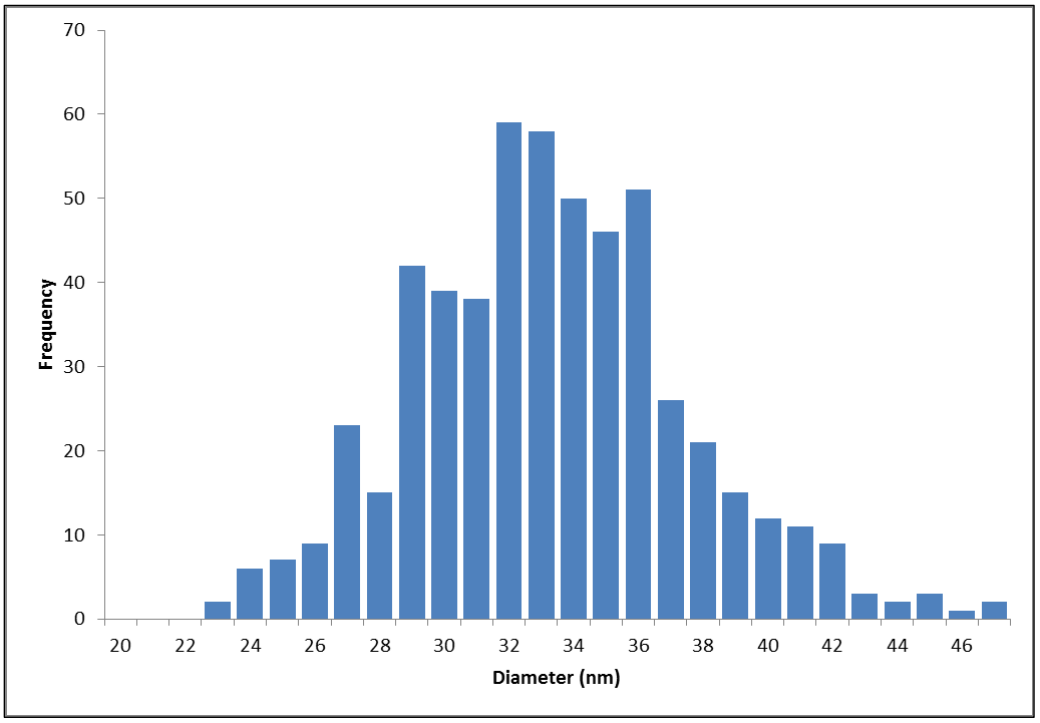

Figure 25. Frequency histogram of diameter measurements of NP/VP24/VP35 nucleocapsid-like particles after hypotonic lysis buffer treatment. Diameters were measured using ImageJ software (n= 550). Mean is 32.8±4.18 nm.

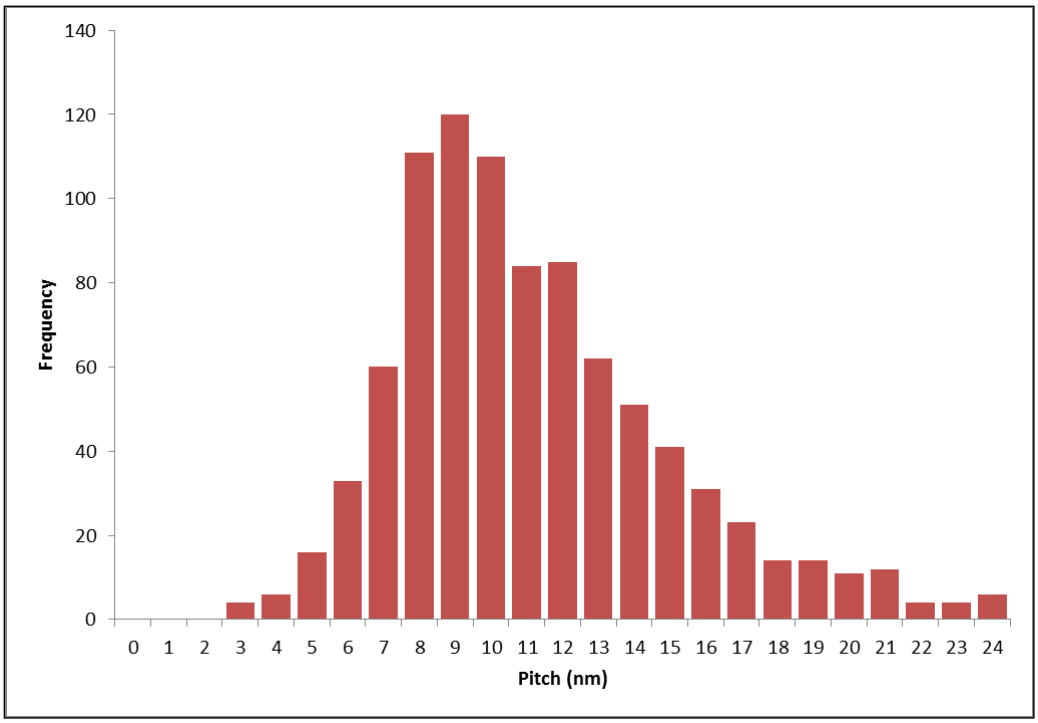

Figure 26. Frequency histogram of pitch measurements of NP/VP24/VP35 nucleocapsid-like particles after hypotonic lysis buffer treatment. Pitches were measured using ImageJ software (n= 902). Mean is 10.83±4.12 nm.

4.4.1.4 Addition of Ebola virus VP30 or VP40

Next, I investigated whether the addition of VP30 or VP40 to the NP, VP24, and VP35 expression panel could lead to perceivable differences in structure (Figures 27-29). The addition of VP30 did not affect the co-distribution of NP, VP24, and VP35 in the density gradient (Figure 27a). Moreover, in confirmation of my earlier observation, VP30 co-migrated with the other three nucleocapsid proteins (Figure 27a). The nucleocapsid-like particles formed in the presence of VP30 did not appear physically different from NP/VP24/VP35 particles when observed by negative stain TEM (Figure 28). However, measurement of the NP/VP24/VP35/VP30 nucleocapsid-like particles revealed that they

were significantly larger than those formed by NP/VP24/VP35 alone, with a mean diameter of 34.77±4.08 nm and a mean pitch of 11.71±3.66 nm (Figure 30, Figure 31).

The Ebola virus matrix protein VP40 has also been implicated in the assembly of the Ebola virus nucleocapsid, potentially as an effector of condensation (Bharat et al. 2012). To investigate whether the addition of VP40 could lead to tighter pitch measurements, 293T cells were transfected with NP, VP24, VP35, and VP40 and particles were isolated by density gradient. Surprisingly, while Coomassie stain did not indicate co-migration of VP40 with the other nucleocapsid proteins, western-blot analysis did detect VP40 in fractions 1-6 (Figure 27b and c). Control transfections of NP/VP24/VP40 and NP/VP35/VP40 revealed that VP40 more strongly co-migrated with NP and VP35 (Figure 27de). Nucleocapsid-like particles isolated from NP/VP24/VP35/VP40 transfected cells had no observable differences from NP/VP24/VP35 particles (Figure 29). Nonetheless, co-expression of VP40 with the other nucleocapsid proteins did result in significantly larger mean pitch (11.95±4.51 nm) and diameter (35.33±5.56 nm) measurements between NP/VP24/VP35 and NP/VP24/VP35/VP40 nucleocapsid-like particles when lysed by hypotonic lysis buffer (Figure 30, Figure 31).

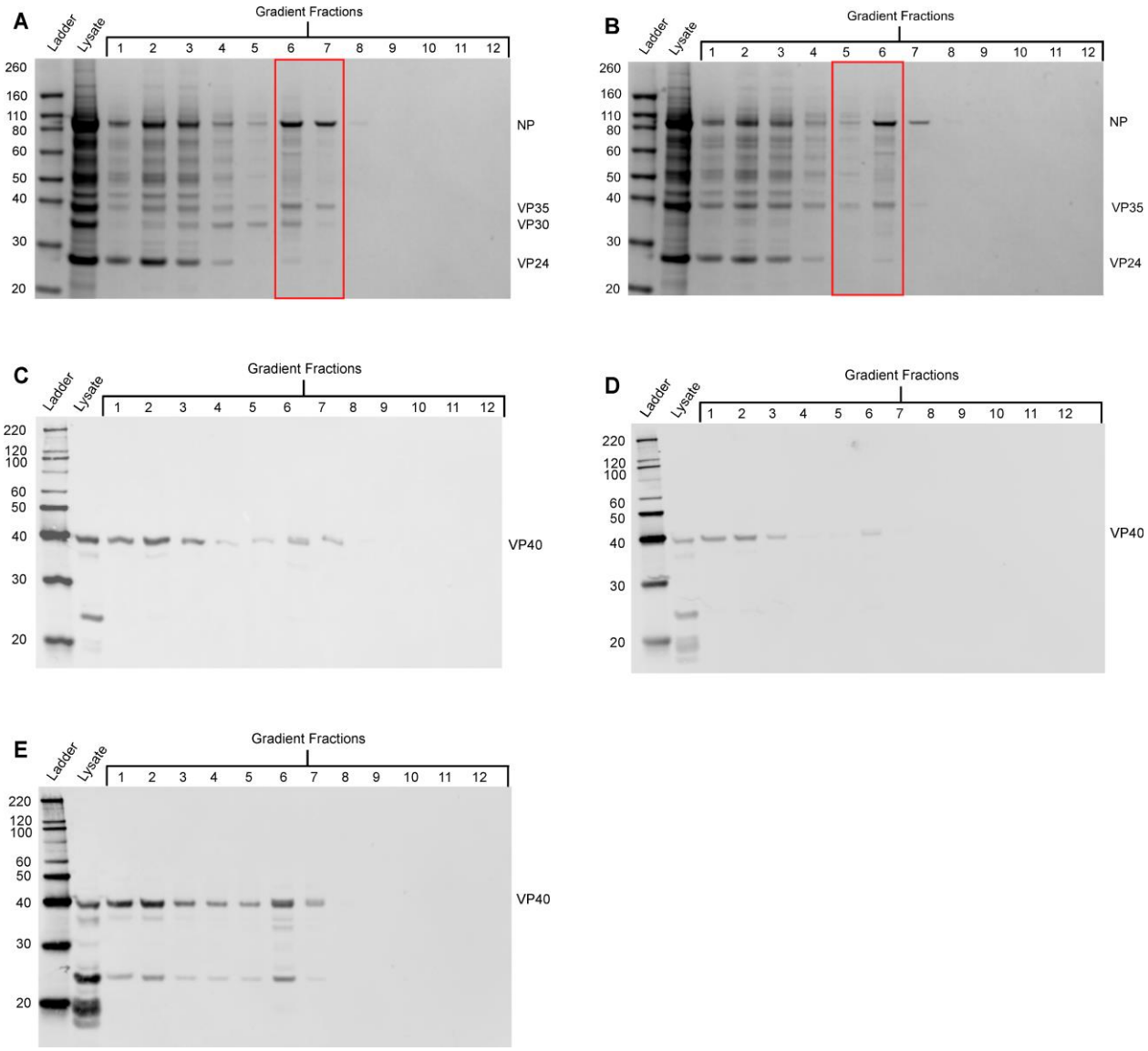

Figure 27. Co-migration of Ebola virus nucleocapsid proteins. 293T cells transfected with (A) NP/VP24/VP35/VP30; (B and C) NP/VP24/VP35/VP40; (D) NP/VP24/VP40; or (E) NP/VP35/VP40 were treated with hypotonic lysis buffer and layered on 15-30% iodixanol gradients. Fractions were collected top-down, with Fraction 1 representing the first fraction collected. (A, B) Protein was detected by SDS-PAGE. Red boxes indicate fractions chosen for further purification. (C, D, E) Anti-VP40 western blots of gradient fractions.

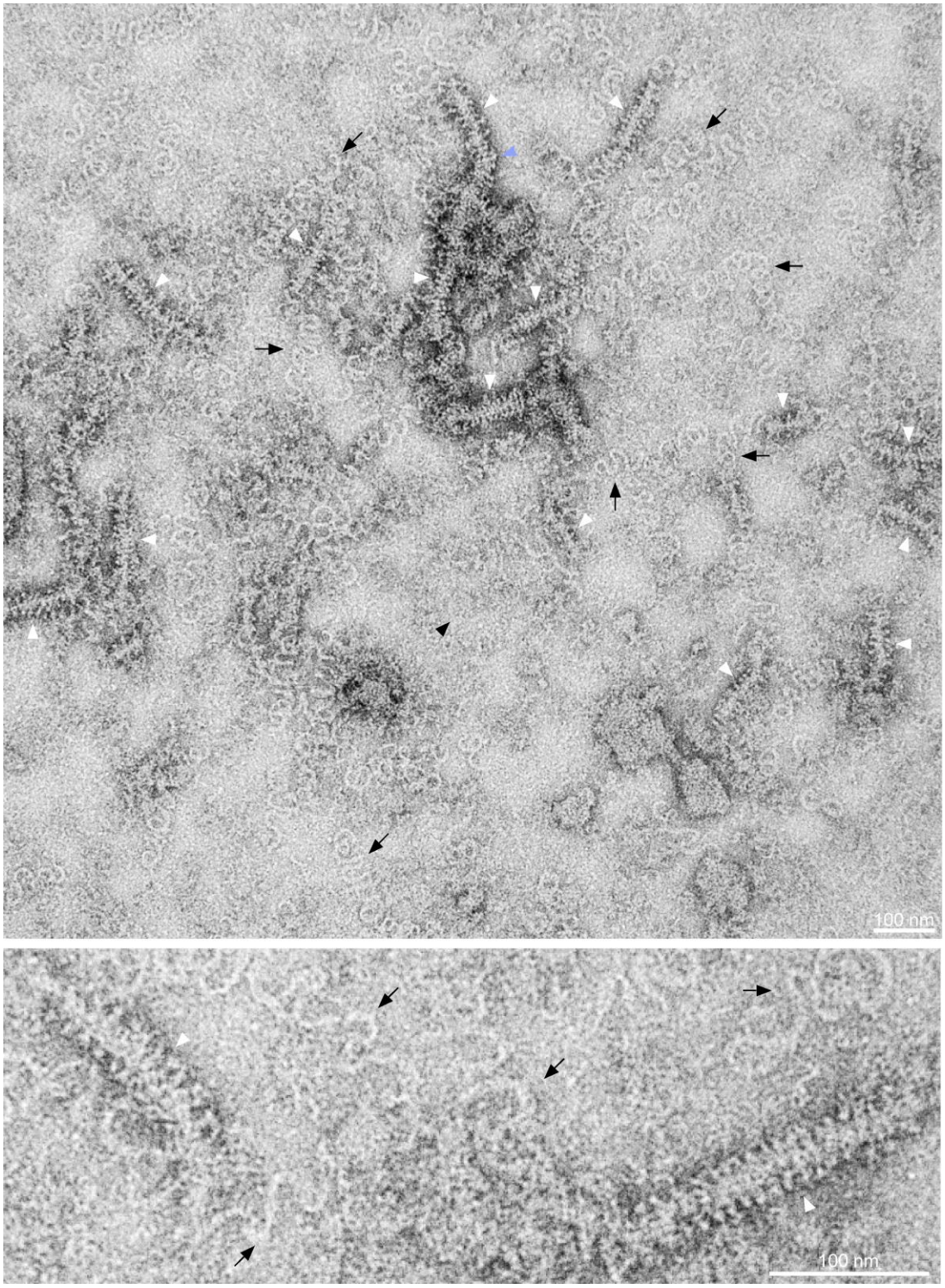

Figure 28. Nucleocapsid-like particles observed after addition of VP30 to NP/VP24/VP35 expression. Selected fractions were purified through 50 mM NaCl and stained with methylamine tungstate. Black arrows: loose NP-RNA coils; black arrowheads: tight NP-RNA coils; white arrowheads: nucleocapsid-like particles; blue arrowheads: kinks in nucleocapsid-like particles.

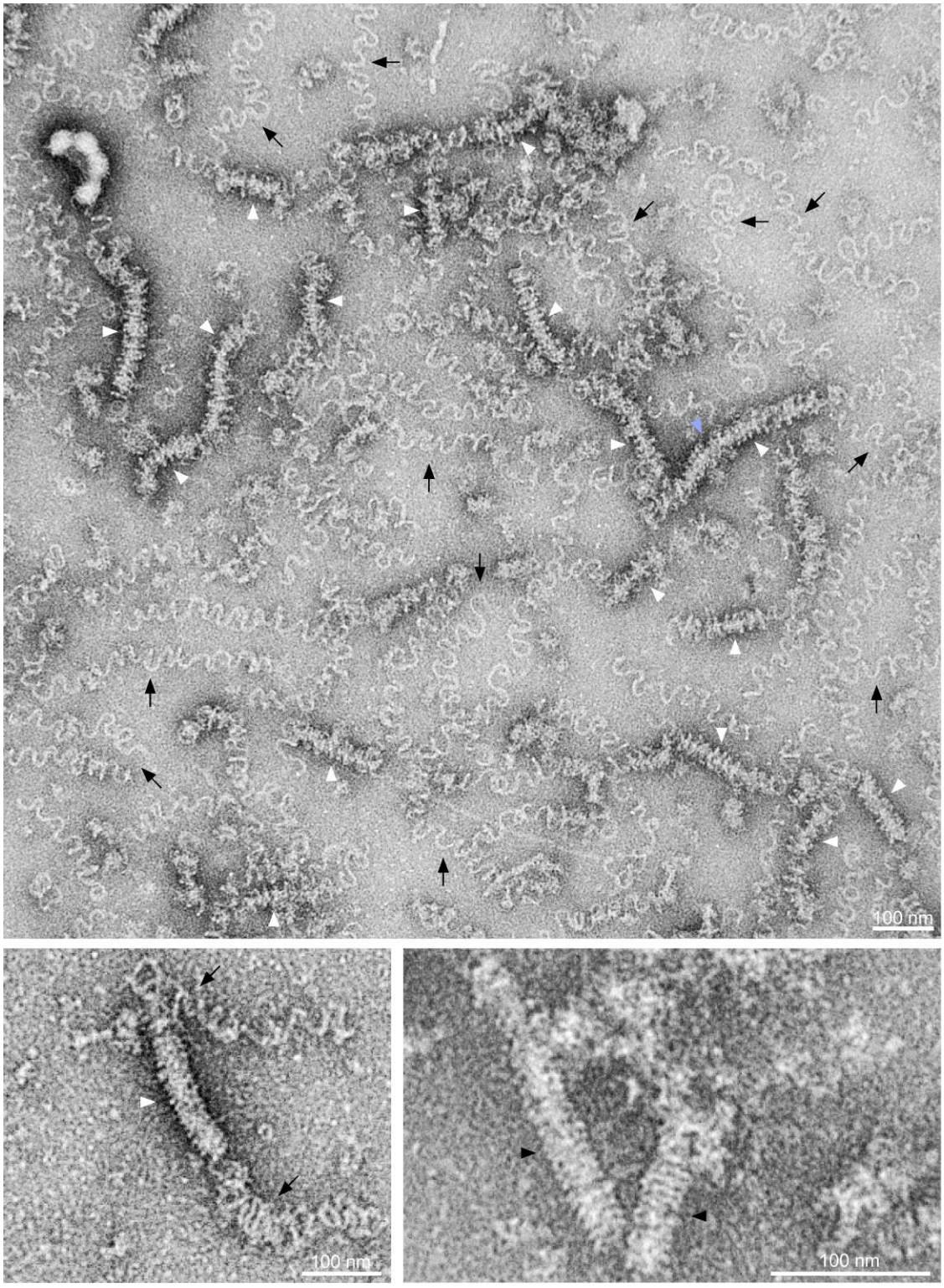

Figure 29. Nucleocapsid-like particles observed after addition of VP40 to NP/VP24/VP35 expression. Selected fractions were purified through 50 mM NaCl and stained with methylamine tungstate. Black arrows: loose NP-RNA coils; black arrowheads: tight NP-RNA coils; white arrowheads: nucleocapsid-like particles; blue arrowheads: kinks in nucleocapsid-like particles.

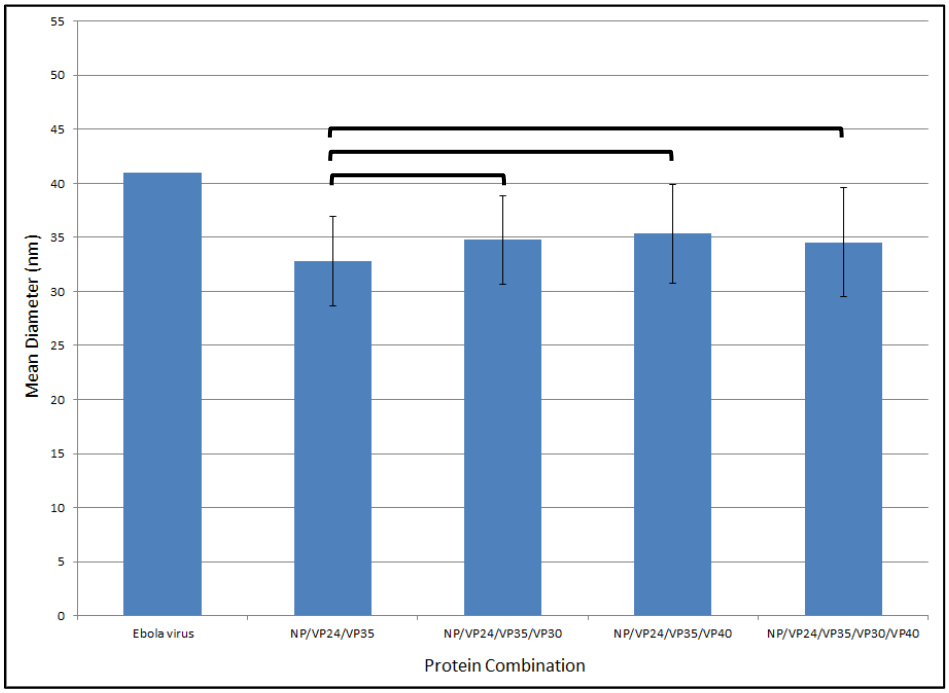

Figure 30. Comparison of mean diameter values for all protein combinations after hypotonic lysis buffer treatment. Diameters were measured using ImageJ software (p=0.000625, student t test; Bonferroni correction).

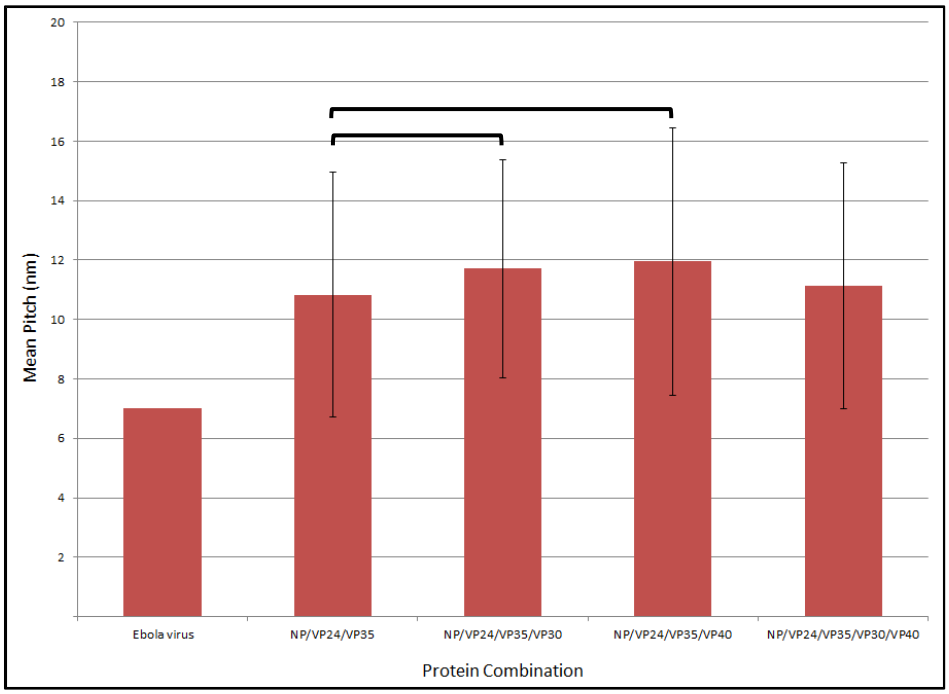

Figure 31. Comparison of mean pitch values for all protein combinations after hypotonic lysis buffer treatment. Pitch of nucleocapsid-like particles was measured using ImageJ software (p=0.000625, Mann-Whitney; Bonferroni correction).

4.4.1.5 Addition of Ebola virus VP30 and VP40

Transfection of all five nucleocapsid proteins was performed to determine if additional protein-protein interactions might account for a tighter pitch or more uniform structure, as observed for the native Ebola virus nucleocapsid. Consistent with my previous results, VP30 and VP40 migrated with NP/VP24/VP35 through the density gradient (Figure 32). Nucleocapsid-like particles isolated from the NP/VP24/VP35/VP30/VP40 transfection were indistinguishable from NP/VP24/VP35 particles and had an average pitch that was not significantly different (11.13±4.14 nm) (Figure 31, Figure 33). In contrast, the mean diameter of NP/VP24/VP35/VP30/VP40 nucleocapsid-like particles was significantly larger than NP/VP24/VP35 (34.55±5.06 nm) (Figure 30). Interestingly, when diameter and pitch measurements of the other protein combinations were compared against each other, the mean pitch and diameters were not significantly different between these protein combinations (Figure 30, Figure 31). Intracellular NP/VP24/VP35 nucleocapsid-like particles were significantly tighter and narrower than the other protein combinations when released by hypotonic lysis buffer. A scatterplot of mean diameter vs. mean pitch also demonstrates the smaller, tighter nature of NP/VP24/VP35 nucleocapsid-like particles. In addition, a linear correlation between diameter and pitch is suggested (Figure 34).

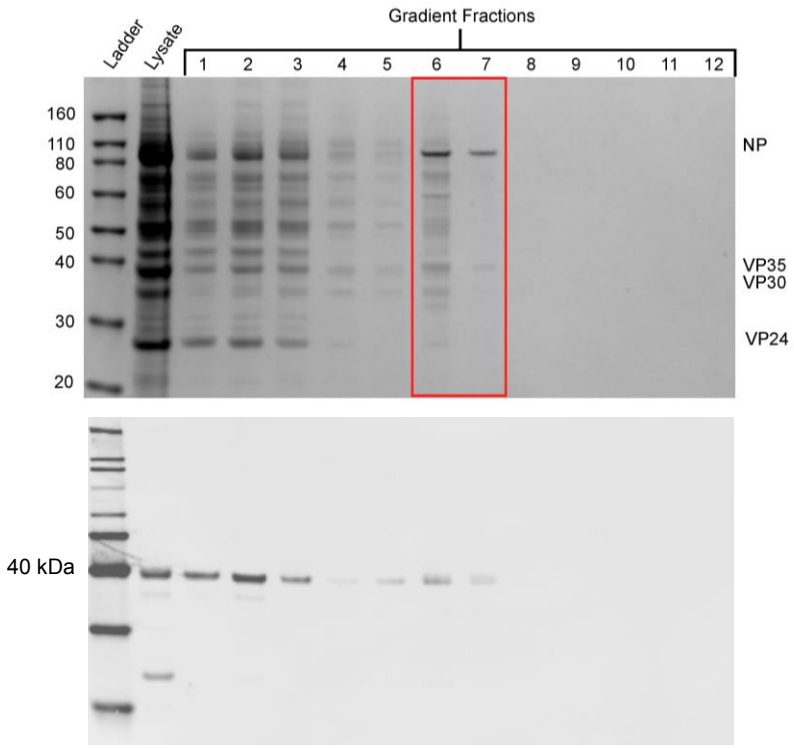

Figure 32. Migration of Ebola virus NP, VP24, VP35, VP30, and VP40 through 15-30% iodixanol gradient. Cells were harvested by hypotonic lysis buffer and differential ultracentrifugation was performed. Fractions were collected top-down, with Fraction 1 representing the first fraction collected. **Upper panel:** SDS-PAGE of gradient fractions, stained with Coomassie blue. Red box indicates fractions chosen for further purification. **Bottom panel:** Anti-VP40 western blot of gradient fractions.

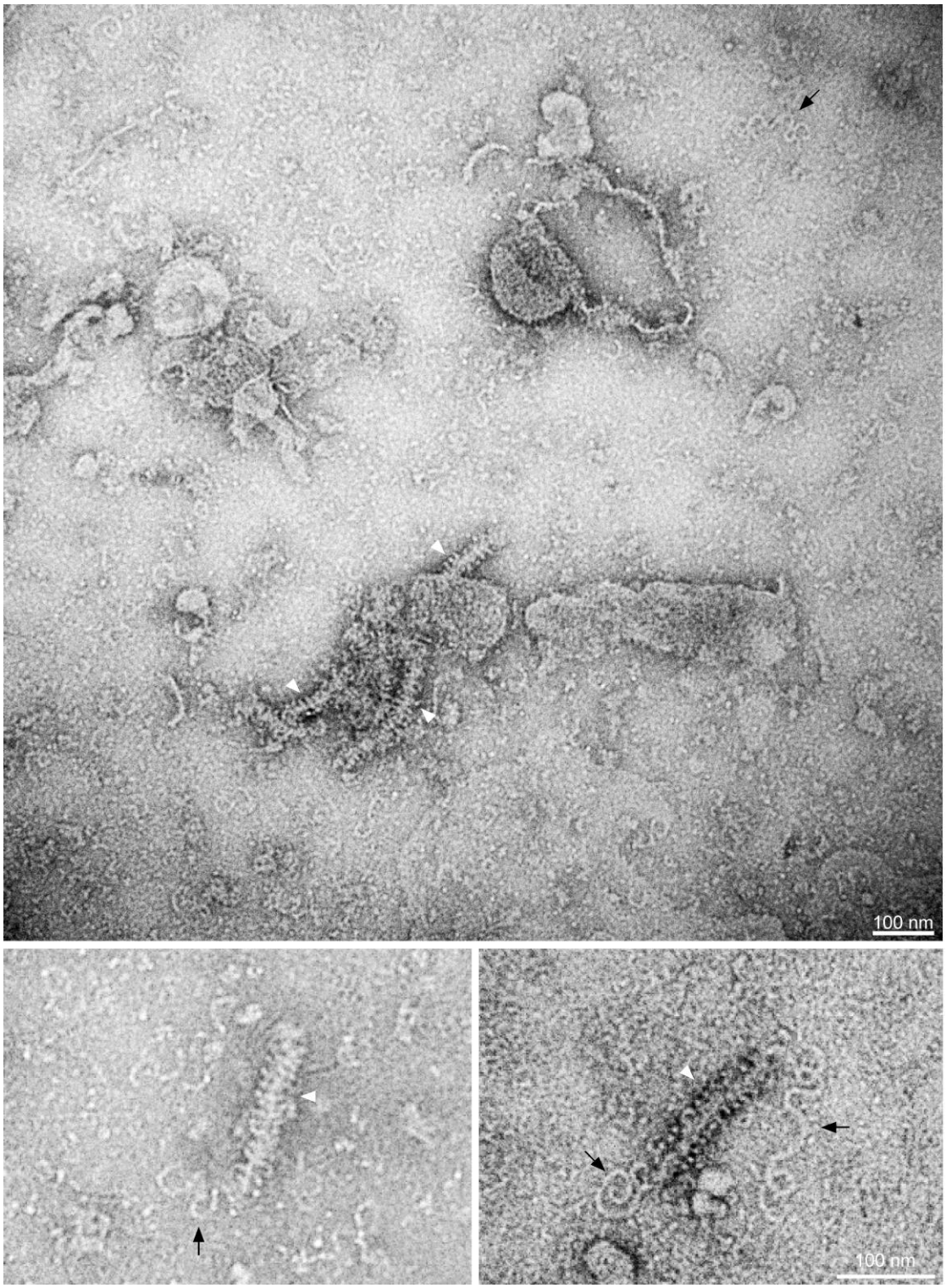

Figure 33. Nucleocapsid-like particles observed after expression of NP/VP24/VP35/VP30/VP40. Fractions 6 and 7 were layered onto 50 mM NaCl and ultracentrifuged. Pellets were resuspended in 50 mM NaCl and stained with methylamine tungstate. Black arrows: loose NP-RNA coils; black arrowheads: tight NP-RNA coils; white arrowheads: nucleocapsid-like particles.

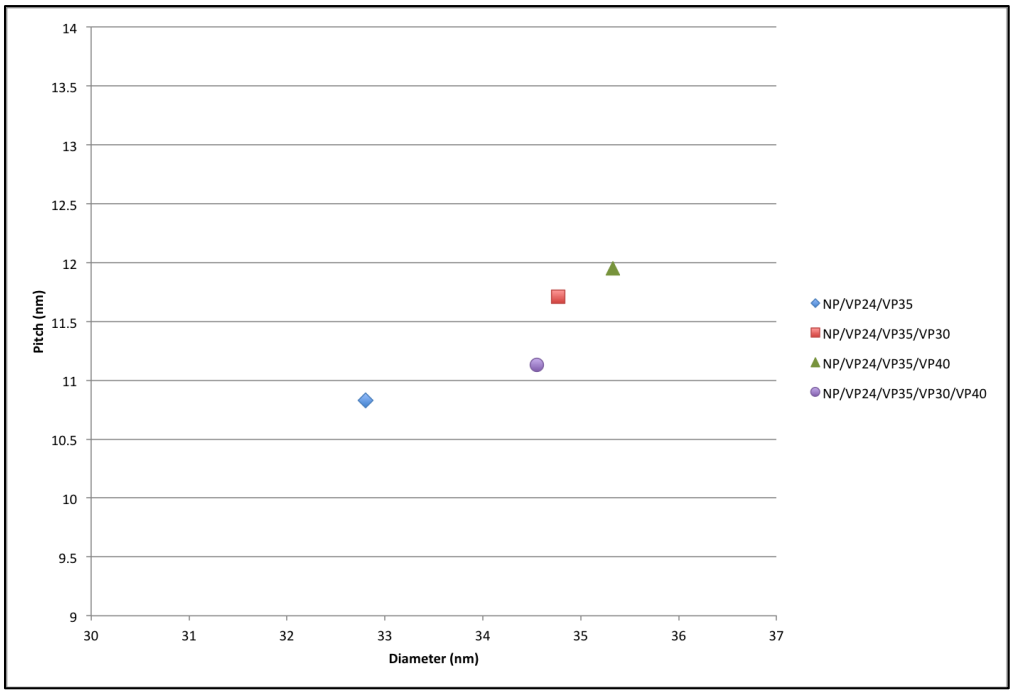

Figure 34. Scatterplot of mean diameter and pitch values for each protein combination when transfected cells were lysed with hypotonic lysis buffer.

4.4.2 Isotonic lysis buffer

The consistent assembly of relatively relaxed nucleocapsid-like particles prompted the investigation into whether alternative methods of lysis could affect the condensation of these particles. To this end, I repeated the experiments described above using lysis buffer with an isotonic sodium chloride concentration (150 mM NaCl).

In contrast to treatment with hypotonic lysis buffer, treatment of transfected cells with isotonic lysis buffer appeared to result in less protein travelling through the gradient overall (Figure 35). Migration of VP24 through the gradient in tandem with NP and VP35 was particularly affected, with the majority of VP24 observed in the upper 3 fractions, while NP and VP35 continued to migrate to fractions 6 and 7 (Figure 35). The presence of VP40 within these gradients is again difficult to differentiate, as is VP30.

Nevertheless, nucleocapsid-like particles were isolated from fractions for each protein combination containing NP, VP24, and VP35 (Figure 36). These nucleocapsid-like particles appeared very similar to those observed after hypotonic lysis buffer, with no discernable changes due to the addition of VP30 and/or VP40 (Figure 36).

In contrast to hypotonic lysis buffer, the mean diameter of NP/VP24/VP35 nucleocapsid-like particles released by isotonic lysis buffer was not significantly different from NP/VP24/VP35/VP30 or NP/VP24/VP35/VP40 particles at 34.53 nm, 34.36 nm, and 34.77 nm, respectively (Figure 37). Instead, these three protein combinations all had significantly larger mean diameters than NP/VP24/VP35/VP30/VP40 (32.52 nm) (Figure 37). NP/VP24/VP35 and NP/VP24/VP35/VP30 nucleocapsid-like particles also had significantly larger mean pitch measurements (12.45 nm and 12.33 nm) than NP/VP24/

VP35/VP40 (11.14 nm) (Figure 38). A scatterplot of mean diameters and pitch values does not show the same linear correlation as observed for hypotonic lysis buffer (Figure 39).

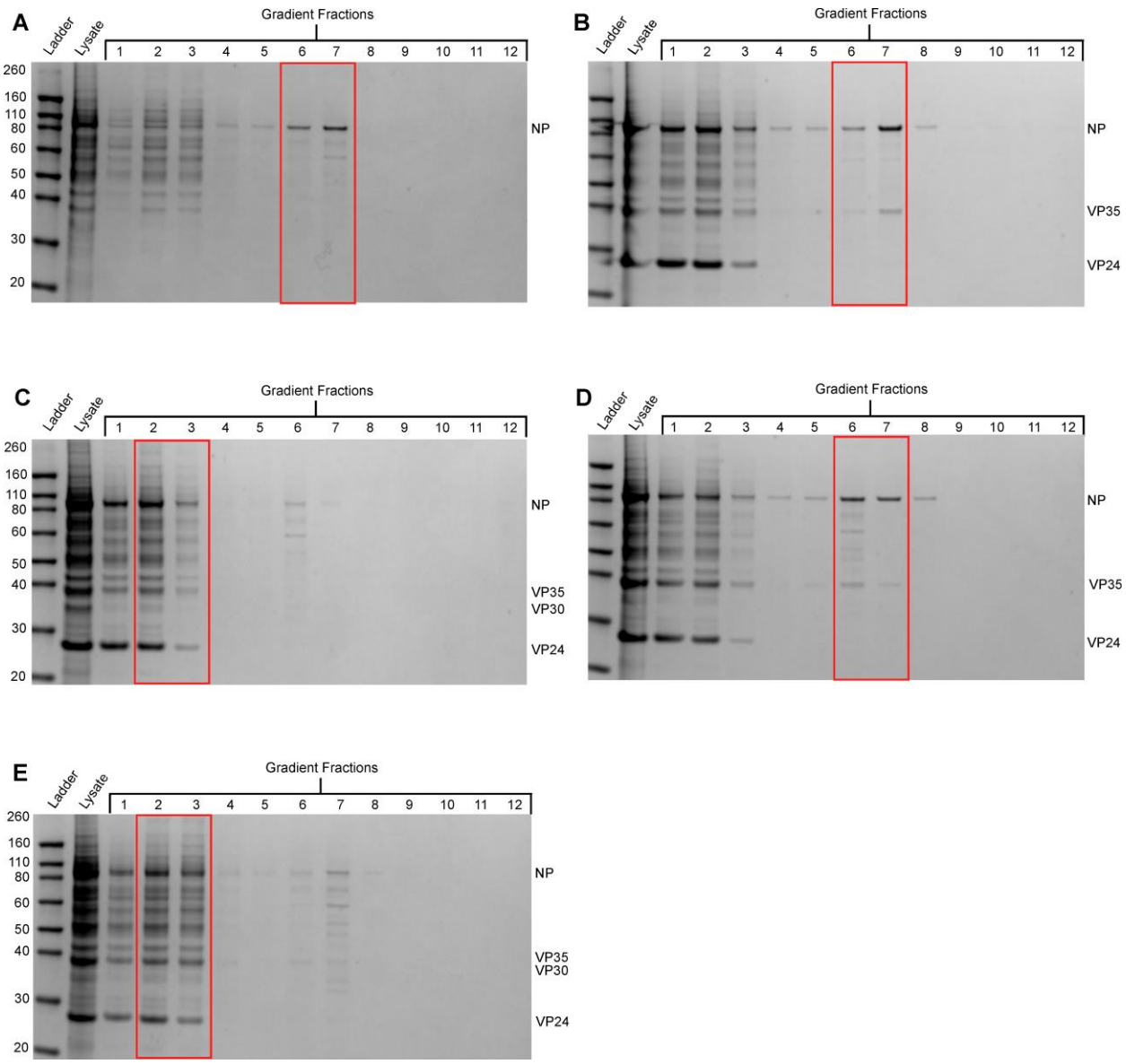

Figure 35. Ebola virus nucleocapsid protein migration through iodixanol density gradient after treatment with isotonic lysis buffer. Forty-eight hours post-transfection, 293T cells were lysed with isotonic lysis buffer and layered onto 15-30% iodixanol gradients. Fractions were collected top-down, with Fraction 1 representing the first fraction collected. Fractions were analyzed by SDS-PAGE. Red boxes indicate fractions chosen for further purification. (A) NP; (B) NP/VP24/VP35; (C) NP/VP24/VP35/VP30; (D) NP/VP24/VP35/VP40; (E) NP/VP24/VP35/VP30/VP40.

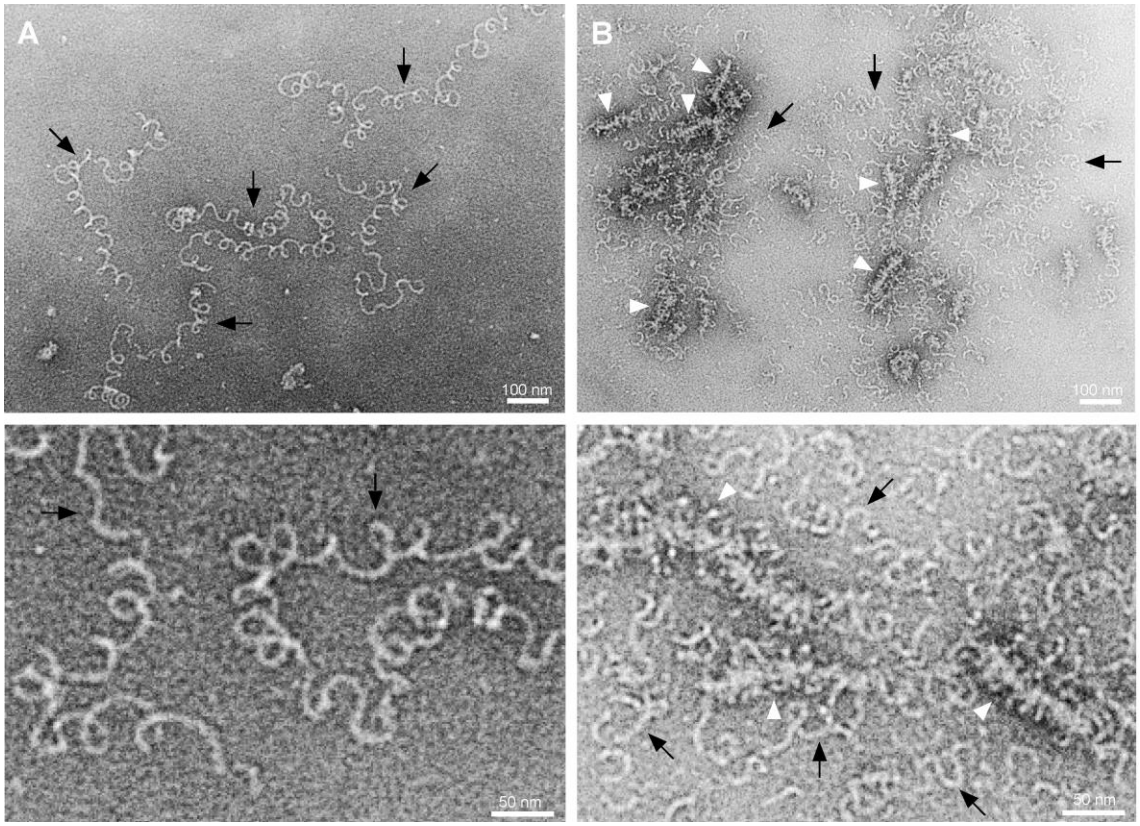

Figure 36. Nucleocapsid-like particles purified after isotonic lysis buffer treatment. Selected fractions were pelleted through PBS and stained with methylamine tungstate. (A) NP; (B) NP/VP24/VP35; (C) NP/VP24/VP35/VP30; (D) NP/VP24/VP35/VP40; (E) NP/VP24/VP35/VP30/VP40. Black arrows indicate loose NP-RNA coils, black arrowheads indicate tight NP-RNA coils, and white arrowheads indicate nucleocapsid-like particles.

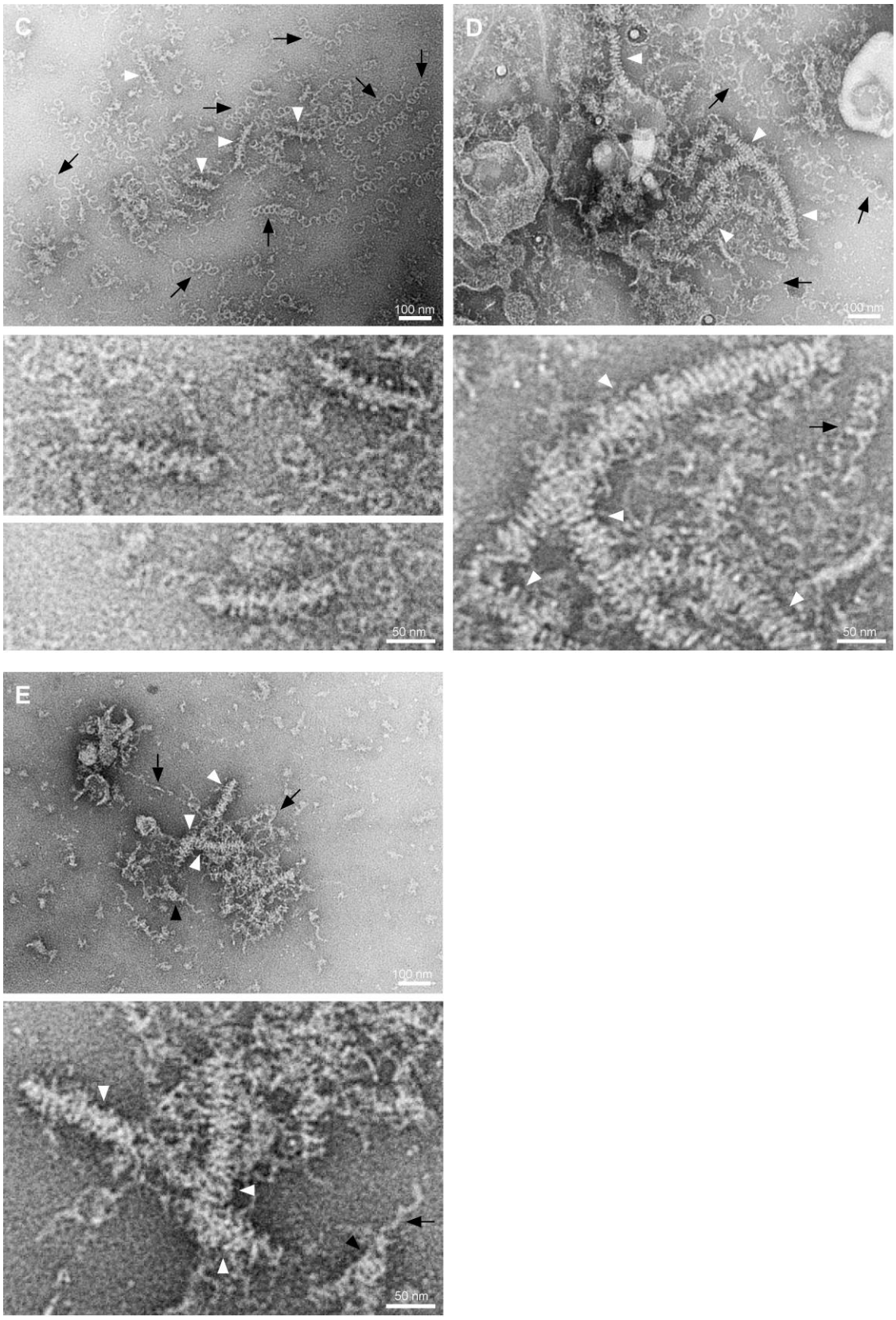

Figure 36 continued.

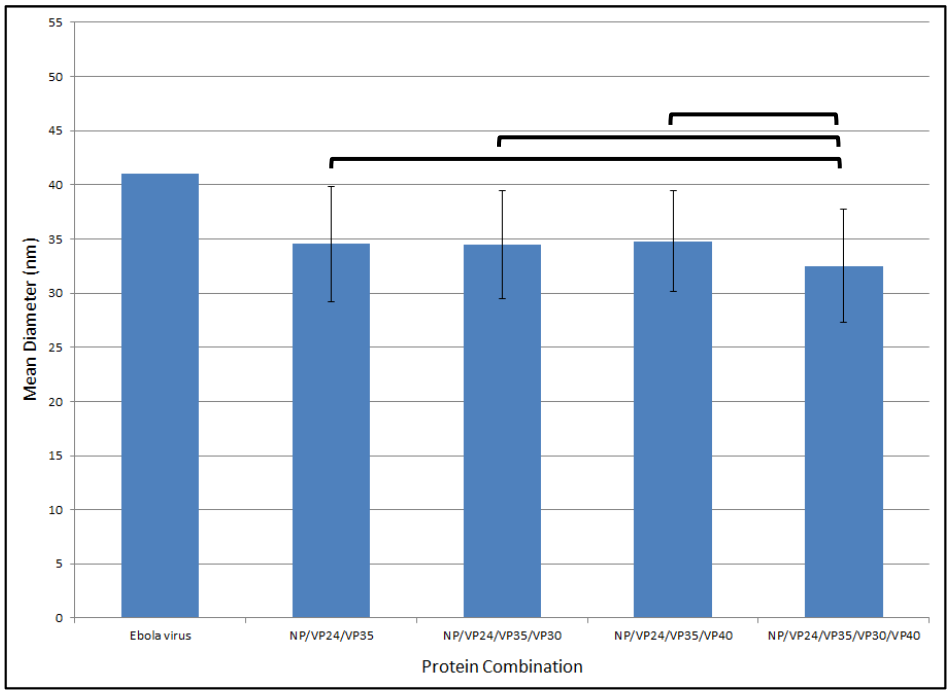

Figure 37. Comparison of mean diameter values for each protein combination after isotonic lysis buffer treatment. Nucleocapsid-like particle diameters were measured using ImageJ software (p=0.000625, student t test; Bonferroni correction).

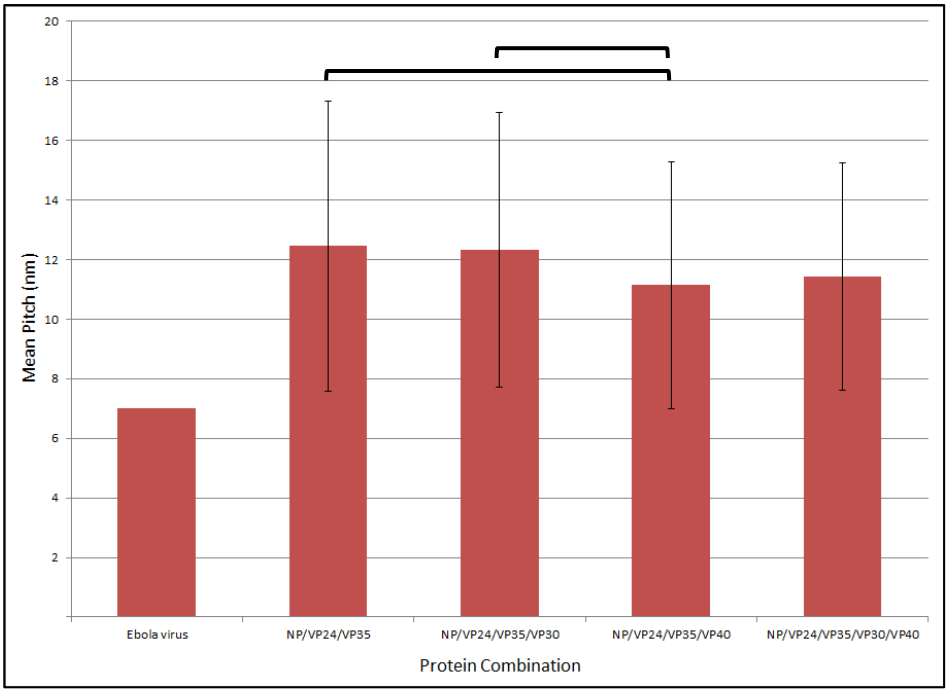

Figure 38. Comparison of mean pitch values for each protein combination after isotonic lysis buffer treatment. Nucleocapsid-like particle pitches were measured using ImageJ software (p=0.000625, Mann-Whitney; Bonferroni correction).

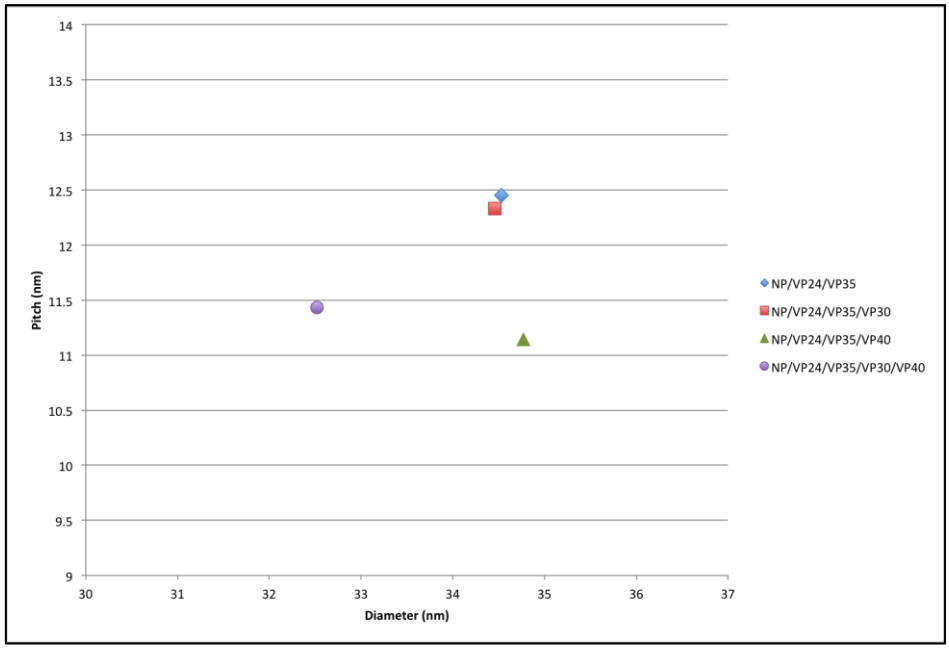

Figure 39. Scatterplot of mean diameter vs. mean pitch values for each protein combination after isotonic lysis buffer treatment.

4.4.3 Hypotonic freeze/thaw

To determine if three cycles of freeze/thaw at -80°C would result in larger, more condensed nucleocapsid-like particles, 293T cells were transfected with various gene combinations and incubated for 48 hours. Cells were lysed by three freeze/thaw cycles in hypotonic PBS and lysates were loaded onto 15-30% 50 mM NaCl iodixanol gradients. Fractions were collected after ultracentrifugation and SDS-PAGE was performed. Selected fractions were further purified by ultracentrifugation and pellets were stained with methylamine tungstate.

Freeze/thaw in hypotonic PBS resulted in strong co-migration of the nucleocapsid proteins (Figure 40). Whereas VP24 was most strongly observed in the upper fractions after treatment with isotonic lysis buffer, release of nucleocapsid-like particles by hypotonic freeze/thaw resulted in a strong VP24 presence in fractions 6 and 7 (Figure 40). Imaging of fractions 6 and 7 by TEM demonstrated the presence of nucleocapsid-like particles when NP, VP24, and VP35 were co-expressed (Figure 41). Similar to the previous experiments, addition of VP30 and/or VP40 did not result any obvious structural changes (Figure 41).

Expression of NP/VP24/VP35/VP30/VP40 resulted in a significantly smaller mean diameter (33.69 nm) compared to the other protein combinations (~35 nm) after hypotonic freeze/thaw (Figure 42). Nucleocapsid-like particles formed in the presence of NP/VP24/VP35/VP30/VP40 also had a significantly smaller mean pitch (12.95 nm) then all other protein combinations except NP/VP24/VP35/VP40 (11.96 nm) (Figure 43). The average pitches of NP/VP24/VP35 and NP/VP24/VP35/VP30 nucleocapsid-like particles were not significantly different from each other and were less condensed then those

particles formed in the presence of VP40. A scatterplot between these two measurements did not show any correlation (Figure 44).

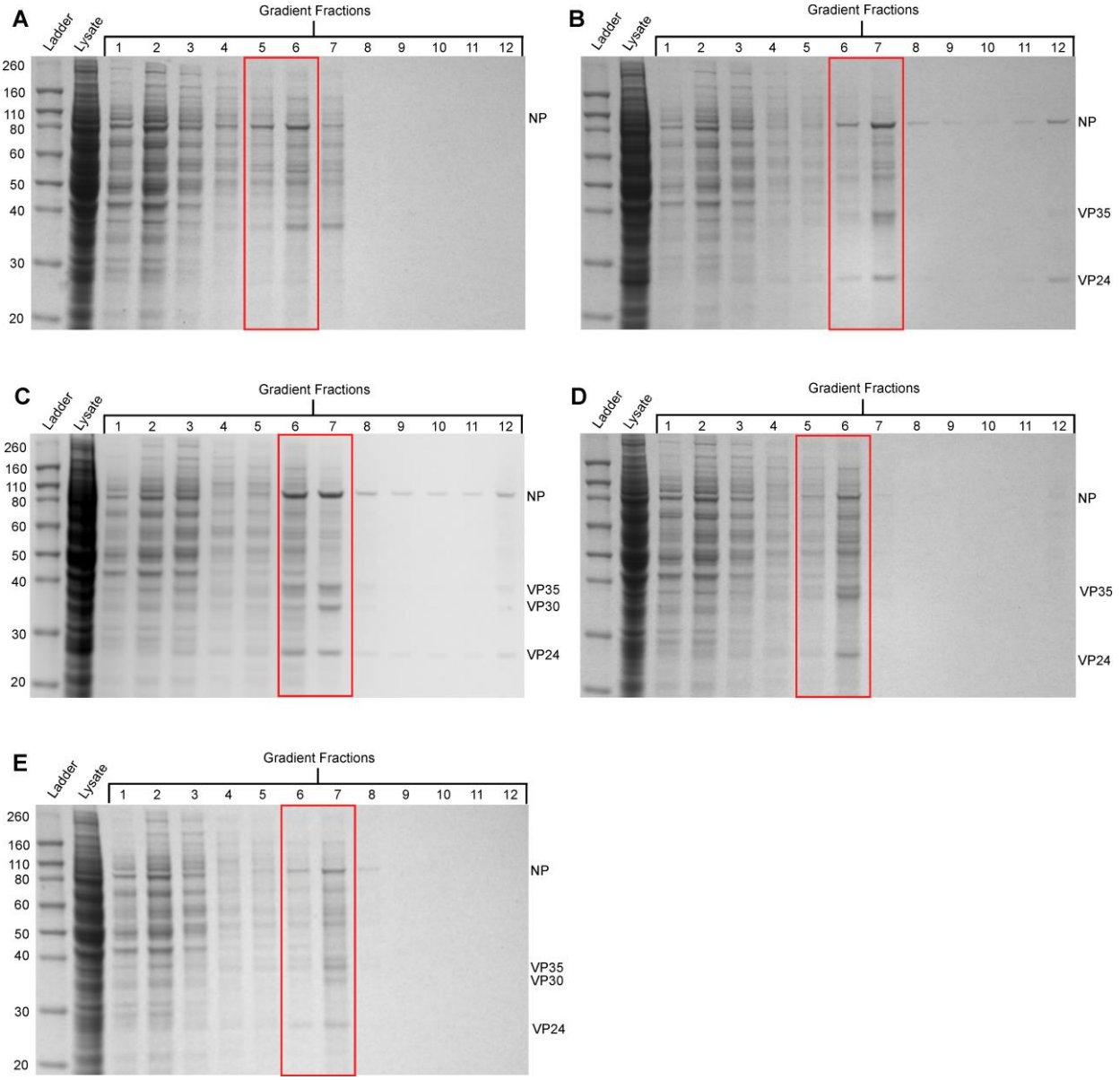

Figure 40. Gradient distribution of Ebola virus nucleocapsid proteins when transfected cells were lysed by hypotonic freeze/thaw. Forty-eight hours post-transfection, 293T cells were lysed by 3 freeze/thaw cycles. Lysates were separated by differential ultracentrifugation. Fractions were collected top-down, with Fraction 1 representing the first fraction collected. Fractions were analyzed by SDS-PAGE. Gels were stained with Coomassie blue. Red boxes indicate fractions selected for further purification. (A) NP; (B) NP/VP24/VP35; (C) NP/VP24/VP35/VP30; (D) NP/VP24/VP35/VP40; (E) NP/VP24/VP35/VP30/VP40.

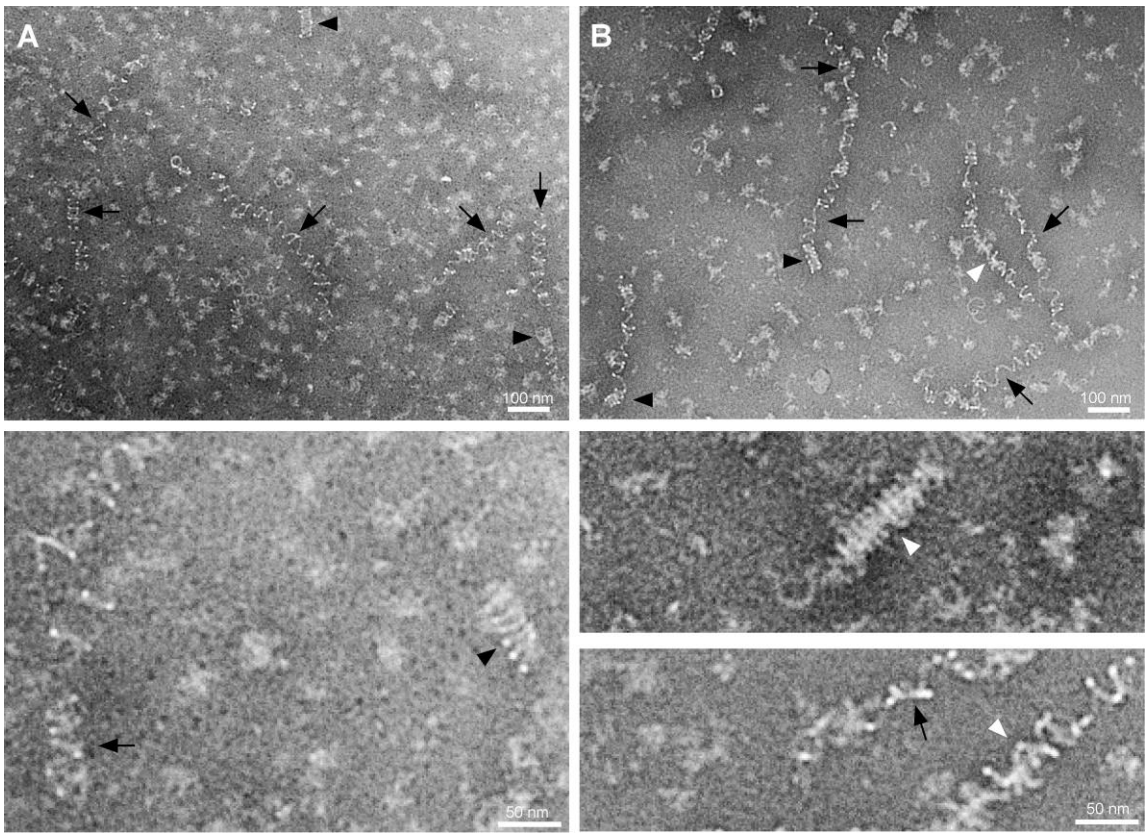

Figure 41. Nucleocapsid-like particles purified after cell lysis by hypotonic freeze/thaw. Selected gradient fractions were ultracentrifuged through 50 mM NaCl PBS. Pellets were resuspended in 50 mM NaCl PBS and stained with methylamine tungstate. (A) NP; (B) NP/VP24/VP35; (C) NP/VP24/VP35/VP30; (D) NP/VP24/VP35/VP40; (E) NP/VP24/VP35/VP30/VP40. Black arrows: loosely coiled NP-RNA; black arrowheads: tightly coiled NP-RNA; white arrowheads: nucleocapsid-like particles.

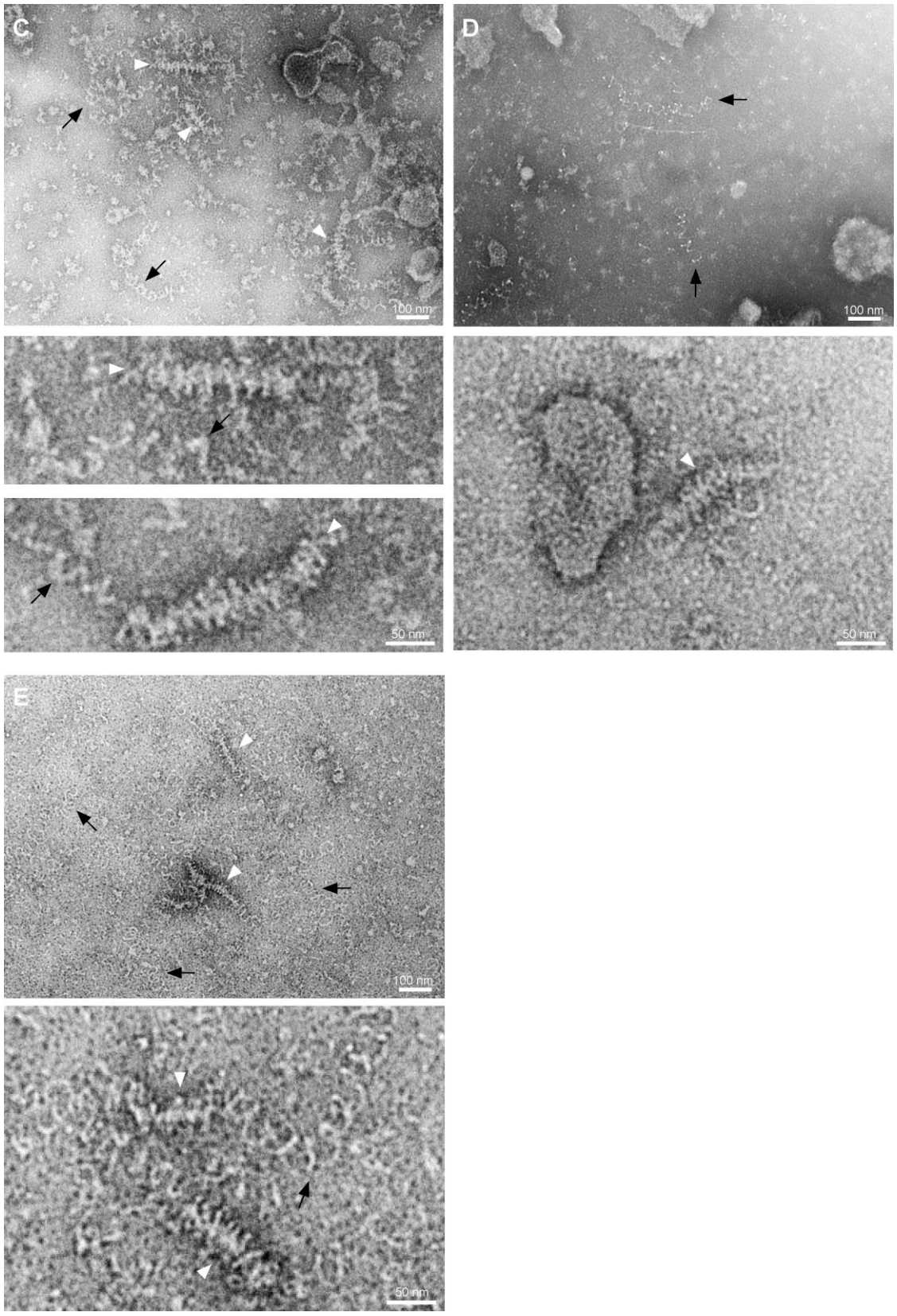

Figure 41 continued.

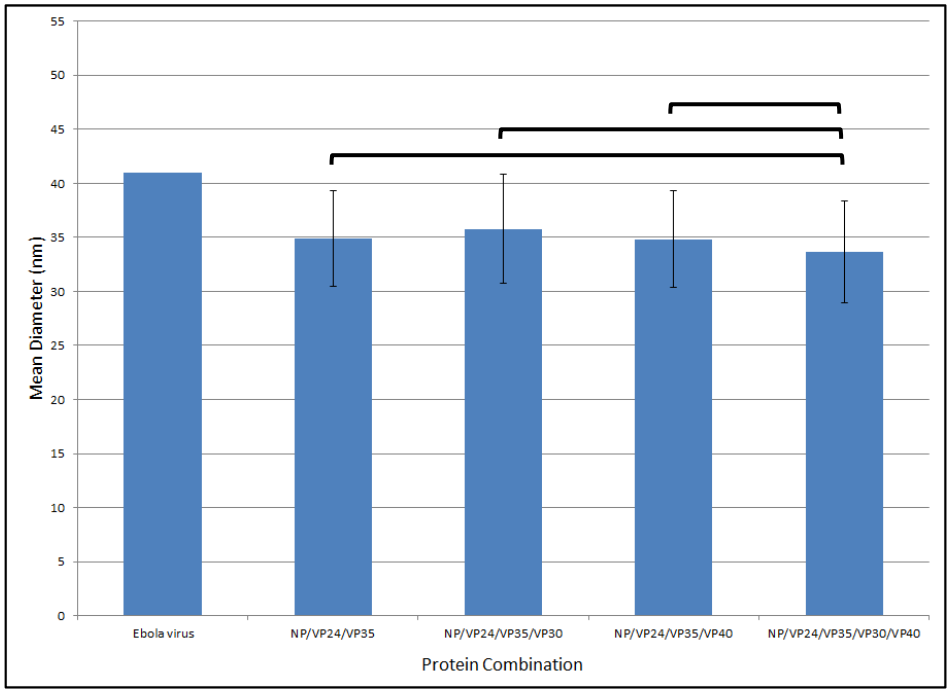

Figure 42. Mean diameters for each protein combination after cell lysis by hypotonic freeze/thaw. Measurements were taken using ImageJ software (p=0.000625, student t test; Bonferroni correction).

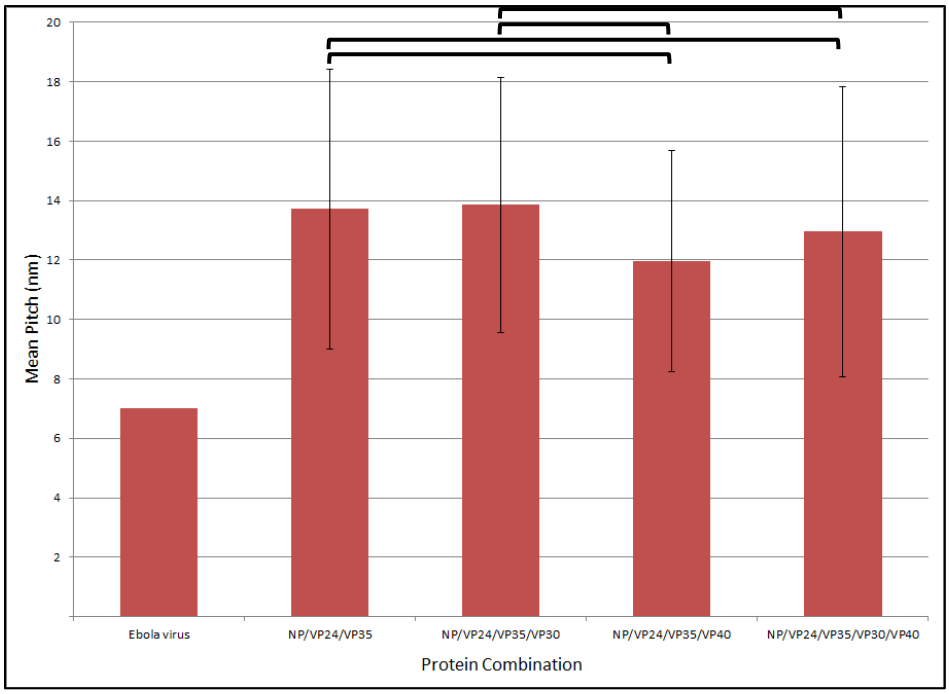

Figure 43. Mean pitch values for each protein combination when transfected cells were lysed by hypotonic freeze/thaw. Pitch of nucleocapsid-like particles was determined using ImageJ software (p=0.000625, Mann-Whitney; Bonferroni correction).

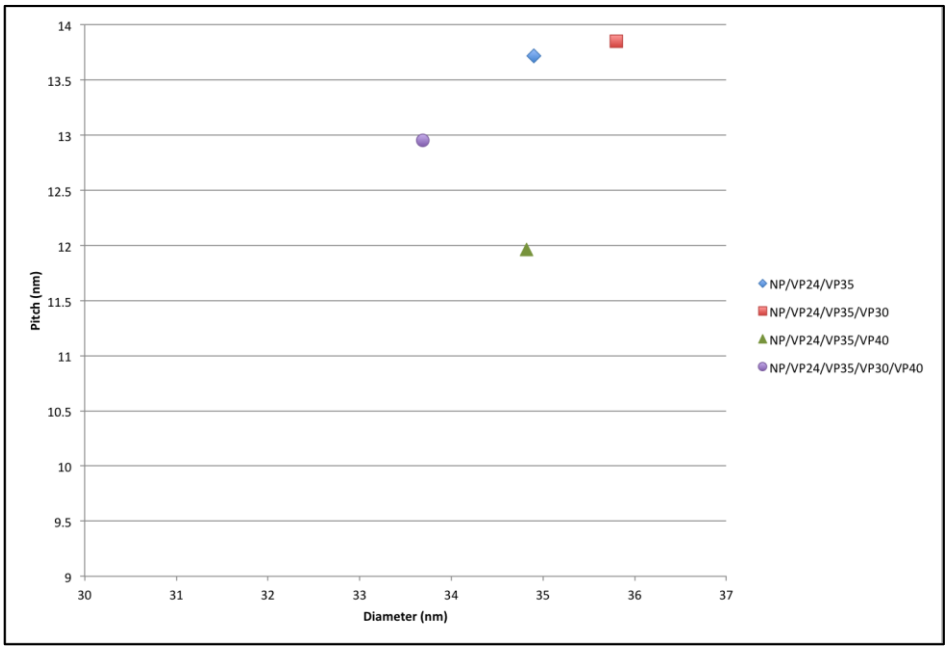

Figure 44. Scatterplot of mean diameter and pitch values for each protein combination after hypotonic freeze/thaw.

4.4.4 Isotonic freeze/thaw

Release of intracellular nucleocapsid-like particles was also attempted by three freeze/thaw cycles in isotonic PBS (150 mM NaCl). Similar to hypotonic freeze/thaw, lysis by isotonic freeze/thaw resulted in strong nucleocapsid protein migration through the iodixanol gradient. VP24 was abundant in fractions 6 and 7 when expressed with NP and VP35 (Figure 45). SDS-PAGE of NP/VP24/VP35±VP30 gradient fractions revealed additional migration of NP, VP24, VP35 and VP30 molecules to the bottom of the gradient (Figure 45bc). Therefore to investigate further, both fractions 6-7 and fraction 12 were selected and purified by ultracentrifugation. Pellets were stained with methylamine tungstate. The clean separation of the nucleocapsid proteins from the cell lysate enabled us to calculate the stoichiometry of these proteins using densitometry based on their

molecular weight (Figure 46; Section 2.18.1). In agreement with previous studies, the densitometry calculations demonstrated a 1:1 ratio of each nucleocapsid protein within these particles (Figure 46).

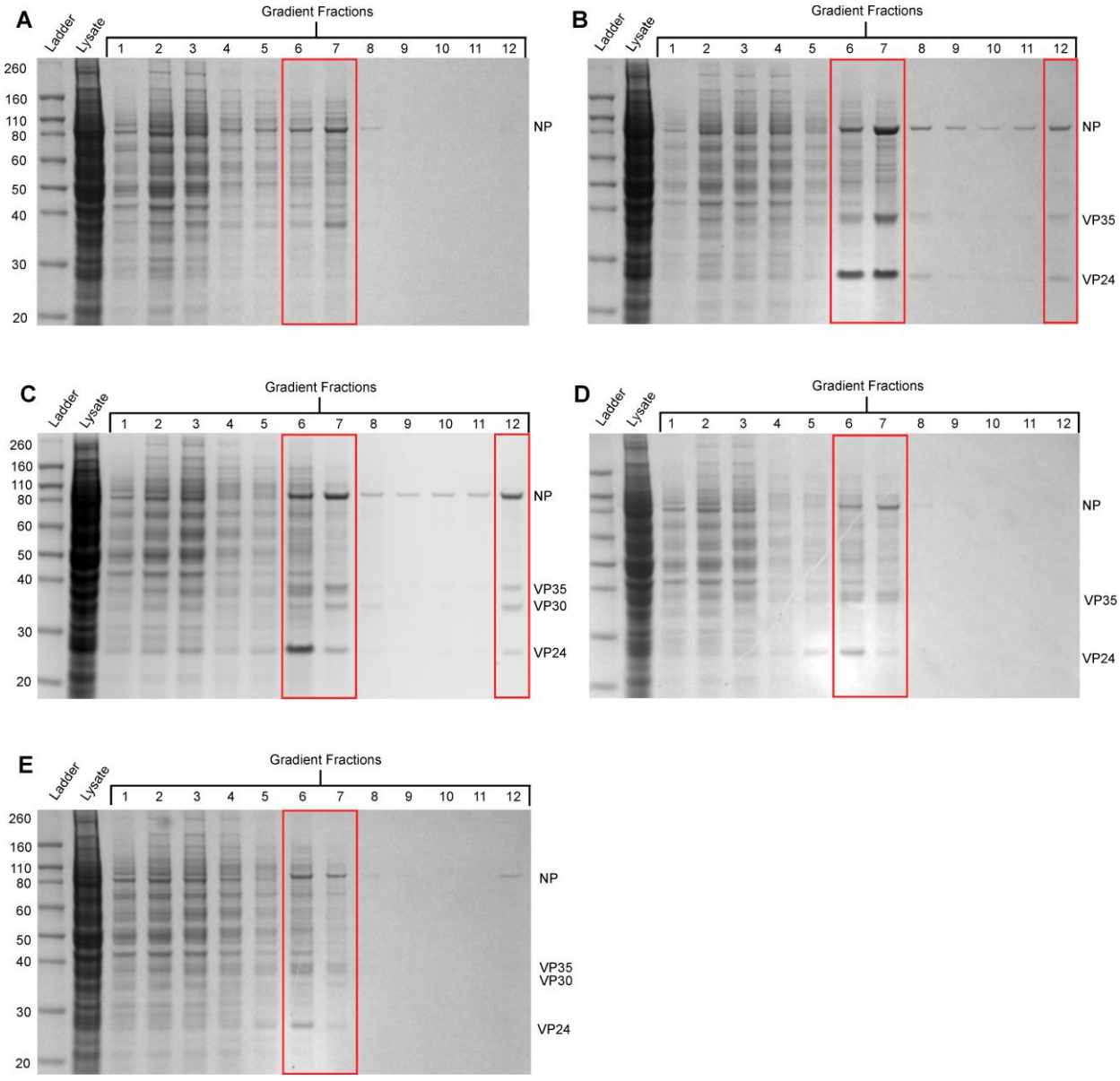

Figure 45. Gradient migration of nucleocapsid proteins after cell lysis by isotonic freeze/thaw. Cells were lysed by 3 freeze/thaw cycles. Fractions were collected top-down, with Fraction 1 representing the first fraction collected. Fractions were analyzed by SDS-PAGE. Gels were stained with Coomassie blue. Red boxes indicate fractions selected for further purification. (A) NP; (B) NP/VP24/VP35; (C) NP/VP24/VP35/VP30; (D) NP/VP24/VP35/VP40; (E) NP/VP24/VP35/VP30/VP40.

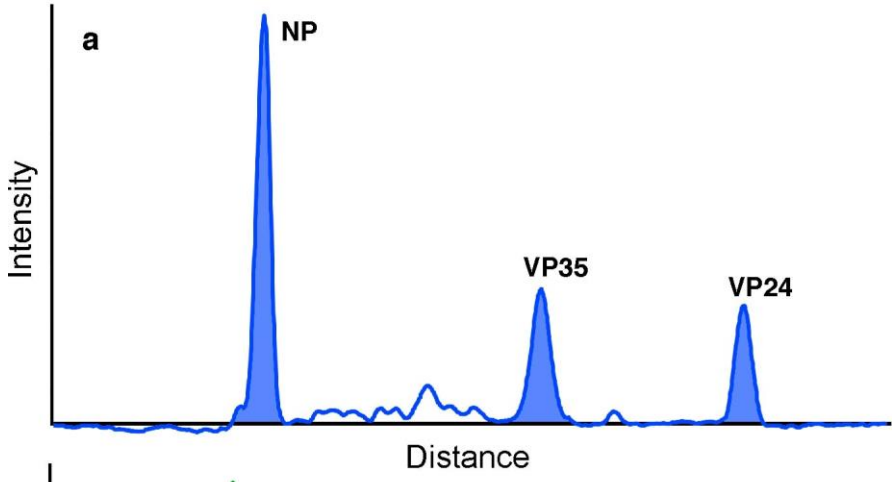

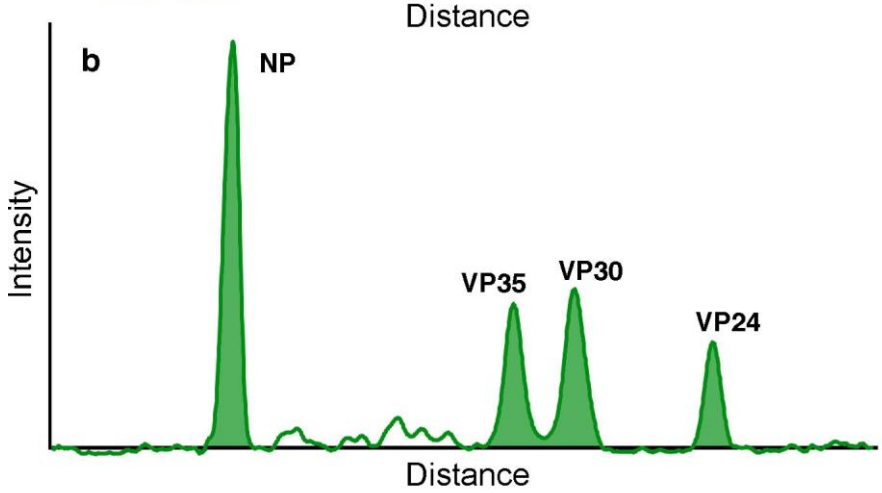

c

Protein	Mean	SD
NP	1	0
VP35	0.89	0.15
VP30	1.17	0.3
VP24	0.89	0.31

Figure 46. Densitometric analysis of SDS-PAGE protein bands. Proteins gels B and C from Figure 45 were scanned onto the computer. SPIDER software was used to determine the band signal levels from lane 12 and Excel was used to generate signal curves (A and B). Molecular weights for each protein were calculated. Estimated stoichiometry was calculated based on the area under the curves divided by the molecular mass. Two gels for each transfection were analyzed and the mean stoichiometry for each calculated. (C) The stoichiometry of NP was set to 1 and the ratio of the other proteins was determined against NP.

TEM revealed no obvious structural changes to nucleocapsid-like particles after isotonic freeze/thaw (Figure 47). As noted for the previous methods, the presence of VP30 and/or VP40 did not lead to any observable differences in structure (Figure 47). While strong protein bands were observed in fraction 12, TEM of these fractions demonstrated few intact nucleocapsid-like particles; in fact more were observed in fractions 2 and 3 than fraction 12 (Figure 48). Those that were observed in fraction 12 were short and relatively unwound.

After isotonic freeze/thaw, nucleocapsid-like particles formed in the presence of NP/VP24/VP35/VP30 had a significantly larger average diameter (36.5 nm) than the other protein combinations after isotonic freeze/thaw (Figure 49). With an average diameter of 35.06 nm, NP/VP24/VP35/VP40 nucleocapsid-like particles were significantly larger than NP/VP24/VP35 (33.77 nm) and NP/VP24/VP35/VP30/VP40 (33.28 nm). In contrast, the average diameters of NP/VP24/VP35 and NP/VP24/VP35/VP30/VP40 nucleocapsid-like particles were not significantly different from each other (Figure 50). The mean pitch measurements of NP/VP24/VP35, NP/VP24/VP35/VP30, and NP/VP24/VP35/VP30/VP40 nucleocapsid-like particles were not significantly different from each other for this lysis method (~13 nm). Similar to hypotonic freeze/thaw, NP/VP24/VP35/VP40 nucleocapsid-like particles were the most condensed, with an average pitch of 11.8 nm (Figure 50). This result is also evident when a scatterplot of average diameter and pitch measurements is created. No strong correlation was observed between diameter and pitch; however, it illustrates the difference observed between NP/VP24/VP35/VP40 and the other protein combinations (Figure 51).

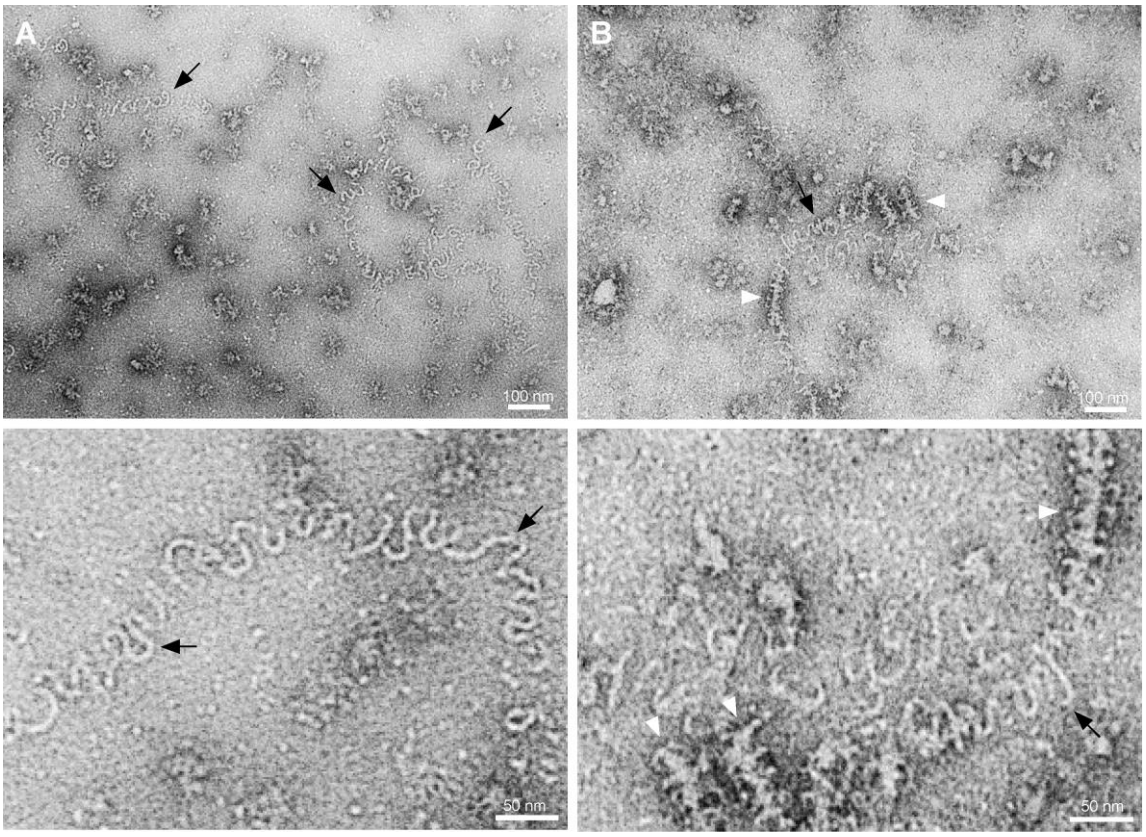

Figure 47. Nucleocapsid-like particles observed after cell lysis by isotonic freeze/thaw. Fractions 6 and 7 were purified by ultracentrifugation through PBS. Pellets were resuspended in PBS and stained with methylamine tungstate. (A) NP; (B) NP/VP24/VP35; (C) NP/VP24/VP35/VP30; (D) NP/VP24/VP35/VP40; (E) NP/VP24/VP35/VP30/VP40. Black arrows indicate loosely coiled NP-RNA and white arrowheads indicate nucleocapsid-like particles.

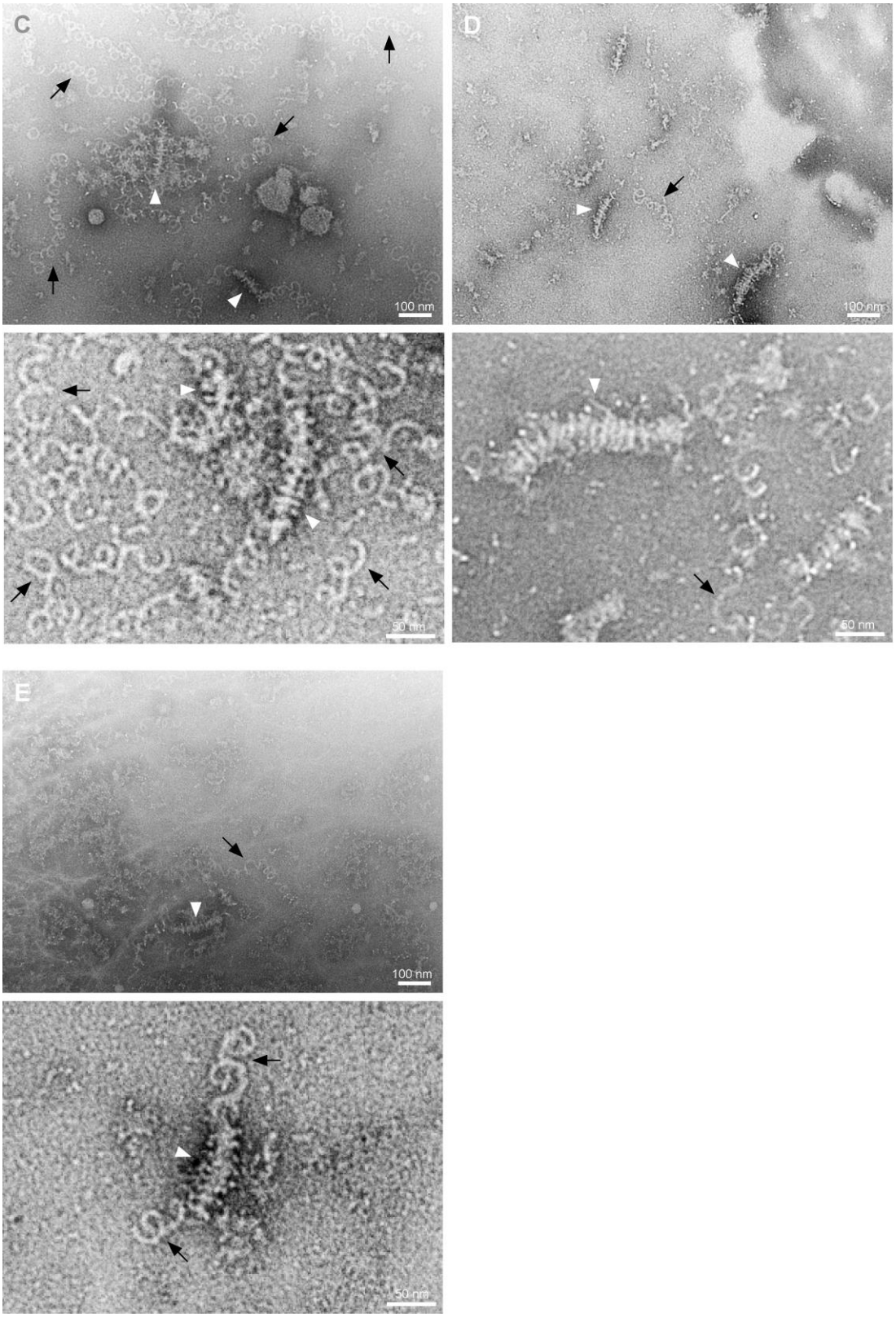

Figure 47 continued.

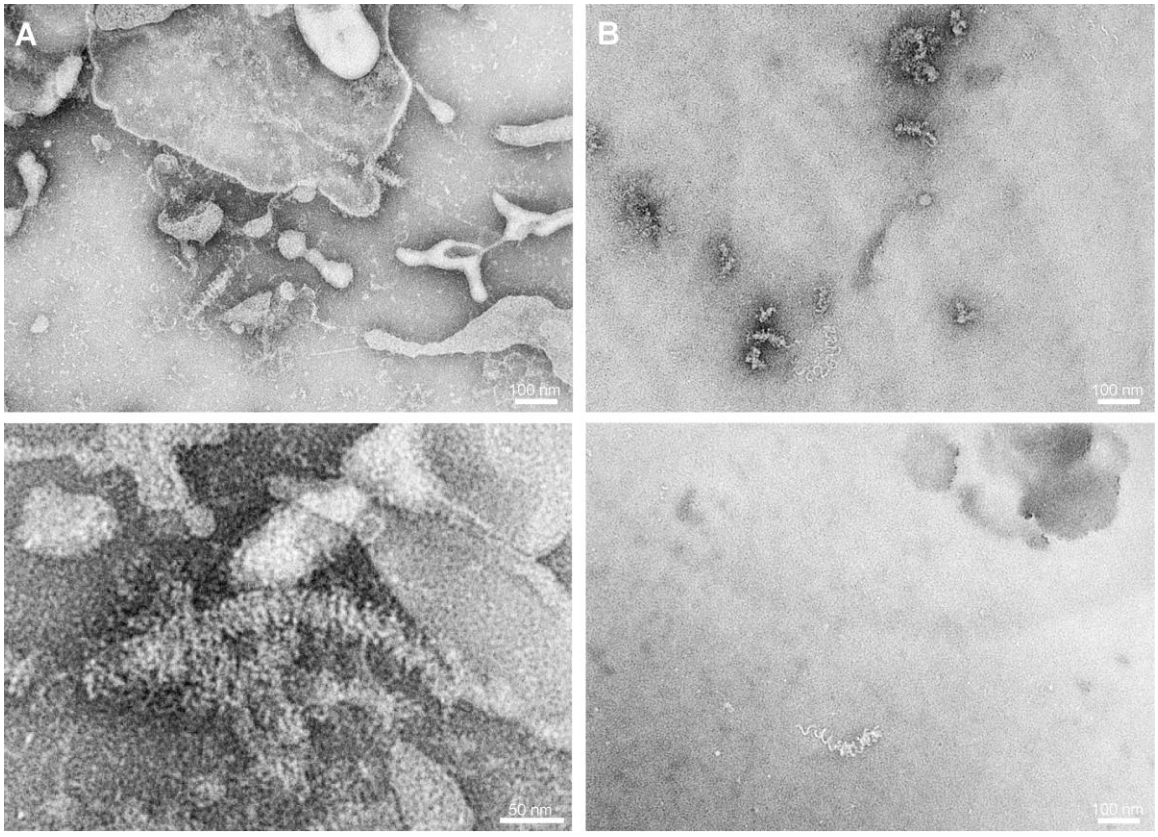

Figure 48. Nucleocapsid-like particles present in fractions 2-3 or fraction 12. Gradient fractions (A) 2 and 3 or (B) 12 were layered onto PBS and ultracentrifuged. Pellets were resuspended in PBS and stained with methylamine tungstate.

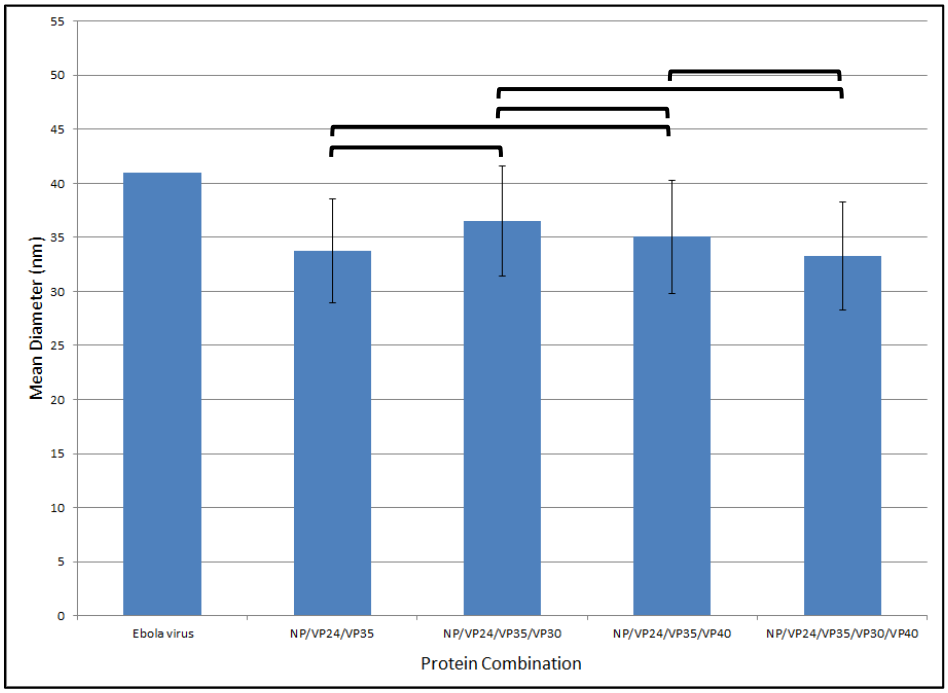

Figure 49. Comparison of mean diameter values after isotonic freeze/thaw. Measurements were made using ImageJ software (p=0.000625, student t test; Bonferroni correction).

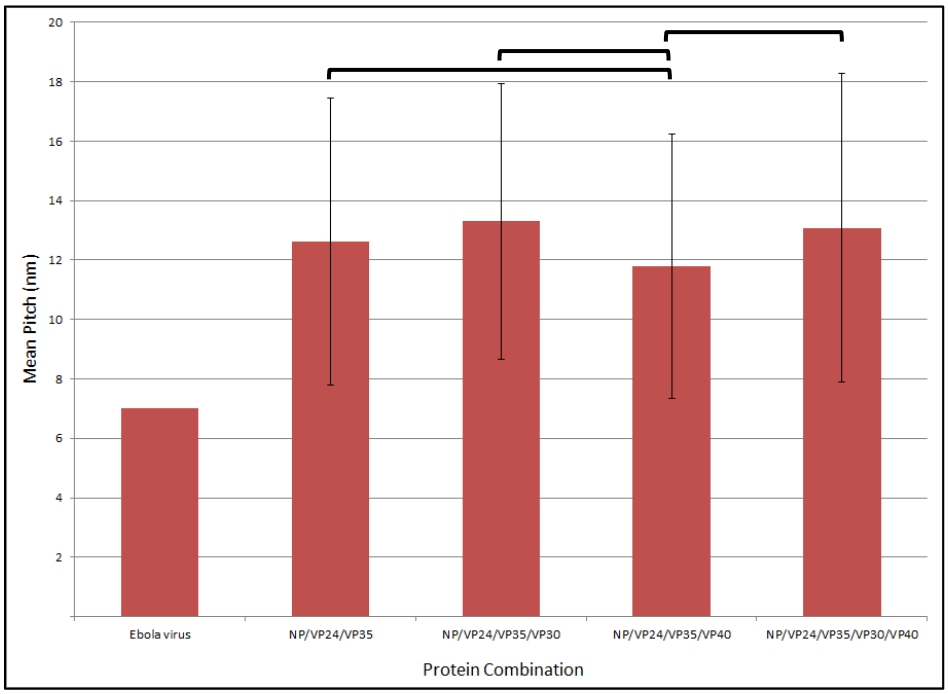

Figure 50. Comparison of mean pitch values after isotonic freeze/thaw. Measurements were made using ImageJ software (p=0.000625, Mann-Whitney; Bonferroni correction).

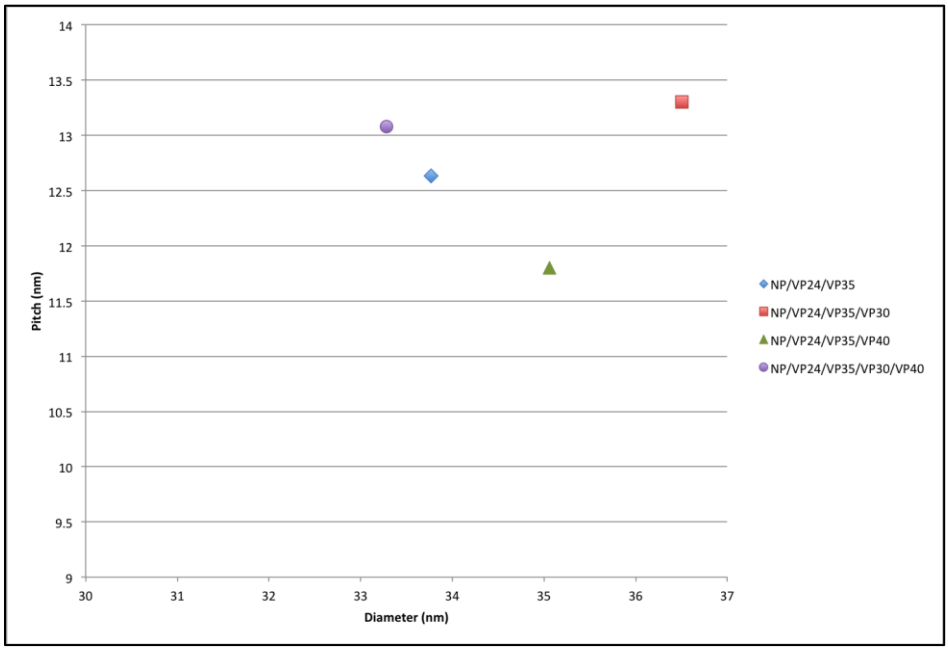

Figure 51. Scatterplot of mean diameter vs. mean pitch values for each protein combination when lysed by isotonic freeze/thaw.

4.4.5 Nucleocapsid-like particles purified from the cell culture supernatant

During the generation of VLP samples it was noted that nucleocapsid-like particles were also found in the cell culture medium when NP, VP24, and VP35 were expressed (Figure 52, Figure 53). Layering the cell culture medium onto of a 20% sucrose cushion followed by ultracentrifugation enabled the collection of these "naturally" released nucleocapsid-like particles. As these particles had not been released from transfected cells by either a) low salt b) detergent or c) freeze/thaw, I decided to measure their pitch and diameter. Nucleocapsid-like particles were present in cell culture medium in the absence of VP40 and no obvious differences in structure were seen with or without VP30 and/or VP40 (Figure 53).

Statistical analysis of the diameter measurements revealed that NP/VP24/VP35, NP/VP24/VP35/VP40, and NP/VP24/VP35/VP30/VP40 nucleocapsid-like particles were not significantly different from each other, at 31.04 nm, 30.19 nm, and 30.86 nm respectively. Particles formed in the presence of NP/VP24/VP35/VP30 had a significantly larger mean diameter than the other protein combinations (32.89 nm) (Figure 54). NP/VP24/VP35/VP30 nucleocapsid-like particles isolated from the cell culture medium were also significantly more relaxed (10.7 nm) than NP/VP24/VP35/VP40 (9.21 nm) or NP/VP24/VP35/VP30/VP40 particles (9.29 nm). The average pitch of NP/VP24/VP35 particles (9.68 nm) was not significantly different from NP/VP24/VP35/VP30 (Figure 55). The scatterplot of these values demonstrated a positive correlation between diameter and pitch (Figure 56).

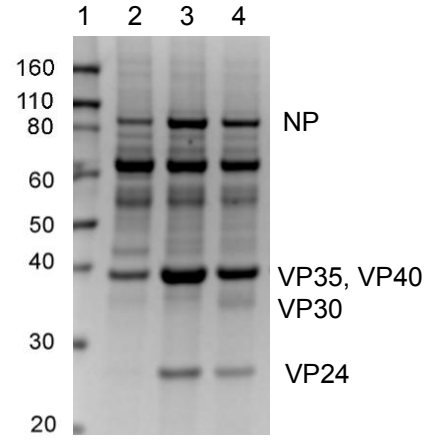

Figure 52. SDS-PAGE analysis of purified VLPs. Cell culture medium was collected 48 hours post-transfection and layered onto 20% sucrose. Pellets were resuspended in PBS and SDS-PAGE was performed. **Lane 1:** Ladder; **Lane 2:** NP/VP40; **Lane 3:** NP/VP24/VP35/VP40; **Lane 4:** NP/VP24/VP35/VP30/VP40.

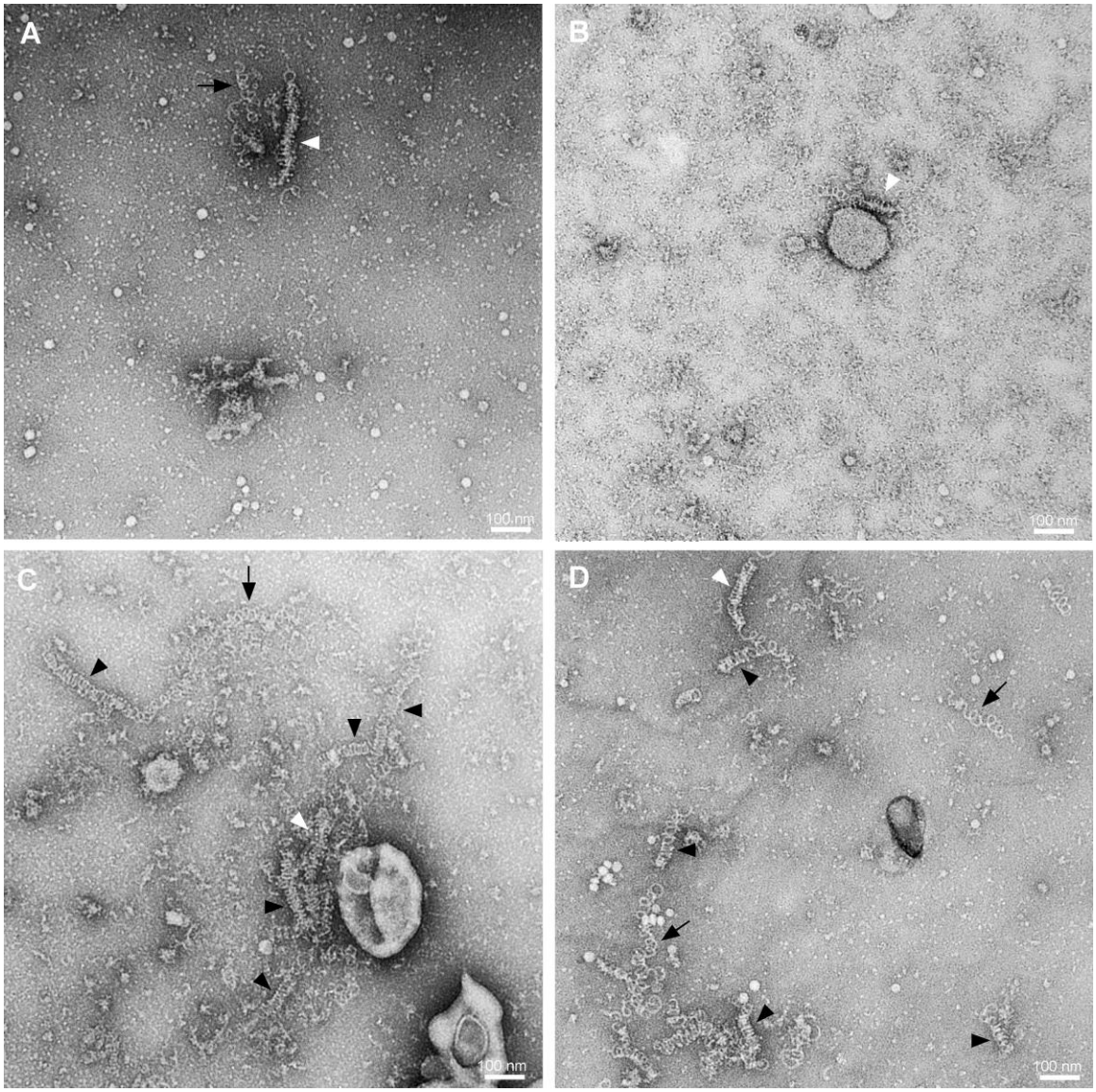

Figure 53. Nucleocapsid-like particles observed in cell culture media. Forty-eight hours post-transfection, cell culture medium was removed and layered onto 20% sucrose. Pellets were resuspended in PBS and stained with methylamine tungstate. (A) NP/VP24/VP35; (B) NP/VP24/VP35/VP30; (C) NP/VP24/VP35/VP40; (D) NP/VP24/VP35/VP30/VP40. Black arrows: loosely coiled NP-RNA; black arrowheads: tightly coiled NP-RNA; white arrowheads: nucleocapsid-like particles.

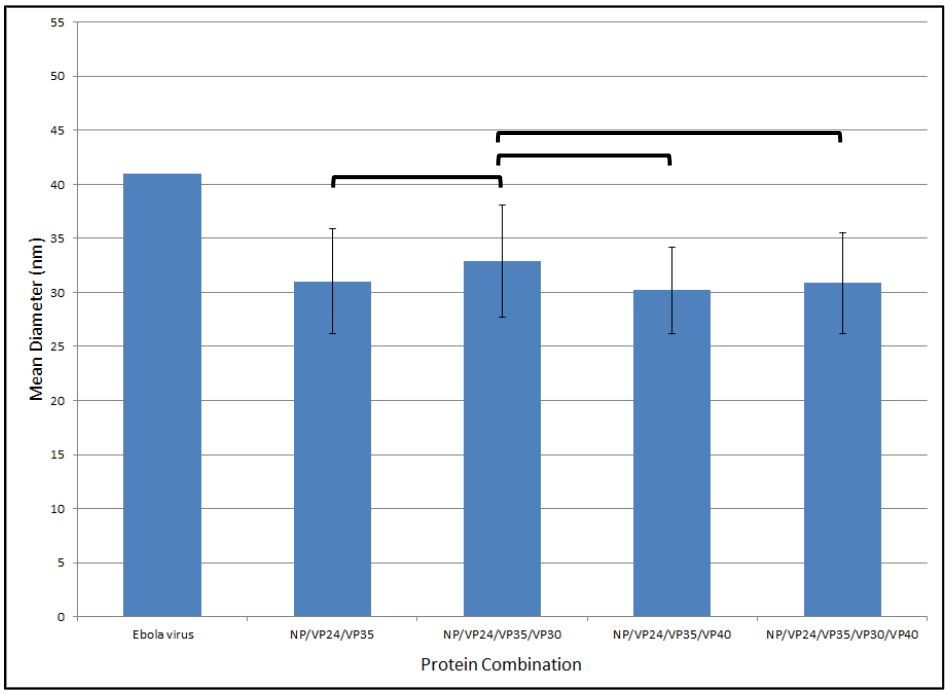

Figure 54. Comparison of mean diameter measurements from nucleocapsid-like particles purified from cell culture medium. Measurements were made using ImageJ software (p=0.000625, student t test; Bonferroni correction).

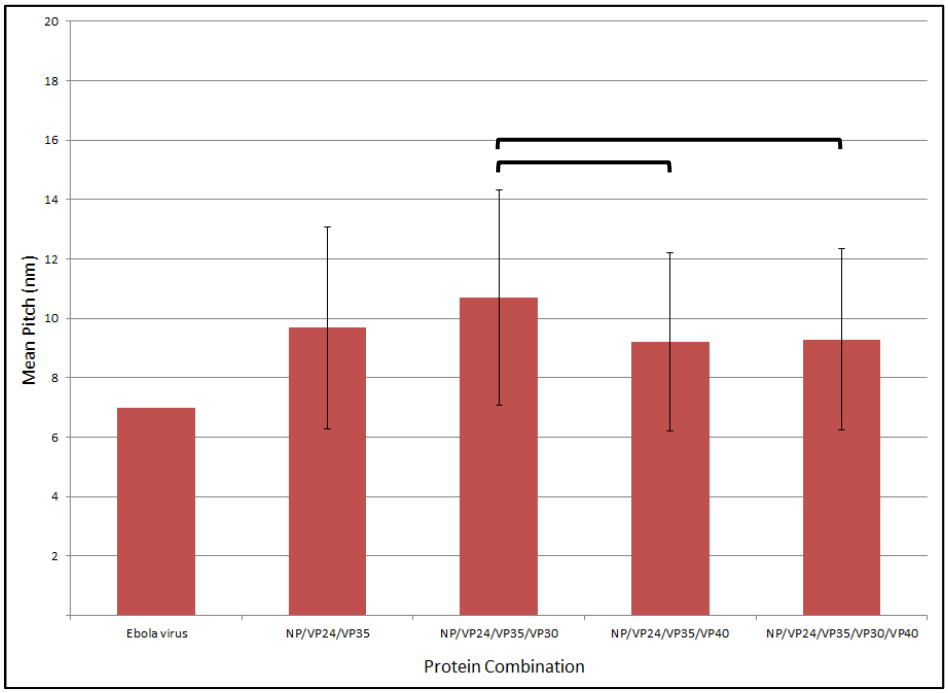

Figure 55. Comparison of mean pitch measurements from nucleocapsid-like particles purified from cell culture medium. Measurements were made using ImageJ software (p=0.000625, Mann-Whitney; Bonferroni correction).

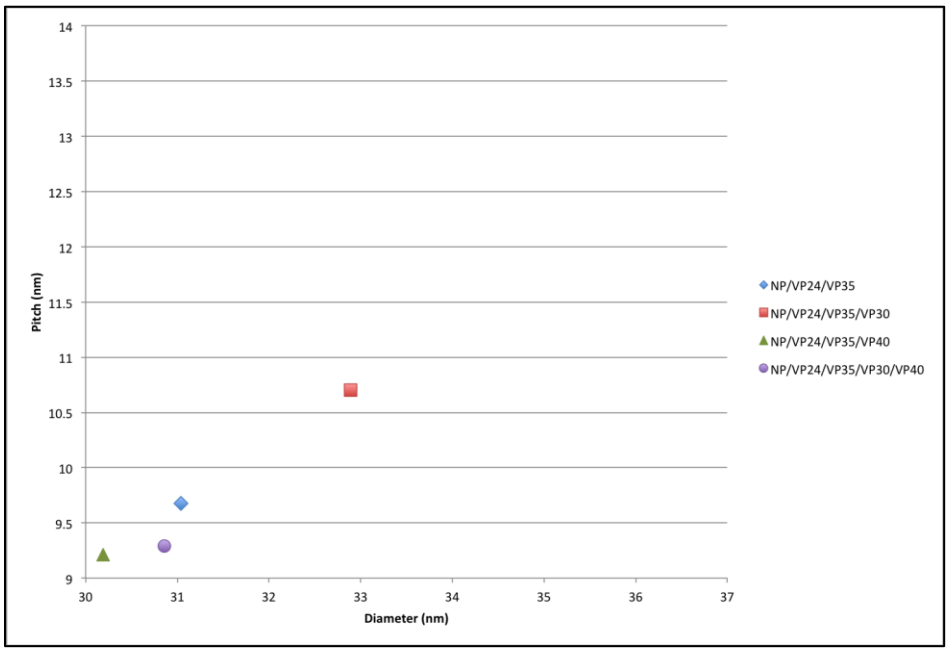

Figure 56. Scatterplot of mean diameter and pitch measurements for each protein combination after isolation from cell culture medium.

4.4.6 Additional analysis of nucleocapsid-like particles

4.4.6.1 Protein combinations

Diameter and pitch measurements were further analyzed within each protein combination in an attempt to discern additional trends (Tables 9-16). Most notably, nucleocapsid-like particles isolated from cell culture media were significantly more condensed and narrower than nucleocapsid-like particles isolated by any other method, regardless of protein combination (Tables 9-16, Figure 57, Figure 58). In addition, the average diameters of NP/VP24/VP35/VP40 nucleocapsid-like particles were not significantly different from each other, regardless of the lysis method used (other than cell culture media) (Table 11, Figure 57, Figure 58). The average pitch measurements of NP/VP24/VP35/VP40 nucleocapsid-like particles were also less likely to be affected by

lysis method (Table 15). In contrast, the diameters and pitches of the other protein combinations were variably affected by lysis method (Tables 9-16).

Table 9. Statistical comparison of diameter measurements after various lysis methods for NP/VP24/VP35 nucleocapsid-like particles.

NP/VP24/VP35	LB150	FT50	FT150	Media
LB50	p<0.000625	p<0.000625	p<0.000625	p<0.000625
LB150	-	NS	NS	p<0.000625
FT50	-	-	p<0.000625	p<0.000625
FT150	-	-	-	p<0.000625

LB50: hypotonic lysis buffer; LB150: isotonic lysis buffer; FT50: hypotonic freeze/thaw; FT150: isotonic freeze/thaw; Media: cell culture media; NS: Not significant. Diameters were compared by two-tailed student t tests. P value was calculated using Bonferroni correction.

Table 10. Comparison of diameter measurements after various lysis methods for NP/VP24/VP35/VP30 nucleocapsid-like particles.

NP/VP24/VP35/VP30	LB150	FT50	FT150	Media
LB50	NS	p<0.000625	p<0.000625	p<0.000625
LB150	-	p<0.000625	p<0.000625	p<0.000625
FT50	-	-	NS	p<0.000625
FT150	-	-	-	p<0.000625

LB50: hypotonic lysis buffer; LB150: isotonic lysis buffer; FT50: hypotonic freeze/thaw; FT150: isotonic freeze/thaw; Media: cell culture media; NS: Not significant. Diameters were compared by two-tailed student t tests. P value was calculated using Bonferroni correction

Table 11. Statistical analyses of diameter measurements after various lysis methods for NP/VP24/VP35/VP40 nucleocapsid-like particles.

NP/VP24/VP35/VP40	LB150	FT50	FT150	Media
LB50	NS	NS	NS	p<0.000625
LB150	-	NS	NS	p<0.000625
FT50	-	-	NS	p<0.000625
FT150	-	-	-	p<0.000625

LB50: hypotonic lysis buffer; LB150: isotonic lysis buffer; FT50: hypotonic freeze/thaw; FT150: isotonic freeze/thaw; Media: cell culture media; NS: Not significant. Diameters were compared by two-tailed student t tests. P value was calculated using Bonferroni correction.

Table 12. Comparison of diameter measurements after various lysis methods for NP/VP24/VP35/VP30/VP40 nucleocapsid-like particles.

NP/VP24/VP35 /VP30/VP40	LB150	FT50	FT150	Media
LB50	p<0.000625	p<0.000625	p<0.000625	p<0.000625
LB150	-	p<0.000625	NS	p<0.000625
FT50	-	-	NS	p<0.000625
FT150	-	-	-	p<0.000625

LB50: hypotonic lysis buffer; LB150: isotonic lysis buffer; FT50: hypotonic freeze/thaw; FT150: isotonic freeze/thaw; Media: cell culture media; NS: Not significant. Diameters were compared by two-tailed student t tests. P value was calculated using Bonferroni correction.

Table 13. Statistical comparison of pitch measurements after various lysis methods for NP/VP24/VP35 nucleocapsid-like particles.

NP/VP24/VP35	LB150	FT50	FT150	Media
LB50	p<0.000625	p<0.000625	p<0.000625	NS
LB150	-	p<0.000625	NS	p<0.000625
FT50	-	-	p<0.000625	p<0.000625
FT150	-	-	-	p<0.000625

LB50: hypotonic lysis buffer; LB150: isotonic lysis buffer; FT50: hypotonic freeze/thaw; FT150: isotonic freeze/thaw; Media: cell culture media; NS: Not significant. Pitches were compared by Mann-Whitney tests. P value was calculated using Bonferroni correction.

Table 14. Comparison of pitch measurements after various lysis methods for NP/VP24/VP35/VP30 nucleocapsid-like particles.

NP/VP24/VP35/VP30	LB150	FT50	FT150	Media
LB50	NS	p<0.000625	p<0.000625	p<0.000625
LB150	-	p<0.000625	p<0.000625	p<0.000625
FT50	-	-	NS	p<0.000625
FT150	-	-	-	p<0.000625

LB50: hypotonic lysis buffer; LB150: isotonic lysis buffer; FT50: hypotonic freeze/thaw; FT150: isotonic freeze/thaw; Media: cell culture media; NS: Not significant. Pitches were compared by Mann-Whitney tests. P value was calculated using Bonferroni correction.

Table 15. Statistical analyses of pitch measurements after various lysis methods for NP/VP24/VP35/VP40 nucleocapsid-like particles.

NP/VP24/VP35/VP40	LB150	FT50	FT150	Media
LB50	p<0.000625	NS	NS	p<0.000625
LB150	-	p<0.000625	NS	p<0.000625
FT50	-	-	NS	p<0.000625
FT150	-	-	-	p<0.000625

LB50: hypotonic lysis buffer; LB150: isotonic lysis buffer; FT50: hypotonic freeze/thaw; FT150: isotonic freeze/thaw; Media: cell culture media. Pitches were compared by Mann-Whitney tests. P value was calculated using Bonferroni correction.

Table 16. Statistical comparison of pitch measurements after various lysis methods for NP/VP24/VP35/VP30/VP40 nucleocapsid-like particles.

NP/VP24/VP35 /VP30/VP40	LB150	FT50	FT150	Media
LB50	NS	p<0.000625	p<0.000625	p<0.000625
LB150	-	p<0.000625	p<0.000625	p<0.000625
FT50	-	-	NS	p<0.000625
FT150	-	-	-	p<0.000625

LB50: hypotonic lysis buffer; LB150: isotonic lysis buffer; FT50: hypotonic freeze/thaw; FT150: isotonic freeze/thaw; Media: cell culture media; NS: Not significant. Pitches were compared by Mann-Whitney tests. P value was calculated using Bonferroni correction.

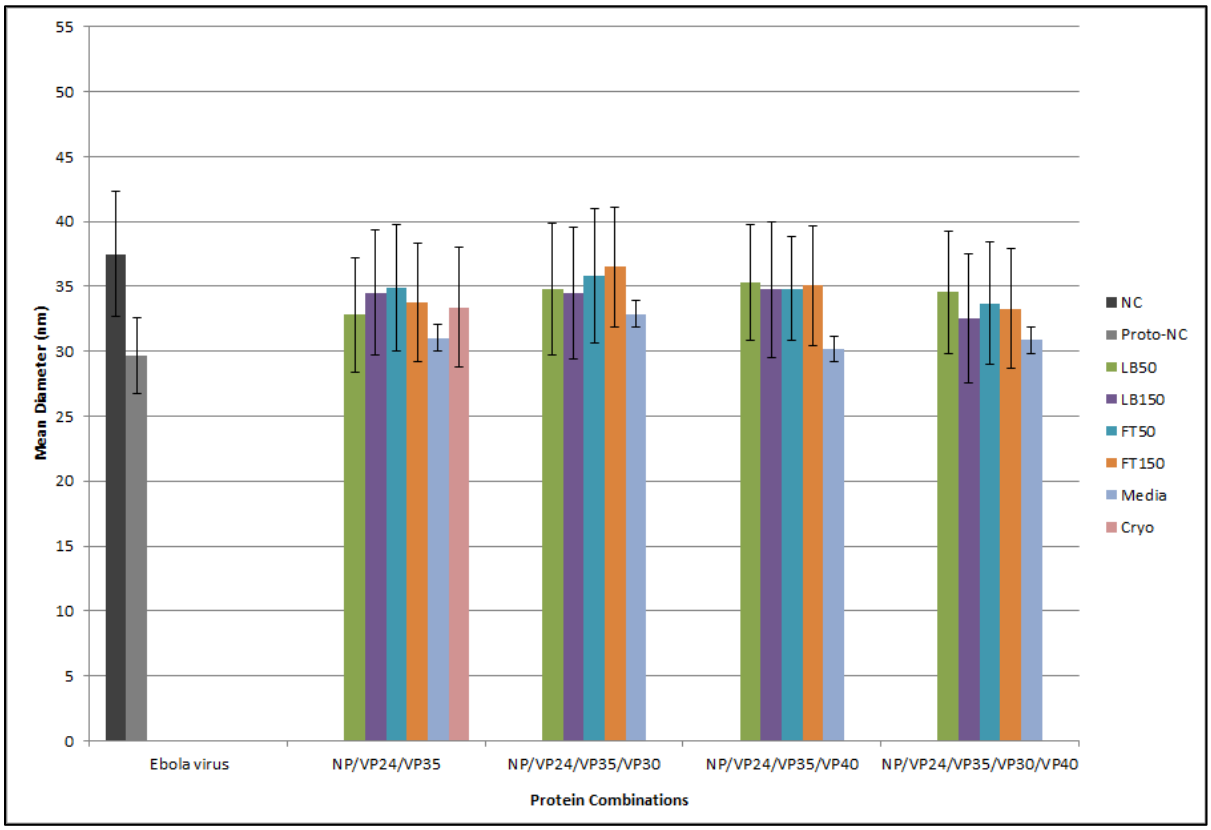

Figure 57. Mean diameter values with standard deviations for each lysis method and protein combination. NC: Cryo-preserved Ebola virus nucleocapsid; Proto-NC: Proto-nucleocapsid isolated from late stage Ebola virus infected cells; LB50: hypotonic lysis buffer; LB150: isotonic lysis buffer; FT50: hypotonic freeze/thaw; FT150: isotonic freeze/thaw; Media: nucleocapsids isolated from cell culture media; Cryo: cryo-preserved NP/VP24/VP35 nucleocapsid-like particles.

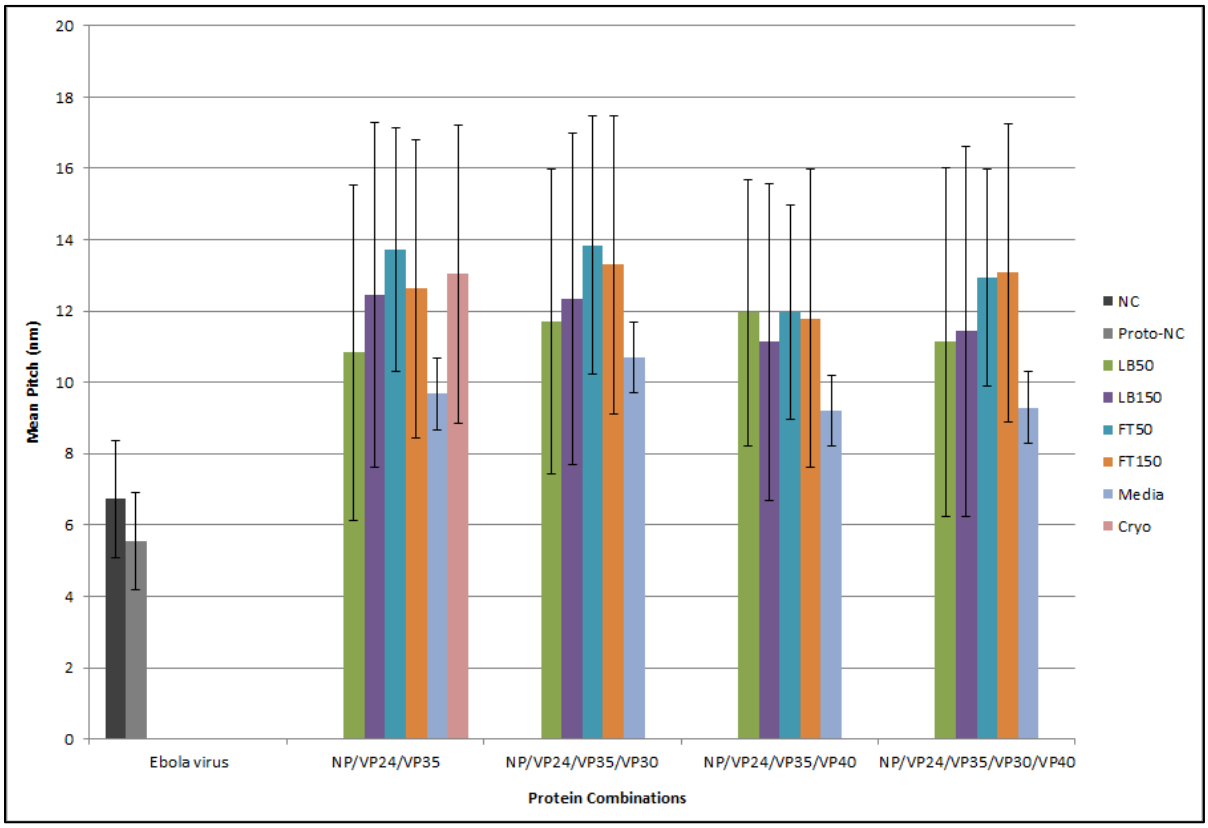

Figure 58. Mean pitch values with standard deviations for each lysis method and protein combination. NC: Cryo-preserved Ebola virus nucleocapsid; Proto-NC: Proto-nucleocapsid isolated from late stage Ebola virus infected cells; LB50: hypotonic lysis buffer; LB150: isotonic lysis buffer; FT50: hypotonic freeze/thaw; FT150: isotonic freeze/thaw; Media: nucleocapsids isolated from cell culture media; Cryo: cryo-preserved NP/VP24/VP35 nucleocapsid-like particles.

A scatterplot of all mean pitch vs. mean diameter values suggests a positive correlation between these two variables with an R^2 value of 0.627 (Figure 59). Within the scatterplot the clustering of nucleocapsid-like particles from cell culture media is apparent, as is the clustering of NP/VP24/VP35/VP40 nucleocapsid-like particles.

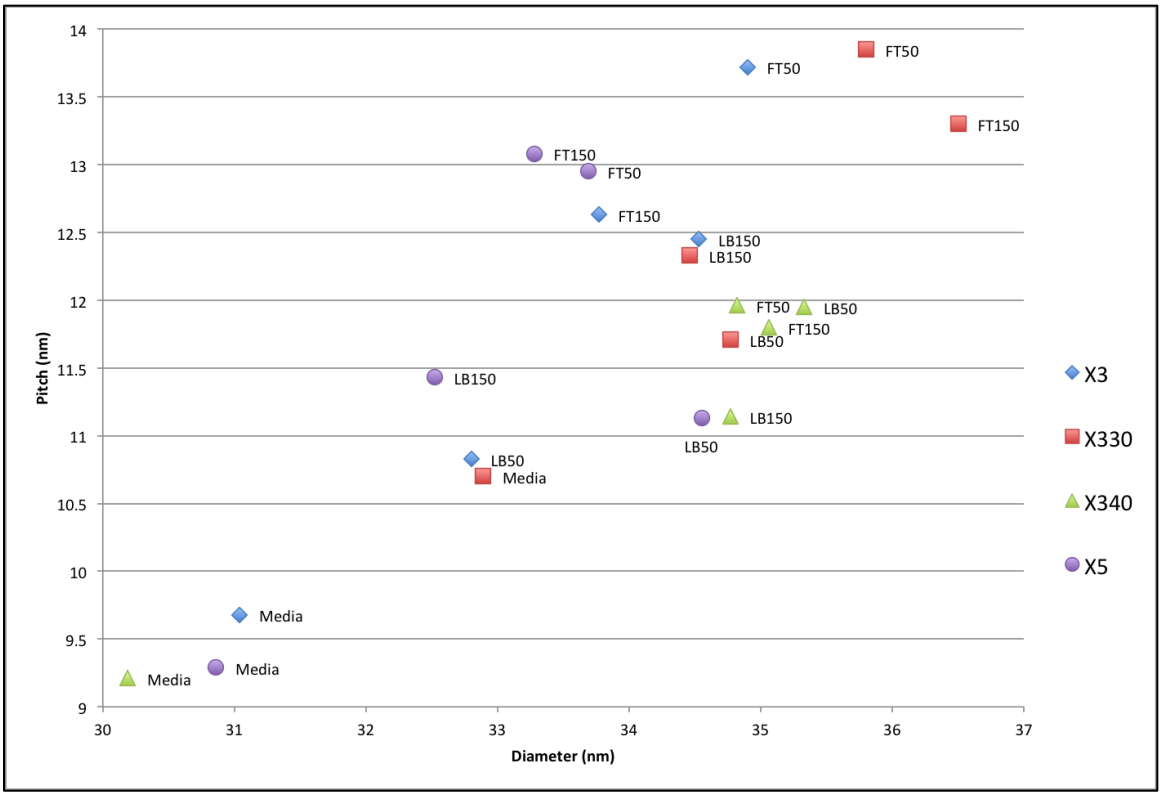

Figure 59. Combined scatterplot of all mean diameter and pitch values for each protein combination and lysis method.

4.4.6.2 Linear regression analysis

Linear regression analysis of paired mean pitch and diameter measurements for each protein combination and lysis method suggests that for every 1 unit increase in diameter, pitch should increase by 0.64 nm (Table 17, Figure 59). However, diameter and pitch measurements were not paired during these experiments and as such, linear regression was more correctly performed within diameter or pitch data sets. The categorical data (protein combination and lysis method) were dummy-coded for these analyses.

Table 17. Linear regression analysis of calculated mean pitch and diameter values.

OVERALL FIT	
Multiple R	0.792
R^2	0.627
Adjusted R^2	0.606
Standard Error	0.854
Observations	20.000

ANOVA				Alpha	0.050	
	df	*SS*	*MS*	*F*	*p-value*	*sig*
Regression	1.000	22.052	22.052	30.223	0.000	yes
Residual	18.000	13.134	0.730			
Total	19.000	35.186				

	coeff	*std err*	*t stat*	*p-value*	*lower*	*upper*
Intercept	-9.877	3.940	-2.507	0.022	-18.155	-1.600
Diameter	0.640	0.116	5.498	0.000	0.395	0.884

When all diameter measurements were taken into account in regards to lysis method and protein composition, only 7.3% of the variation observed in these data sets could be attributed to lysis method and protein combination (Table 18). NP/VP24/VP35 particle diameters were significantly different from all protein combinations except NP/VP24/VP35/VP30/VP40 (X5). Diameters measured within each lysis methods were compared against cell culture media and all were significantly different from that data set (Table 18). When the protein and lysis method data sets were divided, 5.2% of variability could be described by the lysis method and only 1.9% could be described by protein composition (Table 19, Table 20).

Table 18. Regression analysis of diameter measurements by lysis method and protein combination.

OVERALL FIT	
Multiple R	0.272
R^2	0.074
Adjusted R^2	0.073
Standard Error	4.931
Observations	11958

ANOVA					Alpha 0.05	
	df	*SS*	*MS*	*F*	*p-value*	*sig*
Regression	7	23210.458	3315.78	136.39	0	yes
Residual	11950	290506.6	24.31			
Total	11957	313717.06				

	coeff	*std err*	*t stat*	*p-value*	*lower*	*upper*
Intercept	30.59	0.163	188.083	0.000	30.271	30.9
X330-Coded	1.658	0.138	11.998	0.000	1.388	1.929
X340-Coded	0.895	0.134	6.681	0.000	0.632	1.158
X5-Coded	-0.251	0.142	-1.769	0.077	-0.529	0.027
LB50-Coded	3.35	0.153	21.888	0.000	3.05	3.65
LB150-Coded	2.977	0.156	19.142	0.000	2.672	3.282
FT50-Coded	3.622	0.158	22.919	0.000	3.312	3.932
FT150-Coded	3.619	0.154	23.495	0.000	3.317	3.921

X330: NP/VP24/VP35/VP30; X340: NP/VP24/VP35/VP40; X5: NP/VP24/VP35/ VP30/VP40; LB50: hypotonic lysis buffer; LB150: isotonic lysis buffer; FT50: hypotonic freeze/thaw; FT150: isotonic freeze-thaw.

Table 19. Regression analysis of diameter measurements by lysis method only.

OVERALL FIT	
Multiple R	0.230
R^2	0.053
Adjusted R^2	0.052
Standard Error	4.986
Observations	11958

ANOVA				Alpha	0.050	
	df	*SS*	*MS*	*F*	*p-value*	*sig*
Regression	4.000	16550.410	4137.600	166.428	0	yes
Residual	11953.000	297166.651	24.861			
Total	11957.000	313717.061				

	coeff	*std err*	*t stat*	*p-value*	*lower*	*upper*
Intercept	31.330	0.121	259.684	0.000	31.094	31.567
LB50-Coded	3.227	0.154	21.003	0.000	2.926	3.528
LB150-Coded	2.951	0.156	18.863	0.000	2.644	3.257
FT50-Coded	3.464	0.159	21.814	0.000	3.153	3.775
FT150-Coded	3.572	0.155	23.107	0.000	3.269	3.875

LB50: hypotonic lysis buffer; LB150: isotonic lysis buffer; FT50: hypotonic freeze/thaw; FT150: isotonic freeze-thaw.

Table 20. Regression analysis of diameter measurements by protein combination only.

OVERALL FIT	
Multiple R	0.138
R^2	0.019
Adjusted R^2	0.019
Standard Error	5.074
Observations	11958

ANOVA				Alpha	0.05	
	df	*SS*	*MS*	*F*	*p-value*	*sig*
Regression	3	5976.853	1992.284	77.389	0	yes
Residual	11954	307740.21	25.744			
Total	11957	313717.06				

	coeff	*std err*	*t stat*	*p-value*	*lower*	*upper*
Intercept	33.82	0.109	309.931	0.000	33.606	34.034
X330-Coded	1.235	0.141	8.744	0.000	0.958	1.512
X340-Coded	0.554	0.137	4.041	0.000	0.285	0.822
X5-Coded	-0.686	0.145	-4.736	0.000	-0.969	-0.402

X330: NP/VP24/VP35/VP30; X340: NP/VP24/VP35/VP40; X5: NP/VP24/VP35/ VP30/VP40.

Regression analysis of the pitch data sets revealed that only 7.4% of variability within the data set could be attributed to lysis method and protein combination (Table 21). Pitch measurements from NP/VP24/VP35 nucleocapsid-like particles were significantly different than all other protein combinations. As expected, the pitch measurements from nucleocapsid-like particles isolated from cell culture supernatant were significantly different from all other lysis methods (Table 21). Splitting of the two data sets demonstrates that 6.6% of pitch variability is due to the lysis method, while only 1.2% of variability is due to the protein composition (Table 22, Table 23).

Table 21. Linear regression analysis of pitch measurements by lysis method and protein combination.

OVERALL FIT	
Multiple R	0.273
R^2	0.075
Adjusted R^2	0.074
Standard Error	4.266
Observations	13434

ANOVA				Alpha	0.05	
	df	*SS*	*MS*	*F*	*p-value*	*sig*
Regression	7	19689.918	2812.845	154.554	0	yes
Residual	13426	244350	18.2			
Total	13433	264040.16				

	coeff	*std err*	*t stat*	*p-value*	*lower*	*upper*
Intercept	9.786	0.122	79.929	0.000	9.546	10.026
X330-Coded	0.538	0.108	4.987	0.000	0.326	0.749
X340-Coded	-0.549	0.105	-5.253	0.000	-0.754	-0.344
X5-Coded	-0.234	0.111	-2.105	0.035	-0.451	-0.016
LB50-Coded	1.703	0.12	14.187	0.000	1.468	1.939
LB150-Coded	2.065	0.124	16.696	0.000	1.822	2.307
FT50-Coded	3.397	0.125	27.255	0.000	3.153	3.642
FT150-Coded	2.986	0.122	24.393	0.000	2.746	3.226

X330: NP/VP24/VP35/VP30; X340: NP/VP24/VP35/VP40; X5: NP/VP24/VP35/ VP30/VP40; LB50: hypotonic lysis buffer; LB150: isotonic lysis buffer; FT50: hypotonic freeze/thaw; FT150: isotonic freeze-thaw.

Table 22. Regression analysis of pitch measurements by lysis method only.

OVERALL FIT	
Multiple R	0.257
R^2	0.066
Adjusted R^2	0.066
Standard Error	4.285
Observations	13434

ANOVA					Alpha	0.05
	df	*SS*	*MS*	*F*	*p-value*	*sig*
Regression	4	17458.927	4364.732	237.707	0	yes
Residual	13429	246581.23	18.362			
Total	13433	264040.16				

	coeff	*std err*	*t stat*	*p-value*	*lower*	*upper*
Intercept	9.672	0.091	105.868	0.000	9.493	9.851
LB50-Coded	1.755	0.119	14.747	0.000	1.521	1.988
LB150-Coded	2.035	0.124	16.46	0.000	1.793	2.277
FT50-Coded	3.428	0.124	27.667	0.000	3.185	3.671
FT150-Coded	3.091	0.122	25.333	0.000	2.852	3.33

LB50: hypotonic lysis buffer; LB150: isotonic lysis buffer; FT50: hypotonic freeze/thaw; FT150: isotonic freeze-thaw.

Table 23. Regression analysis of pitch measurements by protein combination only.

OVERALL FIT	
Multiple R	0.109
R^2	0.012
Adjusted R^2	0.012
Standard Error	4.408
Observations	13434

ANOVA					Alpha	0.05
	df	*SS*	*MS*	*F*	*p-value*	*sig*
Regression	3	3148.154	1049.385	54.019	0	yes
Residual	13430	260892	19.426			
Total	13433	264040.16				

	coeff	*std err*	*t stat*	*p-value*	*lower*	*upper*
Intercept	12.135	0.081	150.673	0.000	11.9	12.29
X330-Coded	0.279	0.11	2.524	0.012	0.06	0.495
X340-Coded	-0.915	0.107	-8.571	0.000	-1.12	-0.705
X5-Coded	-0.59	0.113	-5.216	0.000	-0.81	-0.368

X330: NP/VP24/VP35/VP30; X340: NP/VP24/VP35/VP40; X5: NP/VP24/VP35/VP30/VP40.

4.4.7 Statistical analysis of combined protein measurements

In an attempt to differentiate any overall trends with regards to protein composition, data sets were merged such that the lysis method was no longer recorded. Due to the significantly smaller diameter and pitch measurements for the "Media" nucleocapsid-like particles, these data sets were left out of this analysis. It was felt that these significantly smaller values might skew the results. Statistical analysis by Mann-Whitney tests reveals that nucleocapsid-like particles formed in the presence of NP/VP24/VP35 or NP/VP24/VP35/VP30/VP40 were not statistically different from each other with regards to diameter or pitch (Figure 60, Figure 61). NP/VP24/VP35/VP30 particles on average had larger diameters and pitches, whereas NP/VP24/VP35/VP40 particles had larger diameters but smaller pitches on average (Figure 60, Figure 61).

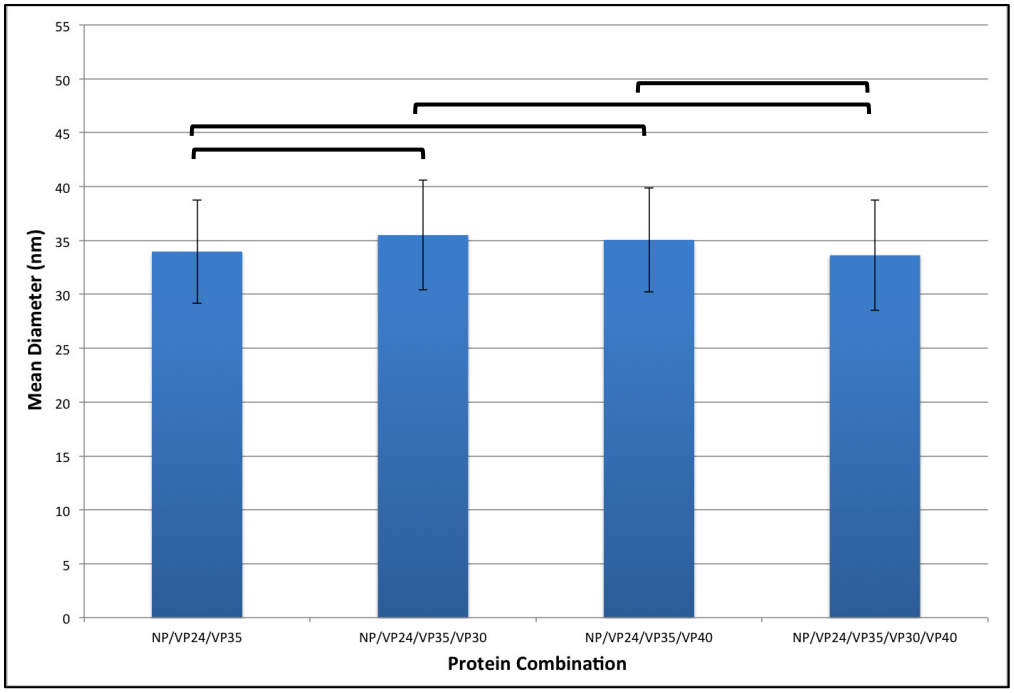

Figure 60. Comparison of mean diameters for each protein combination. All diameter measurements, except media, were combined by protein combination and statistical analysis performed (p=0.000625, Mann-Whitney; Bonferroni correction).

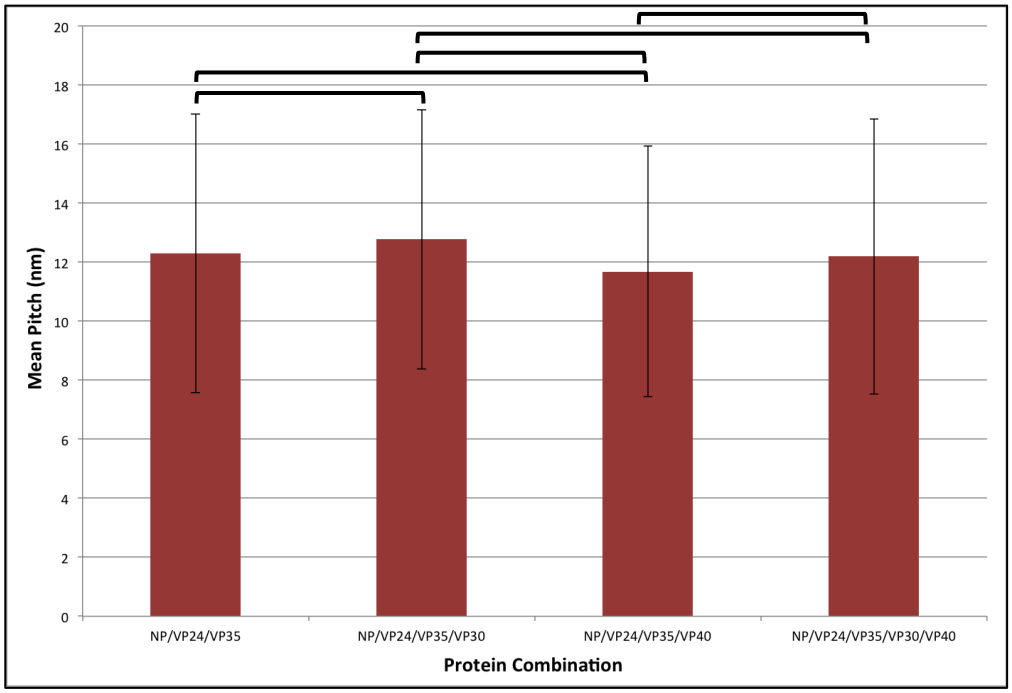

Figure 61. Comparison of mean pitches for each protein combination. All pitch measurements, except media, were combined by protein combination and statistical analysis performed (p=0.000625, Mann-Whitney; Bonferroni correction).

4.5 Summary

Dual transfections of Ebola virus NP with one other nucleocapsid protein resulted in differential protein migration through iodixanol density gradients and the purification of loosely coiled NP-RNA from cell lysates. Both NP/VP35 and NP/VP30 demonstrated strong interactions as evident by their co-migration during density gradient ultracentrifugation. In contrast, NP and VP24 displayed only weak interactions when these two proteins were co-expressed. Expression of NP/VP24/VP35 resulted in the self-assembly and co-migration of all three proteins through the density gradient and the isolation of nucleocapsid-like particles. These particles appeared similar to the Ebola virus nucleocapsid but were less condensed and slightly narrower than the structure determined by cryo-EM. The average pitch of the nucleocapsid-like particles ranged from 9.21-13.85 nm and the average diameter ranged from 30.19-36.5 nm. For comparison, Beniac et al. (2012) calculated the pitch of the Ebola virus nucleocapsid to be 6.96 nm and the diameter to be 41 nm using cryo-EM and tomographic image analysis. Addition of VP30 and/or VP40 did not visibly affect the assembly of these particles; however, upon measurement the diameter and pitch of these helical particles revealed significant differences. Various lysis methods were investigated to determine their effect on the structure of the nucleocapsid-like particles and were found to have small, but statistically significant effects on the diameter and pitch of nucleocapsid-like particles. Nucleocapsid-like particles isolated from transfected cell culture medium were the most narrow and condensed. NP/VP24/VP35/VP40 nucleocapsid-like particles were least likely to be statistically different from each other, regardless of lysis method.

Chapter 5. The effects of ultracentrifugation, fixation, and cryo-preservation on the structure of the nucleocapsid-like particles

5.1 Rationale

The lysis method experiments described in Chapter 4 demonstrated that isolated nucleocapsid-like particles maintained an overall uniform helical structure that displayed a high degree of variability in diameter and pitch. My previous experiments used ultracentrifugation to first separate the particles by density gradient and then pellet protein out of the gradient fractions because iodixanol can affect the appearance of negative stain. To investigate whether this method of purification had an effect on the structure of the nucleocapsid-like particles, I examined nucleocapsid-like particles directly from the cell lysate, from the iodixanol fractions, or after dialysis of the gradient fractions to remove the iodixanol.

In addition, two different methods of fixation were performed to determine if chemical crosslinking could reduce the variation in diameter and pitch (Kastner et al. 2008; Stark 2010). The addition of glutaraldehyde to density gradients (Grafix) is a method that has been successful in stabilizing dynamic structures such as the spliceosomal B complex, the *Trypanosoma brucei* editosome, and 70S *E. coli* ribosome initiation complex for cryo-electron microscopy (Goringer et al. 2011; Kastner et al. 2008; Stark 2010). This fixation technique can reduce the number of intermediate structures visible by cryo-EM resulting in enhanced image analysis and higher resolution images (Kastner et al. 2008; Stark 2010). Therefore, a modified Grafix protocol was investigated as a method for the stabilization of the nucleocapsid-like particles (Kastner et al. 2008; Stark 2010). The use of a chemical cross-linker and subsequent analysis by mass spectrometry is commonly used to elucidate protein-protein interactions both within intact cells and between purified proteins. In this

study, three different chemicals were investigated to determine whether cross-linking of intact transfected cells would stabilize the nucleocapsid-like particles during lysis and purification. PFA, DSS, and EGS are all membrane soluble chemicals with different spacer lengths. Treatment with EGS or DSS leads to covalent interactions between lysine residues that are 16.1 Å or 11.4 Å apart, respectively (Song et al. 2012). PFA has a much shorter spacer length of 2.3-2.7 Å and can be a reversible reaction (Klockenbusch and Kast 2010). The Ebola virus proto-nucleocapsids observed in Chapter 3.4 were fixed by PFA. Crosslinking would also indicate how closely associated the nucleocapsid proteins are; for example, cross-linking after PFA treatment would suggest more closely interacting proteins than DSS or EGS (Klockenbusch and Kast 2010; Song et al. 2012).

Lastly, nucleocapsid-like particles were flash-frozen and imaged by cryo-EM to confirm that the negative staining process had not significantly affected particle structure. Negative staining requires that a sample be dried onto a grid, which can lead to structural deformations. In contrast, vitrification preserves the native structure of a sample and results in a more accurate representation. Thus, diameter and pitch measurements for nucleocapsid-like particles observed by cryo-EM were compared to the negative stain measurements from Chapter 4.

5.2 Hypotheses

1. No difference in nucleocapsid-like particles will be observed in cell lysates, iodixanol fractions, after dialysis, or after pelleting.
2. The addition of glutaraldehyde to the iodixanol gradient will not result in more condensed nucleocapsid-like particles.
3. Fixation of live cells will successfully maintain intracellular nucleocapsid-like particles after cell lysis.
4. No significant difference between cryo-preserved and negative stained nucleocapsid-like particles will be observed.

5.3 Objectives

1. Negative stain cell lysates, iodixanol gradient fractions 6 and 7, and dialysis products and inspect nucleocapsid-like particles
2. Generate iodixanol gradients with either 0.15% glutaraldehyde in the 15% solution or in both the 15% and 30% solutions
3. Inspect nucleocapsid-like particles purified in the glutaraldehyde-iodixanol gradients
4. Treat transfected cells with the chemical cross-linkers DSS, EGS, or PFA
5. Lyse cross-linked cells and perform differential ultracentrifugation. Image purified nucleocapsid-like particles.
6. Prepare nucleocapsid-like particles by hypotonic lysis buffer and differential ultracentrifugation. Flash-freeze these particles using the Vitrobot. Image by cryo-EM.

5.4 Results

5.4.1 Comparison of purification methods

To investigate whether differential ultracentrifugation and/or the pelleting of fractions was affecting the structure of the nucleocapsid-like particles, lysates and iodixanol fractions were negative stained and visualized by TEM. Nucleocapsid-like particles were difficult to find in cell lysates due to the high level of debris and the small size of the particles. The particles appeared similar to those observed after pelleting by ultracentrifugation. No extensive measurements were taken due to the low sample size (Figure 62a). Likewise, nucleocapsid-like particles observed directly from gradient fractions 2-3, 6-7, or 12 did not demonstrate perceivable differences in assembly (Figure 48, Figure 62bc). Dialysis of gradient fractions resulted in a loss of protein and/or dilution of nucleocapsid-like particles (Figure 63). Nucleocapsid-like particles were difficult to find in the dialysis products and were comparable to the particles observed after pelleting (Figure 62f). As such, nucleocapsid-like particles were isolated by ultracentrifugation for most of the remainder of this study.

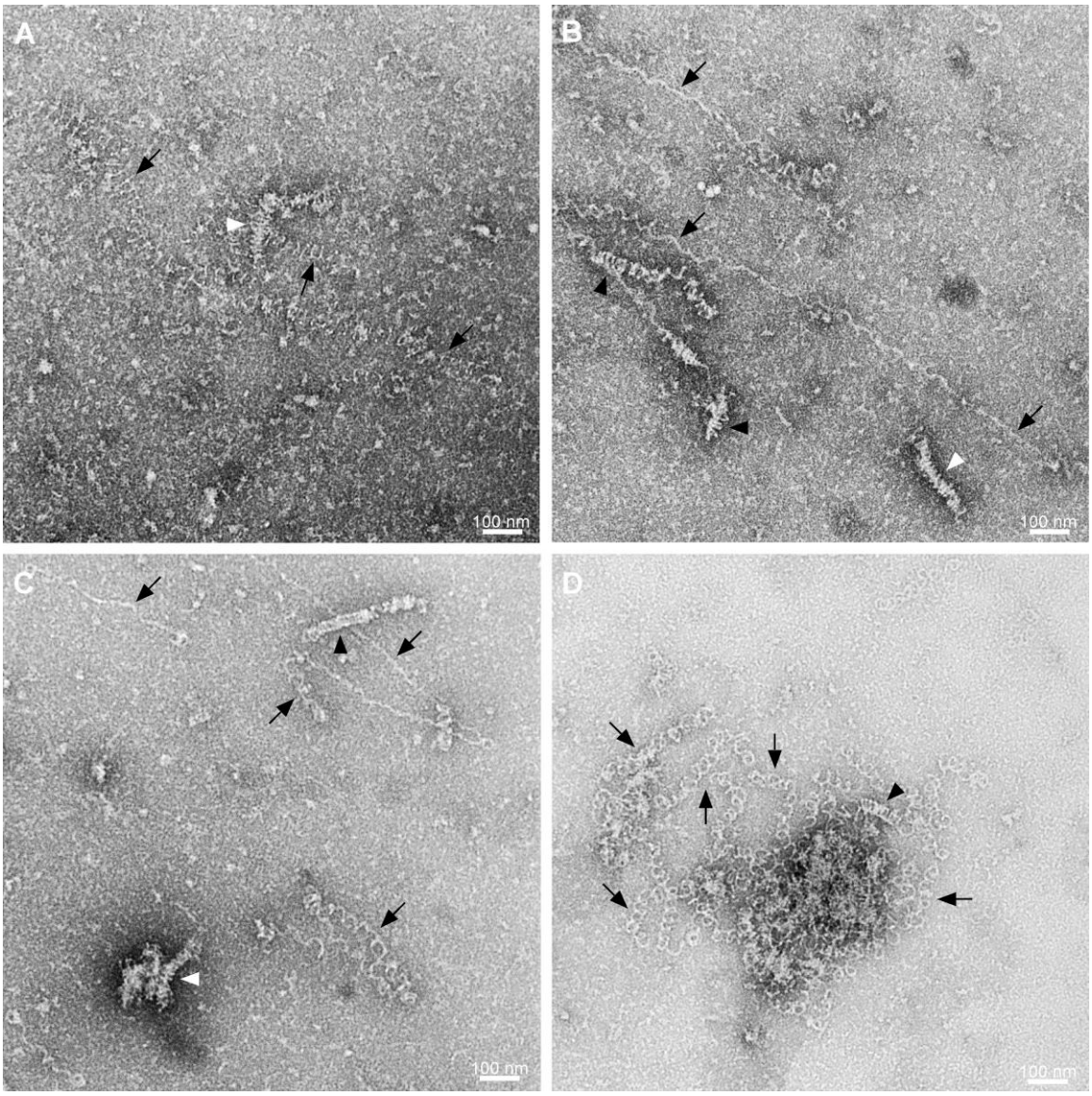

Figure 62. Nucleocapsid-like particles observed during various stages of purification. Cells were transfected with NP, VP24, and VP35 for 48 hours, after which they were lysed using isotonic lysis buffer. Lysates were loaded onto 15-30% iodixanol gradients and ultracentrifuged. Fraction 6 was collected and either dialyzed or further centrifuged to pellet protein. Samples were stained with methylamine tungstate. (A) Direct from lysate; (B, C) Direct from fraction 6; (D, E) After dialysis; (F) From pellet.

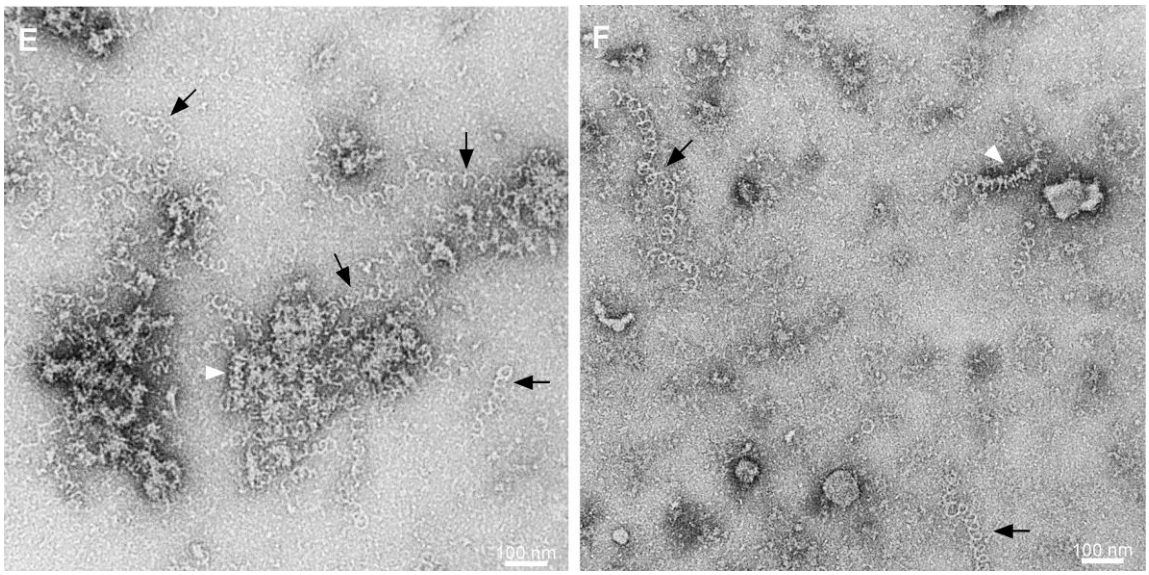

Figure 62 continued.

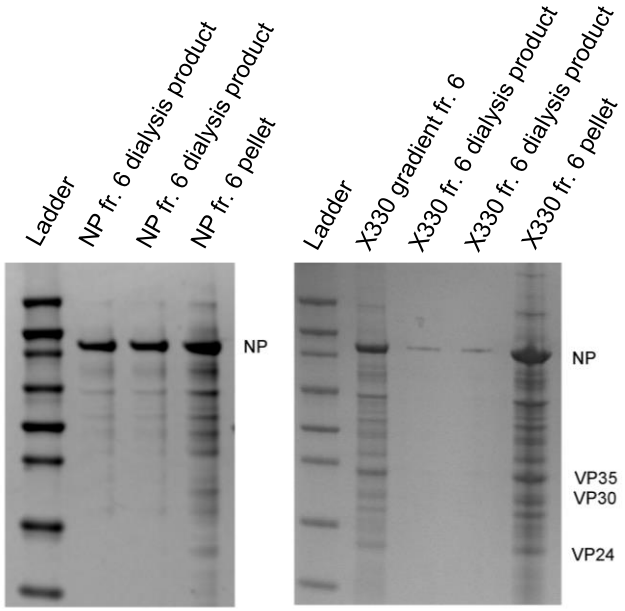

Figure 63. Effects of dialysis on protein concentration. X3: NP/VP24/VP35; X330: NP/VP24/VP35/VP30; Fr: fraction.

5.4.2 Fixation methods

5.4.2.1 Gradient fixation

Glutaraldehyde was added to the density gradients to investigate whether nucleocapsid-like particles could be stabilized during differential ultracentrifugation (Kastner et al. 2008; Stark 2010). Two different iodixanol gradients were made, one with 0.15% glutaraldehyde in the upper 15% layer and the other with 0.15% glutaraldehyde in both the 15% and 30% iodixanol layers (Kastner et al. 2008; Stark 2010). Cells lysed by hypotonic lysis buffer were layered onto gradients and ultracentrifuged. Fraction 6 of each gradient was further ultracentrifuged to remove glutaraldehyde and iodixanol. Fixation of NP alone or in combination with VP30 or VP35 did not result in particles that resembled the proto-nucleocapsids described in Chapter 3.4 (Figure 64). Furthermore, the presence of glutaraldehyde in both the 15% and 30% layer appeared to be detrimental to NP-RNA coils (Figure 65). The migration and purification of NP/VP24/VP35 and NP/VP24/VP35/VP30 particles through the glutaraldehyde gradients was also unfavourable, with drastically fewer nucleocapsid-like particles observed and most appearing disorganized (Figure 64, Figure 65). The SDS-PAGE of gradient fractions was not successful due to the presence of glutaraldehyde.

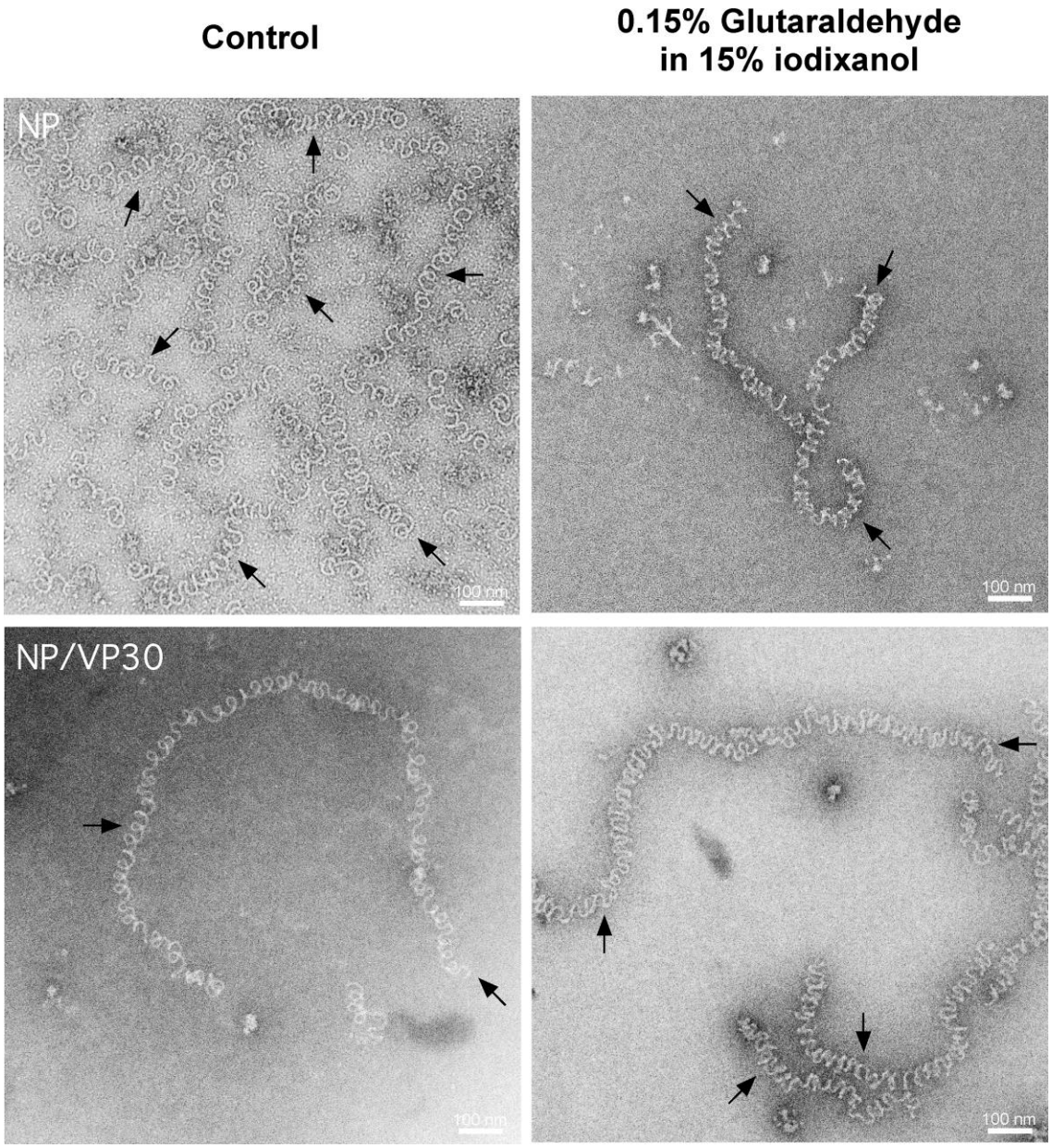

Figure 64. Nucleocapsid-like particles purified from gradients containing 0.15% glutaraldehyde in the 15% layer (panels above and on following page). Cells were lysed in hypotonic lysis buffer and layered onto gradients containing glutaraldehyde. Fraction 6 from each gradient was layered onto 50 mM NaCl PBS and ultracentrifuged. Pellets were resuspended in 50 mM NaCl PBS and stained with methylamine tungstate. Black arrows: loosely coiled NP-RNA; white arrowheads: nucleocapsid-like particles.

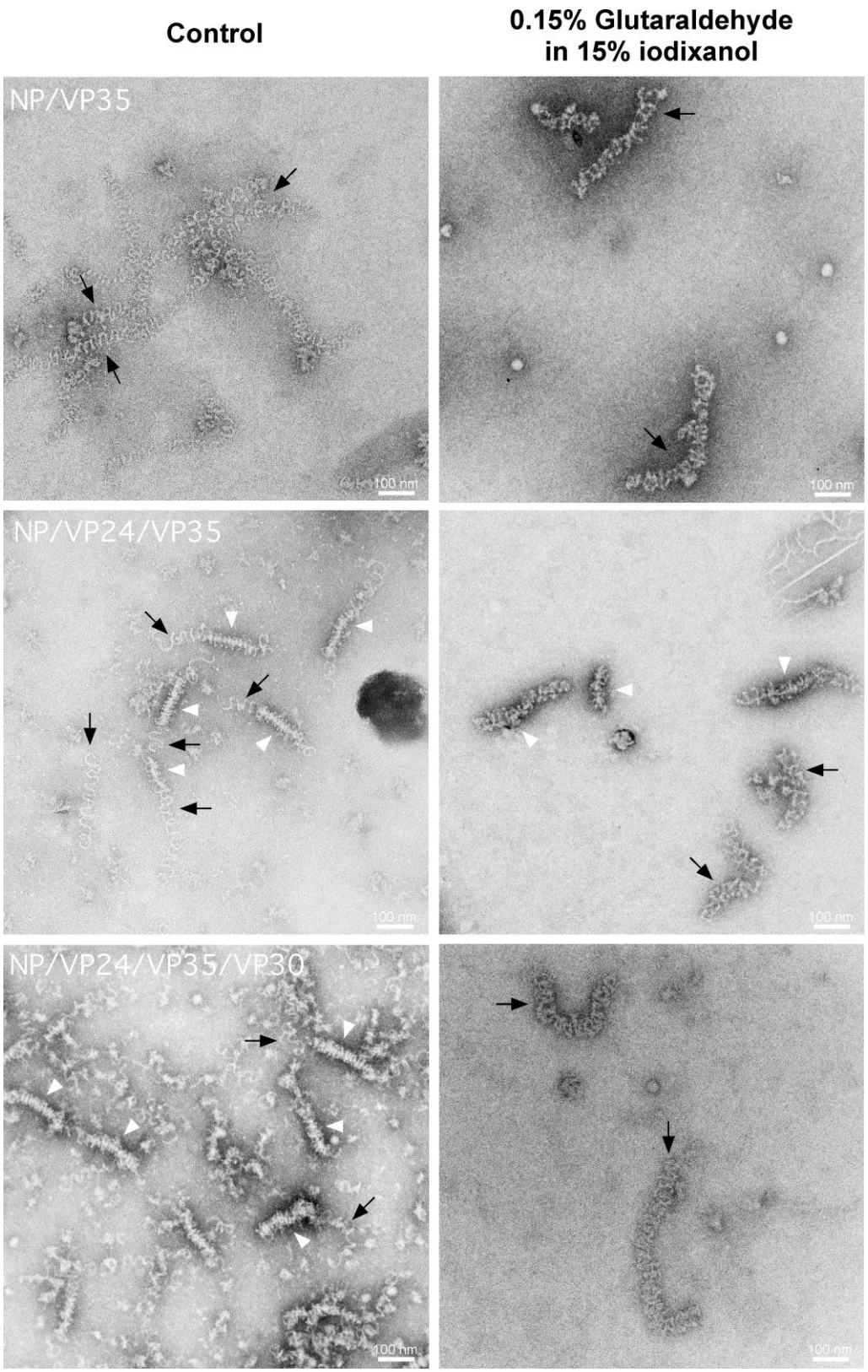

Figure 64 continued.

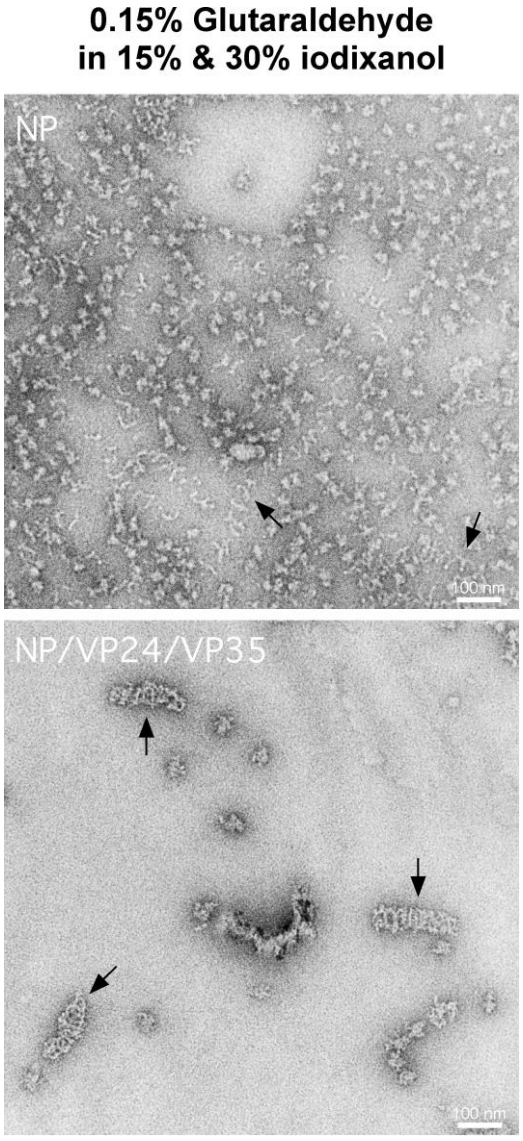

Figure 65. Structures purified from gradients containing 0.15% glutaraldehyde in both 15% and 30% layers. Cells were lysed in hypotonic lysis buffer and layered onto gradients containing glutaraldehyde. Fraction 6 from each gradient was layered onto 50 mM NaCl PBS and ultracentrifuged. Pellets were resuspended in 50 mM NaCl PBS and stained with methylamine tungstate. Black arrows: loosely coiled NP-RNA.

5.4.2.2 Cross-linking of intact cells

To investigate whether cellular or viral proteins might be stabilizing nucleocapsid-like particles within cells, 293T cells transfected with NP, VP24, and VP35 were subjected to the cross-linking chemical DSS, EGS, or PFA. Following cross-linker incubation, cells were lysed by isotonic lysis buffer and lysates were stained by methylamine tungstate. Differential ultracentrifugation was performed and gradient fractions were analyzed by SDS-PAGE to confirm protein expression and observe changes to gradient migration. In comparison to treatment with DMSO, migration of NP, VP24, and VP35 through the gradient was greatly reduced after DSS, EGS, or PFA treatment (Figure 66). In particular, exposure to 2% PFA completely abrogated protein migration (Figure 66fg).

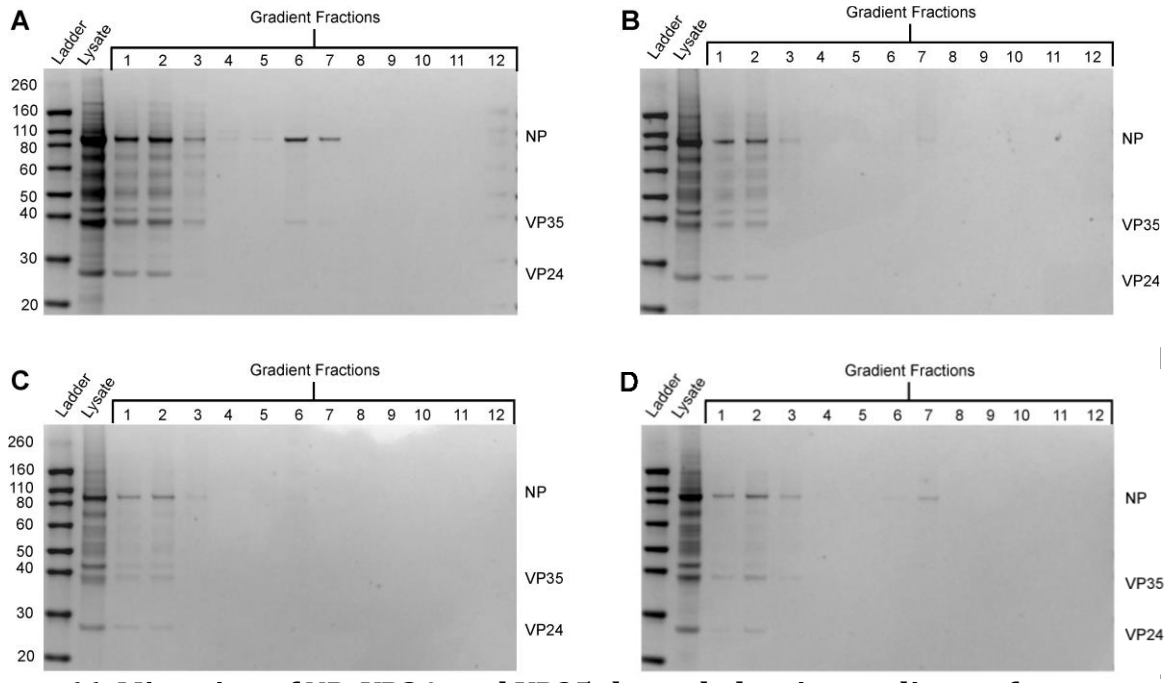

Figure 66. Migration of NP, VP24, and VP35 through density gradients after cross-linking treatment. Forty-eight hours post-transfection cells were harvested and treated with cross-linkers. Cells were lysed with isotonic lysis buffer and lysates were loaded onto 15-30% iodixanol gradients and ultracentrifuged. Fractions were collected top-down. SDS-PAGE was performed and gels were stained with Coomassie Blue. (A) DMSO control; (B) 1 mM DSS, 42 min; (C) 2 mM DSS, 42 min; (D) 1 mM EGS, 42 min; (E) 2 mM EGS, 42 min; (F) 2% PFA, 22 min; (G) 2% PFA, 42 min.

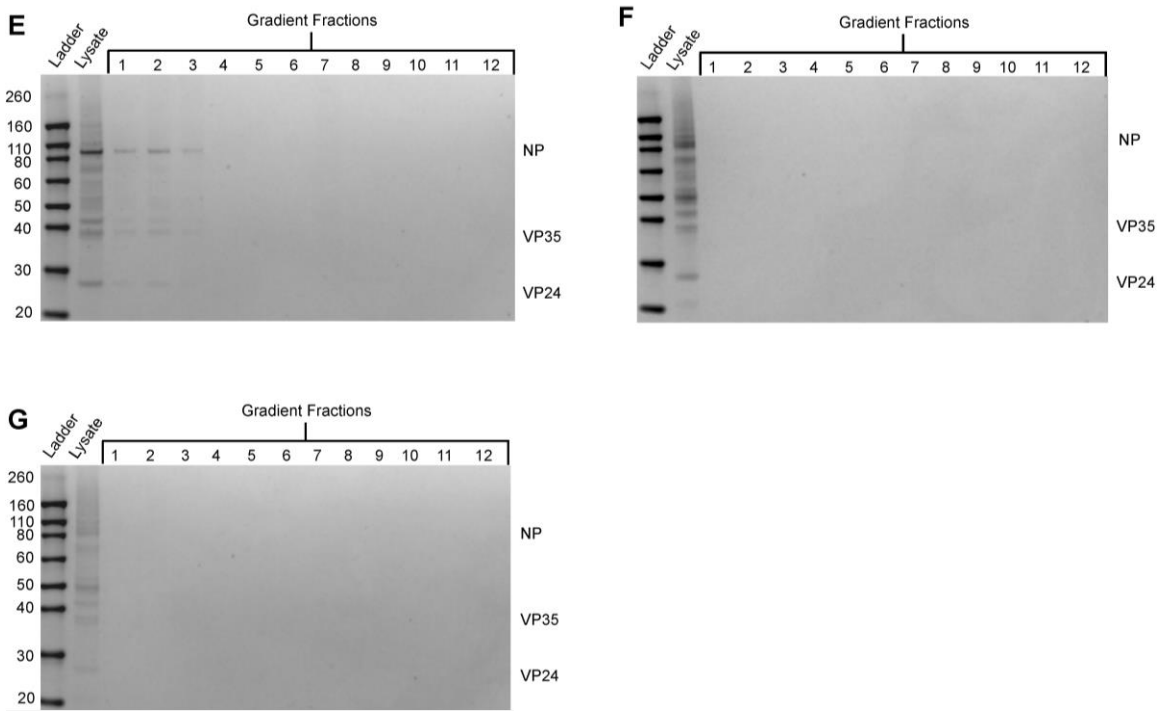

Figure 66 continued.

The visualization of nucleocapsid-like particles in cell lysates was difficult after cross-linker treatment due to the heavy staining and the presence of cellular debris. These experiments were repeated twice, with no improvement to the stain. NP-RNA and nucleocapsid-like particles were observed after all treatments, but there was no apparent increase in condensation of these particles, regardless of chemical or concentration (Figure 67, Figure 68). Structural variability was still noted after cross-linking treatment; however, too few nucleocapsid-like particles were observed for statistical analysis.

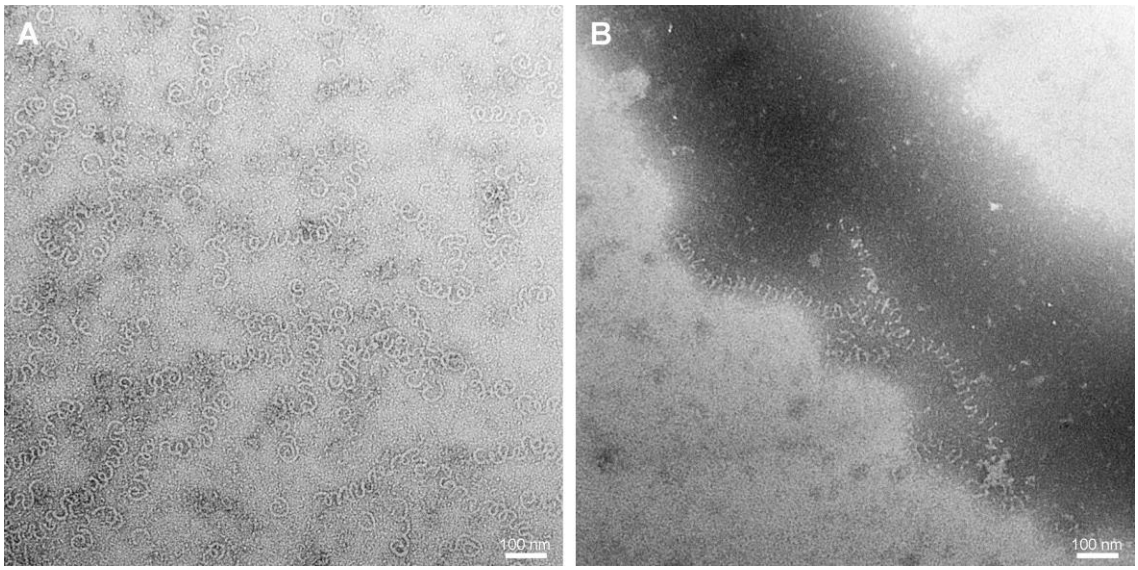

Figure 67. NP structures observed after treatment with 1 mM DSS. Forty-eight hours post transfection cells were harvested and washed. Cells were treated with (A) DMSO or (B) 1 mM DSS, 60 min. After incubation cells were lysed with isotonic lysis buffer. Lysates were directly stained with methylamine tungstate for this experiment.

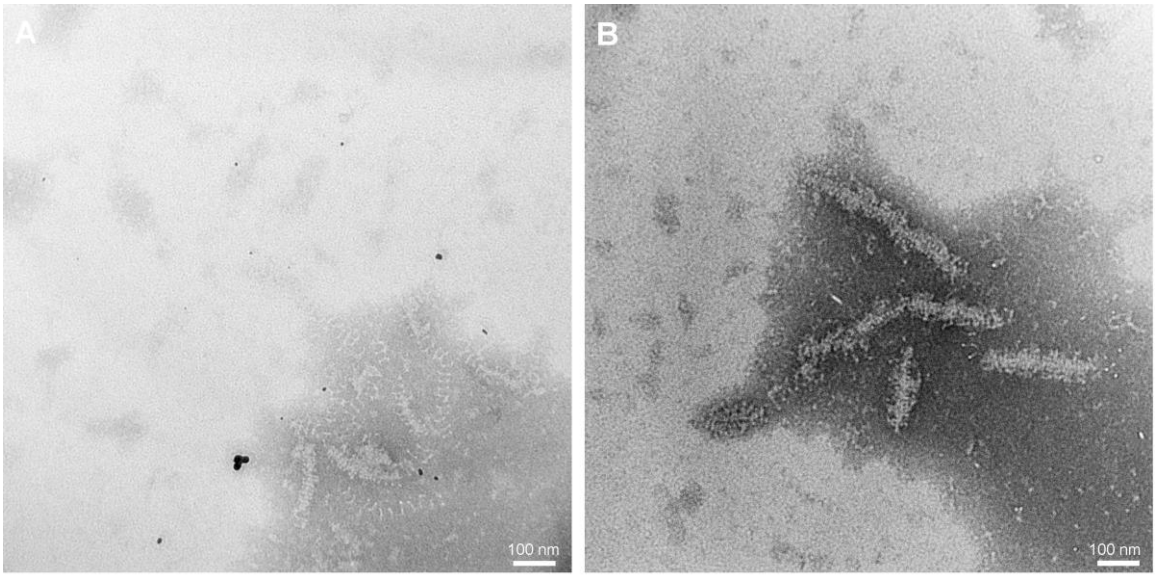

Figure 68. Representative images of nucleocapsid-like particles observed after treatment of intact NP, VP24, VP35 transfected cells with cross-linkers. Forty-eight hours post transfection cells were harvested and washed. Cells were treated with (A) DMSO or (B) 1 mM DSS, 42 min; (C) 2 mM DSS, 42 min; (D) 1 mM EGS, 42 min.

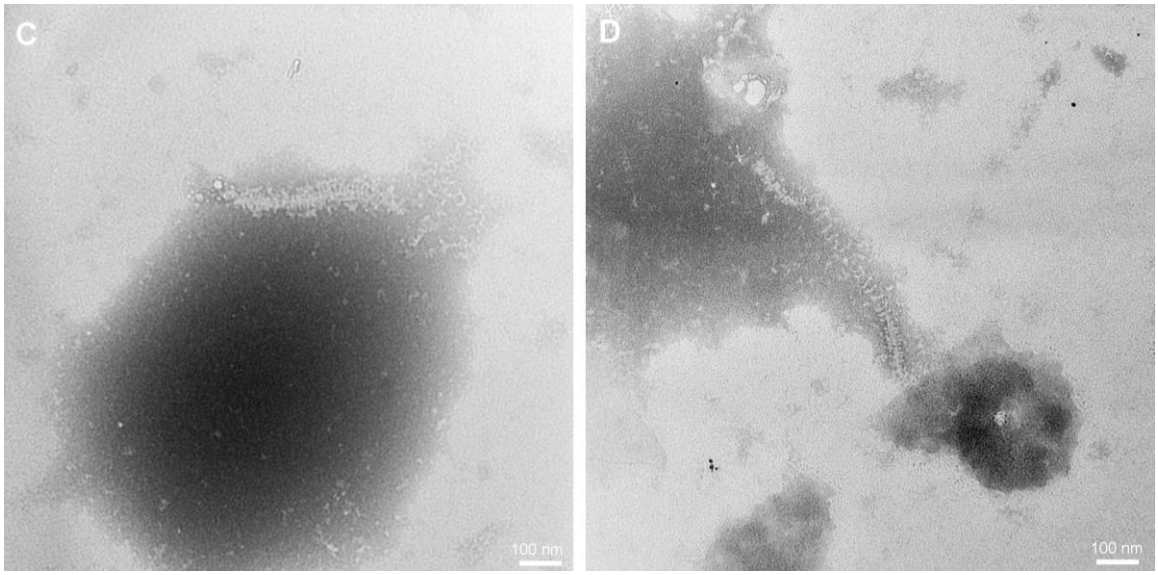

Figure 68 continued.

5.4.3 Cryo-EM

Frozen-hydrated NP/VP24/VP35 nucleocapsid-like particles were visualized by cryo-EM (Figure 69). As described in Chapter 4, hypotonic lysis buffer and density gradient ultracentrifugation were performed to isolate these particles. Nucleocapsid-like particles imaged by cryo-EM demonstrated a helical structure with an average diameter of 33.38±4.59 nm and an average pitch of 13.04±4.18 nm. When these measurements were compared to hypotonic lysis buffer NP/VP24/VP35 negative stain measurements, the cryo-EM images had a significantly larger average pitch than those imaged by negative stain; however, diameters were not significantly different (Table 24, Table 25). In agreement with earlier findings, pitch and diameter measurements from cryo-EM nucleocapsid-like particles were significantly larger than the cell culture media particles. (Table 24, Table 25). Reference-free classification of the cryo-EM nucleocapsid-like particles illustrates the relaxed nature of these helices compared to the intact Ebola virus particles (Figure 70).

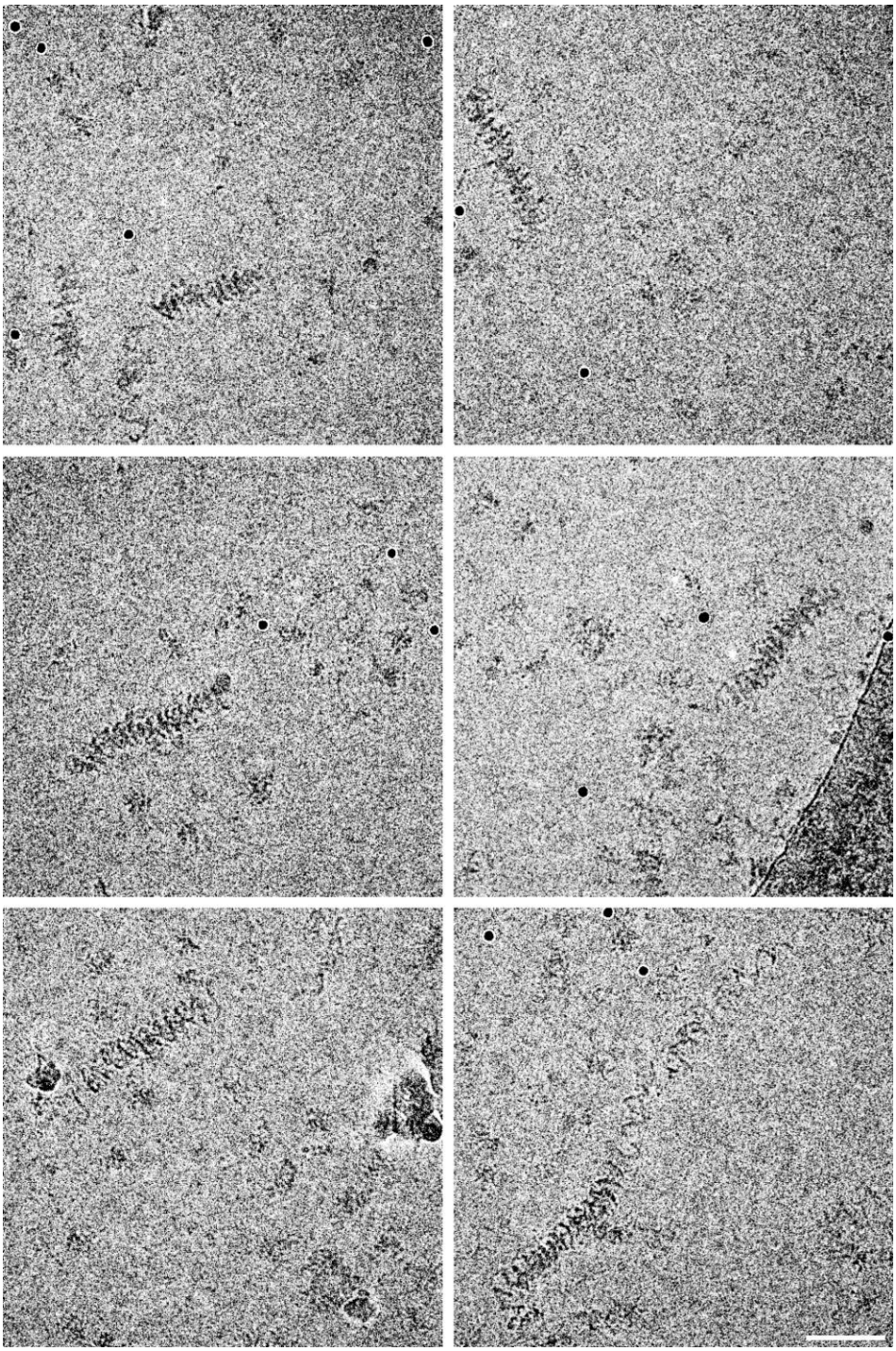

Figure 69. Electron micrographs of cryo-preserved nucleocapsid-like particles. NP/VP24/VP35 transfected cells were lysed in hypotonic lysis buffer and subjected to differential ultracentrifugation. Fraction 6 was further pelleted and resuspended in 50 mM NaCl PBS. Samples were flash-frozen in liquid ethane and imaged at liquid nitrogen temperatures. Scale bar: 100 nm.

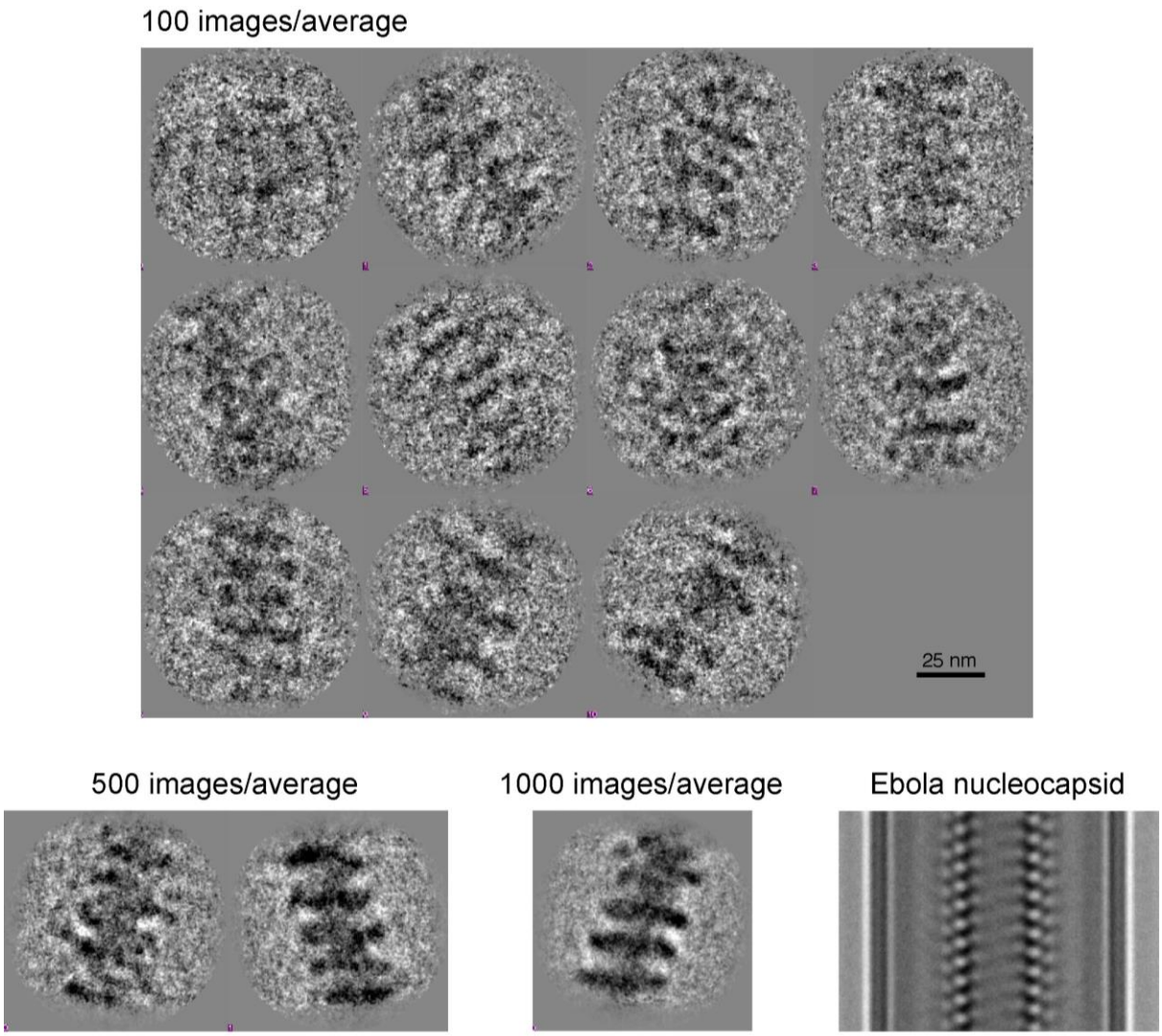

Figure 70. 2D class averages of cryo-preserved NP/VP24/VP35 nucleocapsid-like particles after reference-free analysis. Class averages were calculated using EMAN. Numbers refer to the number of images in each class average. Bottom right hand corner is a 2D class average of the Ebola virus nucleocapsid (Beniac et al., 2012), used with permission.

Table 24. Statistical comparison of the mean diameters of cryo-preserved NP/VP24/VP35 nucleocapsid-like particles and those prepared by negative stain.

Method	Negative stain (nm)	Cryo-EM (nm)	Statistical analysis
LB50	32.8±4.18	33.38±4.59	NS
LB150	34.53±5.32	-	NS
FT50	34.9±4.42	-	p<0.000625
FT150	33.77±4.83	-	NS
Media	31.04±4.38	-	p<0.000625

LB50: hypotonic lysis buffer; LB150: isotonic lysis buffer; FT50: hypotonic freeze/thaw; FT150: isotonic freeze/thaw; Media: cell culture media; NS: Not significant. Pitches were compared by Mann-Whitney tests. P value was calculated using Bonferroni correction.

Table 25. Statistical comparison of the mean pitch measurements of cryo-preserved NP/VP24/VP35 nucleocapsid-like particles and those prepared by negative stain.

Method	Negative stain (nm)	Cryo-EM (nm)	Statistical analysis
LB50	10.83±4.12	13.04±4.18	p<0.000625
LB150	12.45±4.87		NS
FT50	13.72±4.71		NS
FT150	12.63±4.82		NS
Media	9.68±3.4		p<0.000625

LB50: hypotonic lysis buffer; LB150: isotonic lysis buffer; FT50: hypotonic freeze/thaw; FT150: isotonic freeze/thaw; Media: cell culture media; NS: Not significant. Pitches were compared by Mann-Whitney tests. P value was calculated using Bonferroni correction.

5.5 Summary

Nucleocapsid-like particles observed in cell lysates, iodixanol fractions, or after dialysis were not perceivably more condensed than nucleocapsid-like particles observed after pelleting by ultracentrifugation. Glutaraldehyde fixation of nucleocapsid-like particles as they migrated through the density gradient did not increase the stability of these particles. Likewise, fixation of intact transfected cells by PFA, DSS, or EGS was not successful in stabilizing intracellular nucleocapsid-like particles. Analysis of frozen-hydrated nucleocapsid-like particles by cryo-EM demonstrated the same relaxed helical particles observed by negative stain.

Chapter 6. The effect of lysis buffer substitutions, staggered transfections, or VLP incorporation on the structure of the nucleocapsid-like particles

6.1 Rationale

Additional lysis methods were investigated to determine their effects on the structure of the nucleocapsid-like particles. First, removal of the detergent NP-40 from the hypotonic lysis buffer was performed to confirm that this detergent was not the reason for the difference in pitch observed between the nucleocapsid-like particles and the cryo-EM reconstruction. Second, homogenization of transfected cells was undertaken as an alternative method of cell lysis. Whereas freeze/thaw treatment lyses cells by ice crystal formation and expansion upon freezing, the use of a tissue homogenizer lyses cells by applying a shearing force. Homogenized lysates were observed without differential gradient centrifugation to preserve potentially required viral or cellular proteins that were being removed during the purification process. Third, the addition of $MgCl_2$ and KCl was investigated to determine whether the lack of divalent salts was influencing the condensation of nucleocapsid-like particles. Lastly, exposure to low pH was examined. Desfosses *et al*. (2013) demonstrated that exposure of vesicular stomatitis virus (VSV) nucleoprotein (N) to a pH of 5 resulted in the condensation of the N protein into the characteristic rhabdovirus bullet shape. Previous to this work, it was believed that the matrix protein (M) of rhabdoviruses was required for nucleocapsid condensation (Desfosses et al. 2013). As both Ebola virus and VSV are members of the *Mononegavirales*, I replicated this experiment with the Ebola virus nucleocapsid proteins.

In addition to the various lysis methods described above, I also explored whether staggered transfections could increase the yield or the degree of condensation of the nucleocapsid-like particles. Most viruses, including Ebola virus, express their proteins in a

temporally regulated fashion (Nanbo et al. 2013). Expression of NP, VP35, and VP30 was detected in Ebola virus infected cells within 6 hours of infection and increased over time (Nanbo et al. 2013). In contrast, VP24 expression was not detected until 18 hours post-infection (Nanbo et al. 2013). Nanbo *et al*. (2013) also observed that VP40 co-localized with NP and VP35 12 hours post-infection. To mimic the temporal expression of Ebola virus proteins, transfections were staggered by 2 or 6 hours and nucleocapsid-like particles were examined. In a separate experiment, I investigated whether interactions with VP40 and/or the budding process might lead to greater condensation of the nucleocapsid-like particles. Bharat et al. (2012) reported that nucleocapsid-like particles within isolated VLPs were similar in pitch and diameter to the Ebola virus; as such, I co-expressed the nucleocapsid proteins with VP40 and collected VLPs for visualization by TEM.

6.2 Hypotheses

1. Neither the removal of NP-40 nor homogenization of transfected cells will generate more condensed nucleocapsid-like particles.
2. Addition of $MgCl_2$ and KCl to the lysis buffer will not result in tighter nucleocapsid-like particles.
3. Exposure of nucleocapsid-like particles to a pH of 5 will result in more condensed nucleocapsid-like particles.
4. Staggered transfections of the Ebola virus nucleocapsid genes will not affect the assembly of nucleocapsid-like particles.
5. Nucleocapsid-like particles observed within VLPs will be more condensed.

6.3 Objectives

1. Isolate nucleocapsid-like particles from cells lysed by homogenization or hypotonic lysis buffer lacking NP-40
2. Isolate nucleocapsid-like particles from cells lysed with $MgCl_2$ and KCl lysis buffers
3. Expose cell lysates or gradient fractions to a pH of 5 and observe resultant changes to nucleocapsid-like particle
4. Perform staggered transfections of NP(VP24/VP35), NP/VP35(VP24), or NP/VP40 (VP24/VP35) at 2 or 6 hour intervals and image resultant nucleocapsid-like particles by TEM
5. Collect VLPs by ultracentrifugation and examine the structure of the nucleocapsid-like particles found within VLPs

6.4 Results

6.4.1 Additional lysis buffer modifications

6.4.1.1 Removal of NP-40

293T cells transfected with NP, VP24 and VP35 expression plasmids were incubated for 48 hours, after which cells were lysed with hypotonic lysis buffer with or without 1% NP-40. Lysates were loaded onto 15-30% iodixanol gradients and ultracentrifuged. Gradients were analyzed by SDS-PAGE and fraction 6 from each gradient was further purified by ultracentrifugation. While both lysis methods resulted in protein migration through the gradient, higher levels of NP, VP35 and VP24 were present when treated with 1% NP-40 (Figure 23, Figure 71). In particular, the presence of VP24 in the gradient was reduced when NP-40 was not included in the lysis buffer. Imaging of fraction 6 pellets

demonstrated no marked difference between nucleocapsid-like particles in the presence or absence of NP-40 (Figure 71).

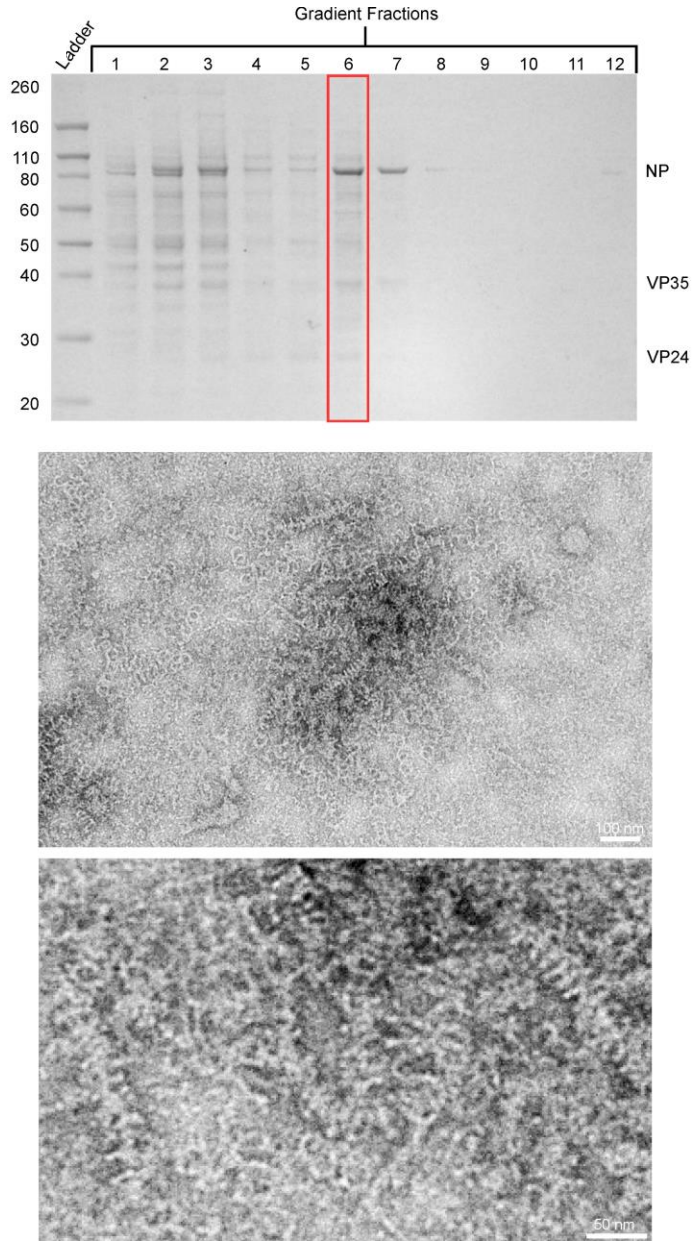

Figure 71. Nucleocapsid-like particles isolated after cell lysis by hypotonic lysis buffer lacking the detergent NP-40. Cells were transfected with NP/VP24/VP35. Lysates were loaded onto 15-30% iodixanol gradients and ultracentrifuged. Fractions were collected top-down, with Fraction 1 representing the first fraction collected. Top panel: SDS-PAGE of gradient fractions, stained with Coomassie Blue; Bottom panels: Negative stain images of fraction 6 pellets.

6.4.1.2 Homogenization

To investigate whether homogenization might lead to more condensed nucleocapsid-like particles, 293T cells expressing Ebola virus nucleocapsid proteins were subjected to a tissue homogenizer for 60 sec on ice. Cell lysates were divided and either stained and imaged by TEM or layered onto iodixanol gradients. Similar to the lysis methods described in Chapter 4, homogenization resulted in the co-migration of nucleocapsid proteins through the gradient, with strong bands in fractions 6 and 7 (Figure 72). In addition, nucleocapsid proteins migrated to fraction 12 as well (Figure 72c and d). Negative staining of homogenization lysates revealed tightly coiled NP-RNA particles, but few nucleocapsid-like particles were observed (Figure 73). To investigate further, fraction 6 from each gradient was stained with methylamine tungstate and observed by TEM. Ultracentrifugation resulted in the unwinding of tight NP-RNA coils, generating the loosely coiled structures observed in previous experiments (Figure 73a, Figure 74a). Nevertheless, nucleocapsid-like particles observed within these fractions were not noticeably different from previous particles generated (Figure 74).

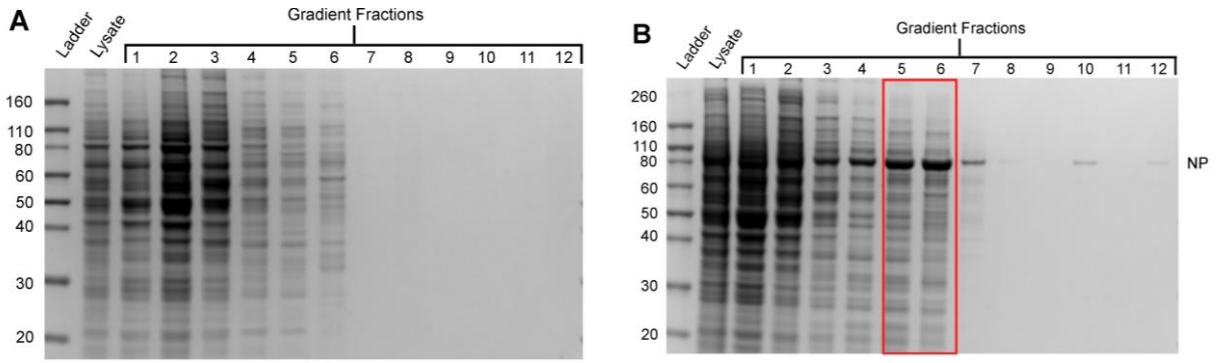

Figure 72. Gradient migration of nucleocapsid proteins after cell lysis by homogenization. Transfected cells were subjected to 60 sec homogenization followed by differential ultracentrifugation. Fractions were collected top-down, with Fraction 1 representing the first fraction collected. Red boxes indicate selected fractions. (A) Empty vector control; (B) NP; (C): NP/VP24/VP35; (D) NP/VP24/VP35/VP30; (E) NP/VP24/VP35/VP30/VP40.

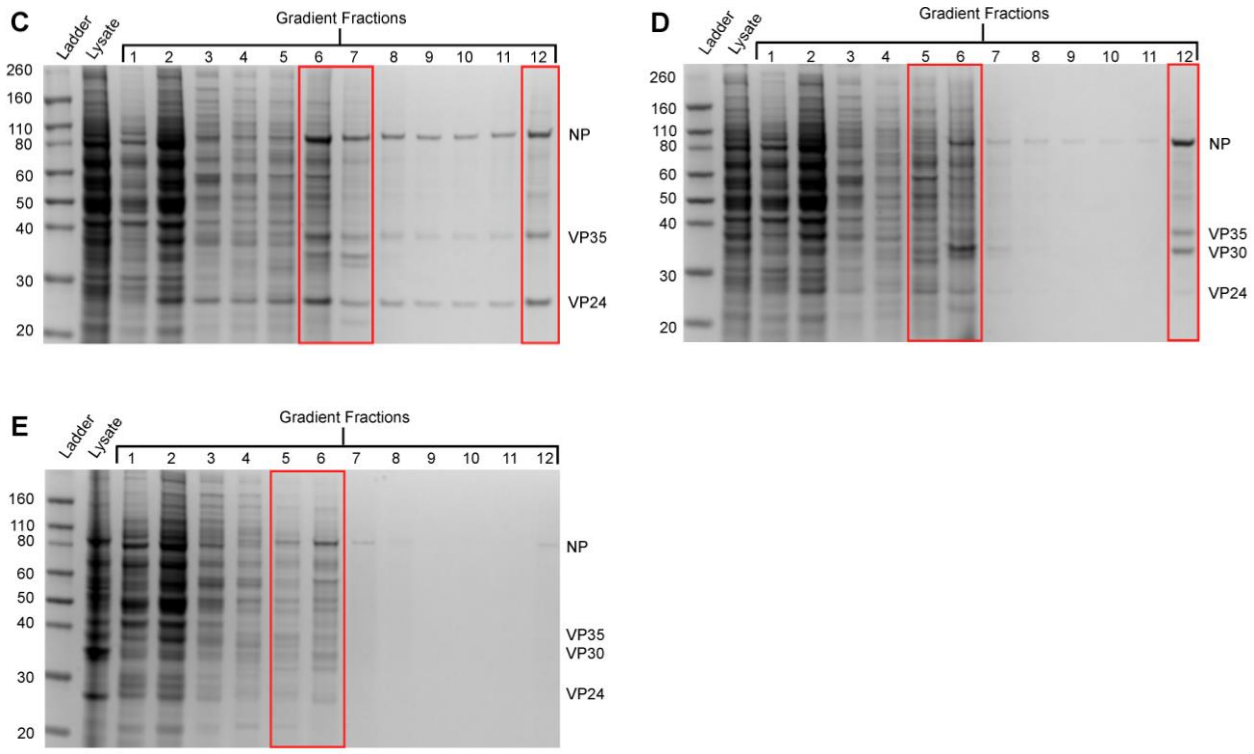

Figure 72 continued.

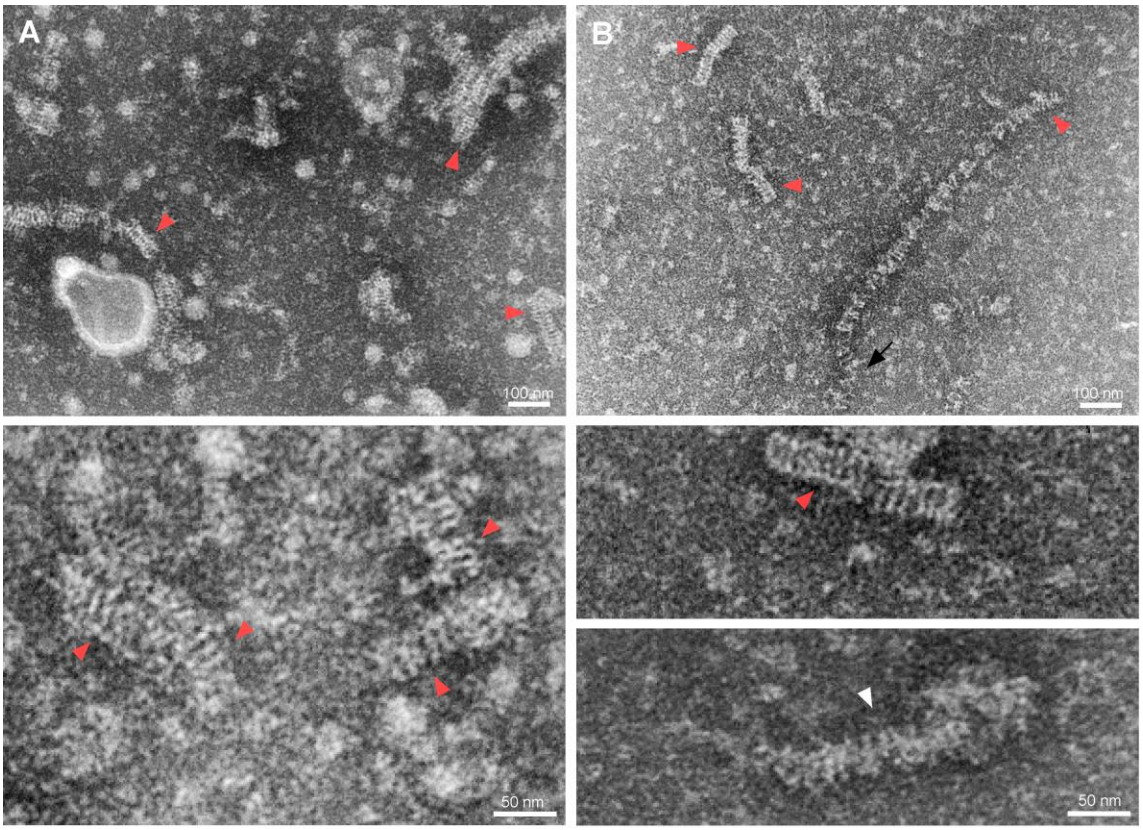

Figure 73. Nucleocapsid-like particles observed in homogenized cell lysates.

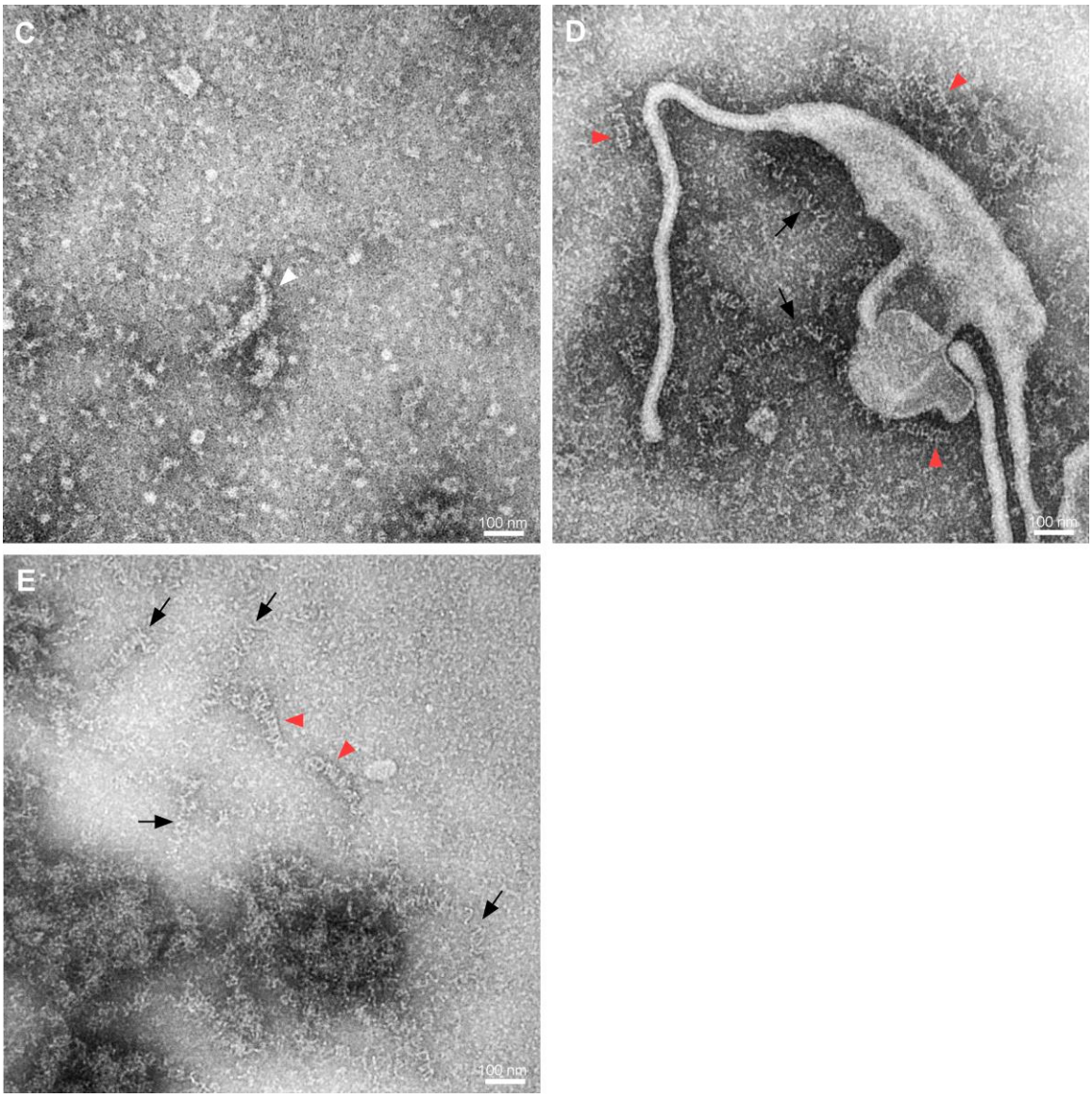

Figure 74. Nucleocapsid-like particles observed in homogenized cell lysates. Forty-eight hours post transfection cells were subjected to 60 sec of homogenization. Samples were taken directly from lysates and stained with methylamine tungstate. (A) NP; (B) NP/VP24/VP35; (C) NP/VP24/VP35/VP30; (D) NP/VP24/VP35/VP40; (E) NP/VP24/VP35/VP30/VP40. Black arrows: loosely coiled NP-RNA; red arrowheads: tightly coiled NP-RNA; white arrowheads: nucleocapsid-like particles.

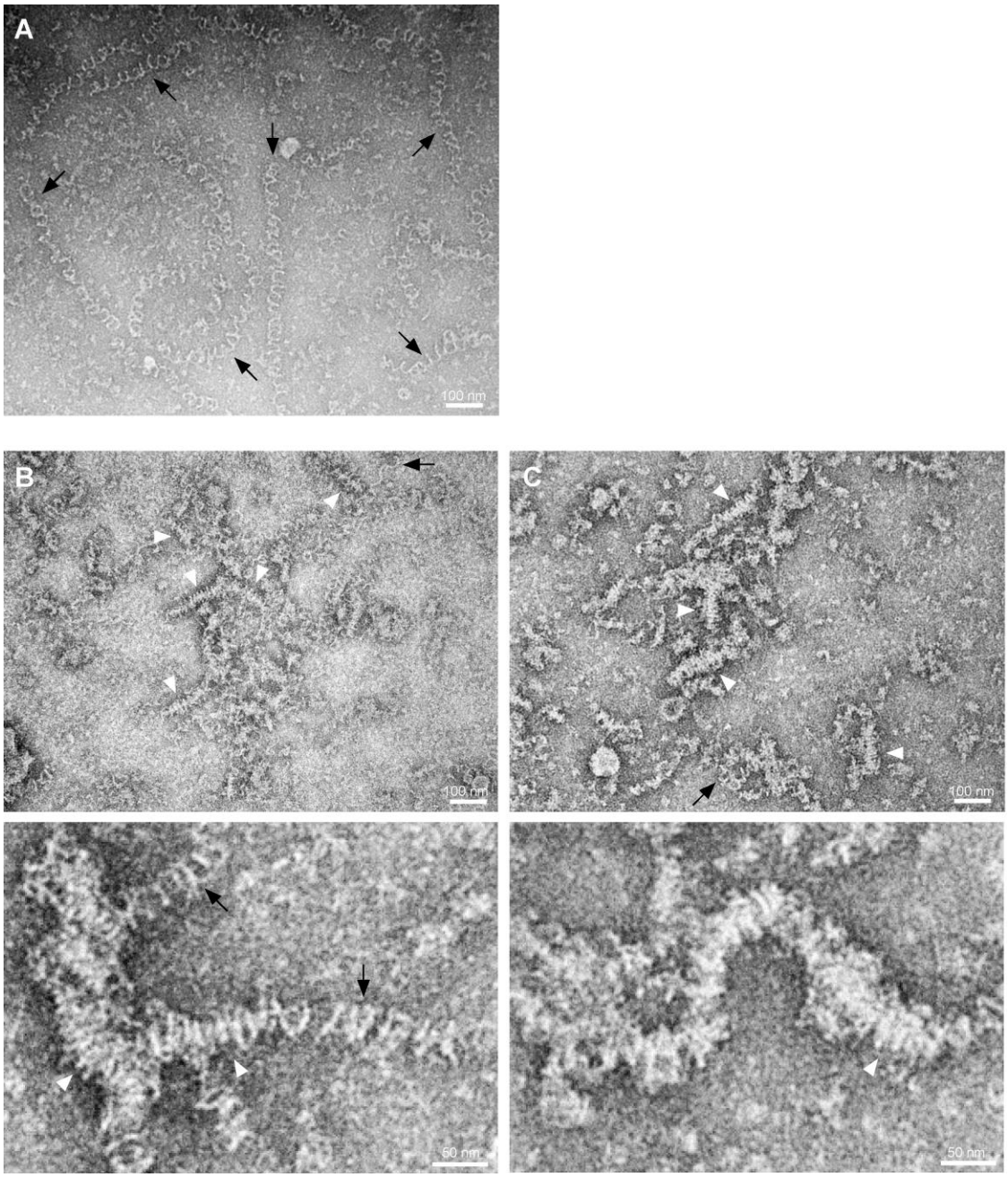

Figure 75. Nucleocapsid-like particles observed in gradient fraction 6 after homogenization. Homogenized cell lysates were layered on top of 15-30% iodixanol gradients and ultracentrifuged. Samples were taken directly from fraction 6 and stained with methylamine tungstate. (A) NP; (B) NP/VP24/VP35; (C) NP/VP24/VP35/VP30. Black arrows: loosely coiled NP-RNA; white arrowheads: nucleocapsid-like particles.

6.4.1.3 Addition of $MgCl_2$ and KCl

The effect of $MgCl_2$ and KCl on nucleocapsid-like particles was studied by generating a lysis buffer containing these reagents (150 mM NaCl, 1% NP-40, 10 mM KCl, 1.5 mM $MgCl_2$, 10 mM Tris-HCl, PIC). Iodixanol gradients were generated to match the concentrations of NaCl, $MgCl_2$ and KCl in the lysis buffers. Compared to the isotonic lysis buffer control, the removal of EDTA and the addition of $MgCl_2$ and KCl did not result in greater protein migration through iodixanol gradients for either NP/VP24/VP35 or NP/VP24/VP35/VP30 (Figure 75, Figure 76).

Lysates were stained with methylamine tungstate and imaged by TEM. Compared to the isotonic control, no NP-RNA or nucleocapsid-like particles were clearly observed when $MgCl_2$ and KCl were added to the lysis buffer (Figure 77). Experiments were repeated twice for both NP/VP24/VP35 and NP/VP24/VP35/VP30 transfections.

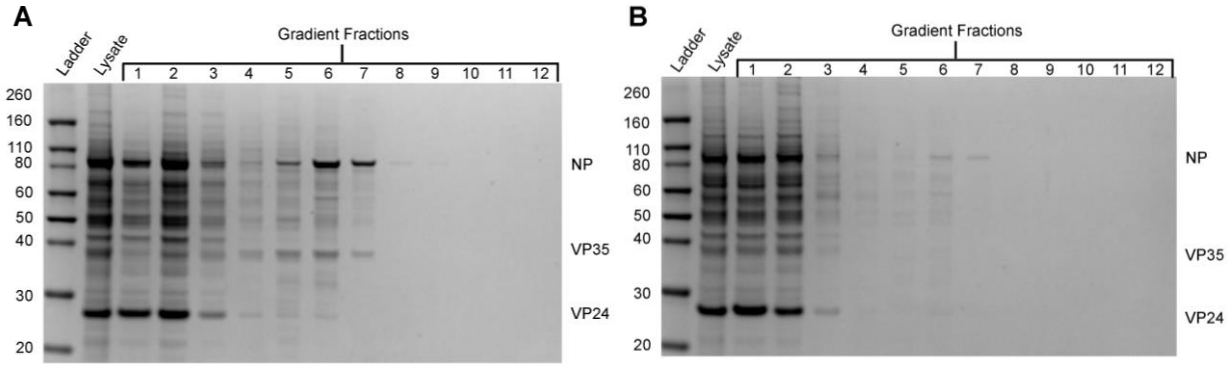

Figure 76. Migration of NP, VP24, and VP35 through the iodixanol gradient after the addition of $MgCl_2$ and KCl to the lysis buffer. Fractions were collected top-down, with Fraction 1 representing the first fraction collected. (A) Control isotonic lysis buffer; (B) Lysis buffer with $MgCl_2$ and KCl.

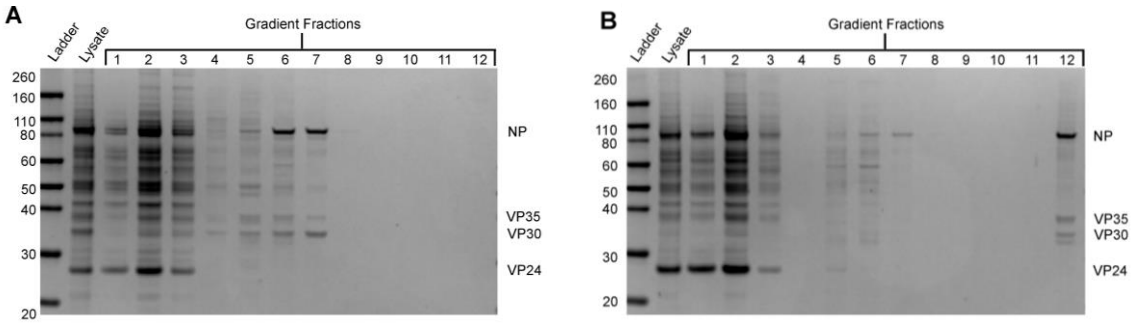

Figure 77. Migration of NP, VP24, VP35, and VP30 through the iodixanol gradient after the addition of $MgCl_2$ and KCl to the lysis buffer. Fractions were collected top-down, with Fraction 1 representing the first fraction collected. (A) Control isotonic lysis buffer; (B) Lysis buffer with $MgCl_2$ and KCl.

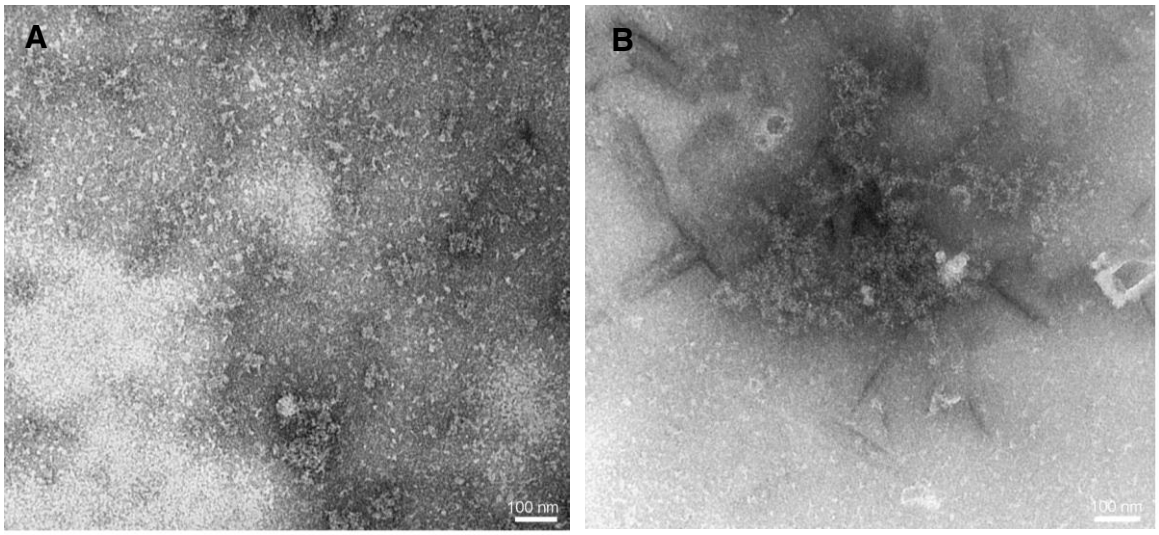

Figure 78. TEM observations after addition of $MgCl_2$ and KCl Samples were taken directly from lysates. (A) NP/VP24/VP35 (B) NP/VP24/VP35/VP30.

6.4.1.4 Exposure to low pH

To investigate whether exposure to low pH could trigger conformational changes and/or greater condensation of the Ebola virus nucleocapsid, cell lysates expressing NP alone, NP/VP24/VP35, or NP/VP24/VP35/VP30 were layered onto neutral or low pH iodixanol gradients. In addition, fractions from neutral pH gradients were dialyzed into either neutral or pH 5 buffers (Desfosses et al. 2013). Migration of NP through a low pH gradient resulted in no clear focusing of NP in fractions 6 and 7, as observed with the controls. Instead, NP is visible throughout the gradient (Figure 78d).

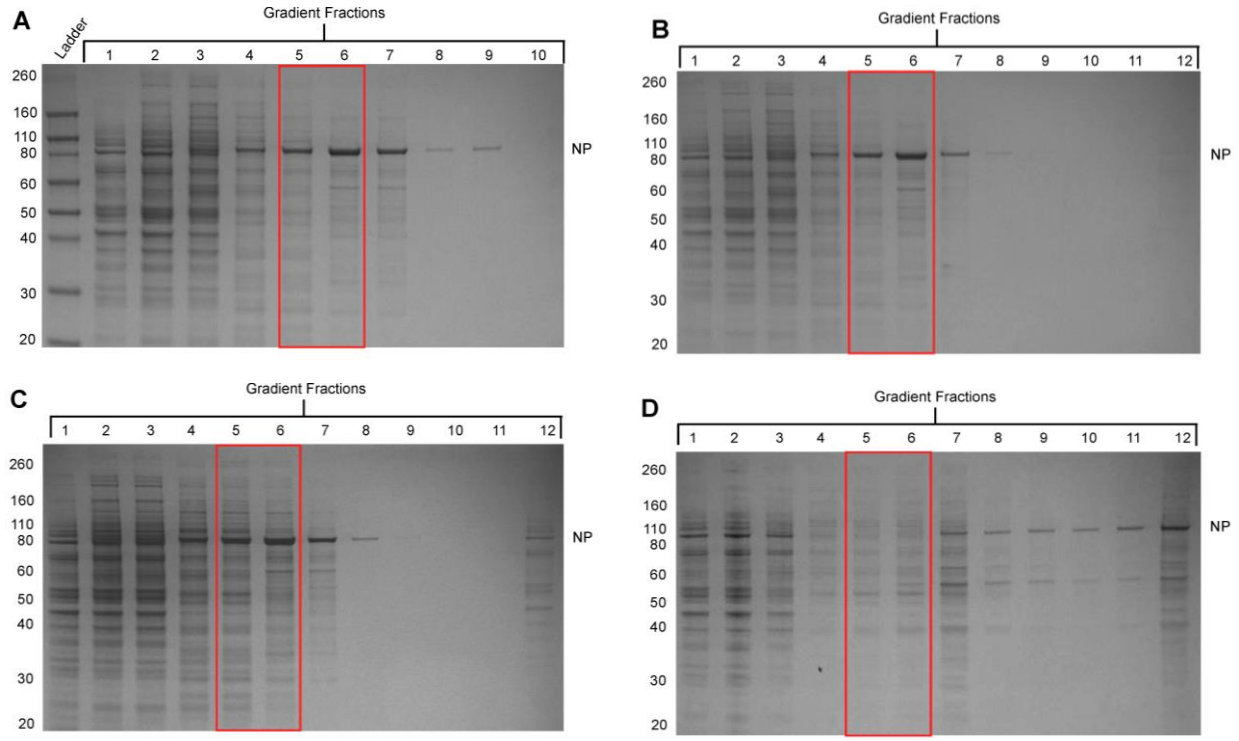

Figure 79. Gradient migration of NP after exposure to low or neutral pH iodixanol. 293T cells were lysed by isotonic lysis buffer and layered onto gradients with altered pH. Fractions were collected top-down, with Fraction 1 representing the first fraction collected. (A) 150 mM NaCl, pH 7.0 ; (B) 150 mM NaCl, 5 mM Tris-HCl, pH 7.5; (C) 5 mM Tris-HCl, pH 7.5; (D) 5 mM NaAc, pH 5.3.

Dialysis of the low pH gradient fractions demonstrated only a few short coils of NP-RNA, which is consistent with the low levels of NP detected by SDS-PAGE (Figure 79c, Figure 80b). In contrast, dialysis and negative stain of the control gradients showed loosely coiled NP-RNA structures (Figure 79, Figure 80). When fractions 6 and 7 from the neutral gradient were dialyzed into low pH or 0 mM NaCl buffers, NP-RNA structures were lost and electron micrographs looked very similar to those observed after exposure of NP cell lysate to the low pH gradients (Figure 81). Furthermore, SDS-PAGE of dialysis products demonstrated a loss of NP, which did not occur after neutral buffer dialysis (Figure 80).

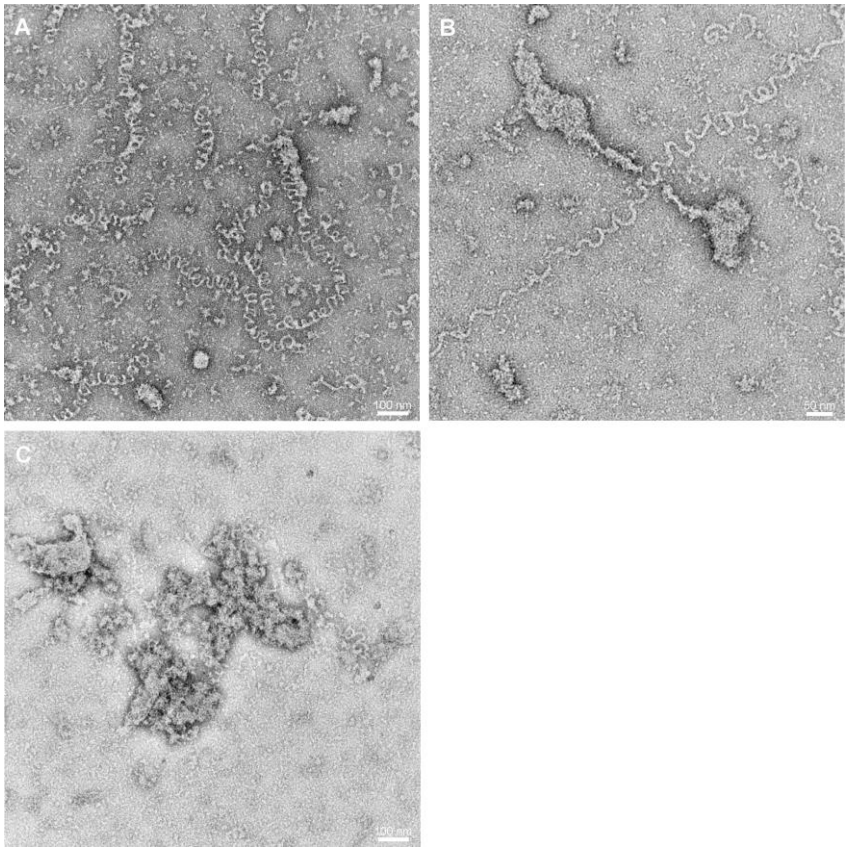

Figure 80. Nucleocapsid-like particles isolated after low pH gradient migration.
Gradient fractions were dialzsed into buffers matching the iodixanol gradient. (A) 150 mM NaCl, 5 mM Tris-HCl, pH 7.5; (B) 5 mM Tris-HCl, pH 7.5; (C) 5 mM NaAc, pH 5.

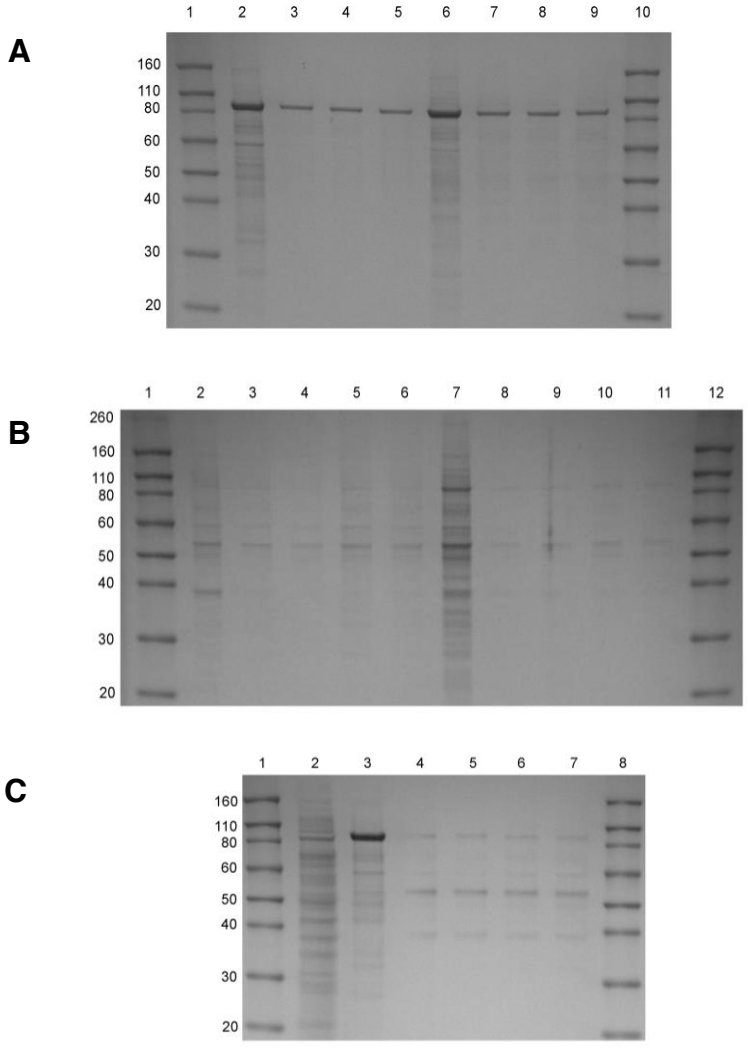

Figure 81. Dialysis products of various NP gradients. Fractions were dialyzed using 10K MWCO Slide-a-Lyzers. Dialysis products were analyzed by SDS-PAGE. **(A)** Matching gradient and dialysis buffer. Lane 2-5: fraction 6 and dialysis products, 150 mM NaCl, 5 mM Tris-HCl, pH 7.5. Lane 6-9: fraction 6 and dialysis products, 5 mM Tris-HCl, pH 7.5. **(B)** Matching gradient and dialysis buffer for 5 mM NaAc, pH 5. Lanes 2 and 7 are fractions 7 and 12 respectively. Following lanes are dialysis products. **(C)** Dialysis of NP into 5 mM NaAc, pH 5. Lane 1. Ladder; Lane 2: untransfected control lysate; Lane 3: fraction 6 from 150 mM NaCl gradient; Lanes 4-7: NP products after 5 mM NaAc pH 5 dialysis of fraction 6.

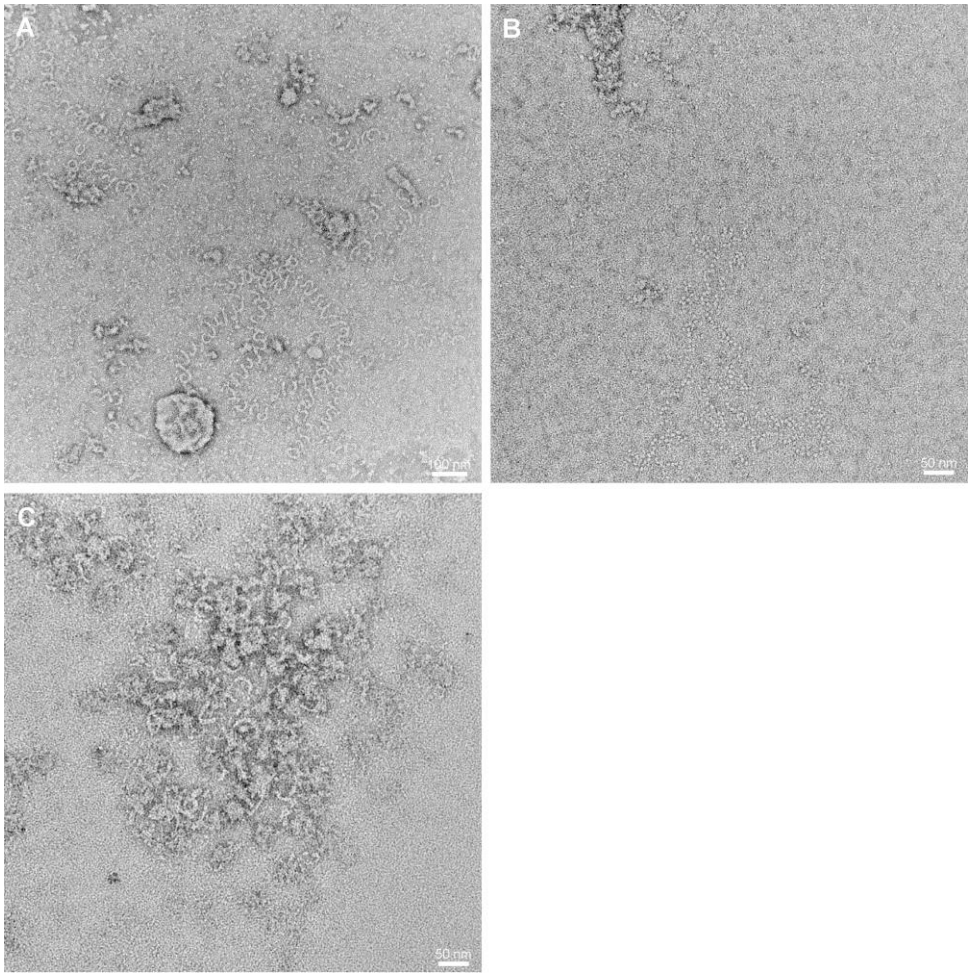

Figure 82. NP structures purified by dialysis in low or neutral pH. Lysates were layered onto neutral 150 mM NaCl gradients and ultracentrifuged. Fraction 6 samples were dialyzed into (A) PBS; (B) 5 mM Tris-HCl, pH 7.5; (C) 5 mM NaAc, pH 5.

This experiment was repeated after expression of the NP/VP24/VP35 and NP/VP24/VP35/VP30 combinations. In both cases, protein migration through the pH 5 gradient led to a loss of protein visible by SDS-PAGE. In addition, reduced focusing of these proteins in fractions 6 and 7 was observed (Figure 82). Dialysis and negative stain of fractions 6 and 7 of the low pH gradients revealed complete disintegration of the nucleocapsid-like particles (Figure 82).

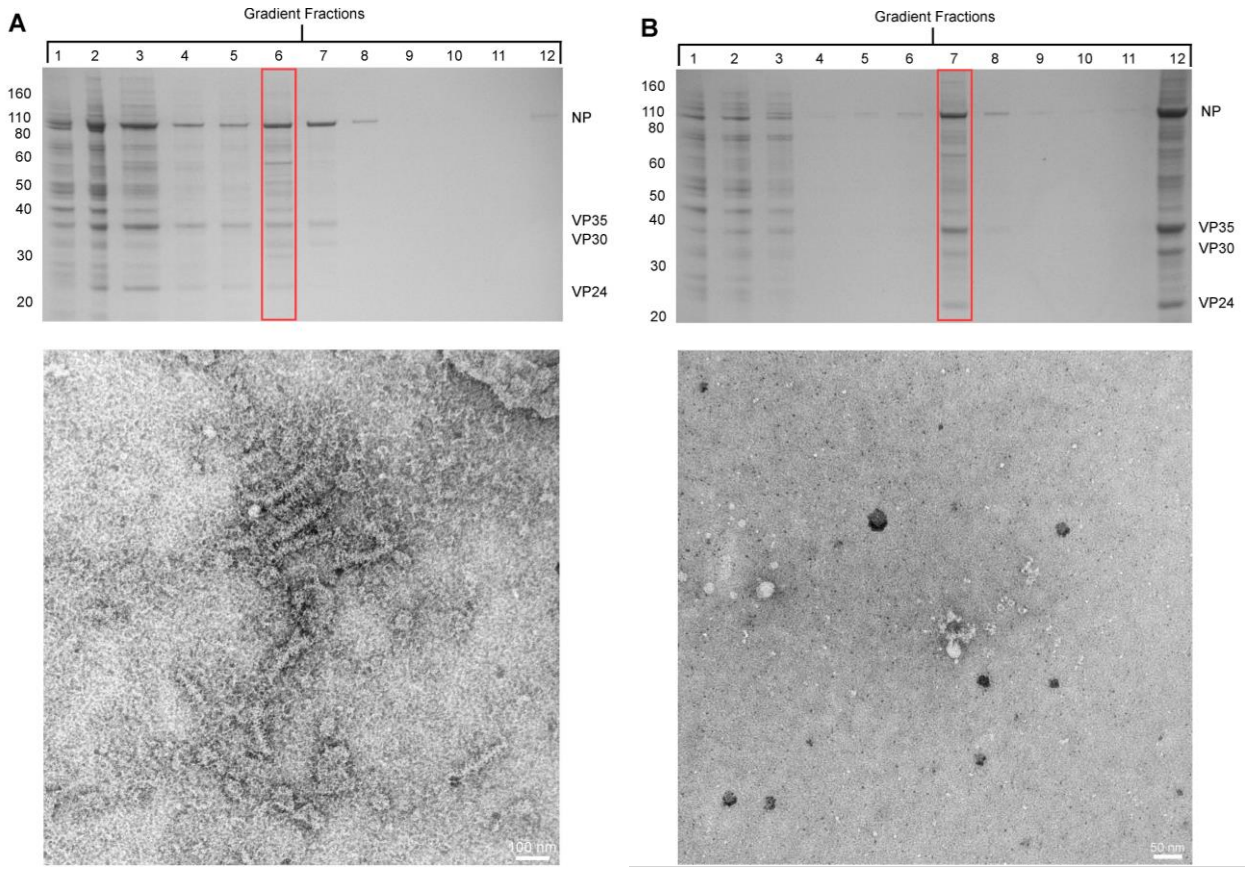

Figure 83. Effect of low pH on nucleocapsid-like particles and gradient migration. 293T cells transfected with NP/VP24/VP35/VP30 were lysed with isotonic lysis buffer and loaded onto 15-30% iodixanol gradients that were modified to be either neutral or low pH. Selected fractions were pelleted and negative stained (red boxes). Fractions were collected top-down, with Fraction 1 representing the first fraction collected. (A) Control gradient, 150 mM NaCl pH 7.0; (B) 5 mM NaAc gradient, pH 5.

6.4.2 Staggered transfections

To investigate whether the unregulated expression of nucleocapsid proteins might be affecting the self-assembly of nucleocapsid-like particles, a staggered transfection experiment was developed (Table 3). Briefly, cells were transfected with NP alone, or in combination with one other expression vector and incubated for 2 or 6 hours. Following incubation, the remaining nucleocapsid genes were transfected and cells were incubated for 48 hours. Cells were lysed by either isotonic freeze/thaw or homogenization.

The shorter timeframe of these transfections (48 hours) versus infections (normally 4-7 days) meant that I was unable to reproduce the exact timing of the Ebola virus protein expression, as described by Nanbo et al. (2013) and still generate sufficient nucleocapsid-like particles to analyze. However, I was able to replicate the sequence of protein expression described in that study. With NP, VP35, and VP40 being detected first in Ebola virus infected cells, these genes were transfected first in this experiment. As VP24 was detected later in infection, this expression plasmid was transfected during the second round (Nanbo et al. 2013).

Regardless of the incubation period, all nucleocapsid proteins co-migrated together through the iodixanol gradient after isotonic freeze/thaw (Figure 83). While these results were promising, negative staining of fraction 6 for each of these experiments demonstrated only loosely coiled nucleocapsid-like particles (Figure 84). In addition, although not quantitatively confirmed, fewer nucleocapsid-like particles were observed after staggered transfection than when the plasmids were co-transfected at one time and isotonic freeze/thaw was applied. Consistent with this finding, fewer nucleocapsid-like particles were observed in homogenized cell lysates after staggered transfections. Instead, homogenized lysates appeared to contain a high concentration of tight NP rod-like particles (Figure 85). The NP rod-like particles were surprisingly unique from the nucleocapsid-like particles. First, they were more rigid, with little curvature observed. Any bends that were observed appeared to be due to jogs or kinks in the rigid structure, rather than the expansion and contraction of the helical components. Second, the NP rod-like particles were more ordered and compact than the nucleocapsid-like particles. These particles were found regardless of the presence of VP40.

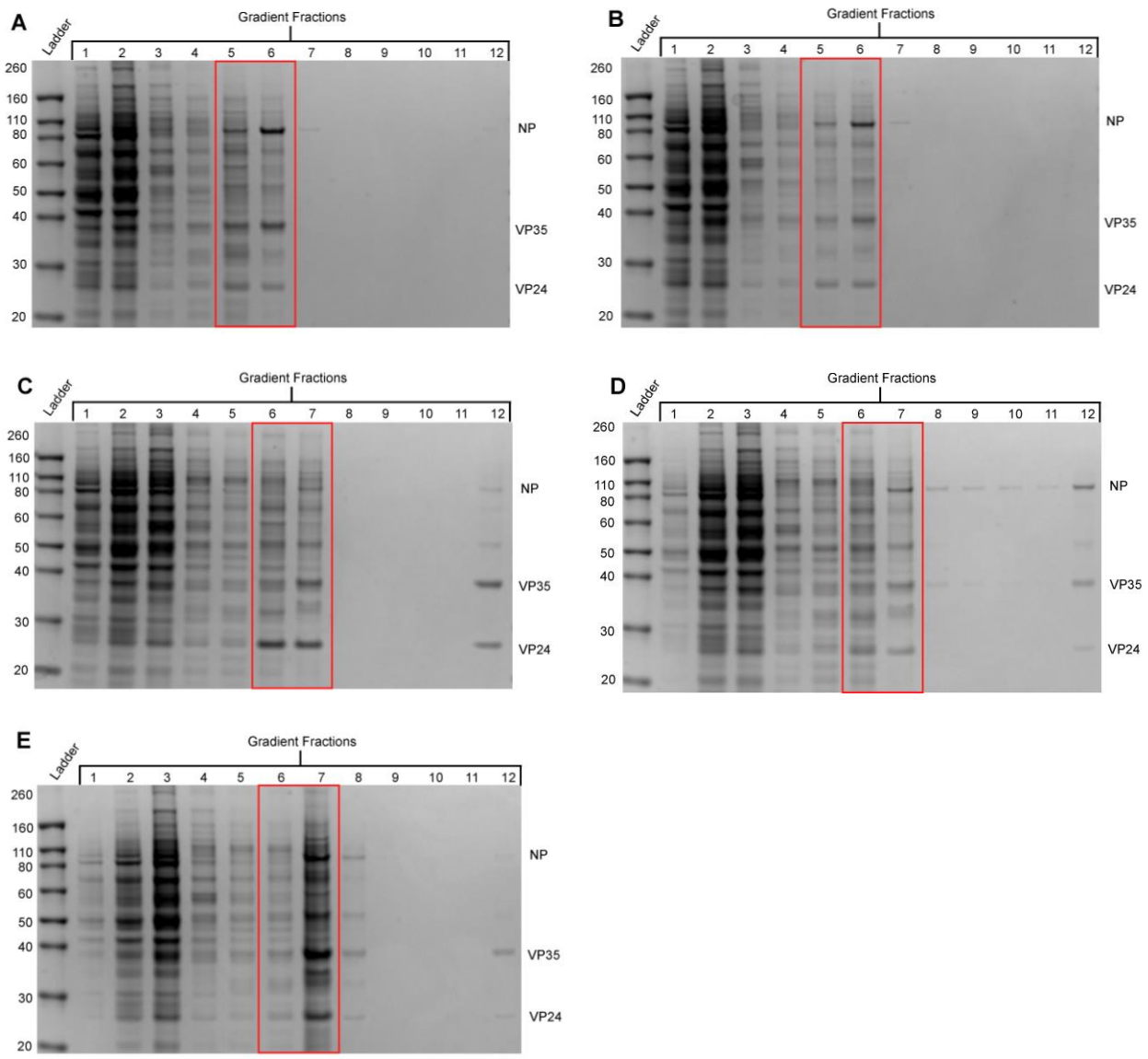

Figure 84. Migration of nucleocapsid proteins after staggered transfections and lysis by isotonic freeze/thaw. Lysates were subjected to differential ultracentrifugation and fractions analyzed by SDS-PAGE. Fractions were collected top-down, with Fraction 1 representing the first fraction collected. (A) NP/VP35, 2 hour incubation, VP24; (B) NP/VP40, 2 hour incubation, VP24/VP35; (C) NP, 6 hour incubation, VP24/VP35; (D) NP/VP35, 6 hour incubation, VP24; (E) NP/VP40, 6 hour incubation, VP24/VP35.

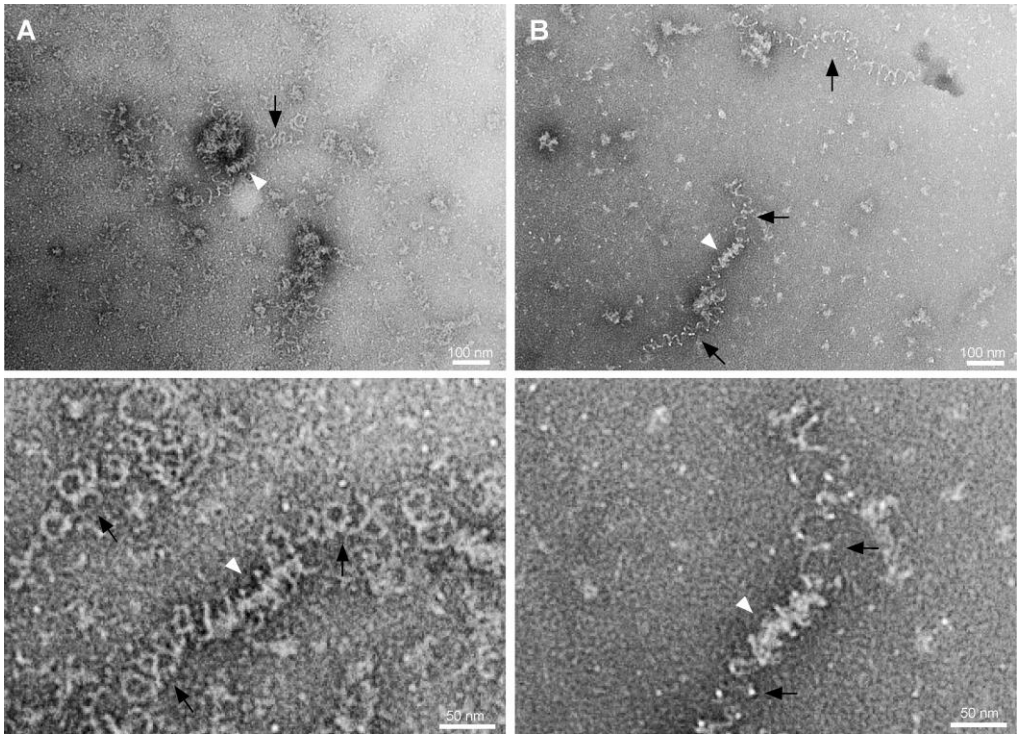

Figure 85. Representative images of nucleocapsid-like particles isolated after staggered transfection and lysis by isotonic freeze/thaw. Selected fractions were pelleted and stained with methylamine tungstate. (A) NP/VP35, 2 hour incubation, VP24; (B) NP/VP40, 2 hour incubation, VP24/VP35.

The high concentration of these particles enabled pitch and diameter measurements. These tight NP rod-like particles were still significantly larger in pitch and diameter than the proto-nucleocapsids described in Chapter 3.4. Two different staggered transfection results were measured: NP transfection, followed 6 hours later by VP35 and VP24 had a mean diameter of 29.19±3.34 nm and pitch of 8.06±2.31 nm and NP/VP35 transfection, followed 2 hours later by VP24 had a mean diameter of 28.09±2.95 nm and pitch of 8.44±2.47 nm (Figure 86). These diameters were significantly different from each other ($p<0.000625$; Mann-Whitney test with Bonferroni correction); however, particles formed by the staggered 6-hour transfection of NP followed by VP35 and VP24 were not

significantly different in terms of diameter from the proto-nucleocapsids. The staggered 2-hour transfection of NP/VP35 followed by VP24 had a significantly smaller diameter than that of the proto-nucleocapsids (29.67±2.93nm). In contrast to the diameter measurements, the mean pitch values of the NP rod-like particles were not significantly different from each other but were significantly larger than the proto-nucleocapsid pitch of 5.56±1.36 nm ($p < 0.000625$; Mann-Whitney test with Bonferroni correction).

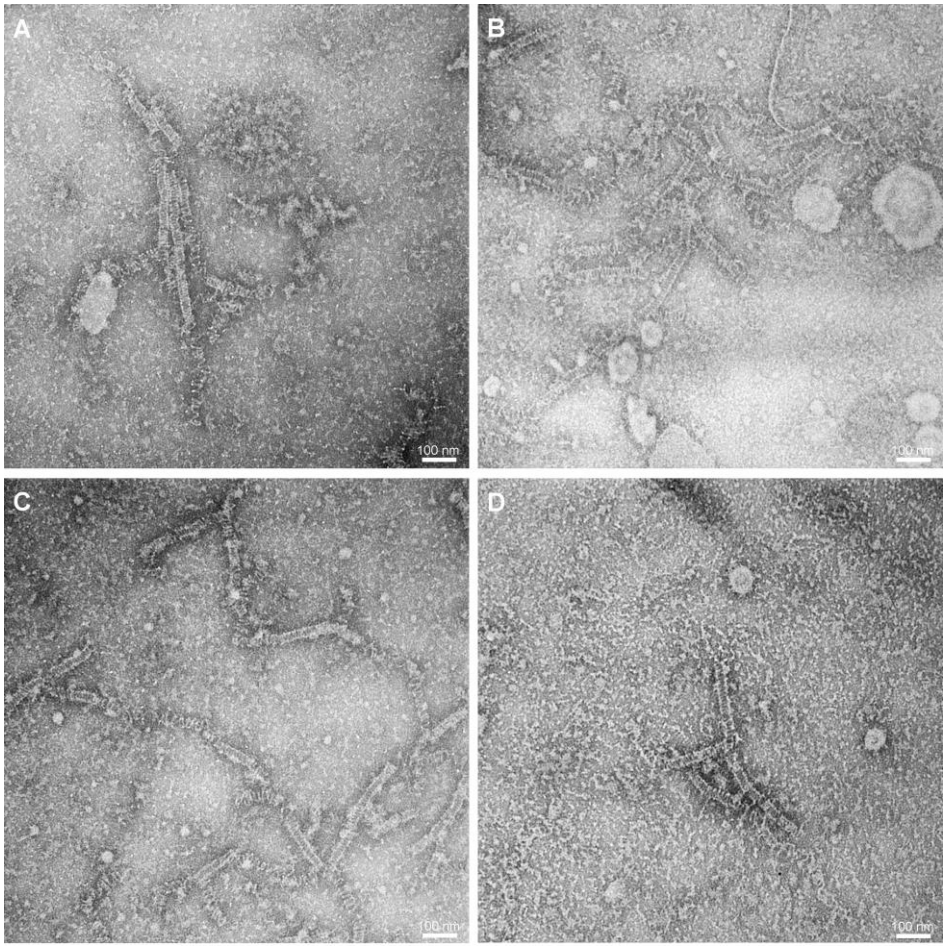

Figure 86. NP rod-like particles observed after staggered transfection of Ebola virus nucleocapsid proteins and cell lysis by homogenization. Forty-eight hours post final transfection, cells were homogenized for 60 sec and lysates were stained directly with methylamine tungstate. (A) NP, 6 hour incubation, VP35/VP24; (B) NP/VP35, 2 hour incubation, VP24; (C) NP/VP35, 6 hour incubation, VP24; (D) NP/VP40, 6 hour incubation, VP35/VP24.

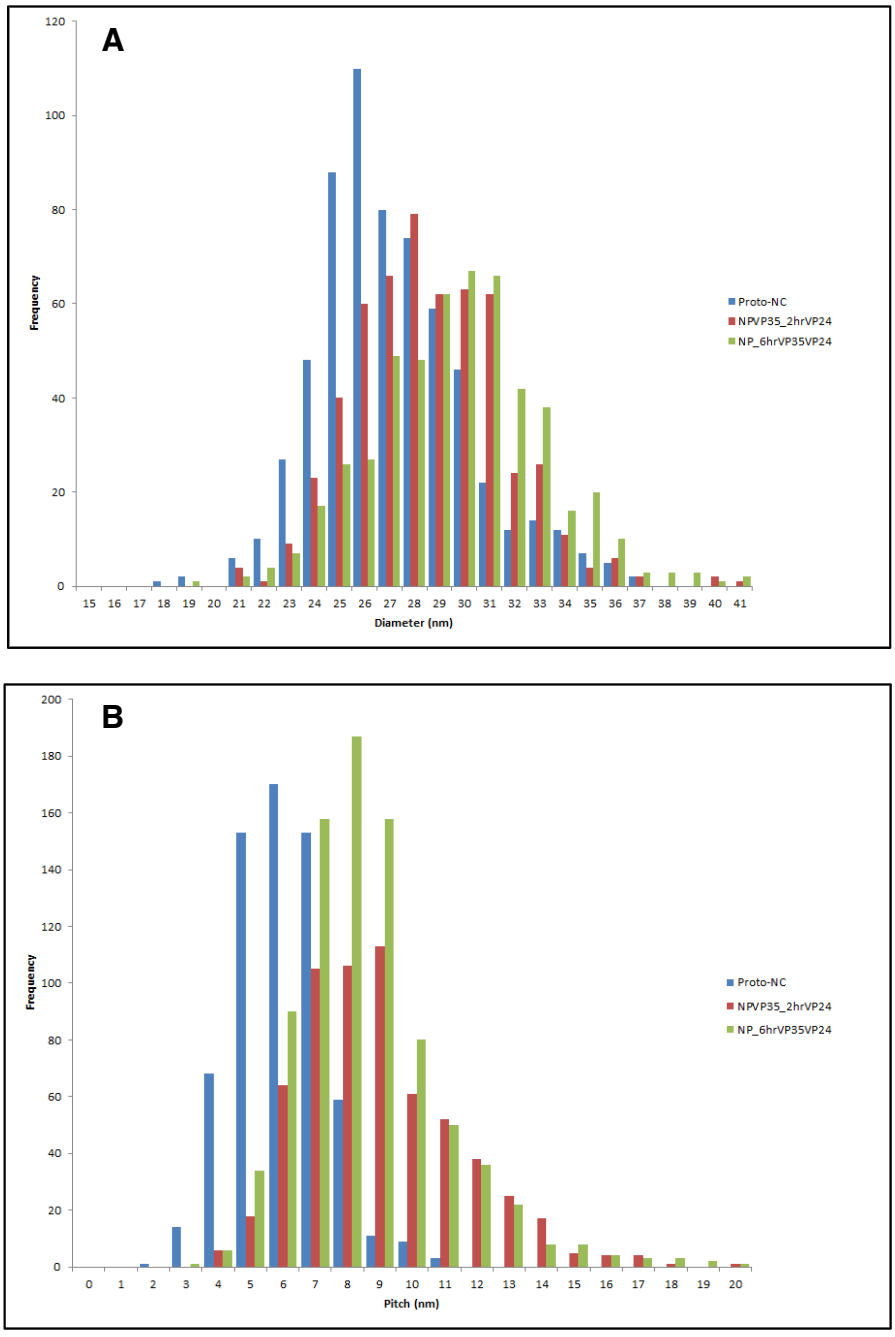

Figure 87. Frequency histograms of NP rod-like particles. (A) Diameter; (B) Pitch. Proto-NC: proto-nucleocapsids from native Ebola virus samples discussed in Chapter 3.4. Staggered transfections were performed with either 2 or 6 hour incubations. Transfected cells were harvested by 60 sec homogenization. Measurements were made using ImageJ software. Diameter: proto-NC (n= 625), NPVP35_2hrVP24 (n= 545), NP_6hrVP35VP24 (n= 514). Pitch: proto-NC (n= 641), NPVP35_2hrVP24 (n= 620), NP_6hrVP35VP24 (n= 851).

6.4.3 VLP incorporation

To investigate the organization of nucleocapsid-like particles within VLPs, 293T cells were transfected and cell culture medium was collected 48 hours later. Co-expression of NP and VP40 resulted in envelope-free NP coils (Figure 87). These particles were not as condensed or rigid as the proto-nucleocapsids observed in Chapter 3.4, but were more condensed than most of the NP-RNA structures observed after cell lysis. Expression of NP/VP24/VP35 with VP40 did result in the budding of nucleocapsid-like particles, visible within VLPs (Figure 88). Likewise, expression of NP/VP24/VP35/VP30 with VP40 also resulted in VLPs containing nucleocapsid-like particles (Figure 89). Unfortunately, these particles were quite rare and while nucleocapsid-like particles did appear more condensed within VLPs, no statistical analysis could be performed. Envelope-free nucleocapsid-like particles were also observed in cell culture media, as described in Chapter 4.

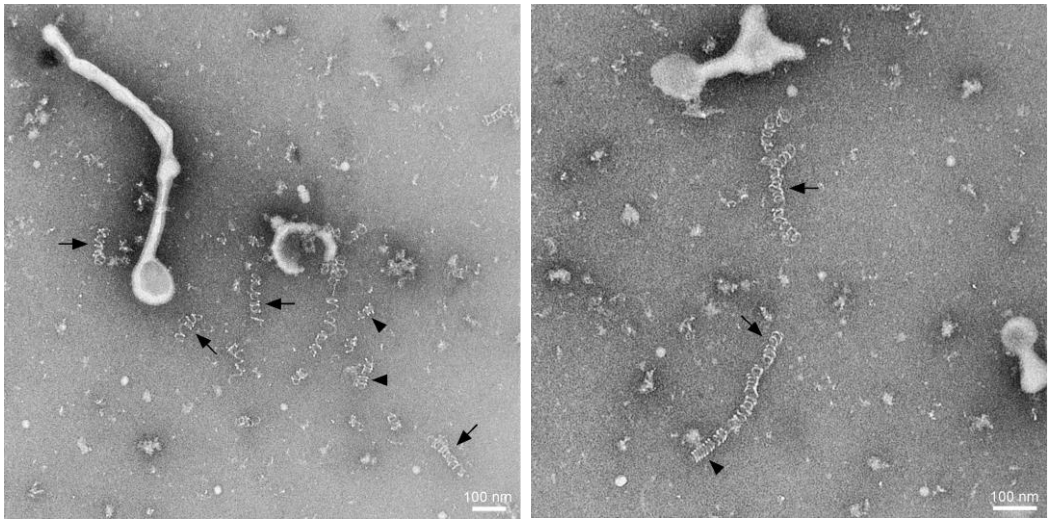

Figure 87. Tight NP-RNA structures observed in VLP samples. 293T cells were transfected with NP and VP40. Forty-eight hours post transfection cell culture medium was collected and layered onto 20% sucrose cushion. Pellets were resuspended in PBS after ultracentrifugation and stained with methylamine tungstate. Black arrows: loosely coiled NP-RNA; black arrowheads: tightly coiled NP-RNA.

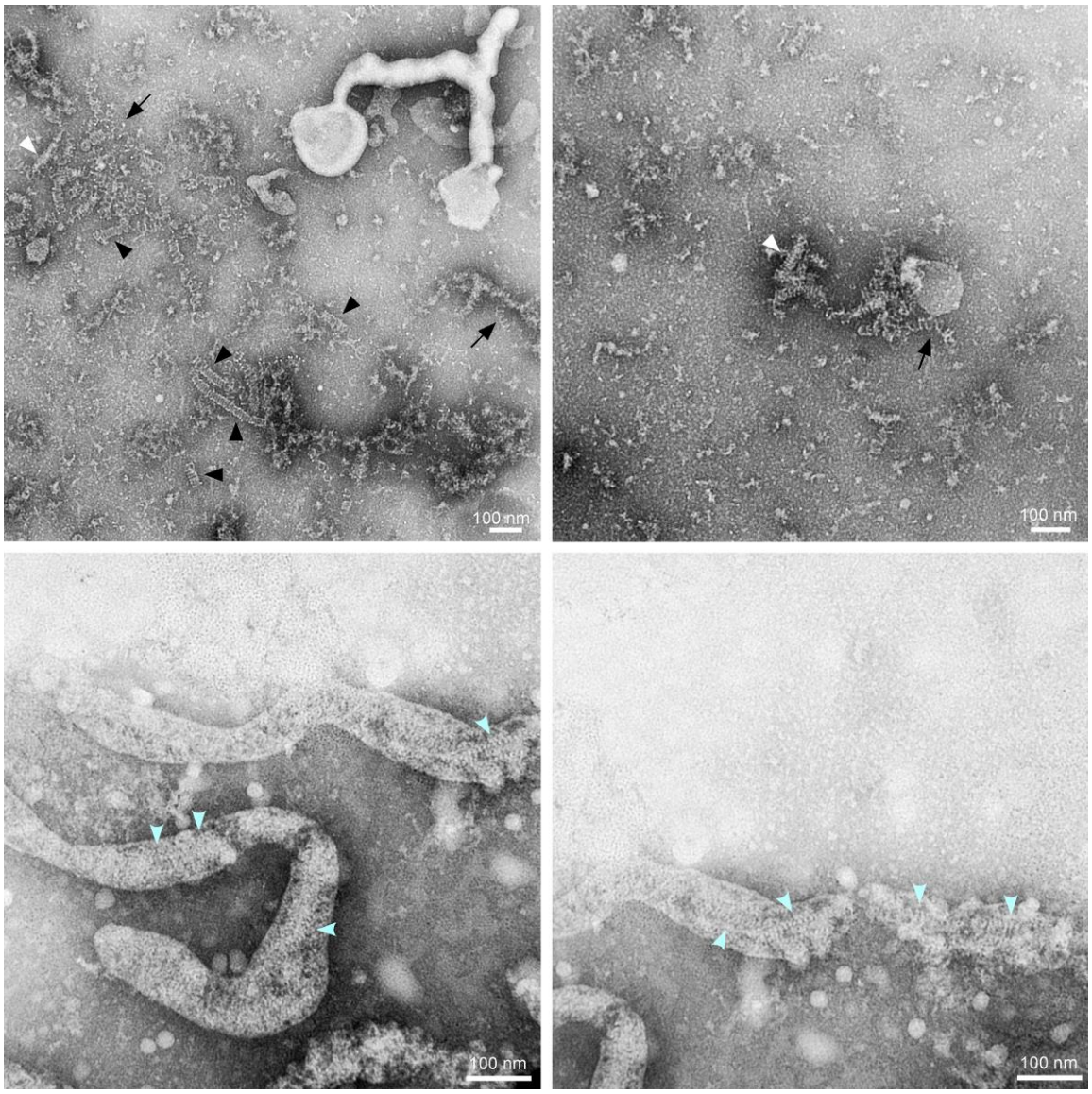

Figure 88. NP/VP24/VP35/VP40 nucleocapsid-like particles observed within VLPs and cell culture media. Ultracentrifugation of cell culture media resulted in VLP pellets, which were resuspended in PBS and stained with methylamine tungstate. Black arrows: loosely coiled NP-RNA; black arrowheads: tightly coiled NP-RNA; white arrowheads: nucleocapsid-like particles; blue arrowheads: regions of tightly wound nucleocapsid-like particles within VLPs.

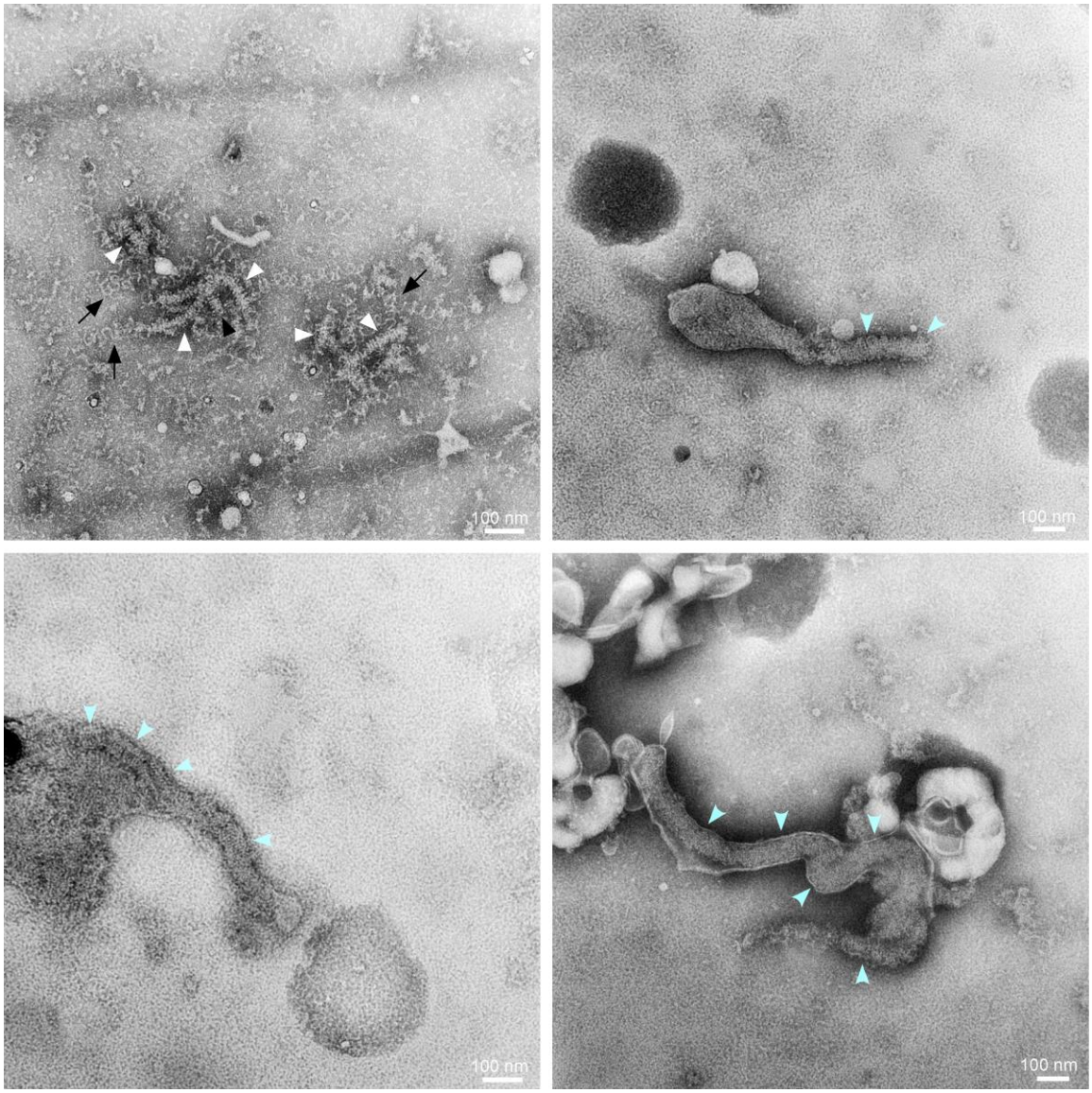

Figure 89. NP/VP24/VP35/VP30/VP40 nucleocapsid-like particles observed within VLPs and cell culture media. Ultracentrifugation of cell culture media resulted in VLP pellets, which were resuspended in PBS and stained with methylamine tungstate. Black arrows: loosely coiled NP-RNA; black arrowheads: tightly coiled NP-RNA; white arrowheads: nucleocapsid-like particles; blue arrowheads: regions of tightly wound nucleocapsid-like particles within VLPs.

6.5 Summary

Removal of the detergent NP-40 from the hypotonic lysis buffer did not cause greater condensation of nucleocapsid-like particles. Tighter nucleocapsid-like particles in either cell lysates or gradient fractions were not observed after homogenization; however, tighter NP-RNA particles were observed much more frequently. In addition, the addition of $MgCl_2$ and KCl did not prevent unwinding of the nucleocapsid-like particles. Attempts to mimic temporal regulation of nucleocapsid proteins by Ebola virus did not result in tighter nucleocapsid-like particles. Interestingly, nucleocapsid-like particles observed within VLPs were rare, but did appear more condensed with a "herring-bone" appearance similar to that of the native Ebola virus nucleocapsid.

Chapter 7. Discussion

An in-depth knowledge of the oligomeric structure and protein-RNA interactions within the filovirus nucleocapsid is essential to understanding how this complex functions in protecting, packaging, and replicating the genome during the viral life cycle. The development of intervention strategies, such as vaccines and therapeutic inhibitors can be expedited by a fuller comprehension of the structural-functional relationships within the nucleoprotein complex of this virus family. This thesis investigated the assembly and protein composition of the Ebola virus nucleocapsid by isolating and analyzing virus-derived and transfection-derived envelope-free Ebola virus nucleocapsids. The main achievement of this thesis project was to ascertain the ability of the four major nucleocapsid proteins to self-assemble (along with cellular RNA) into a stable nucleocapsid structure that could be isolated and purified as a model to study its physical and chemical characteristics. This development is a significant milestone in filovirus research, and paves the way for future studies utilizing synthetic, non-infectious replicase complexes (the nucleocapsid-like particles described in this thesis) to study viral replication and genome packaging. Previous functional studies of the filovirus nucleocapsid-associated proteins have been mostly restricted to investigating the properties of single proteins in isolation, and their interaction with other cellular systems such as the interferon pathway, for example. Structural studies on the whole *bona-fide* viral replication complex (which contains viral RNA and five virally encoded proteins) have been limited due to the pathogenicity of the virus, which restricts work with live specimens to BSL4 laboratories and requires virally-derived extracts and fractions to be inactivated before study. This chemical inactivation can also hinder structural studies, such as IEM. In addition, the

presence of the viral envelope hinders protein identification and higher resolution analyses of the nucleocapsid. Thus, this thesis project investigated noninfectious, envelope-free Ebola virus nucleocapsid-like particles in order to begin to fill these gaps in knowledge. **The central questions of this thesis were (1) could the Ebola virus nucleocapsid be released in a structurally intact state from its viral envelope? and: (2) could synthetic, self-assembled Ebola virus nucleocapsid-like particles be isolated and purified after co-expression of NP, VP24, VP35, and/or VP30 and VP40 in a heterologous, non-infectious expression system?**

7.1 Location of NP, VP24, and VP35 within the Ebola virus nucleocapsid

7.1.1 The inner layer of the Ebola virus nucleocapsid consists of NP-RNA

Reconstructions of the Ebola virus nucleocapsid have revealed that it is a helical, left-handed, double-layered particle (Beniac et al. 2012). The inner helix contains the negative sense, single-stranded RNA genome encapsidated by a single layer of NP molecules (Beniac et al. 2012; Bharat et al. 2012; Booth et al. 2013). Image analysis also suggests that VP30 may be located within this layer, binding in a groove on the top of NP (Figure 2) (Beniac et al. 2012). The structural arrangement of the Ebola virus outer layer is still controversial. Our research group theorizes that the outer shell consists of VP24:VP35 heterodimers that form horizontal bridge-like structures that are relatively globular. Each heterodimer is hypothesized to interact with one NP molecule, giving NP, VP30, VP24, and VP35 equal stoichiometry (Figure 2) (Beniac et al. 2012; Booth et al. 2013). The densitometry results in this thesis support this theory, as I was able to show approx. 1:1

ratios for each of the proteins in the nucleocapsid-like particles (Figure 46). A second theory suggests that VP24 and VP35 interact with alternate copies of NP and form a protuberance that is almost perpendicular to the helical nucleocapsid (Figure 4) (Bharat et al. 2012). The second model is based on a lower resolution reconstruction; however, both reconstructions were hindered by the presence of the viral envelope. At the time of this thesis, release and purification of Ebola virus nucleocapsids from viral envelopes or transfected cells had never been successful.

While investigating chemically fixed Ebola virus particles from a 14-day infection, I discovered hollow, helical particles that appeared similar to the Ebola virus nucleocapsid (Figure 8). These novel proto-nucleocapsid particles were approximately 10 nm narrower than the full Ebola virus nucleocapsid, with an outside diameter of 30.5 nm rather than 41 nm (Beniac et al. 2012). The inner diameter of these hollow rod-like particles was ~20 nm, which closely matches the 16 nm inner diameter of the Ebola virus nucleocapsid. These diameters also closely correspond to the NP tubes visible in cell sections, suggesting that these proto-nucleocapsids consist of the NP subunits (Figure 2, Figure 10, Figure 18). Furthermore, both the pitch (6.96 nm) and number of repeats (10.81) per turn calculated for the proto-nucleocapsids were equivalent to those calculated for the full Ebola virus nucleocapsid. Particles very similar in appearance have been generated by the expression of C-terminally truncated NP mutants. Expression of $NP_{\Delta 451\text{-}739}$ produced condensed, hollow, rod-like particles that were 28-36 nm in diameter and 7.4 nm in pitch (Bharat et al. 2012; Peng et al. 2016). Previous research has also demonstrated the requirement for RNA in the assembly of NP helices (Noda et al. 2010). Dialysis of NP helices into 0 mM NaCl buffer, followed by treatment with RNAse I prevented the reassembly of the NP helices

when dialyzed back into 150 mM NaCl; whereas, the same experiment performed without RNAse I resulted in reassembly of the helices (Noda et al. 2010). Taken together, this is convincing evidence that the proto-nucleocapsids consist of NP-RNA. Furthermore, both the smaller diameter and the lack of external protuberances in the proto-nucleocapsid reconstructions suggest that VP24 and VP35 were not present on this structure (Figure 10, Figure 90).

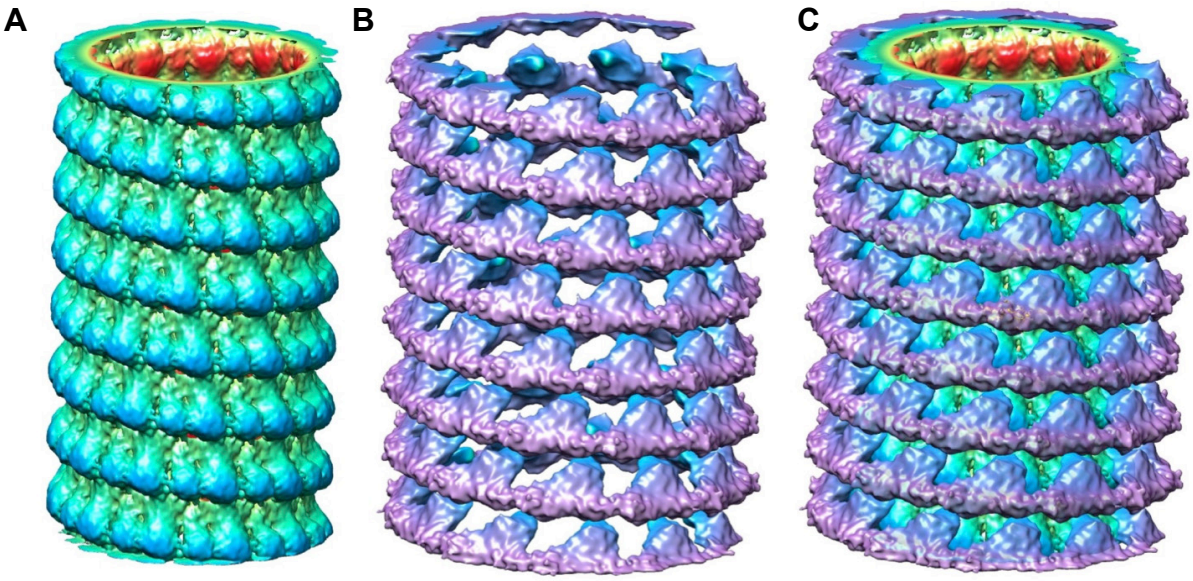

Figure 90. Solid surface reconstructions of the double-layered Ebola virus nucleocapsid. (A) Inner NP layer reconstruction based on the proto-nucleocapsid averages and full Ebola virus nucleocapsid; (B) the outer VP24-VP35 layer based on Ebola virus tomographic and single particle image analysis data; (C) The assembled double-layered Ebola virus nucleocapsid.

The role of these proto-nucleocapsids in Ebola virus infection is currently unknown; however, they could represent an intermediate structure that arises during transcription and replication. These events require the nucleocapsid to at least partially disassemble in order for the polymerase to gain access to the genome. It is possible that the proto-

nucleocapsid is a low energy structure of self-assembled NP that protects the genomic RNA until either packaging or replication/transcription occurs. Whether the proto-nucleocapsids are structural intermediates that occur transiently in the assembly or dis-assembly of the nucleocapsid and what role (if any) they play in infection requires further research into these intriguing structures.

7.1.2 The outer layer of the Ebola virus nucleocapsid consists of VP24 and VP35

Tomographic image analysis of sections of transfected cells confirmed an approximately 20 nm difference between NP only particles and the nucleocapsid-like particles. In contrast, the addition of VP30 to the transfection panel did not affect diameter or morphology of the nucleocapsid-like particles (Figure 18). Inclusion of the proto-nucleocapsid in this analysis demonstrated its similarity in diameter with the NP only particles and confirms the double-layered nucleocapsid model, in which NP-RNA forms the inner helix layer and VP24-VP35 form the outer layer (Figure 90). While previous cell section work has alluded to this conclusion, I am the first to use tomography and image analysis to clearly demonstrate the importance of VP24 and VP35 in generating the full diameter of the Ebola virus nucleocapsid particle (Manuscript in preparation).

In addition, my cell section tomograms illustrated how the nucleocapsid-like particles were positioned within the Z-axis of the cell cytoplasm. The particles were closely packed within the viral inclusion bodies and displayed a high degree of flexibility as the viewpoint was moved through the Z-axis of the tomogram (Chapter 9.4: Movie S1; Movie S2). The resolution of the electron micrographs and tomograms was not sufficient to confirm the pitch of the nucleocapsid-like particles within cell sections. Figure 91 shows an example of a nucleocapsid-like particle with three discernable helical repeats.

Measurement in this region reveals an approximate diameter of 40 nm with a pitch of ~12 nm. Images similar to Figure 91 with light staining and demonstrating a well-defined pitch were rare. It is probable that this relaxed pitch was the norm within transfected cells, since I was unable to isolate nucleocapsid-like particles that consistently matched the Ebola virus nucleocapsid pitch of ~7 nm. Therefore, it is unlikely that the nucleocapsid-like particles assembled in transfected 293T cells are identical in structure to the nucleocapsids synthesized in Ebola virus infected cells.

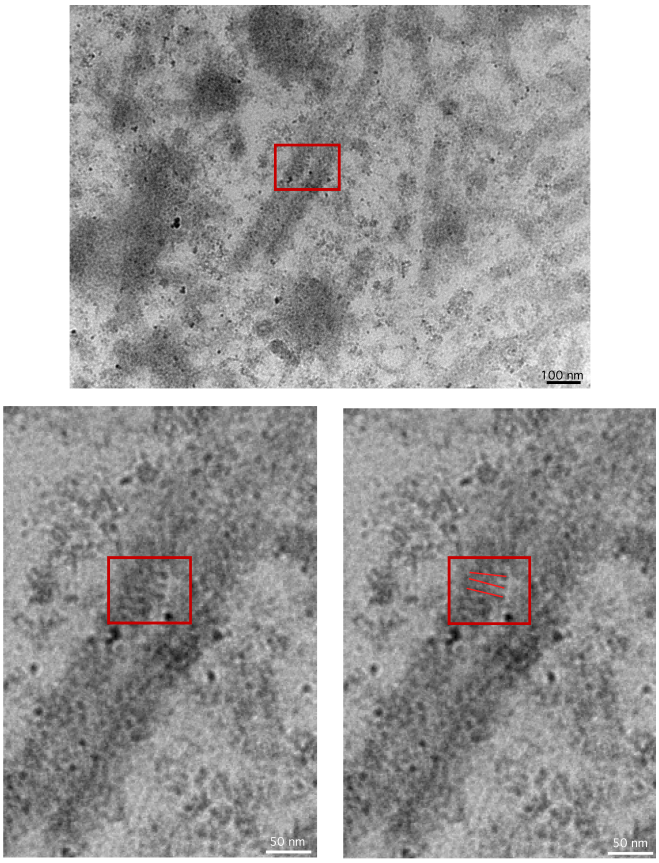

Figure 91. Uncondensed nucleocapsid-like particle from NP/VP24/VP35 transfected cell section. Stained with uranyl acetate and lead citrate. Pitch measured as ~12 nm, diameter as ~ 40 nm.

7.1.3 Summary

My research on the morphology of the virus-derived proto-nucleocapsids and expressed intracellular nucleocapsid-like particles was complementary. The proto-nucleocapsids were novel NP-RNA rod-like particles that were highly condensed and stable. Particles similar in appearance have been generated artificially by overexpression of C-terminal truncated NP mutants, but have never before been observed from Ebola virus infected cells (Bharat et al. 2012; Peng et al. 2016; Watanabe et al. 2006). Thus, it is likely that the Ebola virus-derived proto-nucleocapsids observed in this thesis consist mostly of NP molecules, but may contain other viral proteins, such as VP30 or L. The pitch and number of repeats per turn of the proto-nucleocapsid matches that of the full Ebola virus nucleocapsid, suggesting that the inner NP layer is the foundation of the complete helical nucleocapsid. The difference in diameters observed between particles produced by expression of NP alone (~25 nm) or in combination with VP24 and VP35 (~50 nm) corroborates the double-layered nucleocapsid model, in which the inner NP helix is decorated on the outside with VP24-VP35 heterodimers to assemble the complete Ebola virus nucleocapsid (Figure 90) (Manuscript in preparation). Taken together, the proto-nucleocapsid and cell section data confirms the placement of NP within the inner nucleocapsid layer and reinforces the external location of VP24 and VP35, but still cannot confirm the position of VP30 within the inner NP layer.

7.1.4 Limitations and opportunities

7.1.4.1 Release of Ebola virus nucleocapsids

Treatment with 0.15% NP-40 was not sufficient to release intact nucleocapsids from their viral envelopes, although Bharat et al. (2012) reported the release of VLP-bound NP helices at this concentration. As such, Ebola virus nucleocapsids have still not been successfully isolated from viral particles. Investigation into higher NP-40 or other detergent concentrations should be undertaken, as cryo-EM image processing and analysis of envelope-free nucleocapsids remains a valuable approach to producing a high-resolution reconstruction of the Ebola virus nucleocapsid. I was very lucky to have the opportunity to plan an experiment with Shane Jones and the Special Pathogens group at the NML. Their schedule and the outbreak of Ebola virus in West Africa prevented continued investigation into higher detergent concentrations; however, I know our lab would like to further our studies into late stage Ebola virus infection in the future.

7.1.4.2 Fixation of proto-nucleocapsids

The highly pathogenic nature of filoviruses leads to a stringent fixation protocol before removal from BSL 4 facilities. At the NML, this protocol involves the 24 hour incubation of samples in 4% PFA. As a result, SDS-PAGE, western blot, and/or immunogold labeling cannot be utilized to identify the proteins constituting the proto-nucleocapsids. The fixed Ebola virus samples before and after dialysis to remove the PFA, displayed only a messy smear of protein on SDS-PAGE. While the diameter, pitch, and appearance of the proto-nucleocapsids are consistent with a structure formed by NP-RNA, this conclusion cannot be confirmed until further experiments are performed. Likewise, the theorized

location of VP30 within the inner NP-RNA nucleocapsid layer cannot currently be investigated with regards to the fixed proto-nucleocapsids.

Nonetheless, the discovery of these proto-nucleocapsids provides numerous opportunities for future studies on their structure as well as investigations into the late stages of Ebola virus infection. First, a 14-day Ebola virus infection could be repeated. Isolation of the proto-nucleocapsids from the viral stock would enable protein identification by SDS-PAGE and western blot analyses before the samples are fixed and removed (Welsch et al. 2010). In addition, immunogold labeling prior to fixation could be performed to localize specific nucleocapsid proteins within the proto-nucleocapsid. Alternatively, research on fixed Marburg virus has been successful by embedding purified virus or infected cells in various types of resin. Immunogold labeling of fixed Marburg virus sections enabled the identification and approximate location of NP, VP24, VP35, and VP40 within the virus particle (Bharat et al. 2011). Thus, a similar sectioning approach could be utilized with the fixed proto-nucleocapsids and Ebola virus particles. Second, it is unclear why the proto-nucleocapsids are lacking the outer nucleocapsid layer that consists of VP24 and VP35 (Figure 90). Immunogold labeling of the unfixed or embedded proto-nucleocapsid particles would verify their structural composition, but would not indicate the reason. As mentioned previously, it is possible that the proto-nucleocapsids are intermediate structures required for replication and transcription. *In vitro* transcription assays might help shed light on their role in transcription/replication. Alternatively, as these particles have currently only been observed 14 days post-infection, it is possible that VP24 and VP35 exhaustion could prevent the assembly of the outer nucleocapsid layer. Filovirus gene expression is highly temporally regulated, with genes at the 3' end, such as

NP and VP35 being the most abundantly expressed and those at the 5' end, such as VP24 and the RdRp being expressed less frequently (Muhlberger et al. 1999; Muhlberger 2007). Whether a lack of VP24 and/or VP35 at 14 days post-infection played a role in inhibiting the assembly of the complete Ebola virus nucleocapsid could have implications for novel therapeutic development. TEM of cell sections from the 14 day time point could reveal whether 25 nm proto-nucleocapsids or 50 nm complete nucleocapsids were more abundant within intact cells. To complement the TEM observations, NP, VP24, and VP35 protein and mRNA levels could be measured by western blot and quantitative reverse-transcription PCR, respectively. Lastly, a time course that spans the 14-day infection would be useful to observe if and when NP, VP24, and VP35 expression is reduced.

7.1.4.3 Tomography of cell sections

Cell sections were an ideal specimen for tomography due to their stability and resistance to radiation (Welsch et al. 2010). These features enabled us to easily perform dual-axis tomography and resulted in more complete data for each tomogram (Cope et al. 2011). The disadvantage of using cell sections for tomography is reduced resolution (Welsch et al. 2010). The cell sections utilized in this thesis were triple stained with osmium tetroxide, lead citrate, and uranyl acetate. While stain percentage and incubation period were optimized, stain variability still occurred, resulting in some sections being stained heavier or lighter than others. In addition, section thickness can also influence the resolution of the reconstruction (Sousa et al. 2011) Thus, tomograms of thin cell sections can provide data on a structure's dimensions, placement within cells, and morphology, but cannot provide the finer details of the structural arrangement of small macromolecular complexes (Welsch et al. 2010). This is evident when evaluating the tomograms, which

demonstrate the diameter difference between NP tubes and NP/VP24/VP35 particles, the overall helical morphology of these nucleocapsid-like particles, and the extension of these particles through the cell cytoplasm, but could not distinguish individual protein subunits or the pitch of the nucleocapsid-like particles. One method of enhancing resolution would be to freeze cells at high pressure and then stain and resin embed through slow infiltration (Welsch et al. 2010). Welsch et al. (2010) performed this technique with Marburg virus infected cells and were able to distinguish the "herring-bone" structure of the nucleocapsid within cells and virus particles. Alternatively, cells could be grown on top of prepared TEM grids and prepared immediately for tomography through fixation and/or vitrification (Bharat et al. 2011). Either method could be adapted to investigate the differences in intracellular nucleocapsid particles between virally infected and transfected cells.

7.2 Analysis of nucleocapsid-like particles

7.2.1 VP24 is a critical component of the Ebola virus nucleocapsid

Buoyant density gradient sedimentation of intracellular nucleocapsid-like particles produced by expression of NP, VP24, and VP35 identified only NP and VP35 as the major components of the nucleocapsid (Huang et al. 2002). This observation, along with its early characterization as a matrix protein has led to the longstanding hypothesis that VP24 catalyzes the assembly, but is not itself a major component of the Ebola virus nucleocapsid (Han et al. 2003; Huang et al. 2002; Noda et al. 2006; Noda et al. 2007b).

In contrast to these biochemical studies, more recent structural analyses of the Ebola and Marburg virus nucleocapsids suggest that VP24 is a major component (Beniac et al. 2012; Bharat et al. 2012). Thin-section IEM of Marburg virus nucleocapsids identified

VP24 within this particle (Bharat et al. 2011). This confirmatory data is lacking for Ebola virus, but cryo-electron tomography and single particle image analyses of the Ebola virus nucleocapsid have revealed a density the correct size for VP24 in the outer nucleocapsid layer (Beniac et al. 2012). This location is also consistent with the IEM results from Marburg virus (Bharat et al. 2011).

In this thesis, expression of NP with either VP30 or VP35 resulted in co-migration of these proteins through the density gradient, whereas expression of NP and VP24 did not (Figure 21). Co-migration of VP24 was only achieved upon expression of NP, VP24, and VP35 (Figure 23). Furthermore, nucleocapsid-like particles were only observed after the co-expression of all three proteins (Figure 24). Based on current literature this is the first example of VP24 being directly associated with NP and VP35 with regards to the Ebola virus nucleocapsid. In addition, I am the first to isolate and image ~40 nm diameter Ebola virus nucleocapsid-like particles. The purified nucleocapsid-like particles were similar in appearance to the Ebola virus nucleocapsid and demonstrated characteristic features such as extreme flexibility and disjointed continuations (Figure 24). In contrast to the Ebola virus nucleocapsid, the isolated particles were narrower and less condensed than the native virus. Possible reasons for this discrepancy will be discussed in Section 7.4.

Recently, VP24 was shown to be required for the packaging of tetracistronic, but not monocistronic minigenomes. The infectivity of tetracistronic trVLPs was drastically reduced in the absence of VP24, but the same result was not observed for the monocistronic trVLPs. The authors suggested that monocistronic minigenomes were short enough to be packaged efficiently without VP24 (Watt et al. 2014). Only one study has analyzed VP24-null RNP particles within VLPs. Although Hoenen et al. (2006) initially

labeled these particles as complete nucleocapsids, when I measured these particles recently using ImageJ, a diameter of ~20 nm was recorded for a few short regions of helical NP-RNA, while the rest of the nucleocapsid particle was undefined inside the VLP. I observed similar NP-RNA particles with various degrees of condensation when NP was transfected alone or in combination with one other nucleocapsid-associated protein. This evidence suggests that short sequences of RNA encapsidated by NP, VP35, VP30 and L and packaged into GP-VP40 VLPs are necessary and sufficient for infection and that the full nucleocapsid particle is not required when short RNA sequences are involved. However, VP24 was required for the efficient packaging of loosely coiled L-VP35-VP30-NP-RNA tetracistronic minigenomes, suggesting that the formation of a condensed complete nucleocapsid particle is critical for longer RNA sequences (Watt et al. 2014). The mechanism behind the genome-length dependent effect of VP24 on infectivity was not clear, but Watt et al. (2014) hypothesized that VP24 enabled the condensation of the loosely coiled RNP particle and could be involved in locking the RdRp in the 3' UTR for primary transcription (Hoenen et al. 2006).

My results are consistent with this theory. In most of the transfection studies, expression of NP alone or in combination with one other nucleocapsid-associated protein was characterized by loosely coiled NP-RNA structures. These particles could only be condensed upon co-expression of NP, VP24, and VP35, demonstrating a role for VP24 (and VP35) in nucleocapsid condensation. I have also demonstrated that NP itself can condense into a particle that has the same pitch and number of repeats per turn as the full nucleocapsid, but is 30.5 nm in diameter, rather than 41 nm (Figure 10, Figure 85). In support of the above-mentioned theory, these NP rod-like particles were rare after

transfection, with the exception of the homogenized lysates, and were generally short in length. Thus, interactions between NP subunits appear to be sufficient to generate short segments of condensed helical particles, like those observed in VP24-null infectious VLPs and in my own experiments; however, for efficient assembly into the compact nucleocapsid structure, these NP-NP interactions require VP24 and VP35.

7.2.2 VP40

7.2.2.1 A role in helical condensation

Similar to VP24, the role of VP40 in the structure of the Ebola virus nucleocapsid remains unclear. As the major matrix protein, VP40 is responsible for the "docking" of the nucleocapsid to the plasma membrane and the subsequent budding of the viral particle (Bornholdt et al. 2013; Jasenosky et al. 2001; Noda et al. 2002; Ruigrok et al. 2000). In addition to budding, some researchers have attributed nucleocapsid condensation to VP40. Bharat et al. (2012) reported that tightly coiled NP could only be observed when the C-terminal domain was removed or after release of full-length NP from VLPs. This study also analyzed VLP-bound nucleocapsid-like particles generated by transfection and concluded that VP40 must be an effector that leads to NP and nucleocapsid condensation.

I demonstrated that nucleocapsid-like particles assembled in the presence of VP40 were not perceivably different in appearance from those generated in its absence (Figure 29, Figure 33). However, measurement of the diameter and pitch did reveal that particles assembled in the presence of NP/VP24/VP35/VP40 had the most consistent average diameters, regardless of the lysis method used. These particles also tended to have the tightest pitch. Thus, it is possible that there are two condensation events for the Ebola virus

nucleocapsid. The initial condensation of NP-RNA through NP-NP interactions, which is facilitated by VP24 and VP35, followed by a secondary condensation event when the nucleocapsid associates with VP40 and/or budding occurs.

In agreement with the model, VP40 co-migrated through the density gradient with NP, VP24, VP35 and VP30 (Figure 27). The distribution of VP40 in the density gradient was dependent on the presence of VP35 and only when these two proteins were expressed together did VP40 consistently migrate to fractions 6 and 7, in parallel with the other nucleocapsid-associated proteins (Figure 27, Figure 32). Dual transfection of NP and VP40 did not result in a strong co-migration pattern (Figure 21). Likewise, expression of NP, VP24, and VP40 did not demonstrate an obvious co-distribution (Figure 27). This interaction between VP35 and VP40 has been documented with previous VLP studies. While both NP and VP35 could be detected in VP40 VLPs, VP35 also demonstrated RNA specificity by preferentially selected Ebola virus minigenomes for packaging in VP40 VLPs (Johnson et al. 2006b; Licata et al. 2004). This strong interaction between VP35 and VP40, together with VP40's association with the plasma membrane, suggests that dimeric VP40 and/or components of the hexameric lattice were pulled through the gradient with VP35 and the nucleocapsid-like particles (Bornholdt et al. 2013; Hoenen et al. 2010b; Nanbo et al. 2013). Furthermore, my research points to the interaction between VP40 and VP35 as being the major effector of nucleocapsid packaging, in agreement with the work by Johnson et al. (2006b). It would be interesting to determine the oligomerization state of VP40 in each fraction. In addition, a time course investigating VP35-VP40 interactions and their oligomerization states might also illustrate a change from dimeric to hexameric VP40 during assembly of the nucleocapsid. Deletion mutants of VP35 could be utilized to

determine which domains provide RNA specificity and VP40 binding and confirm that VP35-VP40 interactions are directly responsible for packaging of the viral nucleocapsid.

7.2.2.2 The condensation of NP helices does not require VP40

In contrast to the relationship hinted at between VP40 and nucleocapsid-like particle condensation, I have observed tight NP-RNA coils in both the presence and absence of VP40. Expression of NP and VP40 alone or in combination with the other nucleocapsid-associated proteins resulted in more condensed NP-RNA structures observed from cell culture media (Figure 53c, Figure 87, Figure 88). While VP40 was present in these experiments, encapsidation/release of NP from VLPs was not required for the formation of condensed NP structures. More significantly, I also observed highly condensed NP-RNA particles in the absence of VP40 after homogenization and hypotonic lysis buffer treatment (Figure 24, Figure 73). This condensation was lost after gradient ultracentrifugation of the homogenized lysates, although the nucleocapsid-like particles were unaffected (Figure 74). Staggered transfection of the nucleocapsid-associated proteins, followed by homogenization, resulted in the greatest number of condensed NP rod-like particles and enabled diameter and pitch measurements (Figures 85-86). These particles were also generated in the absence of VP40 (Figure 85abc). Altogether, these observations suggest that a) NP is capable of oligomerization by itself; however, this interaction requires a particular undefined environment to do so; b) VP40 is not required for condensation of full-length NP; and c) NP rod-like particles are more fragile than the full-length nucleocapsid, as ultracentrifugation of homogenized lysates resulted in their unwinding (Figure 74a). More work is needed to determine why homogenization and "natural" release into cell culture medium resulted in a higher concentration of NP rod-like particles. A major

question is whether these methods maintained the proteins and/or cellular environmental conditions required for the NP rod-like particles, or if it is simply that they were more gentle methods of lysis that enabled the fragile NP rod-like particles to remain assembled. It is also possible that the lack of viral RNA may prevent the complete assembly of NP rod-like particles, although this seems like the least likely explanation due to the ability of C-terminal NP mutants to form similar particles using cellular RNA (Bharat et al. 2012; Peng et al. 2016).

The most likely explanation for their fragility may be the absence of VP24 and VP35. I have demonstrated that VP24 and VP35 lead to efficient condensation of the nucleocapsid and in Section 7.2.4 I will discuss the stability of these nucleocapsid-like particles. While NP rod-like particles from NP-only hypotonic lysis buffer lysates were unwound after ultracentrifugation, the same purification method using NP/VP24/VP35 hypotonic lysis buffer lysates resulted in both tight and loosely coiled NP-RNA (compare Figure 22a with Figure 24 and Figure 73a with 74a). The stabilization of NP rod-like particles in the presence of VP24 and VP35 suggests that in addition to stabilizing the full nucleocapsid particle, VP24 and/or VP35 may also be stabilizing NP-RNA particles without the complete assembly of the nucleocapsid. Expression of NP alone lacks this stabilization, and thus the helices easily unwind upon ultracentrifugation. While this fragility is contrasted by the stability of the proto-nucleocapsids, it is possible that fixation and/or the presence of viral RNA prevented the unwinding of these particles isolated from Ebola virus-infected cells.

7.2.3 Influence of protein composition

The range of statistical significance described in Table 26 made it difficult to draw any firm conclusions about the role of protein content on nucleocapsid-like particle assembly. Therefore, I performed linear regression analyses to learn more about data variability and potential correlations. When the average diameter and average pitch values for each lysis method and protein combination were paired, a positive linear regression with an R^2 of 63% was observed by scatterplot (Figure 59). Linear regression analysis of this data suggested that for every 1 nm increase in diameter, pitch would be expected to increase by 0.64 nm (Table 17). This predictive calculation illustrates the relaxed nature of the particles and the danger of using average values. Using this formula, a particle with a diameter of 41 nm would be expected to have a pitch of 26.24 nm, which is drastically larger than the actual ~ 7 nm pitch of the native nucleocapsid (Beniac et al. 2012). This result also indicates that the relationship between diameter and pitch is likely not linear. The measurements I recorded are only a snapshot of the relationship at defined pitch and diameter values. On a larger scale, the relationship is probably more similar to a positive exponential curve, because the pitch and diameter values will never reach zero and may have a preferred value at which they plateau. Indeed, when pitch or diameter datasets are sorted numerically and graphed, the scatterplot takes on a distinctly "S" curved shape. More analysis with paired pitch and diameter measurements will be required to investigate this hypothesis.

Table 26. Summary chart of significant differences between protein combinations.

A Protein Combination			Lysis Method					
			LB50	LB150	FT50	FT150	Media	Combined
X3	<,=,>	X330	<	=	=	<	<	<
X3	<,=,>	X340	<	=	=	<	=	<
X3	<,=,>	X5	<	>	>	=	=	=
X330	<,=,>	X340	=	=	=	>	>	=
X330	<,=,>	X5	=	>	>	>	>	>
X340	<,=,>	X5	=	>	>	>	=	>

B Protein Combination			Lysis Method					
			LB50	LB150	FT50	FT150	Media	Combined
X3	<,=,>	X330	<	=	=	=	=	<
X3	<,=,>	X340	<	>	>	>	=	>
X3	<,=,>	X5	=	=	>	=	=	=
X330	<,=,>	X340	=	>	>	>	>	>
X330	<,=,>	X5	=	=	>	=	>	>
X340	<,=,>	X5	=	=	<	<	=	<

(A) Diameter. (B) Pitch.
(=): The two protein combinations were not significantly different.
(<): The first protein combination had a significantly smaller mean measurement.
(>): The first protein combination had a significantly larger mean measurement.
Mann-Whitney with Bonferroni correction (p=0.000625).
X3: NP/VP24/VP35; X330: NP/VP24/VP35/VP30; X340: NP/VP24/VP35/VP40; X5: NP/VP24/VP35/VP30/VP40; LB50: hypotonic lysis buffer; LB150: isotonic lysis buffer; FT50: hypotonic freeze/thaw; FT150: isotonic freeze/thaw; Media: cell culture media.

Linear regression was then performed on the pitch and diameter data sets separately to determine the influence of lysis method and protein combination on these individual descriptors. Surprisingly, only 7.4-7.5% of the variation observed in the diameter and pitch data sets could be attributed to both lysis method and protein combination. When the data sets were further divided by protein combination or lysis method, protein combination only accounted for 1.9% of the diameter and 1.2% of the pitch variability. As such, protein combination does not appear to be the most significant effector of the nucleocapsid-like particles' diameter and pitch. While more of this variability is described by lysis method, the percentage (5-6%) is still very small. It is likely that sample preparation, image quality, and data collection were the biggest contributors to the variation in data observed, as discussed in Section 7.2.6.1.

Finally, I combined the data sets by protein combination to investigate whether any overall trends could be observed. Diameter and pitch measurements were combined regardless of lysis method, with the exception of the cell culture media data sets. As discussed in Chapter 4.4.5, these measurements were significantly smaller than the other lysis methods investigated. As such, they were removed from this analysis to prevent skewing of the results. When data sets were combined by protein combination only, NP/VP24/VP35 particles were not significantly different from NP/VP24/VP35/VP30/VP40 nucleocapsid-like particles in terms of pitch or diameter (Figure 60, Figure 61, Table 26). On average, NP/VP24/VP35/VP30 nucleocapsid-like particles exhibited the largest diameter and pitch measurements. NP/VP24/VP35/VP40 nucleocapsid-like particles had a similar average diameter to NP/VP24/VP35/VP30, but were significantly more condensed than all other protein combinations (Figure 60, Figure 61) (Manuscript in preparation).

7.2.3.1 The spring model

The flexible Ebola virus nucleocapsid has on average 10.81 repeats per turn, which must be maintained for proper nucleocapsid structure and length (Beniac et al. 2012). This means that as the nucleocapsid is stretched, the pitch should become larger, and the diameter smaller, in order to maintain this 10.81 repeats per turn (Figure 92, Chapter 9.4: Movie S3). The reverse would be true during condensation events, with the diameter growing larger as the pitch decreases (Figure 92, Movie S3). When the nucleocapsid is bent, one side expands while the other contracts. Figures 92 and 93 and the corresponding movies S3 and S4 provide schematic models of two different types of "springs" or helices. For clarity, stretching and condensing of the helices has been exaggerated to enable better visualization of the protein movements; however in reality, the expansion and contraction of the nucleocapsid would be on the nanometer scale, as I have observed.

If we apply this simplified "spring model" to the combined protein observations from the previous section, a hint into the possible mechanism of assembly is revealed. The addition of only VP40 to NP/VP24/VP35 expression led to an increase in diameter in tandem with a decrease in pitch compared to NP/VP24/VP35 alone (Figure 60-61). This pattern is consistent with a spring structure that is condensing as it maintains the same number of repeats per turn, as described above (Figure 92, Movie S3). The NP/VP24/VP35/VP40 nucleocapsid-like particles also maintained the most stable diameter of all the protein combinations, which did not differ significantly after any lysis buffer treatment, as evident in Table 27a. The pitch of NP/VP24/VP35/VP40 nucleocapsid-like particles was more variable, but could still be considered more uniform than the other protein combinations (Table 27b). This data suggests that the addition of VP40 to

NP/VP24/VP35 expression is enabling the assembly of more stable, condensed particles. As VP40 has been attributed to the condensation of VLP bound nucleocapsid-like particles, it is not surprising that I have noticed a similar trend (Figure 88, Figure 89).

In contrast, the addition of VP30 to NP/VP24/VP35 appears to have led to a slight unwinding of the nucleocapsid-like particles. Instead of the expected correlation between increased diameter and decreased pitch, NP/VP24/VP35/VP30 nucleocapsid-like particles were both more relaxed and wider than any of the other protein combinations, suggesting a loss or loosening of the foundational structure that would normally maintain the 10.81 repeats per turn (Figure 60-61, Figure 93, Chapter 9.4: Movie S4).

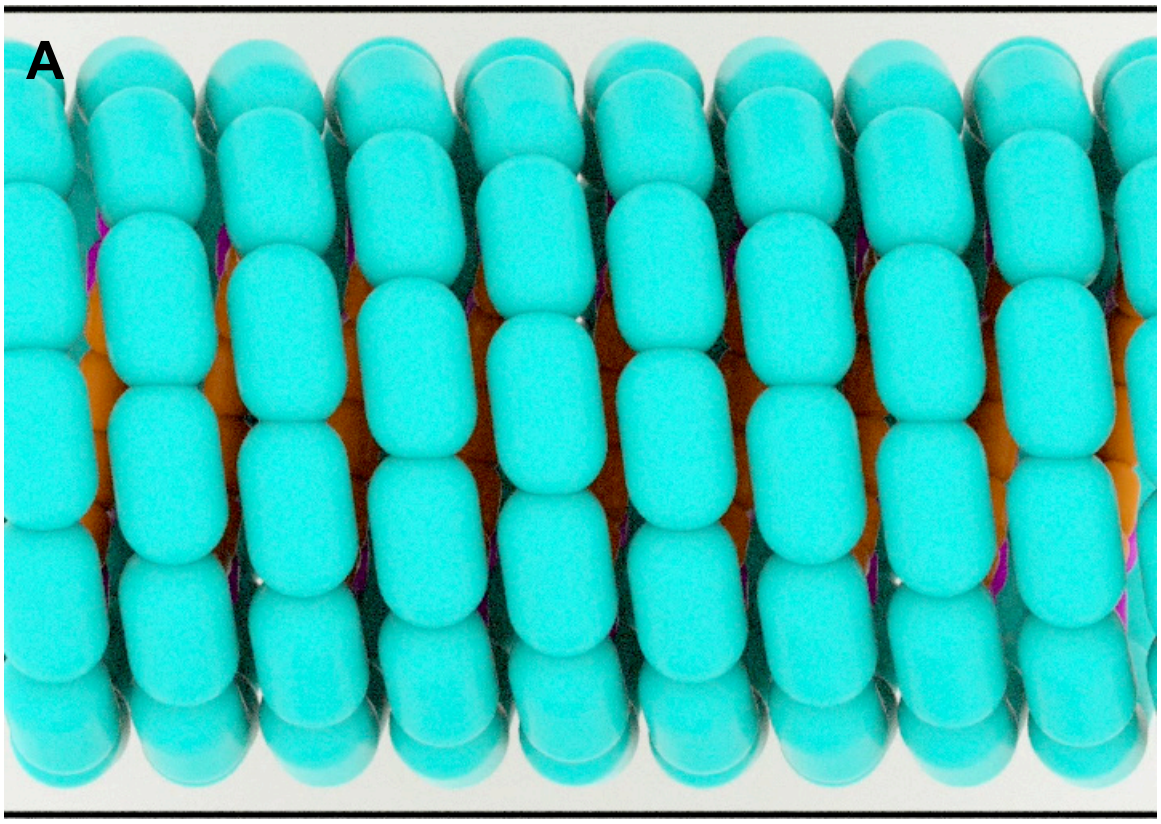

Figure 92. Schematic of a coiled spring that maintains 11 repeats per turn as it is stretched or condensed (Movie S3). (A) Condensed helical structure with a pitch of ~7nm and 11 repeats per turn. (B) Stretching of (A) results in larger pitch but a reduced diameter. (C) Over exaggeration of stretched helical coil to demonstrate smaller diameter and larger pitch. Turquoise: VP24-VP35 heterodimers; magenta: NP molecules; orange: RNA.

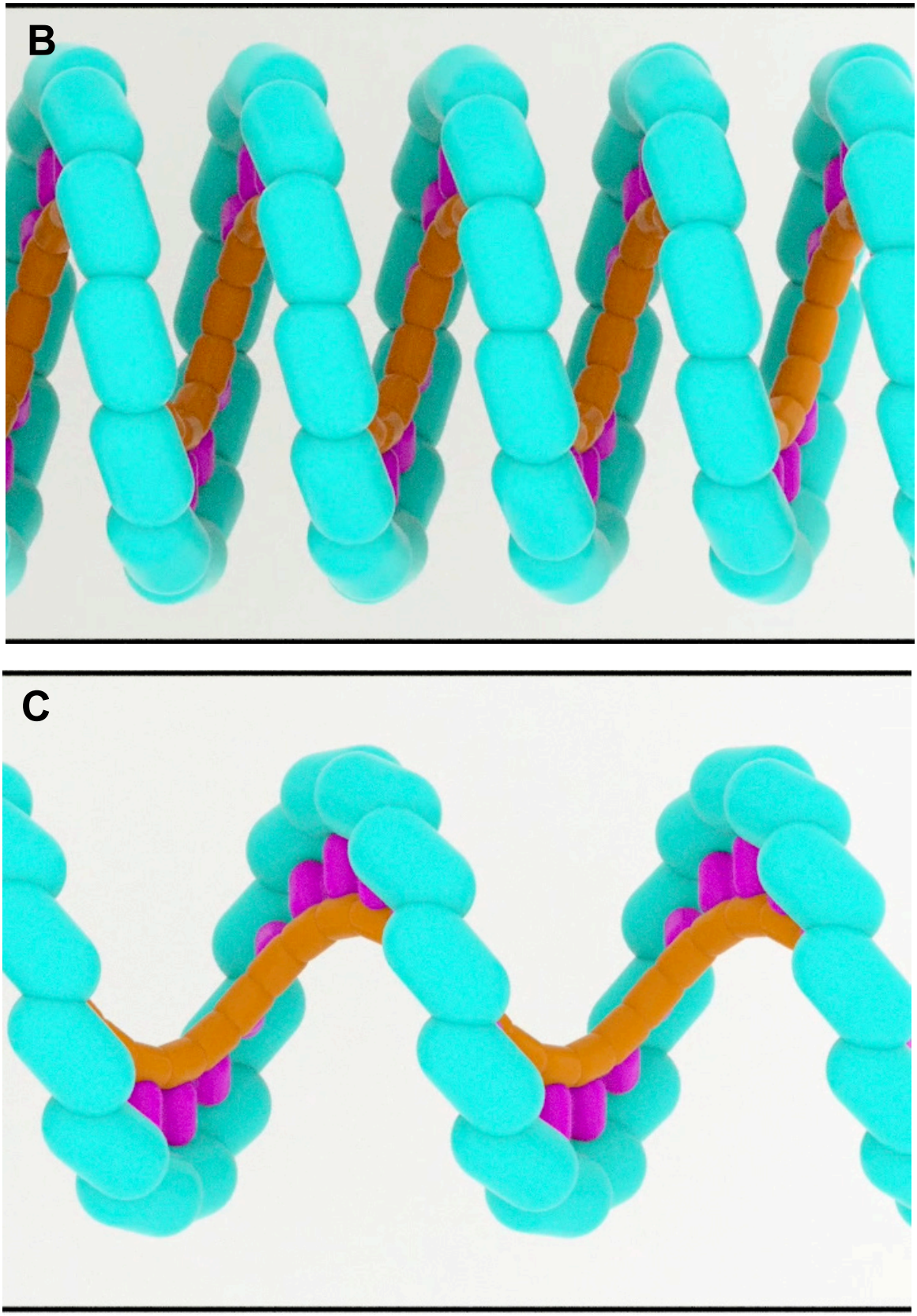

Figure 92 continued.

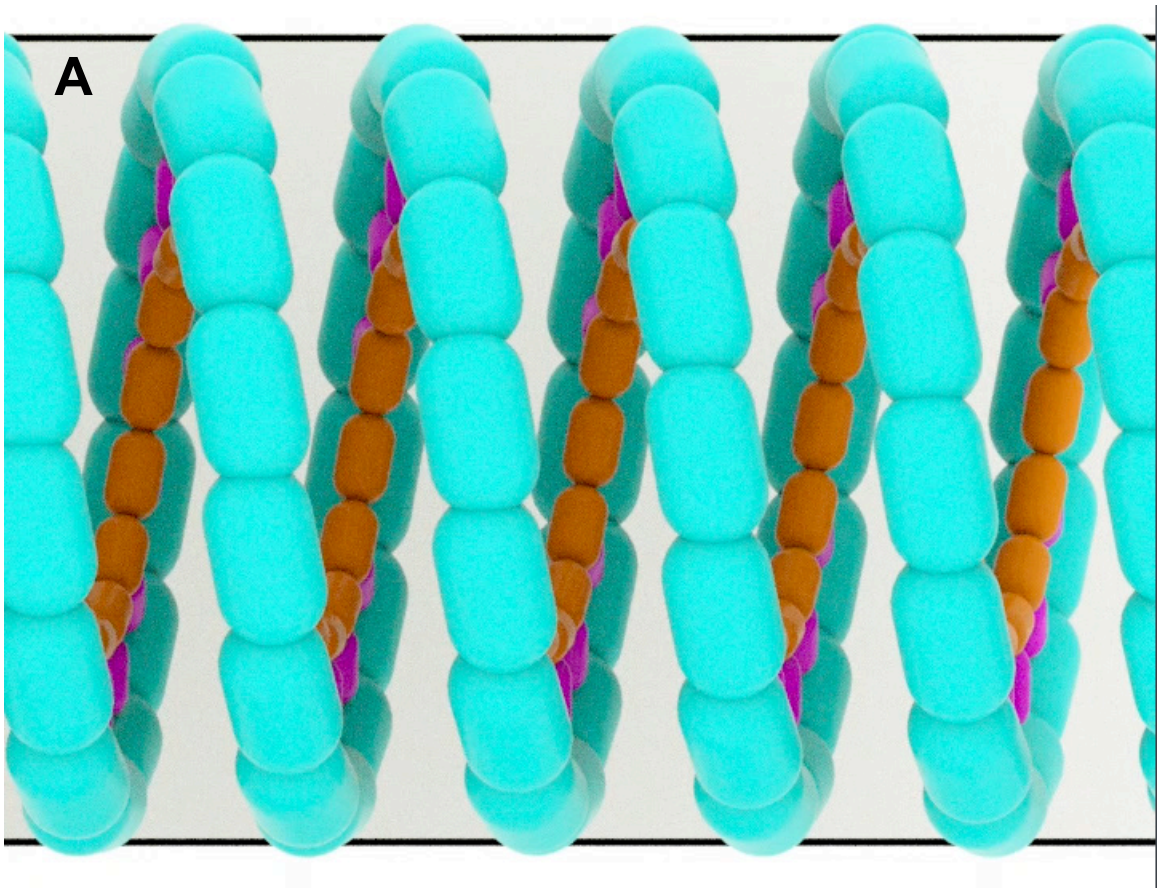

Figure 93. Schematic of a coiled spring that does not maintain 11 repeats per turn as it is stretched or condensed (Movie S4). Helical coil begins with ~ 7 nm pitch and 11 repeats per turn as in Figure 91A. (A) Stretching results in larger pitch and diameter. (B) Over exaggeration of stretched helical coil to demonstrate larger diameter and pitch. Turquoise: VP24-VP35 heterodimers; magenta: NP molecules; orange: RNA.

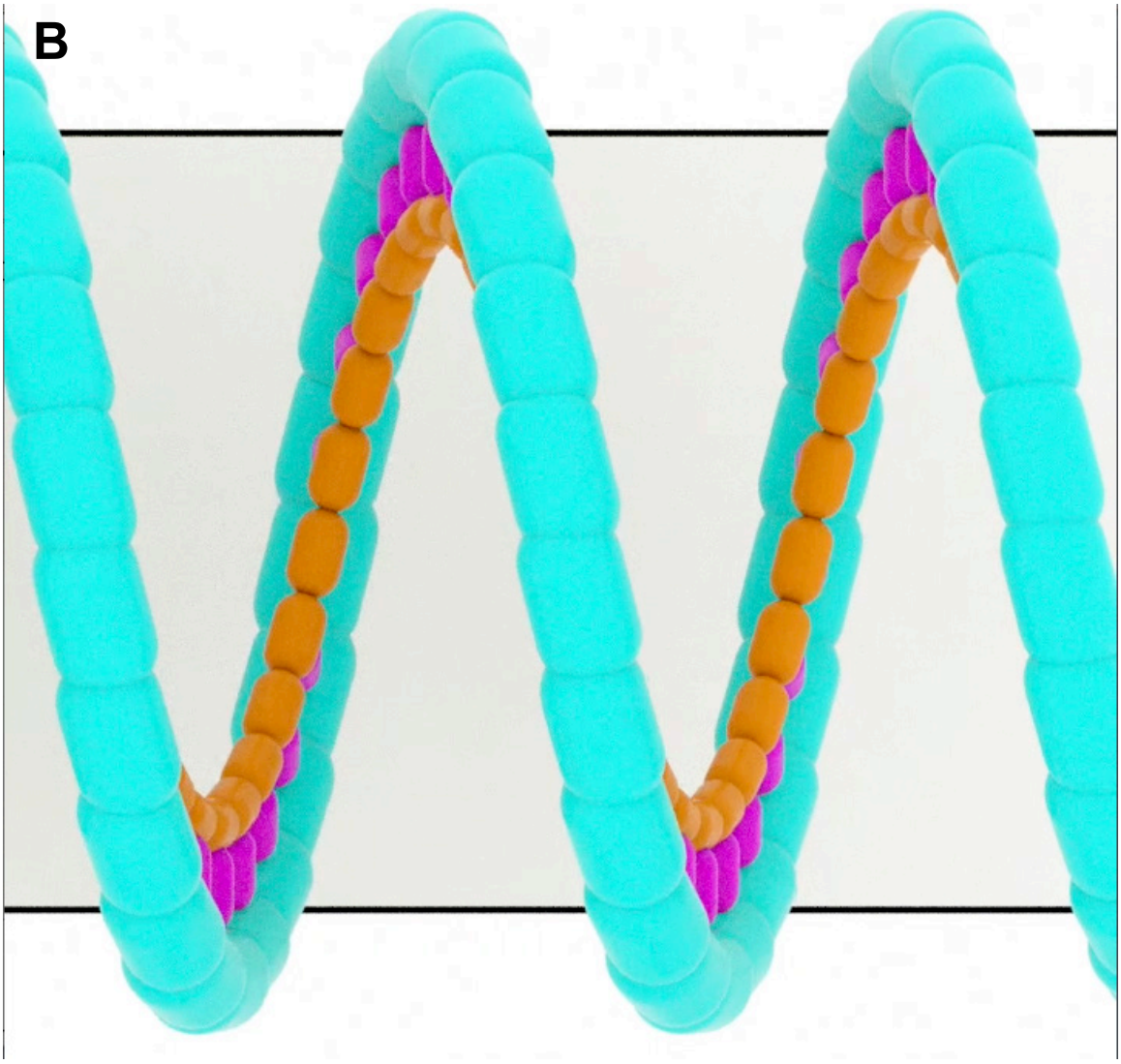

Figure 93 continued.

Table 27. Summary of significant differences by lysis method.

A

Protein Combination	Lysis Method A		Lysis Method B			
			LB150	FT50	FT150	Media
X3	LB50	<,=,>	<	<	<	>
	LB150	<,=,>	-	=	=	>
	FT50	<,=,>	-	-	>	>
	FT150	<,=,>	-	-	-	>
X330	LB50	<,=,>	=	<	<	>
	LB150	<,=,>	-	<	<	>
	FT50	<,=,>	-	-	=	>
	FT150	<,=,>	-	-	-	>
X340	LB50	<,=,>	=	=	=	>
	LB150	<,=,>	-	=	=	>
	FT50	<,=,>	-	-	=	>
	FT150	<,=,>	-	-	-	>
X5	LB50	<,=,>	>	>	>	>
	LB150	<,=,>	-	<	=	>
	FT50	<,=,>	-	-	=	>
	FT150	<,=,>	-	-	-	>

B

Protein Combination	Lysis Method A		Lysis Method B			
			LB150	FT50	FT150	Media
X3	LB50	<,=,>	<	<	<	=
	LB150	<,=,>	-	<	=	>
	FT50	<,=,>	-	-	>	>
	FT150	<,=,>	-	-	-	>
X330	LB50	<,=,>	=	<	<	>
	LB150	<,=,>	-	<	<	>
	FT50	<,=,>	-	-	=	>
	FT150	<,=,>	-	-	-	>
X340	LB50	<,=,>	>	=	=	>
	LB150	<,=,>	-	<	=	>
	FT50	<,=,>	-	-	=	>
	FT150	<,=,>	-	-	-	>
X5	LB50	<,=,>	=	<	<	>
	LB150	<,=,>	-	<	<	>
	FT50	<,=,>	-	-	=	>
	FT150	<,=,>	-	-	-	>

(A): Diameter. (B) Pitch.
(=): The two lysis methods were not significantly different in pitch.
(<): The first lysis method had a significantly smaller mean pitch.
(>): The first lysis method had a significantly larger mean pitch.
Mann-Whitney with Bonferroni correction (p=0.000625).
X3: NP/VP24/VP35; X330: NP/VP24/VP35/VP30; X340: NP/VP24/VP35/VP40; X5: NP/VP24/VP35/VP30/VP40; LB50: hypotonic lysis buffer; LB150: isotonic lysis buffer; FT50: hypotonic freeze/thaw; FT150: isotonic freeze/thaw; Media: cell culture media.

As such, there appears to be an "all or nothing" requirement for VP30 and VP40 in my studies (Figure 94). NP/VP24/VP35 and NP/VP24/VP35/VP30/VP40 nucleocapsid-like particles were not significantly different from each other, whereas the individual addition of VP30 or VP40 resulted in significant changes to pitch and diameter. It is interesting to speculate that VP30 may be unwinding the nucleocapsid for replication and transcription purposes and that this relaxation might be mediated by VP40. VP30 interacts with both NP and VP35, acting as a switch to trigger transcription and halt replication of the genome (Biedenkopf et al. 2013; Biedenkopf et al. 2016; Martinez et al. 2008; Modrof et al. 2002; Weik et al. 2002). It is still unclear how the large polymerase complex gains access to the encapsidated genome and my results hint that VP30 may have a role here as well (Biedenkopf et al. 2016). However, much more research is needed to give credence to this hypothesis.

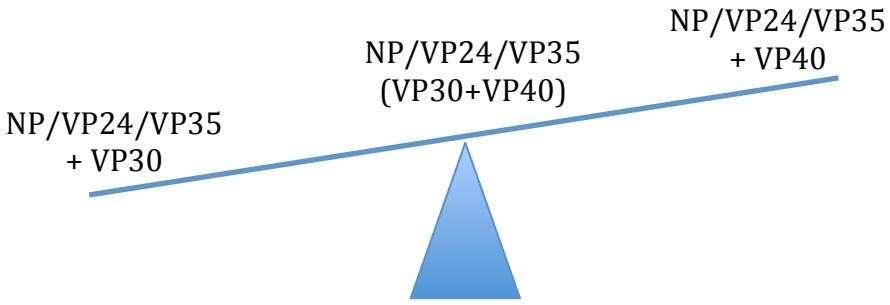

Figure 94. Maintenance of the nucleocapsid structure requires the presence or absence of both VP30 and VP40, not just one of them.

One major caveat to the above observations is that the Ebola virus probably does not continually maintain 10.81 repeats per turn across the whole virus particle. This average value was calculated from tomograms of linear virus particles and does not take into account any differences due to curvature. The nucleocapsid is a dynamic macromolecular structure that is constantly in flux within the environment. The lack of vertical connections between helical rounds enables a large degree of curvature and reduces the risk of breaks (Booth et al. 2013). However, with the diameter limited by the viral envelope and the length of the nucleocapsid limited by the RNA genome and viral envelope, it does seem likely that 10.81 is the ideal number of repeats per turn, and that the nucleocapsid would try to maintain this stable structure.

It should also be noted that while significant differences were observed in the combined data, as well as in the individual lysis method experiments, most of the observed differences were very small, often just a 1-2 nm difference on average. While the large data sets (~19500 measurements for pitch, ~13500 measurements for diameter) gives strength to my observations, the wide range of helical condensation observed suggests that there is more at play in filovirus assembly.

7.2.4 The Ebola virus nucleocapsid proteins assemble into stable, helical structures

To investigate the effect of various lysis methods on the nucleocapsid-like particles, I transfected 293T cells and subjected them to buffers, freeze/thaw, or homogenization. In addition, I also examined the effect of low and physiological salt concentrations on the nucleocapsid-like particles. When lysis buffer and freeze/thaw methods were compared, no major trends were observed. Treatment of transfected cells with isotonic lysis buffer or freeze/thaw did lead to a similar significance pattern when pitch was specifically examined, suggesting that neither lysis method was greatly affecting the assembly or formation of nucleocapsid-like particles (Table 27b).

In addition, a concentration of 50 or 150 mM NaCl did not appear to greatly affect diameter or pitch. The level of significance between hypotonic vs. isotonic lysis buffers varied depending on the protein combination, with no clear trend (Table 27). Comparison of hypotonic vs. isotonic freeze/thaw revealed a strong trend towards comparable average measurements for both diameter and pitch (Table 27). As such, it appears that 50-150 mM NaCl provides a suitable environment for the preservation of the nucleocapsid-like particles and NP-RNA coils generated in this thesis. In contrast, when isotonic NP gradient fractions were dialyzed into a buffer consisting of 5 mM Tris-HCl, 0 mM NaCl, pH 7.5, NP particles appeared to disintegrate (Figure 81b). Similar results were observed when the experiment was repeated for NP/VP24/VP35 with and without VP30 (data not shown). Previous studies have demonstrated the unwinding of NP particles when exposed to 0 mM NaCl. This phenomenon could be reversed when NP was dialyzed back to 150 mM NaCl (Noda et al. 2010). The C-terminal truncated mutant $NP_{\Delta 451\text{-}739}$ was unable to efficiently oligomerize when stored in 0 mM NaCl, whereas mutant NP stored in 150 mM NaCl

assembled into long rod-like particles (Peng et al. 2016). Therefore, like many proteins, NP conformation and protein-protein interactions appear to be dependent on salt concentration, although it is not a permanent affect (Noda et al. 2010; Peng et al. 2016) (Manuscript in preparation).

7.2.4.1 Nucleocapsid-like particles isolated from cell culture media were significantly smaller

When the effect of lysis method is compared by protein combination, the most apparent trend is that nucleocapsid-like particles isolated from cell culture media were significantly narrower and more condensed than those produced by any other method (Table 27). This was a surprising observation, especially as this trend was maintained even in the absence of VP40. All transfected proteins were detected in the VLP samples by SDS-PAGE; however, the average diameter and pitch of the nucleocapsid-like particles isolated from cell culture media more closely matched that of the proto-nucleocapsids from Chapter 3.4. As such, the most likely explanation for these smaller, narrower nucleocapsid-like particles would be that the cell culture medium contained a higher number of NP proto-nucleocapsid-like particles that were measured as nucleocapsid-like particles (Figure 53, Figure 87, Figure 88).

There are several possibilities as to why more proto-nucleocapsid-like particles were observed in the cell culture medium. First, it is possible that purification through a sucrose cushion, rather than a density gradient could be a) more or less detrimental to the overall nucleocapsid-like particle and/or b) separating the nucleocapsid-like particles differently, resulting in an altered sample of observed nucleocapsids. Option (b) seems unlikely as I have visualized nucleocapsid-like particles from fractions 2, 6, and 12 of the iodixanol gradients and observed no increase in the degree of condensation (Figure 48).

Option A is more likely as the sucrose cushion produces a pellet of VLP and cellular material, which could result in the altered particles I observed. Alternatively, the mechanism of release from the transfected cell could be related to the structural differences observed. It is possible that "natural" lysis, rather than the freeze/thaw or osmotic lysis somehow enabled greater condensation of these particles. Another explanation could be that the environment of the cell culture medium was more conducive to preserving these NP helices.

7.2.4.2 Homogenization maintained the assembly of NP rod-like particles

To investigate whether the relaxed nature of the nucleocapsid-like particles was due to the removal of the cellular environment, transfected cells were homogenized and their lysates investigated. Surprisingly, homogenization revealed highly condensed NP rod-like particles in the lysates. Based on this seemingly more efficient assembly or preservation of NP, I expected to observe tighter nucleocapsid-like particles as well, but this was not the case. It was difficult to distinguish the nucleocapsid-like particles due to debris and those that were observed were not noticeably more condensed than those observed after freeze/thaw or lysis buffer treatment (Figure 73, Figure 74). One possible explanation for this difference is the presence or absence of VP24. Analysis of homogenate lysates showed that VP24 did not consistently travel through the iodixanol gradients (Figure 72c-e). Adding 1% NP-40 to the homogenate lysates led to a greater detection of VP24 by SDS-PAGE (data not shown). With its lipophilic tendencies, it is possible that VP24 was dissociating from the nucleocapsid-like particles and/or associating more with cellular membranes, resulting in the reduced number of particles observed when NP-40 was not utilized during homogenization (Han et al. 2003).

In addition to the homogenization of regularly transfected cells, staggered transfections were also exposed to this method of lysis. Transfection of NP alone or in combination with VP35 or VP40 followed by a 2 or 6 hour incubation and subsequent transfection with VP24 and/or VP35 also resulted in a high number of rod-like NP particles, but few nucleocapsid-like particles (Figure 85). A diameter range of 18-41 nm was measured for these rod-like particles, with an average of ~29 nm (Figure 86). The pitch of these proto-nucleocapsid-like particles ranged from 3-20 nm, with an average of ~8 nm (Figure 86). Statistically, these particles were similar in diameter to the proto-nucleocapsids measured by ImageJ, but had a significantly larger pitch.

Staggered transfections were investigated as a means to mimic the temporal regulation of the Ebola virus genome. In Ebola virus infected cells, NP and VP35 can be detected together by 6 hours post-infection, while VP24 is not detected until 18 hours post infection (Nanbo et al. 2013). While staggered transfections can mimic this temporal expression, the relative levels of protein expression cannot be accurately controlled using the single plasmid transfection system. Thus, it is possible that the relative levels of NP protein were not matched by the later expression of VP24 and VP35. The 1:1 stoichiometry of nucleocapsid-associated proteins supported by this thesis suggests that an equal amount of NP, VP24, and VP35 must be present for the assembly of the nucleocapsid (Figure 46). It is also not clear why homogenization, but not freeze/thaw or lysis buffer treatment enabled the higher production of the proto-nucleocapsid-like NP particles, as discussed in Section 7.2.4.1.

7.2.4.3 Addition of $MgCl_2$ and KCl inhibited nucleocapsid-like particle assembly

To observe whether the lack of divalent ions was preventing proper assembly due to the chelating effect of EDTA, I added $MgCl_2$ and KCl to my isotonic lysis buffer (Nyborg and Peersen 2004). Nucleocapsid-associated proteins did migrate through the density gradient, although less protein was detected at fractions 5-7 (Figure 75, Figure 76). While promising, TEM of the purified fractions found little to no evidence of nucleocapsid-like particles (Figure 77). It is unlikely that the presence of EDTA affected the nucleocapsid-like particles as both my freeze/thaw and homogenization experiments were performed in its absence, and no major differences in structure were observed. The reason why $MgCl_2$ and KCl seem to have prevented the assembly of the nucleocapsid-like particles is less clear. It is possible that the concentration of KCl (10 mM) was inhibitory and that a lower concentration would be more beneficial. While the same could be true for the $MgCl_2$ concentration (1.5 mM), it was within the range of 1-2 mM $MgCl_2$ used within many buffers.

7.2.4.4 Exposure to low pH inhibited NP and nucleocapsid-like particle assembly

The nucleoprotein (N) of VSV was recently shown to require an effector to promote condensation into its characteristic bullet shape (Desfosses et al. 2013). This effector could be the direct interaction between matrix and N proteins or exposure of the N protein to low pH, suggesting that a conformational change is required for efficient assembly of VSV N (Desfosses et al. 2013; Iseni et al. 1998). As another member of the *Mononegavirales*, it is possible that Ebola virus NP also requires a conformational change for efficient assembly. To determine if Ebola virus nucleocapsid proteins could also be manipulated by low pH, 293T cells were transfected and lysates were a) run through a neutral pH gradient or b) run through a pH 5 gradient. In addition, fractions 6 and 7 from the neutral gradient were

dialyzed into pH 5 PBS. In contrast to VSV N, Ebola virus NP alone or in combination with VP24, VP35, and VP30 did not self-assemble when exposed to low pH. Rather, a pH of 5 was detrimental to assembly, with few particles visible after purification through a low pH gradient (Figure 79, Figure 82). Furthermore, nucleocapsid-like particles present in the neutral gradient were disintegrated when dialyzed into low pH (Figure 81).

Exposure of the NP-RNA of the mumps paramxyovirus to a pH of 5 or lower led to the loss of RNA, but did not appear to affect NP oligomerization (Cox et al. 2009). Mumps virus NP samples that were resolubilized from low to neutral pH still formed NP ring-like structures (Cox et al. 2009). In contrast, treatment of Ebola virus $NP_{\Delta 451\text{-}739}$ with RNase, followed by sonication, prevented the re-oligomerization of NP, as did treatment with RNase at 0 mM NaCl followed by dialysis into 150 mM NaCl (Noda et al. 2010; Peng et al. 2016). The loss of RNA due to low pH makes it unlikely that the resolubilization of Ebola virus NP would result in the formation of NP particles. Thus, while some sequence and functional similarities between rhabdovirus, paramxyovirus, and filovirus NP are observed, the dependence of Ebola virus NP on the presence of RNA for nucleocapsid assembly differentiates it from the other *Mononegavirales* (Barr et al. 1991; Sanchez et al. 1989; Sanchez et al. 1992). It is interesting to note that filoviruses enter the cell through receptor-mediated endocytosis and must escape from the endosome for productive infection to occur (Aleksandrowicz et al. 2011; Nanbo et al. 2010; Saeed et al. 2010). Inhibition of NPC1, the key filovirus receptor within the endosome, prevents envelope-endosome membrane fusion and subsequent nucleocapsid uncoating into the cytoplasm (Carette et al. 2011; Cote et al. 2011; Miller et al. 2012). The sensitivity of the nucleocapsid-like

particles to a pH close to endosomal levels demonstrates the importance of rapid viral escape before degradation can occur.

7.2.4.5 Neither the fixation of nucleocapsid-like particles during ultracentrifugation nor the fixation of intact cells could enhance the degree of particle condensation

Lastly, I investigated whether fixation could stabilize the nucleocapsid-like particles. To determine if the nucleocapsid-like particles were unwinding during ultracentrifugation, I added 0.15% glutaraldehyde to either the 15%, or both the 15% and 30% iodixanol layers. This "Grafix" method has been demonstrated to stabilize and maintain other protein complexes during density gradient purification (Goringer et al. 2011; Kastner et al. 2008; Stark 2010). Nucleocapsid-like particles observed from Grafix gradients were not perceivably more condensed than untreated gradients, suggesting that the relaxed nature of the particles is not due to ultracentrifugation (Figure 64). Visualization of cell lysates and nucleocapsid-like particles direct from iodixanol fractions supports this conclusion, as particles observed from these solutions were also less condensed than the native Ebola virus nucleocapsid particle (Figure 62). Based on these results and my transfected cell section observations, I next investigated the fixation of intact cells. I fixed live transfected cells with three different chemical cross-linkers with a range of cross-linking distances and examined the nucleocapsid-like particles produced from each. Regardless of the cross-linker arm size, NP-RNA from lysed, fixed cells still displayed a relaxed helical particle, as compared to the proto-nucleocapsids (Figure 67). The smeared bands of fixed cell lysates and gradient fractions when analyzed by SDS-PAGE demonstrated that some cross-linking between proteins did occur (Figure 66). Treatment with 2% PFA appeared to lead to the greatest level of crosslinking, as hardly any protein was evident in the density gradient

fractions. While this result suggests that nucleocapsid-associated protein interactions occur at ~2.3-2.7 Å, it is more likely that PFA treatment led to the mass aggregation of all cellular protein which were then removed during clarification and therefore not sampled. Visualization of nucleocapsid-like particles from fixed intact cells did not demonstrate an increase in condensation (Figure 68). However, on further thought, this is perhaps not surprising. The cross-linker spacer distances of 16.1, 11.4, and 2.3-2.7 Å are too short to span the distance between helical rounds of the native Ebola virus nucleocapsid (~7 nm; 70 Å) and more pointedly, too short for the nucleocapsid-like particles with a pitch ranging on average from 10-15 nm (100-150 Å). Thus, it is still unclear whether the nucleocapsid-like particles visualized within cell sections are more or less condensed than the purified nucleocapsid-like particles. This experiment could be repeated with cross-linker that does have a larger spacer distance, such as SM(PEG)24 with a arm length of 9.52 nm which covalently links amino and sulfhydryl groups (ThermoFisher Scientific, Cat #22114).

7.2.5 Summary

When taken altogether, the data presented in this thesis indicates that the assembly of the Ebola virus nucleocapsid is not a simple process. Numerous viral components must come together to generate the most complex nucleocapsid of the *Mononegavirales* (Booth et al. 2013). Interactions between NP-RNA and NP-NP are required for the formation of the inner nucleocapsid layer (Beniac et al. 2012; Bharat et al. 2012; Noda et al. 2010). I have shown that full-length NP is capable of self-assembly, an observation that has only ever been previously shown with a C terminal truncated mutant or in the presence of VP40. I am also the first to demonstrate a strong interaction between Ebola virus NP, VP24, and VP35,

which was maintained during the migration of the nucleocapsid-like particles through an iodixanol density gradient. In agreement with the theorized location of VP30 within the inner NP-RNA layer, I identified a strong interaction between NP and VP30 that was maintained during ultracentrifugation. These four proteins, in addition to the low copy number L protein must all come together to assemble the nucleocapsid. The densitometry of the gradient protein bands indicates a 1:1 stoichiometry of NP, VP24, VP35, and VP30 within the nucleocapsid, in agreement with the 19Å reconstruction of the Ebola virus nucleocapsid by Beniac et al. (2012) (Figure 2). Both VP24 and VP35 were required for the efficient assembly of the double-layered nucleocapsid-like particles and can therefore be considered the major contributors to nucleocapsid condensation. A second condensation event mediated by VP40 may occur during the budding process, as I noted tightly coiled nucleocapsid-like particles within VLPs and more consistent diameter and pitch measurements when VP40 was present in the nucleocapsid-like particles (Figure 88, Figure 89). In addition, the mechanism behind assembly and condensation is still unknown. Whether it requires the seeding of an NP-RNA rod-like particle to begin assembly or the simultaneous assembly of all proteins around the RNA is unclear. Speculatively, my data supports the latter explanation, as there seemed to be an inverse relationship between NP-RNA rod-like particles and full nucleocapsid-like particles in my studies; however, much more research is required.

Although assembly of the Ebola virus nucleocapsid is not simple, my data does illustrate the stability of these particles. Only extreme conditions such as low pH and 0mM NaCl were able to fully disrupt the structure of the nucleocapsid-like particles. Lysis by various buffers, 3 cycles of freeze/thaw, or homogenization were not able to change the

overall integrity of these particles, although pitch and diameters were affected in small, but significant ways. The nucleocapsid-like particles were also resistant to detergent treatment and hypotonic conditions (50 mM NaCl). Furthermore, the method of purification had no detrimental effects on the overall structural organization, as nucleocapsid-like particles observed in lysates appeared no different than those after ultracentrifugation. Preservation of nucleocapsid-like particles in a thin layer of ice did not reveal any significant changes to condensation or diameter overall, although again small, significant differences where observed when compared to specific lysis methods prepared by negative stain. In brief, my novel nucleocapsid-like particles maintained an extremely stable, helical particle that was on average 32-36 nm in diameter and 10-13 nm in pitch, suggesting that these structures are self-assembling into a low energy state.

7.2.6 Limitations and opportunities

7.2.6.1 Limitations of ImageJ

ImageJ is a useful program for measuring any structure present in an electron micrograph. My measurement of 29.67±2.93 nm for an average diameter of the proto-nucleocapsids was close to the 30.5 nm diameter calculated after single particle image analysis. A chi-square test of this data gives a probability of 0.83, which suggests that these two values are not significantly different. This is reassuring as ImageJ does involve some user bias in which particles are selected and measured, as well as defining what constitutes the middle of a helical round for pitch measurements and what constitutes the end of a helical round for measuring diameter. In addition, poor image quality can hamper accurate measurements. Negative stain is a rapid technique for imaging macromolecular structures,

but does not provide the most consistent results, unlike cryo-preservation. As a result of uneven drying and staining, some nucleocapsid-like particles appeared more clearly than others. In addition, reagents such as iodixanol or the detergent NP-40 can affect negative staining, making imaging more difficult and reducing the quality of the electron micrographs. To the best of my abilities, the same selection and measurement parameters for each nucleocapsid-like particle were used, but as evident by my statistical analyses, high variability in structure still occurred.

7.2.6.2 Single particle image analysis

Single particle image analysis is limited by the requirement for homogeneous 3D structures (Cope et al. 2011; Frank 2002). This thesis project encompassed both extremes of this requirement. The highly stable, symmetrical, and abundant proto-nucleocapsid particles were easily imaged and analyzed to generate an 18.5 Å model of these novel particles (Figure 10). In contrast, I generated nucleocapsid-like particles that were highly dynamic with a wide range of compaction. Preliminary single particle image analysis indicated that the particles were not highly ordered (Figure 69, Figure 70). The nucleocapsid-like particle class averages had low contrast and were relatively undefined even when 500-1000 images were included in the analyses. As such, the use of single particle image analysis was limited to the proto-nucleocapsid study. Furthermore, the low concentration of the nucleocapsid-like particles made it difficult to carry out cryo-ET image analysis.

7.3 Major Findings

In this thesis I have demonstrated that the inner helix of the Ebola virus nucleocapsid consists of NP-RNA. I have also confirmed that VP24, together with VP35 are the major components of the outer layer of the Ebola virus nucleocapsid. Furthermore, I am the first to isolate and characterize envelope-free Ebola virus nucleocapsid-like particles consisting of NP, VP24, and VP35. I demonstrated that VP30 is attached to the nucleocapsid-like particles with high affinity and a 1:1 stoichiometry. Simultaneous expression of NP, VP24, VP35, VP30, and VP40 and subsequent co-migration through an iodixanol density gradient indicated a specific interaction between all five proteins. Furthermore, nucleocapsid-like structures generated by the co-expression of VP40 with NP, VP24, and VP35 had the smallest average pitch, which raises the possibility that further condensation (mediated by VP40) occurs during the budding process. Whereas previously, research has shown an interaction between VP40-VLPs and VP35, I have shown a strong interaction with the nucleocapsid-like particles and VP40. When taken together, these two results provide a strong indication that the VP35-VP40 interaction is critical for encapsidation of the Ebola virus nucleocapsid. Lastly, I have convincingly shown that the Ebola virus nucleocapsid-associated proteins assemble into a consistent structural organization that exhibits a wide range of helical condensation. These particles were stable enough to maintain their overall integrity throughout a variety of conditions, suggesting that they are a low energy state structure. In summary, this thesis has shown that the formation of the Ebola virus nucleocapsid is not simple self-assembly, but rather a complex, coordinated process that we still do not fully understand.

7.4 Future Directions

This thesis focused on external conditions in an attempt to produce condensed nucleocapsid-like particles; however, there are a number of alternative experiments that should be investigated for their effects as well.

1. The Ebola virus nucleocapsid-associated proteins may require additional signals to produce more compacted particles. While both NP and VP35 interact with VP40 and can be incorporated into VLPs, VP35 appears to be responsible for the specific encapsidation of viral RNA (Johnson et al. 2006b). While *Mononegavirales* are well known for their nonspecific encapsidation of cellular RNA, further condensation of the complex Ebola virus nucleocapsid may require specific RNA signals/sequences due to the selectivity of VP35 (Booth et al. 2013; Johnson et al. 2006b). Most research on packaging signals has been concentrated on generating infectious minigenome assays, without the differentiation of what sequences within the 3' and 5' UTRs are necessary for assembly and budding. I recommend the following:
    a. Generation of nucleocapsid-like particles in combination with a minigenome assay and analyzing these particles to determine if the presence of viral RNA is sufficient to induce greater condensation
    b. Generation of nucleocapsid-like particles in combination with specific 3' and 5' Ebola virus RNA genome sequences and truncated sequences to determine whether one might lead to more efficient packaging than the other
    c. Isolation of the cellular RNA that is currently being packaged by the nucleocapsid-like particles to investigate any similarities in sequence or length.

2. It is also possible that the spectrum of condensation observed within this thesis is more biologically relevant than image analysis has led us to believe. Single particle image analysis performed on native Ebola is currently limited to relatively straight regions of the virus in order to perform effective helical analysis (Beniac et al. 2012). Thus, our knowledge of the Ebola virus nucleocapsid is biased towards this idea of a straight, rigid structure. In a review by Booth et al. (2013) some of this bias is dispelled by a model of how the nucleocapsid is constructed such that it can withstand up to 360° movement. Filovirus particles have been observed curved into spherical particles, bent in half to form checkmark shapes, or semi-curved to form comma-shaped particles. The double-layered nucleocapsid contains no vertical connections between its outer VP24-VP35 layer, allowing the structure to condense or expand when necessary within those particles. The nucleocapsid is likely further stabilized by quasi-equivalent interactions between the outer layer and the VP40 matrix lattice (Beniac et al. 2012; Booth et al. 2013). My data showing that VP35 is required for VP40 association with the nucleocapsid-like particles suggests that these two proteins are the major contributors to these quasi-equivalent interactions. While this model agrees with previously published 3D structural data, no high-resolution reconstructions of bent nucleocapsids have been generated. Towards the end of this thesis I attempted to generate a curved nucleocapsid tomogram; however, data was not sufficient to distinguish individual helical rounds, only the overall orientation within the envelope was visible (Figure 3). As such, the range of condensation in the native virus is still unclear and may in fact be more similar to the pitch of some of the isolated nucleocapsid-like particles. Tomographic

image analysis of bent or curved nucleocapsids would be beneficial to confirm the Booth et al. (2013) model and support the biological relevance of the nucleocapsid-like particles.

3. The unregulated expression of the nucleocapsid genes could have produced an inappropriate ratio of proteins, resulting in the inefficient assembly of the nucleocapsid-like particles. Temporal regulation of gene expression should be investigated, since correct assembly of the nucleocapsid may require translation and assembly of protein molecules in a certain order. A multi-cistronic minigenome, such as the one designed by Watt et al. (2014) could be useful for this study.
4. The use of a single plasmid expression system could also have had an effect on the folding or post-translational modifications of the nucleocapsid proteins. Overexpression could have exhausted the number of chaperones needed for proper folding or the cell stores of phosphates, ubiquitin, etc. I expect that regulated protein expression would also reduce these unintended effects of transfection.
5. Cross-linking of intact cells is more generally used for mass spectrometry analysis of protein-protein interactions. This technique is able to identify the specific amino acid interactions between two proteins. As such, I recommend using this technique to investigate the specific interactions between the nucleocapsid-associated proteins. Most of the binding sites between these proteins, especially pertaining to their location within the nucleocapsid are still unknown (Leitner et al. 2014).
6. My research demonstrated that full-length NP can form rod-like helical particles in the absence of VP40, but also demonstrated that the presence of VP40 did lead to small, but significant reductions in the pitch of nucleocapsid-like particles. In

addition, condensed nucleocapsid-like particles were observed within VLPs by ourselves and others (Bharat et al. 2012). VP40 has two relatively well-defined and separate domains, which have been studied in terms of viral transcription/replication and matrix formation (Bornholdt et al. 2013; Gomis-Ruth et al. 2003). It would be interesting to study whether nucleocapsid-like particle assembly and/or condensation would be affected by the deletion or truncation of one of these domains or by modifying the levels of VP40 octamers, dimers, and/or hexamers. Furthermore, the mechanism behind the ability of VP40 to reduce particle pitch should be investigated.

7. Although this study attempted immunogold labeling of purified nucleocapsid-like particles I did not have success with the antibodies that were available (data not shown). As such, additional antibodies could be produced in order to confirm the location of VP30, VP24, and VP35. IEM of resin-embedded proto-nucleocapsids or whole virus could also be attempted to differentiate protein location (Bharat et al. 2011; Welsch et al. 2010).
8. The successful purification of nucleocapsid-like particles provides a basis for future studies into nucleocapsid assembly inhibitors. Instead of requiring costly BSL 4 experiments to first identify these anti-assembly agents, these small molecules could be added to transfected cells and their effect on assembly evaluated by my purification method. Once identified, these small molecule inhibitors could be evaluated on live virus. Similar assembly inhibitors have already been developed for hepatitis B virus (HBV) and dengue virus. In the case of HBV, heteroaryldihydropyrimidines (HAPs) interacting with the capsid protein lead to

the misassembly of viral core particles, where viral DNA replication occurs. As a result, *in vitro* and *in vivo* studies demonstrated a reduction in viral replication (Deres et al. 2003). The small molecule inhibitor ST-148 has been shown to target the dengue virus capsid protein, resulting in capsid stabilization, self-interaction, and reduced dengue virus replication (Byrd et al. 2013; Scaturro et al. 2014). Although both of these viruses express multiple copies of one capsid protein for assembly, the same underlying theory should hold true for filoviruses. Filovirus NP is the most attractive target as it both protects the genomic RNA and acts as a scaffold for VP24 and VP35. Inhibition of NP-RNA interactions similar to the HAPS mode of action or the promotion of NP self-aggregation similar to ST-148 mode of action are both attractive avenues of antiviral research.

Chapter 8. References

Anonymous. Ebola haemorrhagic fever in Sudan, 1976. Report of a WHO/International Study Team. *Bull. World Health Organ.* **56**, 247-270 (1978a).

Anonymous. Ebola haemorrhagic fever in Zaire, 1976. *Bull. World Health Organ.* **56**, 271-293 (1978b).

Abramoff, M. D., Magelhaes, P. J. & Ram, S. J. Image Processing with ImageJ. *Biophotonics International* **11**, 36-42 (2004).

Adrian, M., Dubochet, J., Lepault, J. & McDowall, A. W. Cryo-electron microscopy of viruses. *Nature* **308**, 32-36 (1984).

Adu-Gyamfi, E. *et al*. The Ebola virus matrix protein penetrates into the plasma membrane: A key step in VP40 oligomerization and viral egress. *J. Biol. Chem.* (2013).

Aleksandrowicz, P. *et al*. Ebola virus enters host cells by macropinocytosis and clathrin-mediated endocytosis. *J. Infect. Dis.* **204 Suppl 3**, S957-67 (2011).

Alvarez, C. P. *et al*. C-type lectins DC-SIGN and L-SIGN mediate cellular entry by Ebola virus in cis and in trans. *J. Virol.* **76**, 6841-6844 (2002).

Amman, B. R. *et al*. Seasonal pulses of Marburg virus circulation in juvenile Rousettus aegyptiacus bats coincide with periods of increased risk of human infection. *PLoS Pathog.* **8**, e1002877 (2012).

Amman, B. R. *et al*. Oral shedding of marburg virus in experimentally infected egyptian fruit bats (rousettus aegyptiacus). *J. Wildl. Dis.* **51**, 113-124 (2015).

Baize, S. *et al*. Defective humoral responses and extensive intravascular apoptosis are associated with fatal outcome in Ebola virus-infected patients. *Nat. Med.* **5**, 423-426 (1999).

Baize, S. *et al*. Inflammatory responses in Ebola virus-infected patients. *Clin. Exp. Immunol.* **128**, 163-168 (2002).

Baize, S. *et al*. Emergence of Zaire Ebola virus disease in Guinea. *N. Engl. J. Med.* **371**, 1418-1425 (2014).

Baker, T. S., Olson, N. H. & Fuller, S. D. Adding the third dimension to virus life cycles: three-dimensional reconstruction of icosahedral viruses from cryo-electron micrographs. *Microbiol. Mol. Biol. Rev.* **63**, 862-922, (1999).

Bamberg, S., Kolesnikova, L., Moller, P., Klenk, H. D. & Becker, S. VP24 of Marburg virus influences formation of infectious particles. *J. Virol.* **79**, 13421-13433 (2005).

Barr, J., Chambers, P., Pringle, C. R. & Easton, A. J. Sequence of the major nucleocapsid protein gene of pneumonia virus of mice: sequence comparisons suggest structural homology between nucleocapsid proteins of pneumoviruses, paramyxoviruses, rhabdoviruses and filoviruses. *J. Gen. Virol.* **72 (Pt 3)**, 677-685 (1991).

Barrette, R. W. *et al*. Discovery of swine as a host for the Reston ebolavirus. *Science* **325**, 204-206 (2009).

Baskerville, A., Fisher-Hoch, S. P., Neild, G. H. & Dowsett, A. B. Ultrastructural pathology of experimental Ebola haemorrhagic fever virus infection. *J. Pathol.* **147**, 199-209 (1985).

Basler, C. F. *et al*. The Ebola virus VP35 protein functions as a type I IFN antagonist. *Proc. Natl. Acad. Sci. U. S. A.* **97**, 12289-12294 (2000).

Basler, C. F. *et al*. The Ebola virus VP35 protein inhibits activation of interferon regulatory factor 3. *J. Virol.* **77**, 7945-7956 (2003).

Bausch, D. G. *et al*. Risk factors for Marburg hemorrhagic fever, Democratic Republic of the Congo. *Emerg. Infect. Dis.* **9**, 1531-1537 (2003).

Bausch, D. G. *et al*. Assessment of the risk of Ebola virus transmission from bodily fluids and fomites. *J. Infect. Dis.* **196 Suppl 2**, S142-7 (2007).

Becker, S., Spiess, M. & Klenk, H. D. The asialoglycoprotein receptor is a potential liver-specific receptor for Marburg virus. *J. Gen. Virol.* **76 (Pt 2)**, 393-399 (1995).

Becker, S., Rinne, C., Hofsass, U., Klenk, H. D. & Muhlberger, E. Interactions of Marburg virus nucleocapsid proteins. *Virology* **249**, 406-417 (1998).

Becquart, P. *et al*. High prevalence of both humoral and cellular immunity to Zaire ebolavirus among rural populations in Gabon. *PLoS One* **5**, e9126 (2010).

Beniac, D. R. *et al*. The organisation of Ebola virus reveals a capacity for extensive, modular polyploidy. *PLoS One* **7**, e29608 (2012).

Bharat, T. A. *et al*. Cryo-electron tomography of Marburg virus particles and their morphogenesis within infected cells. *PLoS Biol.* **9**, e1001196 (2011).

Bharat, T. A. *et al*. Structural dissection of Ebola virus and its assembly determinants using cryo-electron tomography. *Proc. Natl. Acad. Sci. U. S. A.* **109**, 4275-4280 (2012).

Biedenkopf, N., Hartlieb, B., Hoenen, T. & Becker, S. Phosphorylation of Ebola virus VP30 influences the composition of the viral nucleocapsid complex: Impact on viral transcription and replication. *J. Biol. Chem.* (2013).

Biedenkopf, N., Lier, C. & Becker, S. Dynamic Phosphorylation of VP30 is essential for Ebola virus life cycle. *J. Virol.* (2016).

Boekema, E. J., Folea, M. & Kouril, R. Single particle electron microscopy. *Photosynth Res.* **102**, 189-196 (2009).

Booth, T. F., Rabb, M. J. & Beniac, D. R. How do filovirus filaments bend without breaking? *Trends Microbiol.* **21**, 583-593 (2013).

Bornholdt, Z. A. *et al*. Structural rearrangement of ebola virus VP40 begets multiple functions in the virus life cycle. *Cell* **154**, 763-774 (2013).

Bosio, C. M. *et al*. Ebola and Marburg viruses replicate in monocyte-derived dendritic cells without inducing the production of cytokines and full maturation. *J. Infect. Dis.* **188**, 1630-1638 (2003).

Busico, K. M. *et al*. Prevalence of IgG antibodies to Ebola virus in individuals during an Ebola outbreak, Democratic Republic of the Congo, 1995. *J. Infect. Dis.* **179 Suppl 1**, S102-7 (1999).

Byrd, C. M. *et al*. A novel inhibitor of dengue virus replication that targets the capsid protein. *Antimicrob. Agents Chemother.* **57**, 15-25 (2013).

Cardenas, W. B. *et al*. Ebola virus VP35 protein binds double-stranded RNA and inhibits alpha/beta interferon production induced by RIG-I signaling. *J. Virol.* **80**, 5168-5178 (2006).

Carette, J. E. *et al*. Ebola virus entry requires the cholesterol transporter Niemann-Pick C1. *Nature* **477**, 340-343 (2011).

Caspar, D. L. D., and Klug, A. Physical principles in the construction of regular viruses. *Cold Spring Harb. Symp. Quant. Biol.* **27,** 1-24 (1962).

Centers for Disease Control and Prevention (CDC). Imported case of Marburg hemorrhagic fever - Colorado, 2008. *MMWR Morb. Mortal. Wkly. Rep.* **58**, 1377-1381 (2009).

Chandran, K., Sullivan, N. J., Felbor, U., Whelan, S. P. & Cunningham, J. M. Endosomal proteolysis of the Ebola virus glycoprotein is necessary for infection. *Science* **308**, 1643-1645 (2005).

Chang, T. H. *et al*. Ebola Zaire virus blocks type I interferon production by exploiting the host SUMO modification machinery. *PLoS Pathog.* **5**, e1000493 (2009).

Cope, J., Gilbert, S., Rayment, I., Mastronarde, D. & Hoenger, A. Cryo-electron tomography of microtubule-kinesin motor complexes. *J. Struct. Biol.* **170**, 257-265 (2010).

Cope, J., Heumann, J. & Hoenger, A. Cryo-electron tomography for structural characterization of macromolecular complexes. *Curr. Protoc. Protein Sci.* **Chapter 17**, Unit17.13 (2011).

Coronel, E. C., Murti, K. G., Takimoto, T. & Portner, A. Human parainfluenza virus type 1 matrix and nucleoprotein genes transiently expressed in mammalian cells induce the release of virus-like particles containing nucleocapsid-like structures. *J. Virol.* **73**, 7035-7038 (1999).

Coronel, E. C., Takimoto, T., Murti, K. G., Varich, N. & Portner, A. Nucleocapsid incorporation into parainfluenza virus is regulated by specific interaction with matrix protein. *J. Virol.* **75**, 1117-1123 (2001).

Cote, M. *et al*. Small molecule inhibitors reveal Niemann-Pick C1 is essential for Ebola virus infection. *Nature* **477**, 344-348 (2011).

Cox, N. J., McCormick, J. B., Johnson, K. M. & Kiley, M. P. Evidence for two subtypes of Ebola virus based on oligonucleotide mapping of RNA. *J. Infect. Dis.* **147**, 272-275 (1983).

Cox, R. *et al*. Characterization of a mumps virus nucleocapsid-like particle. *J. Virol.* **83**, 11402-11406 (2009).

Curran, J. A role for the Sendai virus P protein trimer in RNA synthesis. *J. Virol.* **72**, 4274-4280 (1998).

Curry, A., Appleton, H. & Dowsett, B. Application of transmission electron microscopy to the clinical study of viral and bacterial infections: present and future. *Micron* **37**, 91-106 (2006).

De Rosier, D. J. & Klug, A. Reconstruction of three dimensional structures from electron micrographs. *Nature* **217**, 130-134 (1968).

De Santis, O. *et al*. Safety and immunogenicity of a chimpanzee adenovirus-vectored Ebola vaccine in healthy adults: a randomised, double-blind, placebo-controlled, dose-finding, phase 1/2a study. *Lancet Infect. Dis.* **16**, 311-320 (2016).

Deres, K. *et al*. Inhibition of hepatitis B virus replication by drug-induced depletion of nucleocapsids. *Science* **299**, 893-896 (2003).

Desfosses, A. *et al*. Self-organization of the vesicular stomatitis virus nucleocapsid into a bullet shape. *Nat. Commun.* **4**, 1429 (2013).

Dessen, A., Volchkov, V., Dolnik, O., Klenk, H. D. & Weissenhorn, W. Crystal structure of the matrix protein VP40 from Ebola virus. *EMBO J.* **19**, 4228-4236 (2000).

DiCarlo, A., Moller, P., Lander, A., Kolesnikova, L. & Becker, S. Nucleocapsid formation and RNA synthesis of Marburg virus is dependent on two coiled coil motifs in the nucleoprotein. *Virol. J.* **4**, 105 (2007).

Dong, S. *et al*. Insight into the Ebola virus nucleocapsid assembly mechanism: crystal structure of Ebola virus nucleoprotein core domain at 1.8 A resolution. *Protein Cell.* **6**, 351-362 (2015).

Dube, D. *et al*. The primed ebolavirus glycoprotein (19-kilodalton GP1,2): sequence and residues critical for host cell binding. *J. Virol.* **83**, 2883-2891 (2009).

Dziubanska, P. J., Derewenda, U., Ellena, J. F., Engel, D. A. & Derewenda, Z. S. The structure of the C-terminal domain of the Zaire ebolavirus nucleoprotein. *Acta Crystallogr. D Biol. Crystallogr.* **70**, 2420-2429 (2014).

Ebihara, H. *et al*. Molecular determinants of Ebola virus virulence in mice. *PLoS Pathog.* **2**, e73 (2006).

Egelman, E. H. A robust algorithm for the reconstruction of helical filaments using single-particle methods. *Ultramicroscopy* **85**, 225-234 (2000).

Egelman, E. H. The iterative helical real space reconstruction method: surmounting the problems posed by real polymers. *J. Struct. Biol.* **157**, 83-94 (2007).
Elliott, L. H., Kiley, M. P. & McCormick, J. B. Descriptive analysis of Ebola virus proteins. *Virology* **147**, 169-176 (1985).

Enterlein, S. *et al*. Rescue of recombinant Marburg virus from cDNA is dependent on nucleocapsid protein VP30. *J. Virol.* **80**, 1038-1043 (2006).

Feldmann, H., Klenk, H. D. & Sanchez, A. Molecular biology and evolution of filoviruses. *Arch. Virol. Suppl.* **7**, 81-100 (1993).

Feldmann, H., Jones, S., Klenk, H. D. & Schnittler, H. J. Ebola virus: from discovery to vaccine. *Nat. Rev. Immunol.* **3**, 677-685 (2003).

Flint, S.J., Enquist, L.W., Racaniello, V.R., and Skalka, A.M. Principles of virology: molecular biology, pathogenesis, and control of animal viruses. Second edition. ASM Press, Washington, DC. (2004).

Frank, J. *et al*. SPIDER and WEB: processing and visualization of images in 3D electron microscopy and related fields. *J. Struct. Biol.* **116**, 190-199 (1996).

Frank, J. Single-particle imaging of macromolecules by cryo-electron microscopy. *Annu. Rev. Biophys. Biomol. Struct.* **31**, 303-319 (2002).

Geisbert, T. W. *et al*. Mechanisms underlying coagulation abnormalities in ebola hemorrhagic fever: overexpression of tissue factor in primate monocytes/macrophages is a key event. *J. Infect. Dis.* **188**, 1618-1629 (2003a).

Geisbert, T. W. *et al*. Pathogenesis of Ebola hemorrhagic fever in cynomolgus macaques: evidence that dendritic cells are early and sustained targets of infection. *Am. J. Pathol.* **163**, 2347-2370 (2003b).

Gentile, M. & Gelderblom, H. R. Electron microscopy in rapid viral diagnosis: an update. *New Microbiol.* **37**, 403-422 (2014).

Gerszten, R. E. *et al*. MCP-1 and IL-8 trigger firm adhesion of monocytes to vascular endothelium under flow conditions. *Nature* **398**, 718-723 (1999).

Gomis-Ruth, F. X. *et al*. The matrix protein VP40 from Ebola virus octamerizes into pore-like structures with specific RNA binding properties. *Structure* **11**, 423-433 (2003).

Gonzalez, J. P., Nakoune, E., Slenczka, W., Vidal, P. & Morvan, J. M. Ebola and Marburg virus antibody prevalence in selected populations of the Central African Republic. *Microbes Infect.* **2**, 39-44 (2000).

Goringer, H. U., Stark, H., Bohm, C., Sander, B. & Golas, M. M. Three-dimensional reconstruction of Trypanosoma brucei editosomes using single-particle electron microscopy. *Methods Mol. Biol.* **718**, 3-22 (2011).

Gupta, M., Mahanty, S., Ahmed, R. & Rollin, P. E. Monocyte-derived human macrophages and peripheral blood mononuclear cells infected with ebola virus secrete MIP-1alpha and TNF-alpha and inhibit poly-IC-induced IFN-alpha in vitro. *Virology* **284**, 20-25 (2001a).

Gupta, M., Mahanty, S., Bray, M., Ahmed, R. & Rollin, P. E. Passive transfer of antibodies protects immunocompetent and imunodeficient mice against lethal Ebola virus infection without complete inhibition of viral replication. *J. Virol.* **75**, 4649-4654 (2001b).

Haasnoot, J. *et al*. The Ebola virus VP35 protein is a suppressor of RNA silencing. *PLoS Pathog.* **3**, e86 (2007).

Halfmann, P. *et al*. Generation of biologically contained Ebola viruses. *Proc. Natl. Acad. Sci. U. S. A.* **105**, 1129-1133 (2008).

Han, Z. *et al*. Biochemical and functional characterization of the Ebola virus VP24 protein: implications for a role in virus assembly and budding. *J. Virol.* **77**, 1793-1800 (2003).

Hartlieb, B., Modrof, J., Muhlberger, E., Klenk, H. D. & Becker, S. Oligomerization of Ebola virus VP30 is essential for viral transcription and can be inhibited by a synthetic peptide. *J. Biol. Chem.* **278**, 41830-41836 (2003).

Hartlieb, B., Muziol, T., Weissenhorn, W. & Becker, S. Crystal structure of the C-terminal domain of Ebola virus VP30 reveals a role in transcription and nucleocapsid association. *Proc. Natl. Acad. Sci. U. S. A.* **104**, 624-629 (2007).

Hartman, A. L., Towner, J. S. & Nichol, S. T. A C-terminal basic amino acid motif of Zaire ebolavirus VP35 is essential for type I interferon antagonism and displays high identity with the RNA-binding domain of another interferon antagonist, the NS1 protein of influenza A virus. *Virology* **328**, 177-184 (2004).

Hartman, A. L., Dover, J. E., Towner, J. S. & Nichol, S. T. Reverse genetic generation of recombinant Zaire Ebola viruses containing disrupted IRF-3 inhibitory domains results in attenuated virus growth in vitro and higher levels of IRF-3 activation without inhibiting viral transcription or replication. *J. Virol.* **80**, 6430-6440 (2006).

Hartman, A. L. *et al*. Inhibition of IRF-3 activation by VP35 is critical for the high level of virulence of ebola virus. *J. Virol.* **82**, 2699-2704 (2008).

Harty, R. N., Brown, M. E., Wang, G., Huibregtse, J. & Hayes, F. P. A PPxY motif within the VP40 protein of Ebola virus interacts physically and functionally with a ubiquitin ligase: implications for filovirus budding. *Proc. Natl. Acad. Sci. U. S. A.* **97**, 13871-13876 (2000).

Hensley, L. E., Young, H. A., Jahrling, P. B. & Geisbert, T. W. Proinflammatory response during Ebola virus infection of primate models: possible involvement of the tumor necrosis factor receptor superfamily. *Immunol. Lett.* **80**, 169-179 (2002).

Hoenen, T. *et al*. VP40 octamers are essential for Ebola virus replication. *J. Virol.* **79**, 1898-1905 (2005).

Hoenen, T. *et al*. Infection of naive target cells with virus-like particles: implications for the function of ebola virus VP24. *J. Virol.* **80**, 7260-7264 (2006).

Hoenen, T., Jung, S., Herwig, A., Groseth, A. & Becker, S. Both matrix proteins of Ebola virus contribute to the regulation of viral genome replication and transcription. *Virology* **403**, 56-66 (2010a).

Hoenen, T. *et al*. Oligomerization of Ebola virus VP40 is essential for particle morphogenesis and regulation of viral transcription. *J. Virol.* **84**, 7053-7063 (2010b).

Huang, Y., Xu, L., Sun, Y. & Nabel, G. J. The assembly of Ebola virus nucleocapsid requires virion-associated proteins 35 and 24 and posttranslational modification of nucleoprotein. *Mol. Cell* **10**, 307-316 (2002).

Iseni, F., Barge, A., Baudin, F., Blondel, D. & Ruigrok, R. W. Characterization of rabies virus nucleocapsids and recombinant nucleocapsid-like structures. *J. Gen. Virol.* **79 (Pt 12)**, 2909-2919 (1998).

Ito, H., Watanabe, S., Sanchez, A., Whitt, M. A. & Kawaoka, Y. Mutational analysis of the putative fusion domain of Ebola virus glycoprotein. *J. Virol.* **73**, 8907-8912 (1999).

Jaax, N. K. *et al*. Lethal experimental infection of rhesus monkeys with Ebola-Zaire (Mayinga) virus by the oral and conjunctival route of exposure. *Arch. Pathol. Lab. Med.* **120**, 140-155 (1996).

Jasenosky, L. D., Neumann, G., Lukashevich, I. & Kawaoka, Y. Ebola virus VP40-induced particle formation and association with the lipid bilayer. *J. Virol.* **75**, 5205-5214 (2001).

Jemielity, S. *et al*. TIM-family proteins promote infection of multiple enveloped viruses through virion-associated phosphatidylserine. *PLoS Pathog.* **9**, e1003232 (2013).

John, S. P. *et al*. Ebola virus VP30 is an RNA binding protein. *J. Virol.* **81**, 8967-8976 (2007).

Johnson, E., Jaax, N., White, J. & Jahrling, P. Lethal experimental infections of rhesus monkeys by aerosolized Ebola virus. *Int. J. Exp. Pathol.* **76**, 227-236 (1995).

Johnson, R. F., Bell, P. & Harty, R. N. Effect of Ebola virus proteins GP, NP and VP35 on VP40 VLP morphology. *Virol. J.* **3**, 31 (2006a).

Johnson, R. F., McCarthy, S. E., Godlewski, P. J. & Harty, R. N. Ebola virus VP35-VP40 interaction is sufficient for packaging 3E-5E minigenome RNA into virus-like particles. *J. Virol.* **80**, 5135-5144 (2006b).

Judson, S., Prescott, J. & Munster, V. Understanding ebola virus transmission. *Viruses* **7**, 511-521 (2015).

Kastner, B. *et al*. GraFix: sample preparation for single-particle electron cryomicroscopy. *Nat. Methods* **5**, 53-55 (2008).

Khan, A. S. *et al*. The reemergence of Ebola hemorrhagic fever, Democratic Republic of the Congo, 1995. Commission de Lutte contre les Epidemies a Kikwit. *J. Infect. Dis.* **179 Suppl 1**, S76-86 (1999).

Kirchdoerfer, R. N., Abelson, D. M., Li, S., Wood, M. R. & Saphire, E. O. Assembly of the Ebola Virus Nucleoprotein from a Chaperoned VP35 Complex. *Cell. Rep.* **12**, 140-149 (2015).

Klockenbusch, C. & Kast, J. Optimization of formaldehyde cross-linking for protein interaction analysis of non-tagged integrin beta1. *J. Biomed. Biotechnol.* **2010**, 927585 (2010).

Kobasa, D., Rodgers, M. E., Wells, K. & Kawaoka, Y. Neuraminidase hemadsorption activity, conserved in avian influenza A viruses, does not influence viral replication in ducks. *J. Virol.* **71**, 6706-6713 (1997).

Kobinger, G. P. *et al*. Replication, pathogenicity, shedding, and transmission of Zaire ebolavirus in pigs. *J. Infect. Dis.* **204**, 200-208 (2011).

Kolodziej, S. J., Penczek, P. A. & Stoops, J. K. Utility of Butvar support film and methylamine tungstate stain in three-dimensional electron microscopy: agreement between stain and frozen-hydrated reconstructions. *J. Struct. Biol.* **120**, 158-167 (1997).

Kondratowicz, A. S. *et al*. T-cell immunoglobulin and mucin domain 1 (TIM-1) is a receptor for Zaire Ebolavirus and Lake Victoria Marburgvirus. *Proc. Natl. Acad. Sci. U. S. A.* **108**, 8426-8431 (2011).

Ksiazek, T. G. *et al*. Clinical virology of Ebola hemorrhagic fever (EHF): virus, virus antigen, and IgG and IgM antibody findings among EHF patients in Kikwit, Democratic Republic of the Congo, 1995. *J. Infect. Dis.* **179 Suppl 1**, S177-87 (1999).

Kuhn, J. H. *et al*. Conserved receptor-binding domains of Lake Victoria marburgvirus and Zaire ebolavirus bind a common receptor. *J. Biol. Chem.* **281**, 15951-15958 (2006).

Kuhn, J. H. *et al*. Nomenclature- and database-compatible names for the two Ebola virus variants that emerged in Guinea and the Democratic Republic of the Congo in 2014. *Viruses* **6**, 4760-4799 (2014).

Le Guenno, B. *et al*. Isolation and partial characterisation of a new strain of Ebola virus. *Lancet* **345**, 1271-1274 (1995).

Leitner, A., Walzthoeni, T. & Aebersold, R. Lysine-specific chemical cross-linking of protein complexes and identification of cross-linking sites using LC-MS/MS and the xQuest/xProphet software pipeline. *Nat. Protoc.* **9**, 120-137 (2014).

Leroy, E. M. *et al*. Human asymptomatic Ebola infection and strong inflammatory response. *Lancet* **355**, 2210-2215 (2000).

Leroy, E. M., Baize, S., Debre, P., Lansoud-Soukate, J. & Mavoungou, E. Early immune responses accompanying human asymptomatic Ebola infections. *Clin. Exp. Immunol.* **124**, 453-460 (2001).

Leroy, E. M., Baize, S., Mavoungou, E. & Apetrei, C. Sequence analysis of the GP, NP, VP40 and VP24 genes of Ebola virus isolated from deceased, surviving and asymptomatically infected individuals during the 1996 outbreak in Gabon: comparative studies and phylogenetic characterization. *J. Gen. Virol.* **83**, 67-73 (2002).

Leroy, E. M. *et al*. Multiple Ebola virus transmission events and rapid decline of central African wildlife. *Science* **303**, 387-390 (2004).

Leroy, E. M. *et al*. Fruit bats as reservoirs of Ebola virus. *Nature* **438**, 575-576 (2005).

Leroy, E. M. *et al*. Human Ebola outbreak resulting from direct exposure to fruit bats in Luebo, Democratic Republic of Congo, 2007. *Vector Borne Zoonotic Dis.* **9**, 723-728 (2009).

Leung, D. W. *et al*. Structure of the Ebola VP35 interferon inhibitory domain. *Proc. Natl. Acad. Sci. U. S. A.* **106**, 411-416 (2009).

Leung, D. W. *et al*. Crystallization and preliminary X-ray analysis of Ebola VP35 interferon inhibitory domain mutant proteins. *Acta Crystallogr. Sect. F. Struct. Biol. Cryst. Commun.* **66**, 689-692 (2010a).

Leung, D. W. *et al*. Structural basis for dsRNA recognition and interferon antagonism by Ebola VP35. *Nat. Struct. Mol. Biol.* **17**, 165-172 (2010b).

Leung, D. W. *et al*. An Intrinsically Disordered Peptide from Ebola Virus VP35 Controls Viral RNA Synthesis by Modulating Nucleoprotein-RNA Interactions. *Cell. Rep.* **11**, 376-389 (2015).

Licata, J. M. *et al*. Overlapping motifs (PTAP and PPEY) within the Ebola virus VP40 protein function independently as late budding domains: involvement of host proteins TSG101 and VPS-4. *J. Virol.* **77**, 1812-1819 (2003).

Licata, J. M., Johnson, R. F., Han, Z. & Harty, R. N. Contribution of ebola virus glycoprotein, nucleoprotein, and VP24 to budding of VP40 virus-like particles. *J. Virol.* **78**, 7344-7351 (2004).

Loney et al. Paramyxovirus ultrastructure and genome packaging: cryo-electron tomography of Sendai virus. *J. Virol*. **83**(16), 8191-81-97, (2009).

Ludtke, S. J., Baldwin, P. R. & Chiu, W. EMAN: semiautomated software for high-resolution single-particle reconstructions. *J. Struct. Biol.* **128**, 82-97 (1999).

Lyon, G. M. *et al*. Clinical care of two patients with Ebola virus disease in the United States. *N. Engl. J. Med.* **371**, 2402-2409 (2014).

MacNeil, A. & Rollin, P. E. Ebola and Marburg hemorrhagic fevers: neglected tropical diseases? *PLoS Negl Trop. Dis.* **6**, e1546 (2012).

Maganga, G. D. *et al*. Ebola virus disease in the Democratic Republic of Congo. *N. Engl. J. Med.* **371**, 2083-2091 (2014).

Mahanty, S. *et al*. Protection from lethal infection is determined by innate immune responses in a mouse model of Ebola virus infection. *Virology* **312**, 415-424 (2003).

Manicassamy, B., Wang, J., Jiang, H. & Rong, L. Comprehensive analysis of ebola virus GP1 in viral entry. *J. Virol.* **79**, 4793-4805 (2005).

Mari Saez, A. *et al*. Investigating the zoonotic origin of the West African Ebola epidemic. *EMBO Mol. Med.* **7**, 17-23 (2014).

Martinez, M. J. *et al*. Role of Ebola virus VP30 in transcription reinitiation. *J. Virol.* **82**, 12569-12573 (2008).

Martinez, M. J. *et al*. Role of VP30 phosphorylation in the Ebola virus replication cycle. *J. Infect. Dis.* **204 Suppl 3**, S934-40 (2011).

Martin-Serrano, J., Zang, T. & Bieniasz, P. D. HIV-1 and Ebola virus encode small peptide motifs that recruit Tsg101 to sites of particle assembly to facilitate egress. *Nat. Med.* **7**, 1313-1319 (2001).

Mastronarde, D. N. Dual-axis tomography: an approach with alignment methods that preserve resolution. *J. Struct. Biol.* **120**, 343-352 (1997).

Mateo, M., Reid, S. P., Leung, L. W., Basler, C. F. & Volchkov, V. E. Ebolavirus VP24 binding to karyopherins is required for inhibition of interferon signaling. *J. Virol.* **84**, 1169-1175 (2010).

Mateo, M. *et al*. VP24 is a molecular determinant of Ebola virus virulence in guinea pigs. *J. Infect. Dis.* **204 Suppl 3**, S1011-20 (2011).

Mavrakis, M., Kolesnikova, L., Schoehn, G., Becker, S. & Ruigrok, R. W. Morphology of Marburg virus NP-RNA. *Virology* **296**, 300-307 (2002).

Mehedi, M. *et al*. A new Ebola virus nonstructural glycoprotein expressed through RNA editing. *J. Virol.* **85**, 5406-5414 (2011).

Melito, P. L. *et al*. The creation of stable cell lines expressing Ebola virus glycoproteins and the matrix protein VP40 and generating Ebola virus-like particles utilizing an ecdysone inducible mammalian expression system. *J. Virol. Methods* **148**, 237-243 (2008).

Meltzer, M. I. *et al*. Estimating the future number of cases in the Ebola epidemic--Liberia and Sierra Leone, 2014-2015. *MMWR Suppl.* **63**, 1-14 (2014).

Miller, E. H. *et al*. Ebola virus entry requires the host-programmed recognition of an intracellular receptor. *EMBO J.* **31**, 1947-1960 (2012).

Miranda, M. E. *et al*. Epidemiology of Ebola (subtype Reston) virus in the Philippines, 1996. *J. Infect. Dis.* **179 Suppl 1**, S115-9 (1999).

Modrof, J., Muhlberger, E., Klenk, H. D. & Becker, S. Phosphorylation of VP30 impairs ebola virus transcription. *J. Biol. Chem.* **277**, 33099-33104 (2002).

Modrof, J., Becker, S. & Muhlberger, E. Ebola virus transcription activator VP30 is a zinc-binding protein. *J. Virol.* **77**, 3334-3338 (2003).

Moller-Tank, S., Kondratowicz, A. S., Davey, R. A., Rennert, P. D. & Maury, W. Role of the phosphatidylserine receptor TIM-1 in enveloped-virus entry. *J. Virol.* **87**, 8327-8341 (2013).

Muhlberger, E. *et al*. Termini of all mRNA species of Marburg virus: sequence and secondary structure. *Virology* **223**, 376-380 (1996).

Muhlberger, E., Lotfering, B., Klenk, H. D. & Becker, S. Three of the four nucleocapsid proteins of Marburg virus, NP, VP35, and L, are sufficient to mediate replication and transcription of Marburg virus-specific monocistronic minigenomes. *J. Virol.* **72**, 8756-8764 (1998).

Muhlberger, E., Weik, M., Volchkov, V. E., Klenk, H. D. & Becker, S. Comparison of the transcription and replication strategies of marburg virus and Ebola virus by using artificial replication systems. *J. Virol.* **73**, 2333-2342 (1999).
Muhlberger, E. Filovirus replication and transcription. *Future Virol.* **2**, 205-215 (2007).

Nakata, S., Petrie, B. L., Calomeni, E. P. & Estes, M. K. Electron microscopy procedure influences detection of rotaviruses. *J. Clin. Microbiol.* **25**, 1902-1906 (1987).

Nanbo, A. *et al*. Ebolavirus is internalized into host cells via macropinocytosis in a viral glycoprotein-dependent manner. *PLoS Pathog.* **6**, e1001121 (2010).

Nanbo, A., Watanabe, S., Halfmann, P. & Kawaoka, Y. The spatio-temporal distribution dynamics of Ebola virus proteins and RNA in infected cells. *Sci. Rep.* **3**, 1206 (2013).

Negredo, A. *et al*. Discovery of an ebolavirus-like filovirus in europe. *PLoS Pathog.* **7**, e1002304 (2011).

Nielsen, S. U. *et al*. Association between hepatitis C virus and very-low-density lipoprotein (VLDL)/LDL analyzed in iodixanol density gradients. *J. Virol.* **80**, 2418-2428 (2006).

Niwa, H., Yamamura, K. & Miyazaki, J. Efficient selection for high-expression transfectants with a novel eukaryotic vector. *Gene* **108**, 193-199 (1991).

Noda, T., Sagara, H., Suzuki, E., Takada, A., Kida, H., and Kawaoka, Y. Ebola virus VP40 drives the formation of virus-like filamentous particles along with GP. J. Virol. **76**(10): 4855-4865 (2002).

Noda, T. *et al*. Assembly and budding of Ebolavirus. *PLoS Pathog.* **2**, e99 (2006).

Noda, T., Watanabe, S., Sagara, H. & Kawaoka, Y. Mapping of the VP40-binding regions of the nucleoprotein of Ebola virus. *J. Virol.* **81**, 3554-3562 (2007a).

Noda, T., Halfmann, P., Sagara, H. & Kawaoka, Y. Regions in Ebola virus VP24 that are important for nucleocapsid formation. *J. Infect. Dis.* **196 Suppl 2**, S247-50 (2007b).

Noda, T., Hagiwara, K., Sagara, H. & Kawaoka, Y. Characterization of the Ebola virus nucleoprotein-RNA complex. *J. Gen. Virol.* **91**, 1478-1483 (2010).

Noda, T., Kolesnikova, L., Becker, S. & Kawaoka, Y. The importance of the NP: VP35 ratio in Ebola virus nucleocapsid formation. *J. Infect. Dis.* **204 Suppl 3**, S878-83 (2011).

Nyborg, J. K. & Peersen, O. B. That zincing feeling: the effects of EDTA on the behaviour of zinc-binding transcriptional regulators. *Biochem. J.* **381**, e3-4 (2004).

Olival, K. J. *et al*. Ebola virus antibodies in fruit bats, bangladesh. *Emerg. Infect. Dis.* **19**, 270-273 (2013).

Olival, K. J. & Hayman, D. T. Filoviruses in bats: current knowledge and future directions. *Viruses* **6**, 1759-1788 (2014).

Pandithage, R. Brief introduction to contrasting for EM sample preparation [online]. (2013). Available from: http://www.leica-microsystems.com/science-lab/brief-introduction-to-contrasting-for-em-sample-preparation/.

Paweska, J. T. *et al*. Virological and serological findings in Rousettus aegyptiacus experimentally inoculated with vero cells-adapted hogan strain of Marburg virus. *PLoS One* **7**, e45479 (2012).

Penczek, P., Marko, M., Buttle, K. & Frank, J. Double-tilt electron tomography. *Ultramicroscopy* **60**, 393-410 (1995).

Peng, R. *et al*. In vitro assembly of Ebola virus nucleocapsid-like complex expressed in E. coli. *Protein Cell.* **7**, 888-898 (2016).

Pettersen, E. F. *et al*. UCSF Chimera--a visualization system for exploratory research and analysis. *J. Comput. Chem.* **25**, 1605-1612 (2004).

Peyrol, J. *et al*. Multiple phosphorylable sites in the Zaire Ebolavirus nucleoprotein evidenced by high resolution tandem mass spectrometry. *J. Virol. Methods* (2012).

Prins, K. C., Cardenas, W. B. & Basler, C. F. Ebola virus protein VP35 impairs the function of interferon regulatory factor-activating kinases IKKepsilon and TBK-1. *J. Virol.* **83**, 3069-3077 (2009).

Prins, K. C. *et al*. Basic residues within the ebolavirus VP35 protein are required for its viral polymerase cofactor function. *J. Virol.* **84**, 10581-10591 (2010a).

Prins, K. C. *et al*. Mutations abrogating VP35 interaction with double-stranded RNA render Ebola virus avirulent in guinea pigs. *J. Virol.* **84**, 3004-3015 (2010b).

Reed, D. S., Hensley, L. E., Geisbert, J. B., Jahrling, P. B. & Geisbert, T. W. Depletion of peripheral blood T lymphocytes and NK cells during the course of ebola hemorrhagic Fever in cynomolgus macaques. *Viral Immunol.* **17**, 390-400 (2004).

Reed, D. S., Lackemeyer, M. G., Garza, N. L., Sullivan, L. J. & Nichols, D. K. Aerosol exposure to Zaire ebolavirus in three nonhuman primate species: differences in disease course and clinical pathology. *Microbes Infect.* **13**, 930-936 (2011).

Reid, S. P., Cardenas, W. B. & Basler, C. F. Homo-oligomerization facilitates the interferon-antagonist activity of the ebolavirus VP35 protein. *Virology* **341**, 179-189 (2005).

Reid, S. P. *et al*. Ebola virus VP24 binds karyopherin alpha1 and blocks STAT1 nuclear accumulation. *J. Virol.* **80**, 5156-5167 (2006).

Reid, S. P., Valmas, C., Martinez, O., Sanchez, F. M. & Basler, C. F. Ebola virus VP24 proteins inhibit the interaction of NPI-1 subfamily karyopherin alpha proteins with activated STAT1. *J. Virol.* **81**, 13469-13477 (2007).

Richman, D. D., Cleveland, P. H., McCormick, J. B. & Johnson, K. M. Antigenic analysis of strains of Ebola virus: identification of two Ebola virus serotypes. *J. Infect. Dis.* **147**, 268-271 (1983).

Rollin, P. E. *et al*. Ebola (subtype Reston) virus among quarantined nonhuman primates recently imported from the Philippines to the United States. *J. Infect. Dis.* **179 Suppl 1**, S108-14 (1999).

Rougeron, V., Feldmann, H., Grard, G., Becker, S. & Leroy, E. M. Ebola and Marburg haemorrhagic fever. *J. Clin. Virol.* **64**, 111-119 (2015).

Ruigrok, R. W., Crepin, T. & Kolakofsky, D. Nucleoproteins and nucleocapsids of negative-strand RNA viruses. *Curr. Opin. Microbiol.* **14**, 504-510 (2011).

Ryabchikova, E. I., Kolesnikova, L. V. & Luchko, S. V. An analysis of features of pathogenesis in two animal models of Ebola virus infection. *J. Infect. Dis.* **179 Suppl 1**, S199-202 (1999).

Saeed, M. F., Kolokoltsov, A. A., Albrecht, T. & Davey, R. A. Cellular entry of ebola virus involves uptake by a macropinocytosis-like mechanism and subsequent trafficking through early and late endosomes. *PLoS Pathog.* **6**, e1001110 (2010).

Sanchez, A., Kiley, M. P., Holloway, B. P., McCormick, J. B. & Auperin, D. D. The nucleoprotein gene of Ebola virus: cloning, sequencing, and in vitro expression. *Virology* **170**, 81-91 (1989).

Sanchez, A., Kiley, M. P., Klenk, H. D. & Feldmann, H. Sequence analysis of the Marburg virus nucleoprotein gene: comparison to Ebola virus and other non-segmented negative-strand RNA viruses. *J. Gen. Virol.* **73 (Pt 2)**, 347-357 (1992).

Sanchez, A., Kiley, M. P., Holloway, B. P. & Auperin, D. D. Sequence analysis of the Ebola virus genome: organization, genetic elements, and comparison with the genome of Marburg virus. *Virus Res.* **29**, 215-240 (1993).

Sanchez, A., Trappier, S. G., Mahy, B. W., Peters, C. J. & Nichol, S. T. The virion glycoproteins of Ebola viruses are encoded in two reading frames and are expressed through transcriptional editing. *Proc. Natl. Acad. Sci. U. S. A.* **93**, 3602-3607 (1996).

Sanchez, A. *et al*. Biochemical analysis of the secreted and virion glycoproteins of Ebola virus. *J. Virol.* **72**, 6442-6447 (1998).

Scaturro, P. *et al*. Characterization of the mode of action of a potent dengue virus capsid inhibitor. *J. Virol.* **88**, 11540-11555 (2014).

Schnittler, H. J. & Feldmann, H. Marburg and Ebola hemorrhagic fevers: does the primary course of infection depend on the accessibility of organ-specific macrophages? *Clin. Infect. Dis.* **27**, 404-406 (1998).

Schornberg, K. *et al*. Role of endosomal cathepsins in entry mediated by the Ebola virus glycoprotein. *J. Virol.* **80**, 4174-4178 (2006).

Shi, W. *et al*. A filovirus-unique region of Ebola virus nucleoprotein confers aberrant migration and mediates its incorporation into virions. *J. Virol.* **82**, 6190-6199 (2008).

Slenczka, W. & Klenk, H. D. Forty years of marburg virus. *J. Infect. Dis.* **196 Suppl 2**, S131-5 (2007).

Sousa *et al*. Dual-axis electron tomography of biological specimens: extending the limits of specimen thickness with bright-field STEM imaging. *J. Struct. Biol*. **174**(1): 107-114 (2011).

Stark, H. GraFix: stabilization of fragile macromolecular complexes for single particle cryo-EM. *Methods Enzymol.* **481**, 109-126 (2010).

Stoops, J. K. *et al*. Comparisons of the low-resolution structures of ornithine decarboxylase by electron microscopy and X-ray crystallography: the utility of methylamine tungstate stain and Butvar support film in the study of macromolecules by transmission electron microscopy. *J. Electron Microsc. Tech.* **18**, 157-166 (1991).

Stricker, R., Mottet, G. & Roux, L. The Sendai virus matrix protein appears to be recruited in the cytoplasm by the viral nucleocapsid to function in viral assembly and budding. *J. Gen. Virol.* **75 (Pt 5)**, 1031-1042 (1994).

Stroher, U. *et al*. Infection and activation of monocytes by Marburg and Ebola viruses. *J. Virol.* **75**, 11025-11033 (2001).

Swanepoel, R. *et al*. Experimental inoculation of plants and animals with Ebola virus. *Emerg. Infect. Dis.* **2**, 321-325 (1996).

Takada, A. *et al*. Human macrophage C-type lectin specific for galactose and N-acetylgalactosamine promotes filovirus entry. *J. Virol.* **78**, 2943-2947 (2004).

Timen, A. *et al*. Response to imported case of Marburg hemorrhagic fever, the Netherland. *Emerg. Infect. Dis.* **15**, 1171-1175 (2009).

Towner, J. S. *et al*. Isolation of genetically diverse Marburg viruses from Egyptian fruit bats. *PLoS Pathog.* **5**, e1000536 (2009).

Trunschke, M. *et al*. The L-VP35 and L-L interaction domains reside in the amino terminus of the Ebola virus L protein and are potential targets for antivirals. *Virology* **441**, 135-145 (2013).

Tuthill *et al*. Picornaviruses. *Curr. Top. Microbiol. Immunol.* **343**, 43-89 (2010).

Uyeki, T. M. *et al*. Clinical Management of Ebola Virus Disease in the United States and Europe. *N. Engl. J. Med.* **374**, 636-646 (2016).

van Heel, M. *et al*. Single-particle electron cryo-microscopy: towards atomic resolution. *Q. Rev. Biophys.* **33**, 307-369 (2000).

Volchkov, V. E., Feldmann, H., Volchkova, V. A. & Klenk, H. D. Processing of the Ebola virus glycoprotein by the proprotein convertase furin. *Proc. Natl. Acad. Sci. U. S. A.* **95**, 5762-5767 (1998).

Volchkov, V. E. *et al*. Characterization of the L gene and 5' trailer region of Ebola virus. *J. Gen. Virol.* **80 (Pt 2)**, 355-362 (1999).

Volchkov, V. E., Chepurnov, A. A., Volchkova, V. A., Ternovoj, V. A. & Klenk, H. D. Molecular characterization of guinea pig-adapted variants of Ebola virus. *Virology* **277**, 147-155 (2000).

Volchkov, V. E. *et al*. Recovery of infectious Ebola virus from complementary DNA: RNA editing of the GP gene and viral cytotoxicity. *Science* **291**, 1965-1969 (2001).

Wahl-Jensen, V. M. *et al*. Effects of Ebola virus glycoproteins on endothelial cell activation

and barrier function. *J. Virol.* **79**, 10442-10450 (2005).

Wamala, J. F. *et al*. Ebola hemorrhagic fever associated with novel virus strain, Uganda, 2007-2008. *Emerg. Infect. Dis.* **16**, 1087-1092 (2010).

Wang, H. *et al*. Ebola Viral Glycoprotein Bound to Its Endosomal Receptor Niemann-Pick C1. *Cell* **164**, 258-268 (2016).

Watanabe, S., Noda, T. & Kawaoka, Y. Functional mapping of the nucleoprotein of Ebola virus. *J. Virol.* **80**, 3743-3751 (2006).

Watanabe, S., Noda, T., Halfmann, P., Jasenosky, L. & Kawaoka, Y. Ebola virus (EBOV) VP24 inhibits transcription and replication of the EBOV genome. *J. Infect. Dis.* **196 Suppl 2**, S284-90 (2007).

Watt, A. *et al*. A novel life cycle modeling system for Ebola virus shows a genome length-dependent role of VP24 in virus infectivity. *J. Virol.* **88**, 10511-10524 (2014).

Wauquier, N., Becquart, P., Padilla, C., Baize, S. & Leroy, E. M. Human fatal zaire ebola virus infection is associated with an aberrant innate immunity and with massive lymphocyte apoptosis. *PLoS Negl Trop. Dis.* **4**, 10.1371/journal.pntd.0000837 (2010).

Weik, M., Modrof, J., Klenk, H. D., Becker, S. & Muhlberger, E. Ebola virus VP30-mediated transcription is regulated by RNA secondary structure formation. *J. Virol.* **76**, 8532-8539 (2002).

Weik, M., Enterlein, S., Schlenz, K. & Muhlberger, E. The Ebola virus genomic replication promoter is bipartite and follows the rule of six. *J. Virol.* **79**, 10660-10671 (2005).

Weingartl, H. M. *et al*. Transmission of Ebola virus from pigs to non-human primates. *Sci. Rep.* **2**, 811 (2012).

Weissenhorn, W., Calder, L. J., Wharton, S. A., Skehel, J. J. & Wiley, D. C. The central structural feature of the membrane fusion protein subunit from the Ebola virus glycoprotein is a long triple-stranded coiled coil. *Proc. Natl. Acad. Sci. U. S. A.* **95**, 6032-6036 (1998a).

Weissenhorn, W., Carfi, A., Lee, K. H., Skehel, J. J. & Wiley, D. C. Crystal structure of the Ebola virus membrane fusion subunit, GP2, from the envelope glycoprotein ectodomain. *Mol. Cell* **2**, 605-616 (1998b).

Welsch, S. *et al*. Electron tomography reveals the steps in filovirus budding. *PLoS Pathog.* **6**, e1000875 (2010).

WHO. 2016. Ebola Situation Report: 17 February 2016 [online]. Available from:

http://apps.who.int.uml.idm.oclc.org/ebola/current-situation/ebola-situation-report-17-february-2016.

Yang, Z. Y. *et al*. Identification of the Ebola virus glycoprotein as the main viral determinant of vascular cell cytotoxicity and injury. *Nat. Med.* **6**, 886-889 (2000).

Zhang, A. P. *et al*. The ebola virus interferon antagonist VP24 directly binds STAT1 and has a novel, pyramidal fold. *PLoS Pathog.* **8**, e1002550 (2012).

Chapter 9. Appendices

9.1 Solutions

TNE Buffer
20 mM Tris
100 mM NaCl
0.1 mM EDTA, pH 7.4

Conventional fix
0.1 M Sorenson's Phosphate Buffer, pH 7.2
2% Paraformaldehyde
2.5% Gluteraldehyde
DH_2O

0.2 M Sorenson's Phosphate Buffer, pH 7.2
0.2 M Dibasic phosphate buffer: 28.39 g Na_2HPO_4 in 1 L ddH_20
0.2 M Monosodium phosphate buffer: 31.21 g $NaH_2PO_42{\bullet}H_20$ in 1 L ddH_20
Mix together: 180 ml dibasic + 70 ml monosodium phosphate buffers

0.1 M Phosphate Buffer with 2.8% Sucrose (Wash Buffer)
250 ml 0.2 M phosphate buffer
250 ml ddH_2O
14.45 g sucrose

0.2 M Phosphate Buffer with 7% Sucrose (Wash Buffer)
250 ml 0.2 M phosphate buffer
17.5 g sucrose

1% Osmium Tetroxide
10 ml 2% osmium tetroxide
10 ml 0.2 M phosphate buffer
(Electron Microscopy Sciences)

Infiltration Media (resin)
15% Araldite 502
25% Embed-812
55% DDSA

Embedding Media (resin + accelerator)
15% Araldite 502
25% Embed-812
55% DDSA
1.5-1.9% DMP-30
(Electron Microscopy Sciences)

9.2 Mass Spectrometry Results

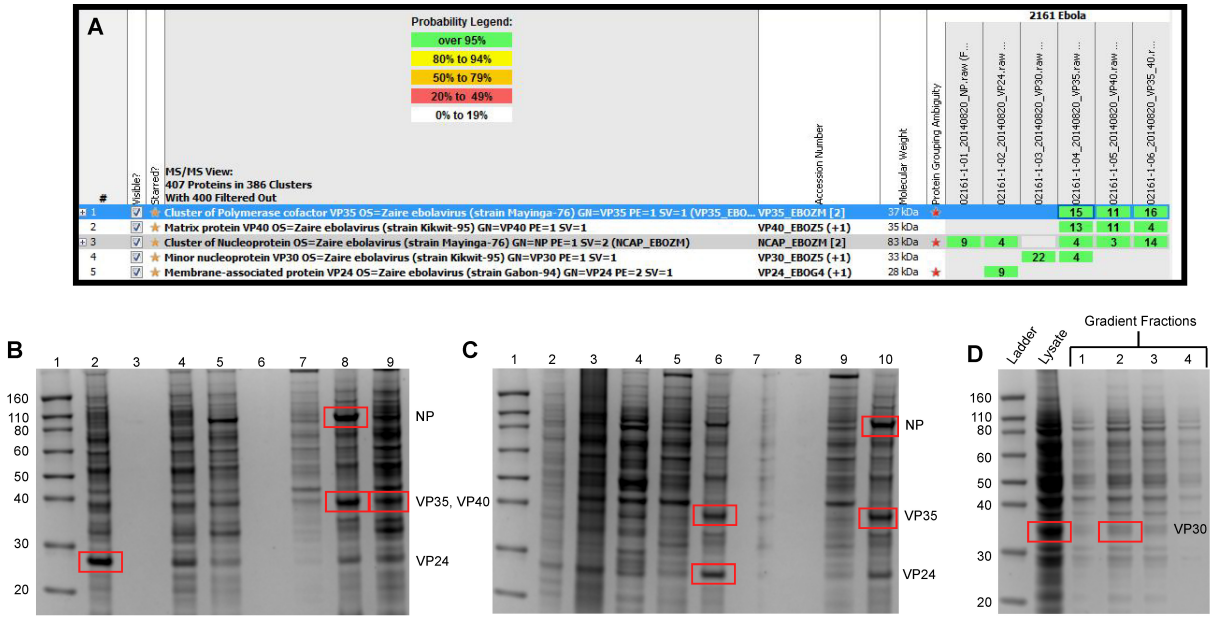

Figure 95. Protein identification by mass spectrometry. Bands of interest were cut from SDS-PAGE (red boxes), in gel digestion was performed and proteins were analyzed by mass spectrometry.

A: Initial mass spectrometry results.
B: SDS-PAGE of fractions and pellets. Lane 1: Ladder; Lane 2: Fraction 6 of NP/VP24/VP35 transfection; Lane 8: Fraction 6 of NP/VP24/VP35/VP40 transfection; Lane 9: Pellet of fraction 6 from NP/VP24/VP35/VP40 transfection.
C: SDS-PAGE of hypotonic freeze/thaw fractions and pellets. Lane 1. Ladder; Lane 6 and 10: Fraction 6 from NP/VP24/VP35 transfections.
D: SDS-PAGE of VP30 only gradient migration.
E: Repeat mass spectrometry results for NP and VP40.
F: SDS-PAGE of NP only gradient.
G: SDS-PAGE of truncated NP only gradient.
H: SDS-PAGE of sucrose purified VLPs. Lane 1: Ladder; Lane 3: VP40 VLP.

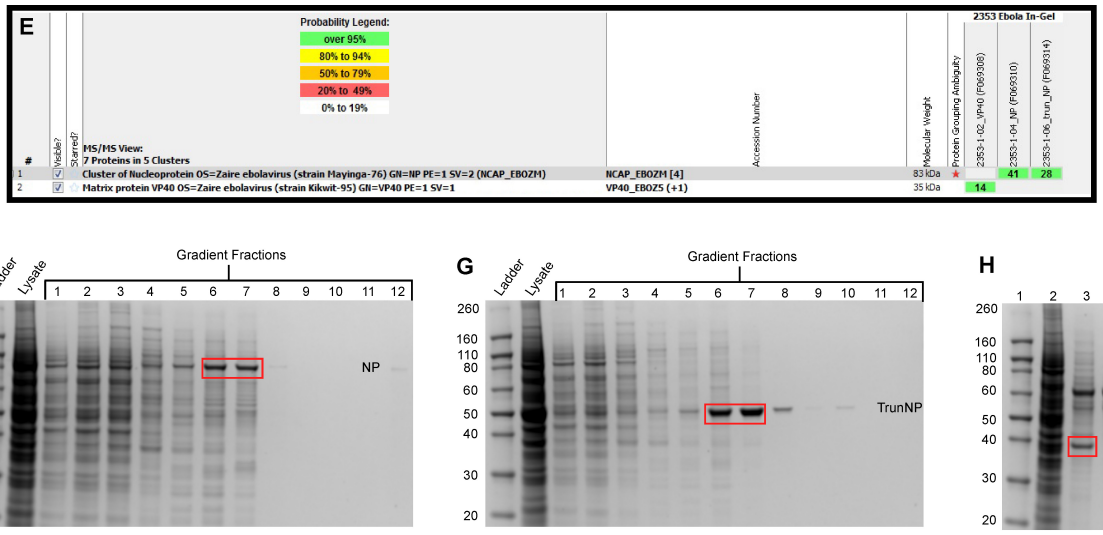

Figure 95 continued.

9.3 Tissue Processing Protocol

Vial	Solution	Agitation	Duration (hrs)	Temperature (°C)
1	Conventional Fixative	Yes	02:00	4
2	0.1 M Sorenson's buffer, pH 7.2	Yes	00:20	4
3	0.1 M Sorenson's buffer, pH 7.2	Yes	00:20	4
4	0.1 M Sorenson's buffer, pH 7.2	Yes	00:20	4
5	1% osmium tetroxide	Yes	01:00	20
6	ddH_20	Yes	00:15	20
7	ddH_20	Yes	00:15	20
8	ddH_20	Yes	00:15	20
9	50% ethanol	Yes	00:15	20
10	70% ethanol	Yes	00:15	20
11	95% ethanol	Yes	00:15	20
12	100% ethanol	Yes	00:10	20
13	100% ethanol	Yes	00:10	20
14	Propylene oxide	Yes	00:10	20
15	Propylene oxide	Yes	00:10	20
16	1:1 Propylene oxide:resin	Yes	04:00	20
17	1:3 Propylene oxide:resin	Yes	04:00	20
18	Resin (-acc)	Yes	04:00	20
19	Resin (-acc)	Yes	04:00	20
20	Resin (+ acc)	Yes	24:00	20

9.4 Supplementary Movies

Movies S1 and S2. Tomograms of NP, VP24, and VP35 transfected cell section. These movies show the compiled "Z" slices from two separate dual axis tomograms. The slices travel through the Z axis of the cell and viral inclusion bodies and demonstrate the flexibility and length of the nucleocapsid-like structures.

Movie S3. Moving model of a coiled spring that maintains 11 repeats per turn as it is stretched or condensed. Movie was modelled in Cinema 4D software by Aaron Simoes, based on a spring that maintains 11 repeats per turn, with a 1:1 ratio for each protein. Turquoise: VP24-VP35 heterodimer; magenta: NP molecules; orange: RNA.

Movie S4. Moving model of a coiled spring that does not maintain 11 repeats per turn as it is stretched or condensed. Movie was modelled in Cinema 4D software by Aaron Simoes, with a 1:1 ratio for each protein. Turquoise: VP24-VP35 heterodimer; magenta: NP molecules; orange: RNA.

9.5 Copyright Approval

Part of Figure 2 and Figure 70 was adapted from Beniac et al. (2012) published by PLoS ONE. This journal applies the Creative Commons Attribution license, meaning that reuse permission is granted upon publication and copyright approval is not required.

Figure 4 was adapted from Bharat et al. (2012) published by PNAS. This journal enables the use of original figures for noncommercial and educational use without requesting permission. As such, copyright approval was not required.

Part of Figure 2 was adapted from Booth et al. (2013). Please see copyright approval on following page.

This Agreement between Melissa Rabb ("You") and Elsevier ("Elsevier") consists of your license details and the terms and conditions provided by Elsevier and Copyright Clearance Center.

License Number	4061420783230
License date	
Licensed Content Publisher	Elsevier
Licensed Content Publication	Trends in Microbiology
Licensed Content Title	How do filovirus filaments bend without breaking?
Licensed Content Author	Tim F. Booth,Melissa J. Rabb,Daniel R. Beniac
Licensed Content Date	November 2013
Licensed Content Volume	21
Licensed Content Issue	11
Licensed Content Pages	11
Start Page	583
End Page	593
Type of Use	reuse in a thesis/dissertation
Portion	figures/tables/illustrations
Number of figures/tables/illustrations	1
Format	both print and electronic
Are you the author of this Elsevier article?	Yes
Will you be translating?	No
Order reference number	
Original figure numbers	Figure 4b
Title of your thesis/dissertation	Ebola virus nucleocapsid-like structures are dynamic, but stable
Expected completion date	May 2017
Estimated size (number of pages)	300